Uniwersytet im. Adama Mickiewicza w Poznaniu

Szkoła Doktorska Nauk Przyrodniczych

Rozprawa doktorska

Struktury deformacyjne powstałe w efekcie upłynnienia osadu – podejście doświadczalne

Liquefaction-induced soft-sediment deformation structures – experimental approach

mgr Szymon Świątek

Promotorki rozprawy doktorskiej
Prof. dr hab. Małgorzata Pisarska-Jamroży
Dr hab. inż. Karolina Lewińska, prof. UAM

Poznań, 2025

Spis treści

Podziękowania

Pragnę złożyć serdeczne podziękowania osobom, bez których wsparcia, zaangażowania i życzliwości ta praca nie mogłaby powstać.

Dziękuję mojej Promotorce, Pani Profesor Małgorzacie Pisarskiej-Jamroży, za zaszczepienie we mnie pasji do paleosejsmologii oraz sedymentologii, a także za wprowadzenie mnie w świat badań naukowych z ogromną cierpliwością i naukową przenikliwością. To dzięki Pani kierunkowi i inspiracji możliwe było ukształtowanie tematu i charakteru tej rozprawy.

Podziękowania kieruję także mojej Drugiej Promotorce, Pani Profesor Karolinie Lewińskiej, za nieocenione wsparcie merytoryczne w zakresie geochemii i gleboznawstwa, za pomoc na każdym etapie pracy, a przede wszystkim – za stworzenie atmosfery otwartości i zaufania, która sprzyjała naukowemu rozwojowi i osobistej motywacji.

Dziękuję wszystkim Współautorom publikacji naukowych powstałych w ramach niniejszej rozprawy, w szczególności dr. Szymonowi Belzytowi za cenne wskazówki merytoryczne oraz rozmowy, które miały istotny wpływ na kształt i jakość prowadzonych badań.

Dziękuję Pracownikom i Pracowniczkom oraz Doktorantom i Doktorantkom Wydziału Nauk Geograficznych i Geologicznych za wszystkie rozmowy, pomoc i codzienne kontakty. Dziękuję Wiktorii, Oli, Kasi, Darkowi, Michałowi i Pawłowi.

Dziękuję także tym, którzy nie wierzyli – ich wątpliwości stały się impulsem do jeszcze większego zaangażowania i konsekwencji w dążeniu do celu.

Szczególne podziękowania kieruję do Konrada – za obecność, wsparcie, zrozumienie, motywację i pomoc.

Nullum magnum ingenium sine mixtura dementiae fuit

Lista publikacji wchodzących w skład rozprawy doktorskiej

Rozprawa doktorska składa się z trzech recenzowanych artykułów naukowych stanowiących spójny tematycznie zbiór publikacji:

1. **Świątek, S.***, Belzyt S., Pisarska-Jamroży, M., Woronko, B. 2023. Sedimentary records of liquefaction: implications from field studies. *Journal of Geophysical Research: Earth Surface* 128, e2023JF007152. https://doi.org/10.1029/2023JF007152 [A1]

   Dostępność online: 09.08.2023 r.
   Q1 WoS / 89. percentyl według bazy Scopus$_{2023}$ / IF$_{2023}$ = 3,5 / MEiN$_{2023}$ = 140 pkt
   Liczba cytowań: 16 (Google Scholar), 14 (Scopus), 11 (Web of Science)

2. **Świątek, S.***, Pisarska-Jamroży, M. 2025. Seismogenic liquefaction with M~3.5 in fine-grained sediments: An experimental approach. *Sedimentary Geology* 478, 106833. https://doi.org/10.1016/j.sedgeo.2025.106833 [A2]

   Dostępność online: 15.02.2025 r.
   Q1 WoS / 82. percentyl według bazy Scopus$_{2025}$ / IF$_{2025}$ = 2,7 / MNiSW$_{2025}$ = 100 pkt
   Liczba cytowań: 0 (Google Scholar), 0 (Scopus), 0 (Web of Science)

3. **Świątek, S.***, Lewińska, K., Pisarska-Jamroży, M., Günter, C. 2025. An application of quartz grain analyses in earthquake-induced (palaeo)liquefaction studies. *Journal of Structural Geology* 193, 105357. https://doi.org/10.1016/j.jsg.2025.105357 [A3]

   Dostępność online: 12.02.2025 r.
   Q1 WoS / 84. Percentyl według bazy Scopus$_{2025}$ / IF$_{2025}$ = 2,6 / MNiSW$_{2025}$ = 100 pkt
   Liczba cytowań: 1 (Google Scholar), 1 (Scopus), 1 (Web of Science)

* *autor korespondencyjny*

Łączna liczba punktów MNiSW$_{2025}$ = 340 pkt, a łączny IF$_{2025}$ = 8,8. Wskaźniki bibliometryczne wskazano na dzień publikacji artykułu naukowego, a liczbę cytowań na dzień 04.05.2025 r.

Streszczenie

Upłynnienie osadu to proces, w którym wskutek nagłego wzrostu ciśnienia porowego w nawodnionych osadach nieskonsolidowanych dochodzi do chwilowej utraty kontaktów międzyziarnowych. W efekcie tego, osad zaczyna zachowywać się jak ciecz, co prowadzi do jego mobilizacji i powstania charakterystycznych struktur deformacyjnych. Zjawisko to odgrywa istotną rolę zarówno we współczesnych procesach sedymentacyjnych, jak i w interpretacji dawnych zdarzeń naturalnych, takich jak trzęsienia ziemi.

Celem rozprawy było zbadanie warunków sprzyjających upłynnieniu osadu oraz określenie, czy i w jakim stopniu może ono wystąpić nawet przy słabszych wstrząsach sejsmicznych, niż dotychczas uznawane za krytyczne (powyżej magnitudy 4,2). Przeprowadzone badania objęły zarówno dokumentację terenową struktur deformacyjnych, jak i kontrolowane doświadczenia laboratoryjne. Próbki osadów poddano analizie teksturalnej i statystycznej, a ich podatność na upłynnienie była testowana w warunkach symulowanych wstrząsów sejsmicznych. Doświadczenia przeprowadzono w zróżnicowanych warunkach chemicznych, m.in. z zastosowaniem wody o różnym stopniu mineralizacji oraz z dodatkiem związków żelaza.

Wyniki pokazały, że szczególnie istotną rolę w procesie upłynnienia odgrywa frakcja pylasta – jej wysoka zawartość sprzyja mobilizacji osadu, nawet przy niskiej zawartości iłu i niewielkim udziale piasku. Co więcej, wykazano, że upłynnienie może być inicjowane już przy magnitudzie M~3,5, czyli niższej niż dotychczas zakładano.

Nowym i istotnym elementem badań była również analiza mikroskopowa, która ujawniła obecność mikropęknięć i śladów korozji na ziarnach kwarcu, a także, co szczególnie interesujące, osadzania się złota w szczelinach powstałych w wyniku wstrząsu. Sugeruje to, że drgania sejsmiczne mogą inicjować mikroobieg cieczy porowej, sprzyjając mobilizacji metali i ich wtórnej krystalizacji. Tego typu zapis może stanowić trwały ślad w strukturze mineralnej osadu, otwierając nowe perspektywy dla badań paleosejsmologicznych.

Rozprawa doktorska ukazuje, że proces upłynnienia osadu jest znacznie bardziej złożony i wieloczynnikowy, niż dotąd sugerowano. Proces ten obejmuje nie tylko mechaniczne właściwości osadu i siłę drgań, lecz także jego teksturę, stan nawodnienia oraz warunki chemiczne. Wyniki badań wnoszą nową jakość do rozpoznawania sejsmogenicznych struktur deformacyjnych i mogą znaleźć zastosowanie zarówno w rekonstrukcjach zdarzeń sejsmicznych, jak i w geologii inżynierskiej. Odkrycia te mogą mieć istotne znaczenie dla aktualizacji map zagrożeń sejsmicznych.

Abstract

Sediment liquefaction is a process in which, as a result of a sudden increase in pore pressure within water-saturated, unconsolidated sediments, intergranular contacts are temporarily lost. As a consequence, the sediment begins to behave like a fluid, leading to its mobilization and the formation of characteristic deformation structures. This phenomenon plays a significant role both in modern sedimentary processes and in the interpretation of past natural events, such as earthquakes.

The aim of this dissertation was to investigate the conditions that promote sediment liquefaction and to determine whether it can occur under weaker seismic shocks than previously considered critical (i.e., those exceeding magnitude 4.2). The research included both field documentation of deformation structures and controlled laboratory experiments. Sediment samples were subjected to textural and statistical analyses, and their susceptibility to liquefaction was tested under simulated seismic shock conditions. The experiments were conducted in varied chemical environments, including the use of water with different degrees of mineralization and the addition of iron compounds.

The results showed that the silt fraction plays a particularly important role in the liquefaction process, its high content promotes sediment mobilization, even when clay content is low and sand is present only in small amounts. Furthermore, it was demonstrated that liquefaction can be triggered at magnitudes as low as M~3.5, which is below the threshold previously assumed in the literature.

A novel and important aspect of the research was also the microscopic analysis, which revealed the presence of microcracks and signs of chemical corrosion in quartz grains, as well as, most notably, the occurrence of gold precipitated in fractures formed during the shock. This suggests that seismic vibrations may initiate a micro-circulation of pore fluids enriched in chemical elements, promoting the mobilization of metals and their secondary crystallization. Such a record may constitute a durable geochemical signal preserved in the mineral structure of the sediment, opening new perspectives in paleoseismological studies.

This doctoral dissertation demonstrates that the liquefaction process is far more complex and multi-factorial than previously suggested. It involves not only the mechanical properties of sediments and the intensity of seismic vibrations but also textural parameters, water saturation, and chemical conditions. The results of the study contribute new insights into the recognition of seismogenic deformation structures and may find application in the reconstruction of seismic events as well as in engineering geology and geohazard assessment.

1. Wprowadzenie

Procesy geologiczne mogą prowadzić do tymczasowych lub trwałych zmian właściwości osadów nieskonsolidowanych. W przebiegu tych procesów często dochodzi do wzrostu ciśnienia porowego, co skutkuje utratą kontaktów międzyziarnowych i mobilizacją osadu (Seed, 1979; Maltman i Bolton, 2003; Rensbergen i in., 2003). Mobilizacja ta następuje wtedy, gdy siły inicjujące ruch ziaren przekraczają siły wewnętrzne mogące im przeciwdziałać (Obermeier, 1996). Wyróżnia się kilka sposobów mobilizacji ziaren w osadzie: przesiąkanie, tiksotropię, upłynnienie oraz uwodnienie. W niniejszej rozprawie szczególną uwagę poświęcono procesom upłynnienia oraz uwodnienia, które stanowią najczęstsze i najlepiej udokumentowane mechanizmy mobilizacji osadów nieskonsolidowanych w odpowiedzi na dynamiczne obciążenia, w tym przede wszystkim na wstrząsy sejsmiczne.

Upłynnienie (ang. *liquefaction*) definiowane jest jako przejściowa utrata wytrzymałości osadu na ścinanie (Owen i Moretti, 2011; Brandes i Winsemann, 2013; Wahyudi i in., 2013). Zjawisko to zachodzi, gdy ziarna w osadzie tracą spójność, a masa osadu przekształca się w plastyczną zawiesinę wskutek reorganizacji ziaren, obciążenia przez nadległe warstwy osadu lub gwałtownego wzrostu ciśnienia porowego (Seed, 1979; Galli, 2000; Maltman i Bolton, 2003). Woda porowa powoduje, że osad nasycony wodą może zachowywać się jak plastyczna masa o zerowej lub bardzo niskiej granicy plastyczności (Van Loon i in., 2020). Upłynnienie może być całkowite (wszystkie kontakty ziarnowe zostają zerwane i struktura pierwotna ulega zniszczeniu) lub częściowe (część kontaktów zostaje zachowana, a struktura pierwotna pozostaje widoczna; Doe i Dott, 1980; Owen i Moretti, 2011).

Uwodnienie (ang. *fluidization*) to z kolei zjawisko występujące wtedy, gdy przepływ cieczy porowej, skierowany ku górze, jest na tyle silny, że znosi ciężar ziaren, zmniejszając ich efektywną wytrzymałość na ścinanie. W tym przypadku kontakty ziarnowe nie zostają całkowicie przerwane, a osad zachowuje pewien poziom spójności (Allen, 1977, 1982; Owen, 2003; Campbell, 2003; Davies i in., 2004). Uwodnienie umożliwia zawieszenie pojedynczych ziaren lub ich transport ku górze (Lowe, 1976; Brandes i Winsemann, 2013).

Upłynnienie (ang. *liquefaction*) oraz uwodnienie (ang. *fluidization*) to zjawiska, które w warunkach naturalnych często współwystępują i bywają łącznie określane terminem *liquidization* (Świątek i in., 2023). Niestety, w polskiej nomenklaturze geologicznej brakuje odpowiednika tego pojęcia, co sprawia, że oba procesy są często traktowane zbiorczo i opisywane jako stan upłynnienia (ang. *liquefaction*) w sensie ogólnym. Na potrzeby niniejszej pracy przyjęto więc termin upłynnienie jako stan obejmujący zarówno upłynnienie, jak i uwodnienie, co jest zabiegiem typowym, stosowanym w wielu pracach naukowych.

Czas trwania naturalnego zjawiska upłynnienia uzależniony jest od wielkości ziaren oraz miąższości deformowanej warstwy, a także czasu trwania sił go inicjujących i zgodnie z szacunkami nie przekracza kilkunastu sekund (Allen, 1982; Owen, 1996). Po zakończeniu procesu, kontakty międzyziarnowe są przywracane (Campbell, 2003) i powstają zróżnicowane struktury deformacyjne w literaturze anglojęzycznej znane jako *soft-sediment deformation structures* (SSDS).

Struktury deformacyjne, powstałe w efekcie upłynnienia osadów, stanowią jedne z najważniejszych sedymentologicznych dowodów dynamicznych przekształceń środowisk geologicznych (Van Loon, 2009). Powstają one w wyniku utraty spójności (kohezji) mechanicznej osadu, spowodowanej gwałtownym wzrostem ciśnienia porowego i przejściowym upłynnieniem osadu nieskonsolidowanego, takiego jak np. piasek czy pył. Wśród najczęściej rozpoznawanych typów SSDS wyróżnić można: (1) struktury obciążeniowe (ang. *load structures*), takie jak pogrązy (ang. *load casts*) i pseudonodule (ang. *pseudonodules*); (2) struktury płomieniowe (ang. *flame structures*), (3) struktury iniekcyjne (ang. *injection structures*), czyli dajki i wulkany klastyczne (ang. *clastic dykes, siliclastic volcanoes*), a także (4) struktury typu piłek i poduszek (ang. *ball-and-pillow structures*) oraz (5) struktury konwolutne i fałdowe (ang. *convolute lamination and folded structure*) (ryc. 1; Lowe, 1976; Allen, 1982; Obermeier, 1996, 2009; Owen, 2003; Davies i in., 2004; Castilla i Audemard, 2007; Van Loon, 2009; Owen i Moretti, 2011; Brandes i Winsemann, 2013; Pisarska-Jamroży i in., 2019; Pisarska-Jamroży i Woźniak, 2019; Müller i in., 2020; Van Loon i in., 2020).

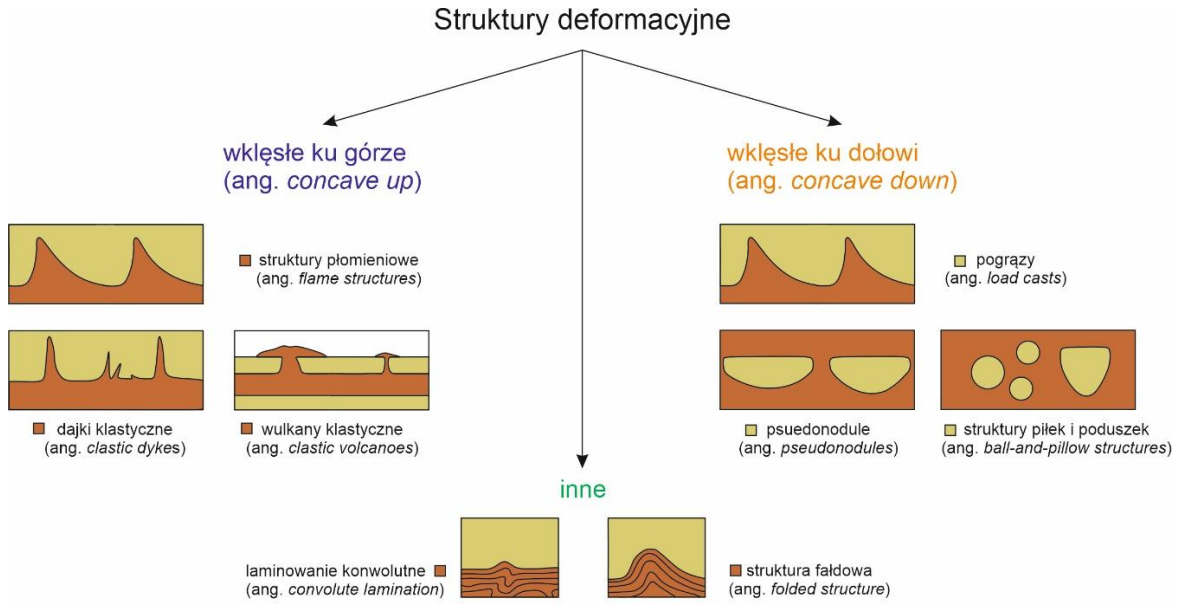

Ryc. 1. Uproszczony schemat podziału sejsmogenicznych struktur deformacyjnych wraz z przykładami.

Deformacje sejsmogeniczne mogą rozwijać się w efekcie: (a) przemieszczania osadów o różnej gęstości, (b) przepływu płynu porowego ku górze, (c) przeciążenia osadu prowadzącego do niestabilności gęstościowej, jak również (d) działania siły ścinającej wywołanej propagacją fal sejsmicznych (m.in. fal typu S; Allen, 1982; Owen, 2003; Van Loon, 2009, 2014; Van Loon i in., 2020). Typ powstałej struktury deformacyjnej zależy m.in. od stosunków gęstości sąsiadujących ze sobą osadów, stopnia ich nawodnienia, cech teksturalnych, szybkości wzrostu ciśnienia porowego w osadach oraz kierunku działania siły deformującej (Sims, 1975; Owen, 1985; Moretti i in., 2014). Struktury deformacyjne mogą być ograniczone do pojedynczej warstwy / laminy lub obejmować ich zestawy. Obecność SSDS, ich morfologia oraz rozmieszczenie są kluczowe dla identyfikacji i interpretacji zdarzeń sejsmicznych (Moretti i in., 1999; Owen i Moretti, 2011; Świątek i Pisarska-Jamroży, 2025). Warstwy osadów, które uległy deformacji w wyniku aktywności sejsmicznej, określane są mianem sejsmitów (ang. *seismites*). Termin ten po raz pierwszy wprowadził Seilacher (1969), opisując deformacje w formacji Monterey w Kalifornii jako rezultat jednorazowego, sejsmicznego zdarzenia. W kolejnych dekadach przeprowadzono szereg badań terenowych i kilkanaście eksperymentalnych, które potwierdziły, że trzęsienia ziemi mogą inicjować procesy upłynnienia oraz powstawania struktur typu SSDS o złożonej budowie (m.in. Nichols i in., 1994; Owen, 1996; Moretti i in., 1999).

Pomimo znacznego postępu w badaniach nad procesami upłynnienia osadów, jednym z najtrudniejszych wyzwań w interpretacji struktur deformacyjnych pozostaje rozpoznanie mechanizmu sprawczego (ang. *trigger mechanism*), który odpowiadał za ich powstanie. Współcześnie znanych jest kilkadziesiąt czynników powodujących deformacje – od procesów, takich jak fale sztormowe, tsunami, szybka i nagła sedymentacja, procesy glacjalne i peryglacjalne, aż po trzęsienia ziemi czy impakty meteorytów (Allen, 1982; Owen, 1996; Maltman i Bolton, 2003; He i in., 2018). Różne mechanizmy mogą prowadzić do powstania struktur o bardzo zbliżonej morfologii, co znacząco utrudnia ich jednoznaczną interpretację w zapisie geologicznym (Van Loon, 2009; Van Loon i in., 2020). Wiele struktur deformacyjnych, jak np. struktury płomieniowe, pseudonodule czy struktury typu piłek i poduszek, może powstawać zarówno w warunkach sejsmicznych (ang. *seismogenic*), jak i niezwiązanych z aktywnością sejsmiczną (ang. *nonseismogenic*), co prowadzi do znacznych trudności w ich interpretacji. Dodatkowo, wiele struktur deformacyjnych może powstawać w efekcie trwania kilku mechanizmów w tym samym czasie lub występujących krótko po sobie (por. Van Loon i in., 2020). Brak spójnych, uniwersalnych narzędzi rozpoznawczych może prowadzić do niepewności interpretacyjnych i potencjalnych błędów w rekonstrukcjach paleogeograficznych

oraz paleotektonicznych. W tym kontekście, niniejsza rozprawa doktorska stanowi próbę zintegrowania podejścia terenowego oraz eksperymentalnego, w celu zaproponowania nowych kryteriów diagnostycznych sejsmogenicznych struktur deformacyjnych, a także warunków, które pomogą je odróżnić od deformacji o innej genezie.

Znaczne trudności w interpretacji budzi kwestia minimalnej magnitudy wstrząsów sejsmicznych niezbędnych do inicjacji upłynnienia. W literaturze najczęściej przyjmuje się wartości progowe w zakresie M 4,2–5,0 (Zhong i in., 2022), jednak dane terenowe sugerują, że proces ten może być inicjowany również przy słabszych wstrząsach, zwłaszcza w odpowiednio uwodnionych i drobnoziarnistych osadach (por. McCalpin i in., 2023).

Początki badań eksperymentalnych sięgają drugiej połowy XX wieku (Stewart, 1958; Gill i Kuenen, 1958; Selley, 1969), jednak przełomowe znaczenie miały prace Owena (1996), który wykazał, że w warunkach laboratoryjnych możliwe jest odtworzenie sejsmogenicznych struktur deformacyjnych, analogicznych do tych obserwowanych w zapisie geologicznym, jak: struktury fałdowe czy płomieniowe, dajki i wulkany klastyczne. Kolejne eksperymenty, m.in. Moretti'ego i in. (1999), z wykorzystaniem cyfrowych stołów do wstrząsów (ang. *shaking table*), pozwoliły symulować fale sejsmiczne i badać ich wpływ na osady piaszczyste i pylaste, wskazując na możliwość deformacji przy zróżnicowanych progach magnitudy, różnych parametrach sejsmologicznych i poziomach nawodnienia. Z kolei Owen i Moretti (2011) podkreślili, że wywołanie deformacji jest wynikiem złożonej interakcji między intensywnością drgań, teksturą osadu a stopniem jego nawodnienia. Eksperymenty przeprowadzane w kolejnych latach przez m.in. Liang'a i in., 2018; Zhong'a i in., 2022; Cui'iego i in., 2022 oraz Liang'a i in., (2024), dostarczyły cennych wskazówek do identyfikacji struktur sejsmogenicznych, umożliwiając również testowanie modeli rekonstrukcji intensywności trzęsień ziemi na podstawie zapisu deformacji w osadach.

Proces sejsmogenicznego upłynnienia osadów jest zjawiskiem złożonym, którego przebieg i zapis są kontrolowane przez trzy główne grupy czynników: (1) parametry sejsmologiczne, (2) właściwości osadu oraz (3) warunki geologiczne (Tang i in., 2016; Van Loon i in., 2016). Do pierwszej grupy należą cechy samego wstrząsu sejsmicznego, takie jak: magnituda (Galli, 2000), czas trwania wstrząsu (Youd i Idriss, 2011), częstotliwość i kierunek propagacji fali (Zhang i in., 1990), a także odległość od epicentrum (Papadopoulos i Lefkopoulos, 1993; Obermeier, 1996). Drugą grupę stanowią właściwości osadów, przede wszystkim cechy teksturalne, takie jak uziarnienie i kształt ziaren (Arias, 1970; Seed, 1979), zawartość frakcji ilastej (Chang i Hong., 2008; Monkul, 2012; Park i Kim, 2013), stopień konsolidacji, gęstość właściwa i względna, nasycenie wodą (Owen i Moretti, 2011) oraz warunki drenażowe

(Umehara, 1985). Trzecia grupa obejmuje uwarunkowania geologiczne, w tym miąższość i głębokość warstw osadów (Einsele i in., 1996), poziom wód gruntowych (Hannich i in., 2007), rzeźbę terenu, wiek osadu (Youd i Perkins, 1973) oraz historię jego naprężeń (Seed i in., 1964). Nadal jednak nieznany pozostaje wpływ składu chemicznego osadów, a w szczególności obecność i formy związków pierwiastków takich, jak Fe czy Mn w warstwach przypowierzchniowych, które mogą mieć znaczący wpływ na plastyczność, na potencjał redoks i ostateczny zapis deformacji osadu.

Fale sejsmiczne poruszają się z różną prędkością w zależności od gęstości ośrodka, przez które przechodzą, np. 400–1200 m/s w suchym piasku, 1500 m/s w wodzie. Ich propagacja powoduje nie tylko drgania ziaren, ale też zmiany energetyczne i zmiany potencjału oksydacyjno-redukcyjnego na poziomie atomowym (Bielański, 2002; 2004), co może prowadzić do przemian chemicznych w osadach np. mobilizacji i krystalizacji poszczególnych pierwiastków chemicznych jak Fe, Mn lub Au.

Badania prowadzone w ramach niniejszej pracy były, według mojej wiedzy, pierwszymi obejmującymi nie tylko wpływ parametrów teksturalnych, nawodnienia, magnitudy wstrząsów sejsmicznych, ale także udział i wpływ procesów oksydacyjno-redukcyjnych na wykształcenie i sposób zachowania (=zapisu) struktur deformacyjnych w osadach nieskonsolidowanych. Do tej pory nie brano pod uwagę, obecnych w osadach, związków chemicznych jako czynników wpływających na proces upłynnienia osadu. Niniejsze badania stanowiły próbę wypełnienia tej luki poznawczej oraz zaproponowanie nowego zintegrowanego podejścia doświadczalnego, w którym analizowane były równocześnie: siła dynamiczna (parametry wstrząsu sejsmicznego), cechy teksturalne osadu (udział frakcji osadu, stopień mineralizacji wody niezbędnej do nawodnienia osadu) oraz warunki geochemiczne (pH, potencjał redoks, obecność Fe i Au). Dzięki zastosowaniu symulacji sejsmicznych w warunkach kontrolowanych, możliwe stało się nie tylko określenie progów inicjujących deformacje, ale także identyfikacja potencjalnych wskaźników morfometrycznych charakterystycznych dla deformacji o genezie sejsmicznej.

Badania, prowadzone w ramach rozprawy doktorskiej, miały na celu udzielenie odpowiedzi m.in. na następujące pytania:

→ W jaki sposób wstrząsy sejsmiczne wpływają na nieskonsolidowane osady o różnych cechach teksturalnych?

→ Czy deformacje osadu mogą powstać przy niższej magnitudzie niż dotychczas uznawano?

→ Jakie struktury deformacyjne powstają w warunkach sejsmicznych w sekwencjach osadowych, ale ze zmienną miąższością?

→ Jaka jest rola poszczególnych frakcji granulometrycznych w rozwoju SSDS?

→ Jaki wpływ na deformacje mają pierwiastki i tworzące je związki chemiczne obecne w osadzie?

→ Czy i jak stopień mineralizacji wody wpływa na przebieg upłynnienia?

→ Jakie zmiany zachodzą w ziarnach kwarcu po przejściu fali sejsmicznej?

→ Czy i jak czas nawodnienia osadów wpływa na proces i zapis zjawiska upłynnienia?

→ Czy warunki oksydacyjno-redukujące wpływają na zapis procesu upłynnienia osadów?

2. Cele badań

Wyznaczono następujące szczegółowe cele badawcze:

1. **Określenie zależności pomiędzy teksturą osadu, w szczególności udziałem poszczególnych frakcji, a rozwojem struktur deformacyjnych powstałych w wyniku upłynnienia.** Obejmowało to analizę wpływu proporcji frakcji pylastej, piaszczystej i ilastej na rodzaj oraz stopień wykształcenia struktur deformacyjnych. Następnie wyodrębniono charakterystyczne cechy morfologiczne struktur deformacyjnych oraz cechy teksturalne, takie jak stopień wysortowania, średnia średnica ziarna, skośność i kurtoza. Na podstawie uzyskanych wyników opracowano model statystyczny umożliwiający przewidywanie typu deformacji w zależności od parametrów osadu. [A1 oraz A2]
2. **Zbadanie zależności między tworzeniem się struktur deformacyjnych, ich cechami teksturalnymi, udziałem wody oraz parametrami wstrząsów sejsmicznych, tj. magnituda, częstotliwość, czas trwania, miąższość osadów, rodzaj osadów i ich gęstość właściwa, wymiary struktur oraz lokalizacja względem całego układu.** Wskazano wpływ konkretnych wartości wybranych parametrów sejsmologicznych, takich jak magnituda (~3,5), częstotliwość (60 Hz) i czas trwania wstrząsu (15 s), na powstanie sejsmogenicznych struktur deformacyjnych. Przeanalizowano również zależności pomiędzy cechami sedymentologicznymi (np. teksturą osadów, miąższością) a działaniem sił zewnętrznych (falami sejsmicznymi) oraz oceniono ich wpływ na przebieg formowania się struktur deformacyjnych. Badania miały charakter zarówno jakościowy, jak i ilościowy. [A2]
3. **Określenie zależności między strukturami deformacyjnymi a właściwościami chemicznymi osadu (np. pH i Eh).** Sprawdzono, czy i w jaki sposób reakcje chemiczne wpływają na proces tworzenia się oraz zapis zmian w upłynnionym osadzie. [A3]
4. **Wskazanie metod umożliwiających rozróżnianie struktur deformacyjnych powstałych w wyniku upłynnienia wywołanego sejsmicznie od tych, które powstały w**

wyniku innych mechanizmów, takich jak obciążenie osadem, działalność sztormów czy erupcje wulkaniczne. Szczególną uwagę poświęcono możliwościom wykorzystania mikromorfologii i cech teksturalnych ziaren kwarcu oraz parametrom morfometrycznym poszczególnych struktur deformacyjnych. [A2 oraz A3]

5. **Określenie wpływu warunków redukcyjnych oraz czasu zapisu zmian w upłynnionym osadzie.** Przeanalizowano wpływ dodatku związków żelaza na tworzenie się struktur deformacyjnych w warunkach ograniczonego dostępu światła i tlenu oraz w dłuższych przedziałach czasowych. [A3]

3. Materiał i metody badań

W niniejszej rozprawie zastosowano podejście doświadczalne, które integruje i wzajemnie uzupełnia zarówno badania terenowe [A1], jak i laboratoryjne [A2 oraz A3]. Taka dwutorowa metodologia wynika z potrzeby jednoczesnego zrozumienia naturalnej zmienności struktur deformacyjnych w rozpoznanych sekwencjach osadowych oraz ich odtworzenia i kontroli w warunkach laboratoryjnych. Badania terenowe dostarczyły nie tylko danych empirycznych dotyczących uziarnienia, morfologii i rozmieszczenia struktur deformacyjnych, lecz także umożliwiły rozpoznanie szerszego kontekstu środowiskowego i statygraficznego. Z kolei badania laboratoryjne pozwoliły odtworzyć wybrane czynniki oraz warunki fizyczne i chemiczne prowadzące do upłynnienia, kontrolować parametry wejściowe (m.in. skład granulometryczny, stopień nasycenia wodą, intensywność sił deformujących, obecność związków żelaza czy stopień mineralizacji wód), analizować powtarzalność obserwowanych struktur, a przede wszystkim uzyskać informacje o roli tych parametrów w procesie upłynnienia i deformacji osadu.

3.1. Materiał badawczy

3.1.1. Badania terenowe

Materiał badawczy, wykorzystany w pierwszym etapie pracy, stanowiły 144 próby pobrane ze struktur deformacyjnych powstałych w efekcie upłynnienia osadu [A1]. Próby zostały pobrane podczas realizacji projektu GREBAL z ośmiu stanowisk zlokalizowanych w północno-wschodnich Niemczech, a także na Litwie i Łotwie (ryc. 2; Nartišs i in., 2018; Pisarska-Jamroży i in., 2018, 2019a, 2019b; Woronko i in., 2018; Belzyt i in., 2021; Woźniak i in., 2021).

Obszar, na którym znajdują się analizowane stanowiska badawcze, charakteryzują się złożoną historią geologiczną związaną z działalnością lądolodu fennoskandzkiego oraz późniejszymi

procesami izostatycznymi. Zidentyfikowane struktury deformacyjne, obecne na tym obszarze, powstały w osadach deponowanych w środowiskach glacilimnicznych, glacifluwialnych, lagunowych oraz płytkomorskich, a ich rozmieszczenie i budowa litologiczna odzwierciedlają zmienne warunki sedymentacji w trakcie i po ustąpieniu lądolodu (Nartišs i in., 2018; Pisarska-Jamroży i in., 2018, 2019a, 2019b; Woronko i in., 2018; Woźniak i in., 2021). Szczególne znaczenie mogło mieć położenie analizowanych stanowisk w strefach przejściowych między lądem a wodą, charakteryzujących się zmiennym poziomem wód, lokalnymi różnicami batymetrycznymi oraz obecnością warstw o zróżnicowanej przepuszczalności. Takie warunki sprzyjają rozwojowi procesów prowadzących do upłynnienia osadów i powstawania struktur deformacyjnych (por. Seed i Idriss, 1983).

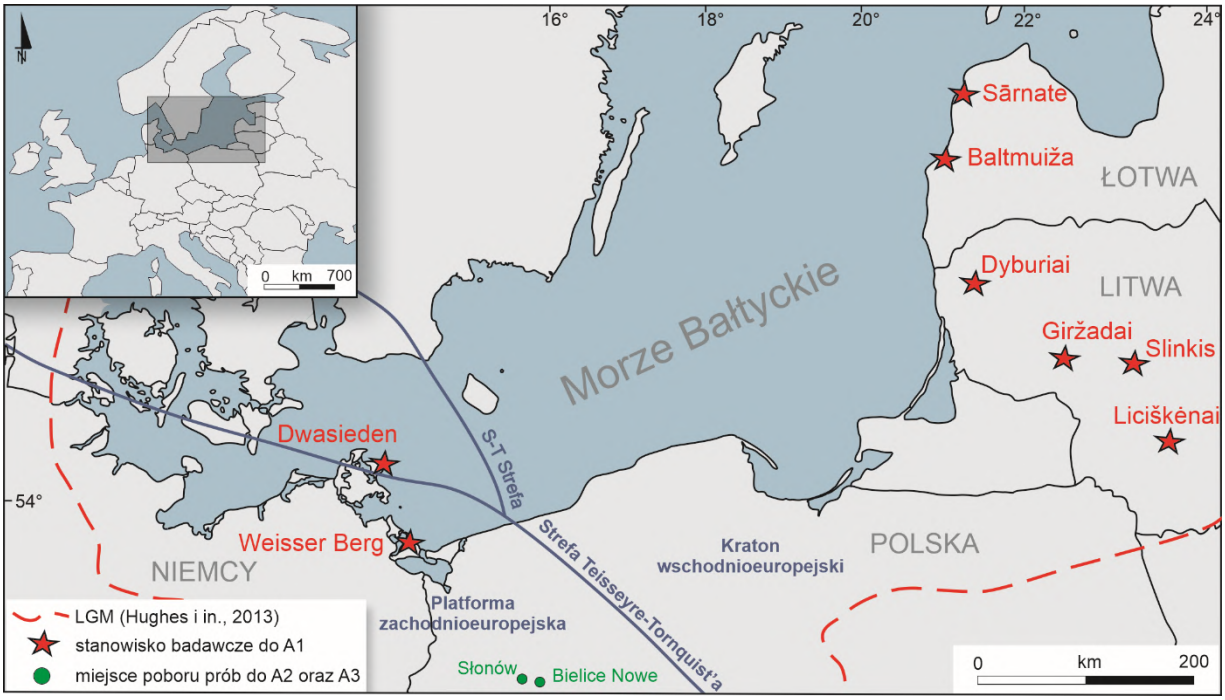

Ryc. 2. Lokalizacja stanowisk badawczych. Strefa S-T – strefa uskokowa Sorgenfrei-Tornquist. LGM – maksymalny zasięg lądolodu fennoskandzkiego podczas ostatniego zlodowacenia. (Świątek i in., 2023; zmodyfikowane).

3.1.2. Badania laboratoryjne

W badaniach laboratoryjnych wykorzystano dwa główne typy osadów nieskonsolidowanych: pył (o udziale frakcji 2–63 μm wynoszącym 93%) oraz drobnoziarnisty piasek (o udziale frakcji 125–250 μm wynoszącym 56%). Osady te zostały pobrane z naturalnych odsłonięć zlokalizowanych w północno-zachodniej Polsce (ryc. 2, 3A).

Symulację sejsmogenicznego upłynnienia osadu oraz dalszą analizę przeprowadzono w cylindrach z przezroczystego pleksi o wysokości 10 cm i średnicy 10 cm (ryc. 3B) [A2]. Łącznie przygotowano pięć wariantów różniących się litologią, z których każdy powtórzono pięciokrotnie.

Symulację rozszerzono następnie o badanie wpływu i zależności związków chemicznych [A3]. W celu stworzenia różnych warunków geochemicznych, osady nasycano trzema rodzajami wody: destylowaną, średniozmineralizowaną oraz wysokozmineralizowaną (ryc. 3C). Wody mineralne stanowiły komercyjnie dostępne produkty, różniące się składem jonowym. Dodatkowo, aby odtworzyć obecność żelaza w środowisku osadowym, do próbek dodano siarczan żelaza(II) ($FeSO_4$) odpowiadający naturalnej zawartości żelaza na poziomie 0,5–1%. Zabieg ten wynikał z wcześniejszych obserwacji terenowych, podczas których zidentyfikowano związki żelaza występujące w upłynnionym osadzie (Świątek i in., 2025). W tym eksperymencie [A3] przygotowane próbki umieszczono w cylindrach z pleksi o wysokości 10 cm i średnicy 15 cm (ryc. 3C), a następnie inkubowano je w warunkach ograniczonego dostępu światła w celu stworzenia warunków redukcyjne [A3]. Łącznie przygotowano 36 próbek, które badano w sześciu punktach czasowych: w dniu rozpoczęcia eksperymentu (dzień zero), po upływie 1,5 miesiąca, 3 miesięcy, 6 miesięcy, 9 miesięcy oraz po 12 miesiącach (ryc. 3D).

3.2. Metody badawcze i metodyka

3.2.1. Analiza statystyczna prób osadu pobranego z terenu

W każdej próbie zidentyfikowano i sklasyfikowano występujące struktury deformacyjne na podstawie ich morfologii i orientacji. Wyróżniono struktury deformacyjne wygięte ku dołowi (ang. *concave down;* np. *pseudonodules*, *load casts*) oraz struktury wygięte ku górze (ang. *concave up*; np. *flame structures*, *clastic dykes*, *injection features*). Dodatkowo struktury przyporządkowano do jednej z czterech grup procesowych: AU (*active up*), AD (*active down*), PU (*passive up*), PD (*passive down*), zgodnie z mechanizmem ich powstawania i relacją względem sąsiednich warstw (ryc. 2 w artykule Świątek i in., 2023). Dla wszystkich próbek wykonano analizy granulometryczne z wykorzystaniem dyfrakcji laserowej (Malvern Mastersizer 2000), a następnie przetworzono dane w programie GRADISTAT, uzyskując podstawowe parametry statystyczne uziarnienia, takie jak średnia średnica ziarna, stopień wysortowania, skośność i kurtoza. Zebrane dane posłużyły do przeprowadzenia analiz statystycznych (m.in. testu t-Studenta, Manna-Whitneya oraz F-Snedecora), których celem było określenie istotnych statystycznie różnic w uziarnieniu poszczególnych typów struktur

deformacyjnych oraz wskazanie teksturalnych cech predysponujących osady do rozwoju określonych struktur deformacyjnych.

3.2.2. Badania laboratoryjne

Część laboratoryjna rozprawy obejmowała dwa uzupełniające się etapy badań eksperymentalnych, których celem było odtworzenie warunków kontrolowanych prowadzących do powstawania struktur deformacyjnych w efecie upłynnienia [A2 oraz A3]. Pierwszy etap [A2] polegał na przeprowadzeniu serii eksperymentów w skali makroskopowej, w których modelowano deformację nieskonsolidowanych osadów pod wpływem drgań o charakterystyce zbliżonej do trzęsień ziemi o niskiej magnitudzie [A2]. Do badań wykorzystano próbki osadów o znanym uziarnieniu (pył, piasek drobnoziarnisty, piasek gruboziarnisty), umieszczone w przezroczystych cylindrach i poddawane działaniu drgań generowanych przez urządzenie imitujące wstrząsy sejsmiczne (Analysette 3 SPARTAN). Parametry drgań odpowiadały w przybliżeniu sile wstrząsu o magnitudzie ~3,5 (ryc. 3B). W trakcie eksperymentów rejestrowano rozwój struktur deformacyjnych, a po ich zakończeniu wykonano szczegółową dokumentację fotograficzną oraz pomiary morfometryczne powstałych struktur deformacyjnych (wysokość, szerokość, kąt nachylenia struktur, odległość między nimi).

Drugi etap obejmował analizy mikroskalowe, których celem było zidentyfikowanie wpływu procesów mechanicznych i chemicznych, towarzyszących upłynnieniu, na ziarna kwarcu [A3]. Do eksperymentów zastosowano drobnoziarnisty piasek kwarcowy nawodniony trzema typami wód: destylowaną, średnio- i wysokozmineralizowaną, wzbogacony o siarczan żelaza (II) o stężeniu ok. 0,5-1% (ryc. 3C). Przed i po każdej symulacji sejsmicznej dokonywano pomiarów pH i Eh, a po zakończeniu każdego etapu wykonano cienkie przekroje osadów i przeprowadzono szczegółową analizę mikromorfologiczną przy użyciu skaningowego mikroskopu elektronowego (SEM) z zastosowaniem spektroskopii dyspersji rentgenowskiej (EDX). Na podstawie cech teksturalnych porównano ziarna kwarcu z osadów sejsmogenicznych struktur deformacyjnych rozpoznanych w warunkach naturalnych, z osadów poddanych symulacji sejsmogenicznego upłynnienia, a także z próbek niepoddanych wstrząsom. Zidentyfikowano liczne mikrotekstury, takie jak mikropęknięcia, ślady korozji brzegów ziaren, powierzchniowe rozwarstwienia oraz wtórne produkty (np. złoto, tlenki żelaza). Na podstawie cech mikroteksturalnych i właściwości chemicznych podjęto próbę określenia wpływu wstrząsów sejsmicznych, warunków geochemicznych oraz czasu nawodnienia osadu na obecność i stopień spękań ziaren kwarcu.

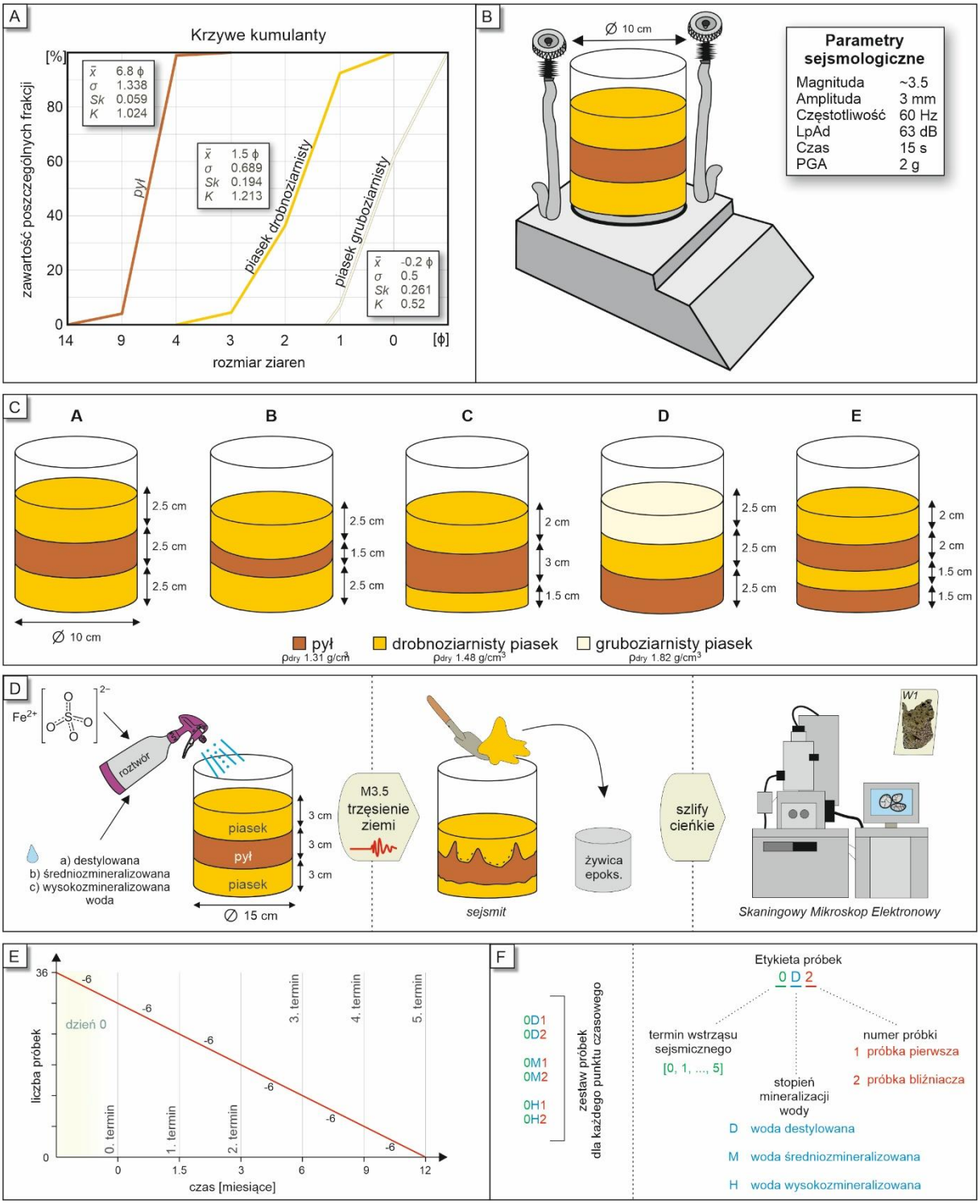

Ryc. 3. Kluczowe elementy eksperymentalnych badań laboratoryjnych dotyczących symulacji upłynnienia osadów (Świątek i Pisarska-Jamroży, 2025; Świątek i in., 2025; zmodyfikowane): A – skład granulometryczny wykorzystanych osadów [A2 oraz A3], B – parametry urządzenia imitującego wstrząsy sejsmiczne [A2 oraz A3], C – sukcesje osadów poddanych symulacji [A2], D – schemat doświadczenia inkubacyjnego [A3], E – schemat symulacji upłynnienia w doświadczeniu inkubacyjnym [A3], F – schemat analizowanych próbek [A3].

4. Zarys treści publikacji wchodzących w skład rozprawy doktorskiej

[A1] **Świątek, S.***, Belzyt S., Pisarska-Jamroży, M., Woronko, B. 2023. Sedimentary records of liquefaction: implications from field studies. *Journal of Geophysical Research: Earth Surface* 128, e2023JF007152. https://doi.org/10.1029/2023JF007152

W publikacji opisano zależność między teksturą osadu a występowaniem struktur deformacyjnych powstałych w wyniku upłynnienia. Badania przeprowadzono na 144 próbkach osadów zidentyfikowanych jako zdeformowane, pobranych z ośmiu stanowisk terenowych zlokalizowanych w północno-wschodnich Niemczech, na Litwie i Łotwie (ryc. 2). Osady te reprezentują różnorodne środowiska sedymentacyjne, w tym płytkomorskie, rzeczne, lagunowe oraz glacilimniczne. Zidentyfikowane struktury deformacyjne podzielono na dwie grupy (ryc. 1): (1) formy wklęsłe ku dołowi (ang. *concave down*, np. *pseudonodules, load casts*) oraz (2) formy wklęsłe ku górze (ang. *concave up*, np. *flame structures, clastic dykes, injection structures*). Dodatkowo każdą ze struktur deformacyjnych przyporządkowano do jednej z czterech grup procesowych: AU (*active up*), AD (*active down*), PU (*passive up*), PD (*passive down*).

Próbki poddano analizie granulometrycznej z zastosowaniem dyfrakcji laserowej (Malvern Mastersizer 2000), a dane przetworzono w programie GRADISTAT, uzyskując podstawowe parametry statystyczne uziarnienia: średnią średnicę ziarna, wskaźnik wysortowania, skośność i kurtozę. Analizy statystyczne (testy t-Studenta, Manna-Whitneya, Snedecora) wykazały, że osady towarzyszące struktury *concave up* różnią się istotnie od tych, w których występują struktury *concave down* – zarówno pod względem granulometrii, jak i parametrów statystycznych. Stwierdzono, że struktury typu *concave up* występują głównie w osadach drobnoziarnistych, słabo wysortowanych, z wysoką zawartością frakcji pylastej i ilastej, podczas gdy struktury *concave down* rozwijają się w osadach piaszczystych, lepiej wysortowanych. Dodatkowo wyznaczono zależności między udziałem poszczególnych frakcji osadu a podstawowymi parametrami statystycznymi.

Integralną częścią pracy było przeprowadzenie modelowania statystycznego, które pozwoliło wskazać wartości progowych oraz kombinacje cech teksturalnych istotnie wpływających na rozwój poszczególnych typów struktur. Opracowany model statystyczny może pełnić funkcję narzędzia prognostycznego, umożliwiającego ocenę potencjału deformacyjnego osadu oraz przewidywanie typu struktur, które mogą się rozwinąć w danej sekwencji osadowej. Wyniki badań stanowią istotny wkład w zrozumienie zależności między teksturą osadu a jego podatnością na upłynnienie oraz rozwój określonych struktur deformacyjnych.

[A2] **Świątek, S.***, Pisarska-Jamroży, M. 2025. Seismogenic liquefaction with M~3.5 in fine-grained sediments: An experimental approach. *Sedimentary Geology* 478, 106833. https://doi.org/10.1016/j.sedgeo.2025.106833

Artykuł prezentuje oryginalne i nowatorskie podejście do eksperymentalnych badań laboratoryjnych nad deformacjami osadów wywołanymi przez trzęsienia ziemi o niskiej magnitudzie (blisko 3,5). Celem pracy było sprawdzenie, czy wstrząsy o tak niskiej magnitudzie mogą inicjować procesy upłynnienia i prowadzić do rozwoju struktur deformacyjnych w nasyconych wodą osadach drobnoziarnistych. W badaniach wykorzystano trzy rodzaje osadów (pył, piasek drobno- i gruboziarnisty), które zestawiono w pięć różnych sekwencji warstw (różniących się miąższością warstw, liczbą warstw i układem litologicznym) i poddano działaniu drgań generowanych przez urządzenie symulujące fale sejsmiczne (Analysette 3 SPARTAN). Drgania miały ściśle określone parametry: magnitudę ~3,5, częstotliwość 60 Hz, amplitudę drgań 3 mm i czas trwania 15 sekund.

Podczas symulacji oraz po jej zakończeniu każdą próbkę szczegółowo analizowano pod kątem przebiegu procesu upłynnienia osadu, oraz jego zapisu w postaci struktur deformacyjnych. Zidentyfikowano sześć głównych typów struktur: w grupie struktur wklęsłych ku górze wyróżniono struktury płomieniowe, struktury iniekcyjne (pylaste i piaszczyste) oraz wulkany klastyczne, natomiast w grupie struktur wklęsłych ku dołowi – struktury obciążeniowe, takie jak pogrązy i pseudonodule. Przeprowadzono analizy morfometryczne, obejmujące pomiary wysokości, szerokości oraz obliczenia współczynników kształtu. Wyniki wskazały wyraźne korelacje między szerokością a wysokością struktur, zwłaszcza dla struktur płomieniowych, pogrązów i wulkanów klastycznych. Eksperyment potwierdził, że nawet przy niewielkiej magnitudzie możliwe jest upłynnienie osadu oraz powstawanie struktur deformacyjnych.

W dalszej części pracy wyniki eksperymentów porównano z wynikami terenowymi, wskazując na silne analogie między strukturami powstałymi w warunkach laboratoryjnych a tymi obserwowanymi w naturalnych odsłonięciach. Dyskusja dotyczyła również kryteriów rozpoznawania struktur pochodzenia sejsmicznego oraz znaczenia morfometrii jako narzędzia potencjalnie pomocnego w rozróżnianiu liczby zdarzeń deformujących. Wnioski płynące z pracy mogą znaleźć zastosowanie nie tylko w rekonstrukcji przeszłych wstrząsów, lecz także w ocenie zagrożeń związanych z upłynnieniem osadów w regionach dotąd uznawanych za obszary o niskiej aktywności sejsmicznej.

[A3] **Świątek, S.***, Lewińska, K., Pisarska-Jamroży, M., Günter, C. 2025. An application of quartz grain analyses in earthquake-induced (palaeo)liquefaction studies. *Journal of Structural Geology* 193, 105357. https://doi.org/10.1016/j.jsg.2025.105357

Artykuł przedstawia innowacyjne podejście do analizy struktur deformacyjnych powstałych w wyniku sejsmogenicznego upłynnienia osadów, koncentrując się na mikroteksturalnych cechach ziaren kwarcu. Celem badania było ustalenie, czy mikromorfologia ziaren kwarcu oraz cechy współistniejące (np. nagromadzenie złota, koncentracja pierwiastków) mogą służyć jako wskaźnik potwierdzające deformacje sejsmogeniczne, a także czy zmiany te mogą być wykorzystane do rekonstrukcji dawnych zdarzeń sejsmicznych. Eksperyment przeprowadzono w kontrolowanych warunkach laboratoryjnych, wykorzystując pył i piasek drobnoziarnisty nasycone trzema typami wód o różnym stopniu mineralizacji. Przed i po każdym wstrząsie wykonano pomiary pH i Eh. Próbki poddano działaniu symulowanego wstrząsu sejsmicznego (M~3,5), a następnie analizowano mikroskopowo płytki cienkie przy użyciu skaningowego mikroskopu elektronowego (SEM), skupiając się na cechach ziaren kwarcu.

W artykule zidentyfikowano szereg cech mikrostrukturalnych, od subtelnych pęknięć i korozji krawędzi po zaawansowaną fragmentację ziaren. Stwierdzono, że stopień mineralizacji wody oraz czas ekspozycji istotnie wpływały na intensywność zmian. W próbkach nasyconych wodą wysokozmineralizowaną zaobserwowano większy zakres uszkodzeń mechanicznych i chemicznych. Dodatkowo wykazano obecność złota w mikroszczelinach i na powierzchni ziaren, co sugeruje, że aktywność sejsmiczna może odgrywać rolę w mobilizacji i redepozycji pierwiastków metalicznych w środowisku sedymentacyjnym. Oprócz udziału sił mechanicznych szczegółowo opisano wpływ warunków geochemicznych (pH, Eh, obecność kwasu fluorowodorowego i kwasu ortokrzemowego) na stopień korozji ziaren kwarcu oraz potencjał tworzenia nowych struktur mineralnych.

W części dyskusyjnej zaproponowano siedmioetapowy „cykl sejsmiczny ziarna kwarcu” – od inicjalnego pęknięcia poprzez fragmentację, agregację i rekrystalizację, aż po ponowne wejście ziarna w obieg sejsmicznej deformacji. Podkreślono, że połączenie sił mechanicznych i chemicznych prowadzi do złożonej, często wielofazowej transformacji ziaren, która może być rejestrowana w osadzie jako wskaźnik aktywności sejsmicznej. Wnioski z pracy sugerują, że mikromorfologia kwarcu, w połączeniu z analizą chemiczną i teksturalną, może stanowić obiecujące narzędzie do identyfikacji i interpretacji struktur deformacyjnych pochodzenia sejsmicznego, a także do oceny ryzyka związanego z upłynnieniem osadów.

5. Dyskusja

5.1. Cechy osadu podatnego na upłynnienie

Dotychczasowe badania nad procesami upłynnienia osadów koncentrowały się głównie na określeniu krytycznego udziału frakcji ilastej jako parametru decydującego o możliwości wystąpienia upłynnienia i deformacji (Wang, 1979; Zhou, 1981; Figueroa i in., 1995; Tuttle i in., 1990; Andrews i Martin, 2000). Rola frakcji pylastej była natomiast w dużej mierze pomijana lub marginalizowana. Wyniki prezentowane w niniejszej rozprawie jednoznacznie wskazują jednak, że to właśnie frakcja pylasta (ang. *silt*) odgrywa kluczową rolę w inicjowaniu deformacji osadów, szczególnie w przypadku struktur iniekcyjnych.

Dla struktur wklęsłych ku górze (np. struktur płomieniowych, struktur iniekcyjnych) mediana udziału frakcji pylastej wynosi aż 73%, podczas gdy dla struktur wklęsłych ku dołowi (pogrązy, pseudonodule) jedynie 20%. Tak znacząca różnica została potwierdzona zarówno przez wcześniejsze badania terenowe (Van Loon i Pisarska-Jamroży, 2014; Van Loon i in., 2016; Pisarska-Jamroży i in., 2018, 2019a, 2019b, 2022; Belzyt i in., 2021; Woźniak i in., 2021), jak i eksperymenty laboratoryjne (Othman i in., 2019; Othman i Marto, 2019) oraz modele matematyczne (Bronikowska i in., 2021). Wyniki badań zaprezentowane w artykule [A1] wyraźnie pokazują, że to właśnie mobilność frakcji pylastej w warunkach wysokiego nasycenia wodą odgrywa decydującą rolę w inicjowaniu deformacji oraz ułatwia wtórną mobilizację ziaren piasku [A1].

Wbrew wnioskom Obermeiera (1996), który twierdził, że dodatek iłu i pyłu do piasków obniża podatność osadów na upłynnienie, przedstawione wyniki dowodzą, że **osady pylaste są wyjątkowo podatne na mobilizację**, podczas gdy osady z wyższym udziałem frakcji ilastej ulegają deformacji jedynie wtedy, gdy udział tej frakcji nie przekracza wartości granicznej (maks. 14%; Świątek i in., 2023).

5.2. „Siła" trzęsienia ziemi niezbędna do zainicjowania upłynnienia osadu

Eksperymenty przeprowadzone w ramach drugiego etapu badań, tj. symulacji upłynnienia w warunkach laboratoryjnych [A2], dostarczyły przełomowych danych dotyczących granicznej wartości energii sejsmicznej niezbędnej do zainicjowania procesu upłynnienia osadów. W warunkach laboratoryjnych zaobserwowano rozwój struktur deformacyjnych w wyniku zastosowania drgań sejsmicznych odpowiadających magnitudzie M~3,5. Jest to wartość niższa od progów podawanych w większości wcześniejszych prac, w których sugerowano, że minimalna magnituda zdolna do wywołania upłynnienia wynosi co najmniej M 4,2 (Youd, 1978; Galli, 2000), a częściej M 5,0 lub więcej (Ambraseys, 1988; Papadopoulos i Lefkopoulos,

1993). Co więcej, według Zhong'a i in. (2022), formowanie struktur takich jak pseudonodule czy struktury typu piłek i poduszek jest możliwe dopiero przy magnitudzie M 6–6,5.

Wyniki przeprowadzonych eksperymentów wskazują na znacznie niższe wartości progowe, które mogą inicjować upłynnienie. Pomimo niskiej magnitudy, zastosowane drgania o wysokim przyspieszeniu szczytowym gruntu (PGA), szacowanym na około 2 g, spowodowały intensywną mobilizację osadu oraz rozwój złożonych struktur deformacyjnych, takich jak wulkany klastyczne, pogrązy czy struktury płomieniowe. Są to struktury charakterystyczne dla deformacji sejsmogenicznych, opisywane również przez Liang'a i in. (2024), którzy uzyskali podobne efekty przy PGA na poziomie 0,5–0,8 g.

Nowatorskim aspektem przeprowadzonych badań jest również fakt, że zastosowana „magnituda eksperymentalna" miała charakter pośredni, wynikający z parametrów układu laboratoryjnego: masy próbek, odległości od źródła wstrząsu oraz geometrii cylindrów z pleksi. Oznacza to, że nie została określona bezpośrednio za pomocą sejsmografu, lecz oszacowana na podstawie empirycznych zależności. Tym bardziej interesujące jest to, że mimo tak niskiej wartości magnitudy, deformacje nie tylko powstały, ale często miały charakter rozbudowany, co potwierdziły pięciokrotne powtórzenia eksperymentu. **Wyniki te podkreślają kluczowe znaczenie lokalnych warunków geologicznych i geotechnicznych w rozwoju struktur deformacyjnych, które nie są determinowane wyłącznie przez wartość energii sejsmicznej.**

5.3. Kryteria rozpoznawcze sejsmogenicznie upłynnionych osadów

Jednym z kluczowych wyzwań w interpretacji struktur deformacyjnych jest prawidłowe określenie czynnika deformującego osad (np. Obermeier i in., 1990; Hilbert-Wolf i in., 2009; Owen i Moretti, 2011; Owen i in., 2011; Moretti i in., 2014; He i Qiao, 2015). Wyniki przedstawione w artykułach [A2] (Świątek i Pisarska-Jamroży, 2025) oraz [A3] (Świątek i in., 2025) umożliwiły sformułowanie nowych kryteriów identyfikacyjnych dla struktur o pochodzeniu sejsmicznym.

Eksperymenty wykazały, że określone typy struktur deformacyjnych, takie jak struktury płomieniowe, wulkany klastyczne czy pseudonodule, charakteryzują się powtarzalnymi, typowymi proporcjami wysokości do szerokości. Może to stanowić istotne narzędzie w rozpoznawaniu charakteru siły deformującej (por. Owen i Moretti, 2011; Belzyt i Pisarska-Jamroży, 2017). Morfometria tych struktur, analizowana w warunkach eksperymentalnych, sugeruje możliwość wykorzystania współczynników kształtu jako dodatkowego wskaźnika określającego liczbę zdarzeń deformujących osad. Co istotne, korelacje między wymiarami

struktur a takimi czynnikami jak układ litologiczny, poziom nawodnienia czy szacowana magnituda wskazują, że podejście to może być zastosowane również na badaniach terenowych – w celu wstępnej klasyfikacji typu deformacji oraz identyfikacji zdarzeń wieloprocesowych. Nowatorskim i unikalnym wkładem niniejszych badań jest również zastosowanie skaningowej mikroskopii elektronowej (SEM) i spektroskopii EDX do analizy ziaren kwarcu poddanych działaniu fali sejsmicznej. Zidentyfikowano liczne mikropęknięcia, deformacje brzegów ziaren, korozję chemiczną ich powierzchni, a co szczególnie istotne – obecność złota (Au) osadzonego w szczelinach ziaren. Obecność złota w mikrospękaniach może świadczyć o tym, że drgania sejsmiczne nie tylko inicjują deformację mechaniczną, lecz również powodują krótkotrwałe, lokalne przemieszczenia cieczy porowej, prowadzące do mobilizacji i krystalizacji metali. Tego rodzaju mikroobieg może sprzyjać transportowi jonów metali i ich osadzaniu w strefach największego naprężenia. W konsekwencji, struktury deformacyjne mogą stanowić mikroślady zarówno procesów mechanicznych, jak i chemicznych związanych z aktywnością sejsmiczną (Świątek i in., w recenzji).

6. Wnioski

Analiza zebranych w terenie prób, przeprowadzenie eksperymentów laboratoryjnych i ich szczegółowe analizy pozwoliły na kompleksowe ujęcie problematyki powstawania sejsmogenicznych struktur deformacyjnych. Zidentyfikowano, a także zweryfikowano udział czynników kontrolujących proces upłynnienia, jak i dopracowano kryteria rozpoznawania sejsmogenicznych struktur deformacyjnych. Prezentowana rozprawa doktorska, składająca się z trzech recenzowanych artykułów, pozwoliła wyciągnąć następujące wnioski:

1. Analiza i interpretacja struktur deformacyjnych typu *soft-sediment deformation structures* (SSDS) powinna opierać się m.in. na szczegółowych cechach litologicznych osadów. Nawet trzęsienia ziemi o wysokich magnitudach (>6) nie doprowadzą do upłynnienia, jeżeli osady nie są odpowiednio nawodnione lub posiadają „niekorzystny" skład granulometryczny, np. nadmiar piasku przy niedoborze frakcji pylastej. [A1]
2. Spośród wszystkich analizowanych frakcji, wchodzących w skład osadów upłynnionych, to frakcja pylasta wykazuje najwyższą mobilność i najczęściej uczestniczy bezpośrednio w inicjacji upłynnienia. Jej obecność sprzyja utracie spójności osadu, zwłaszcza w warunkach wysokiego nawodnienia i przy obecności drobnych frakcji piasku. W wielu przypadkach to właśnie pył stanowi główną frakcję w strukturach płomieniowych czy klastycznych dajkach. [A1]

3. Podstawowe parametry statystyczne uziarnienia takie jak średnia średnica ziarna, skośność, wysortowanie i kurtoza mogą stanowić obiektywne kryteria ilościowe klasyfikacji typów struktur deformacyjnych. Wyniki badań wykazały, że pogrązy czy struktury typu pseudonodule najczęściej rozwijają się w dobrze wysortowanych i piaszczystych osadach (65-95%), natomiast struktury płomieniowe czy dajki klastyczne występują przede wszystkim w osadach słabiej wysortowanych o wyższej zawartości frakcji pylastej (do 89%). [A1]
4. Na podstawie analizy modeli statystycznych można oszacować podatność osadu na upłynnienie. Analiza ta pozwoliła na wskazanie wartości progowych oraz kombinacji cech teksturalnych, które statystycznie istotnie wpływają na rozwój poszczególnych typów struktur deformacyjnych. Model statystyczny uzyskany na tej podstawie może stanowić narzędzie prognostyczne, umożliwiające ocenę potencjału deformacyjnego osadu. [A1]
5. Eksperymenty laboratoryjne dowiodły, że możliwe jest wywołanie procesu upłynnienia i powstania struktur deformacyjnych przy zastosowaniu niskiej magnitudy (M~3,5), pod warunkiem wysokiego nawodnienia osadu i odpowiedniego układu litologicznego warstw. Wyniki te stanowią istotne uzupełnienie dotychczasowej wiedzy, która wskazywała próg $M \geq 4{,}2–5{,}0$ jako minimalny dla wystąpienia upłynnienia osadu. [A2]
6. Wyniki badań eksperymentalnych wykazały, że im bardziej zróżnicowana sukcesja osadów podatnego na upłynnienie (pod względem frakcji osadu, gęstości właściwej i przepuszczalności), tym większe prawdopodobieństwo wystąpienia złożonych i dobrze widocznych struktur deformacyjnych. W przypadku prostych układów litologicznych (np. profili z dominującą jedną frakcją) struktury deformacyjne były słabo rozwinięte i trudniejsze do identyfikacji. [A2]
7. Analiza morfometrii struktur deformacyjnych wykazała wysoką powtarzalność proporcji (wysokość : szerokość) w obrębie danych struktur deformacyjnych, co może stanowić narzędzie pomocnicze w terenowej klasyfikacji struktur oraz przybliżonej ocenie liczby zdarzeń, jak i intensywności siły deformującej, np. analizując współczynniki korelacji między wysokością a szerokością w obrębie dwóch różnych litologicznie warstw osadu. [A2]
8. W efekcie eksperymentów laboratoryjnych zaobserwowano, powstałe w ich trakcie, mikropęknięcia ziaren kwarcu. Analiza wykorzystująca skaningowy mikroskop elektronowy ujawniła, że pęknięcia te mają zróżnicowany charakter: od prostych, liniowych szczelin przełamujących ziarno, po rozgałęzione mikroszczeliny

przypominające siatkę spękań powstałych wskutek gwałtownego przeciążenia mechanicznego. Mikropęknięcia o genezie sejsmicznej mają ostre zarysy, są nieregularne oraz zazwyczaj głębokie. [A3]

9. W warunkach laboratoryjnych wykazano, że w osadach wzbogaconych w związki metali (np. złota) może dochodzić do ich mobilizacji i wtórnej krystalizacji w mikropęknięciach ziaren kwarcu, bezpośrednio podczas lub tuż po zdarzeniu deformacyjnym. Na podstawie obserwacji wykazano, że drgania sejsmiczne mogą aktywować mikroobieg cieczy bogatej w pierwiastki chemiczne, co może pozostawiać trwały sygnał geochemiczny w strukturze mineralnej osadu, w postaci nagromadzeń złota. Kwestia ta pozostaje otwarta i wymaga dalszych analiz. [A3]
10. Po raz pierwszy zwrócono uwagę na rolę warunków chemicznych środowiska, w szczególności odczynu (pH) i potencjału oksydacyjno-redukcyjnego (Eh) w procesie deformacji osadu i jego zapisie geochemicznym. W literaturze przedmiotu zagadnienie to było dotąd pomijane, a dominowały interpretacje oparte niemal wyłącznie na aspektach fizycznych, takich jak ciśnienie porowe, siła wstrząsu, czy tekstura osadu. Wyniki badań sugerują, że deformacje mechaniczne ziaren mogą być współkształtowane przez środowisko geochemiczne, w którym zachodzi upłynnienie. [A3]
11. Zaproponowane w pracy podejście, łączące analizy terenowe, eksperymenty i badania mikroskopowe, umożliwiło nie tylko skuteczne rozpoznanie struktur deformacyjnych, ale również ocenę charakteru procesów odpowiedzialnych za ich powstanie. Jest to szczególnie istotne w kontekście badań paleosejsmologicznych i rekonstrukcji zdarzeń z przeszłości, zwłaszcza w obszarach o niskiej aktywności sejsmicznej. [A1-A3]
12. Wyniki, na podstawie przeprowadzonych eksperymentów, wskazują na możliwość wywołania procesu upłynnienia w osadach drobnoziarnistych przy magnitudzie ~3,5, stawiają pod znakiem zapytania dotychczasowe założenia leżące u podstaw map ryzyka sejsmicznego i hazardu sejsmicznego, szczególnie w regionach uznawanych dotychczas za obszary o niskiej aktywności sejsmicznej. Tradycyjne podejście zakładało, że istotne deformacje osadu mogą powstać dopiero przy trzęsieniach ziemi o magnitudzie ≥M4,2–5,0. Tymczasem uzyskane, w efekcie przeprowadzonych badań laboratoryjnych, wyniki wskazują, że przy odpowiednim nawodnieniu i teksturze osadu, nawet słabe drgania sejsmiczne są wystarczające do zainicjowania procesu upłynnienia i powstania złożonych struktur deformacyjnych. Co więcej, szczegółowe badania nad cechami teksturalnymi osadów, w tym rola frakcji pylastej, jej proporcja do piasku i iłu ujawniają

nowe kryteria predykcyjne, które mogą zostać wykorzystane do aktualizacji modeli ryzyka związanego z upłynnieniem, zarówno w kontekście paleosejsmologicznym, jak i inżynierskim. Wyniki te mają bezpośrednie znaczenie dla planowania inwestycji infrastrukturalnych, modelowania zagrożeń oraz oceny stabilności osadów w obszarach dotąd niedoszacowanych sejsmicznie. [A1-A3]

Spis literatury

Allen, J.R.L. (1977). The possible mechanics of convolute lamination in graded sand beds. Journal Geology of Society, 134, 19–31. https://doi.org/10.1144/gsjgs.134.1.0019.

Allen, J.R.L. (1982). Developments in Sedimentology. Sedimentary structures, their character and physical basis. (Vol. 30A). Elsevier Scientific Publishing Company.

Ambraseys, N.N. (1988). Engineering seismology: Part I. Earthquake Engineering and Structural Dynamics, 17, 1–105. https://doi.org/10.1002/eqe.4290170101.

Andrews, C.A.D. & Martin, G.R. (2000). Criteria for liquefaction of silty soils. Paper presented at 12th World Conference on Earthquake Engineering, Auckland, New Zealand.

Arias, A. (1970). A measure of earthquake intensity. W: Seismic Design for Nuclear Power Plants. (Ed Hansen, Robert J.). Cambridge, Mass. Massachusetts Inst. of Tech. Press, 438–483.

Belzyt, S. & Pisarska-Jamroży, M. (2017). W jaki sposób badać sejsmity? Przegląd metod badawczych. Acta Geographica Lodziensia, 106, 171–180.

Belzyt, S., Pisarska-Jamroży, M., Bitinas, A., Woronko, B., Phillips, E. R., Piotrowski, J. A. & Jusienė, A. (2021). Repetitive Late Pleistocene soft-sediment deformation by seismicity-induced liquefaction in north-western Lithuania. Sedimentology, 68(7), 3033–3056. https://doi.org/10.1111/sed.12883.

Bielański, A. (2002). Podstawy chemii nieorganicznej. Tom I. Polskie Wydawnictwo Naukowe PWN. 1-546.

Bielański, A. (2004). Podstawy chemii nieorganicznej. Tom II. Polskie Wydawnictwo Naukowe PWN. 1-520.

Brandes, C. & Winsemann, J. (2013). Soft-sediment deformation structures in NW Germany caused by Late Pleistocene seismicity. International Journal of Earth Sciences, 102(8), 2255–2274. http://dx.doi.org/10.1007/s00531-013-0914-4.

Bronikowska, M., Pisarska-Jamroży, M. & Van Loon, A.J. (2021). First attempt to model numerically seismically-induced soft-sediment deformation structures – a comparison with field examples. Geological Quarterly, 65(4), 60. http://dx.doi.org/10.7306/gq.1629.

Campbell, C.S. (2003). Rapid granular flows. Annual Review of Fluid Mechanics, 22(1), 57–90. http://dx.doi.org/10.1146/annurev.fl.22.010190.000421.

Castilla, R.A. & Audemard, F.A. (2007). Sand blows as a potential tool for magnitude estimation of pre-instrumental earthquakes. Journal of Seismology, 11, 473–487. https://doi.org/10.1007/s10950-007-9065-z.

Chang, W.J. & Hong, M.L. (2008). Effects of clay content on liquefaction characteristics of gap-graded clayey sand. Soils and Foundations, 48, 1, 101–114.

Cui, M., Peng, N., Liu, Y., Wang, Z., Li, C., Xu, K. & Kuang, H. (2022). Recognizing deformation origins: a review of deformation structures and hypothesis on the perspective of sediment consolidation. International Geology Review, 65(9), 1500–1523. https://doi.org/10.1080/00206814.2022.2094840.

Davies, N., Turner, P. & Sansom, I.J. (2004). Soft-sediment deformation structures in the Late Silurian Stubdal Formation: the result of seismic triggering. Norwegian Journal of Geology, 85(3), 233–243.

Doe, T. W. & Dott, R.H.Jr. (1980). Genetic significance of deformed cross bedding; with examples from the Navajo and Weber sandstones of Utah. Journal of Sedimentary Petrology, 50(3), 793–812. https://doi.org/10.1306/212F7AEF-2B24-11D7-8648000102C1865D.

Einsele, G., Chough, S.K. & Shiki, T. (1996). Depositional events and their records - an introduction. Sedimentary Geology, 104, 1-4, 1–9.

Figueroa, J.L., Saada, A.S. & Liang, L. (1995). Effect of the grain size on the energy per unit volume at the onset of liquefaction. Paper presented at 3rd International Conference on Recent Advances in Geotechnical Earthquake Engineering and Soil Dynamics. St. Louis, Missouri.

Galli, P. (2000). New empirical relationships between magnitude and distance for liquefaction. Tectonophysics, 324(3), 169–187. https://doi.org/10.1016/S0040-1951(00)00118-9.

Gill, W.D. & Kuenen, P.H. (1958). Sand volcanoes on slumps in the Carboniferous of County Clare. Quarterly Journal of the Geological Society, 113(1-4), 441–460.

Hannich, D., Hoetzl, H. & Ehret, D. (2007). Liquefaction probability in Bucharest and influencing factors. Proceedings, International Symposium on Strong Vrancea earthquake and Ris Mitigation, Bucharest, Romania, 4(6), 205–222.

He, B. & Qiao, X. (2015). Advances and overview of the study on paleo-earthquake events: a review of seismite. Acta Geologica Sinica, 89, 1702–1746.

He, B., Qiao, X., Li, H. & Su, D. (2018). Soft sediment deformation structures triggered by the earthquakes: response to the high frequent tectonic events during the main tectonic movements. W: E. Sharkov (Eds.), Tectonics – Problems of Regional Settings. IntechOpen. http://dx/doi/org/10.5772/intechopen.72941.

Hilbert-Wolf, H.L., Simpson, E.L., Simpson, W.S., Tindall, S.E. & Wizevich, M.C. (2009). Insights into syndepositional fault movement in a foreland basin; trends in seismites of Upper Cretaceous Wahweap Formation, Kaiparowits Basin, Utah, USA. Basin Research, 21, 856–871. https://doi.org/10.1111/j.1365-2117.2009.00398.x.

Liang, L., Dai, F., Jiang, H. & Zhong N. (2018). A preliminary study on the soft-sediment deformation structures in the Late Quaternary lacustrine sediments at Tashkorgan, northeastern Pamir. Acta Geologica Sinica, 92(4), 1574–1591. https://doi.org/10.1111/1755-6724.13644.

Liang, L., Lu, Z., Zhang, Q., Tian, H., Dai, F. & Jiang, H. (2024). Shaking table simulation of soft sediment deformation structures in lacustrine sediments. Sedimentary Geology, 472, 106756. https://doi.org/10.1016/j.sedgeo.2024.106756.

Lowe, D.R. (1976). Subaqueous liquefied and fluidised sediment flows and their deposits. Sedimentology, 23(2), 285–308. https://doi.org/10.1111/j.1365-3091.1976.tb00051.x.

Maltman, A.J. & Bolton, A. (2003). How sediments become mobilized. W: P. van Rensbergen, R.R. Hillis, A.J. Maltman & C.K. Morley (Eds.), Subsurface Sediment Mobilization (pp. 9–20). London, Geological Society Special Publications. (Vol. 216). https://doi.org/10.1144/GSL.SP.2003.216.01.02.

McCalpin, J.P., Ferrario, F., Figueiredo, P., Livio, F., Grützner, C., Pisarska-Jamroży, M., Quigley, M., Reicherter, K., Rockwell, T., Štěpančíková, P. & Tábořiki, P. (2023). New developments in onshore paleoseismic methods, and their impact on Quaternary tectonic studies. Quaternary International, 664, 59–76. https://doi.org/10.1016/j.quaint.2023.03.008.

Monkul, M.M. (2012). On some of the factors influencing the fines' role on liquefaction of silty sands. Proceedings, GeoCongress 2012 State of the Art and Practice in Georechnical Engineering, Oakland, 799–808.

Moretti, M., Alfaro, P., Caselles, O. & Canas, J.A. (1999). Modelling seismites with a digital shaking table. Tectonophysics, 304, 369–383. https://doi.org/10.1016/S0040-1951(98)00289-3.

Moretti, M., Van Loon, A.J., Liu, M. & Wang, Y. (2014). Restrictions to the application of 'diagnostic' criteria for recognizing ancient seismite. Journal of Palaeogeography, 3, 162–173. https://doi.org/10.3724/SP.J.1261.2014.00050.

Müller, K., Winsemann, J., Pisarska-Jamroży, M., Lege, T., Spies, T. & Brandes, C. (2020). Limitations of soft-sediment deformation structures as indicators for paleo-earthquakes in formerly periglacial and glaciated areas. Paper presented at EGU General Assembly 2020.

Nartišs, M., Woronko, B., Pisarska-Jamroży, M., Belzyt, S. & Bitinas, A. (2018). Injection structures and load casts in lagoon sediments (Sārnate outcrop, W Latvia). Paper presented at International Palaeoseismological Field Workshop, Lithuanian Geological Survey, Lithuanian Geological Society, Vilnius, Lithuania.

Nichols, R.J., Sparks, R.S.J. & Wilson, C.J.N. (1994). Experimental studies of the fluidization of layered sediments and the formation of fluid escapes structures. Sedimentology, 41(2), 233–253. https://doi.org/10.1111/j.1365-3091.1994.tb01403.x.

Obermeier, S. (1996). Use of liquefaction-induced features for paleoseismic analysis – An overview of how seismic liquefaction features can be distinguished from other features and how their regional distribution and properties of source sediment can be used to infer the location and strength of Holocene paleo-earthquakes. Engineering Geology, 44(1–4), 1–76. https://doi.org/10.1016/S0013-7952(96)00040-3.

Obermeier, S., Jacobson, R.B., Smoot, J.P., Weems, R.E., Gohn, G.S., Monroe, J.E. & Powars, D.S. (1990). Earthquake-induced liquefaction features in the coastal setting of South Carolina and in the fluvial setting of the New Madrid seismic zone. US Geological Survey Professional Papers, 1504, 44.

Othman, B.A. & Marto, A. (2019). Laboratory test on maximum and minimum void ratio of tropical sand matrix soils. IOP Conference Series: Earth and Environmental Science, 140(1), 012084. https://doi.org/10.1088/1755-1315/140/1/012084.

Othman, B.A., Marto, A., Yunus, N.Z.M., Soon, C.T. & Pakir, F. (2019). The grading effect of coarse sand on consolidated undrained strength behaviour of sand matrix soils. International Journal of Recent Technology and Engineering, 7(5), 88–92.

Owen, G. (1985). Mechanisms and controls of deformation in unconsolidated sands: an experimental approach. Unpublished PhD thesis, University of Reading.

Owen, G. (1996). Experimental soft-sediment deformation: structures formed by the liquefaction of unconsolidated sands and some ancient examples. Sedimentology, 43(2), 279–293. https://doi.org/10.1046/j.1365-3091.1996.d01-5.x.

Owen, G. (2003). Load structures: gravity-driven sediment mobilization in the shallow subsurface. W: P. van Rensbergen, R.R. Hillis, A.J. Maltman & C.K. Morley (Eds.), Subsurface Sediment Mobilization (pp. 21–34). London, Geological Society Special Publications. (Vol. 216). https://doi.org/10.1144/GSL.SP.2003.216.01.03.

Owen, G. & Moretti, M. (2011). Identyfying triggers for liquefaction-induced soft-sediment deformation in sands. Sedimentary Geology, 235(3–4), 141–147. https://doi.org/10.1016/j.sedgeo.2010.10.003.

Papadopoulos, G.A. & Lefkopoulos, G. (1993). Magnitude–distance relations for liquefaction in soil from earthquakes. Bulletin of the Seismological Society of America, 83, 925–938. https://doi.org/10.1785/BSSA0830030925.

Park, S.S. & Kim, Y.S. (2013). Liquefaction resistance of sands containing plastic fines with different plasticity. Journal of Geotechnical and Geoenvironmental Engineering, ASCE, 139(5), 825–830.

Pisarska-Jamroży, M. & Woźniak, P.P. (2019). Debris flow and glacioisostatic-induced soft-sediment deformation structures in a Pleistocene glaciolacustrine fan: The southern Baltic Sea coast, Poland. Geomorphology, 326, 225–238.

Pisarska-Jamroży, M., Belzyt, S., Bitinas, A., Jusienė, A. & Woronko B. (2019a). Seismic shocks, periglacial conditions and glaciotectonics as causes of the deformation of a Pleistocene meandering river succession in central Lithuania. Baltica, 32(1), 63–77. http://dx.doi.org/10.5200/baltica.2019.1.6.

Pisarska-Jamroży, M., Belzyt, S., Bitinas, A., Jusienė, A., Damušytė, A. & Woronko, B. (2018). A glaciolacustrine succession (Dyburiai outcrop, NW Lithuania) with numerous deformed layers sandwiched between undeformed layers. Paper presented at International Palaeoseismological Field Workshop, Lithuanian Geological Survey, Lithuanian Geological Society, Vilnius, Lithuania.

Pisarska-Jamroży, M., Belzyt, S., Börner, A., Hoffmann, G., Hüneke, H., Kenzler, M., Obst, K., Rother, H., Steffen, H., Steffen, R. & Van Loon, A.J. (2019b). The sea cliff at Dwasieden: soft-sediment deformation structures triggered by glacial isostatic adjustment in front of the advancing Scandinavian Ice Sheet. DEUQUA Special Publications, 2, 61–67. https://doi.org/10.5194/deuquasp-2-61-2019.

Pisarska-Jamroży, M., Belzyt, S., Börner, A., Hoffmann, G., Kenzler, M., Rother, H., Steffen, R. & Steffen, H. (2022). Late Pleistocene earthquakes imprinted on glaciolacustrine

sediments on Gnitz Peninsula (Usedom Island, NE Germany). Quaternary Science Reviews, 296, 107807. https://doi.org/10.1016/j.quascirev.2022.107807.

van Rensbergen P., Hillis, R.R. Maltman, A.J. & Morley C.K. (2003). Subsurface Sediment Mobilization (pp. 9–20). London, Geological Society Special Publications. (Vol. 216). https://doi.org/10.1144/GSL.SP.2003.216.01.02.

Seed, H.B. (1979). Soil liquefaction and cyclic mobility evaluation for level ground during earthquakes. Journal of the Geotechnical Engineering Division, 105(2), 201–255. https://doi.org/10.1061/AJGEB6.0000768.

Seed, H.B., Woodward, R.J. & Lundgren, R. (1964). Fundamental aspects of the Atterberg limits. Journal of the Soil Mechanics and Foundations Division, 90(6), 75–105. https://doi.org/10.1061/JSFEAQ.0000685.

Seilacher, A. (1969). Fault-graded beds interpreted as seismites. Sedimentology, 13, 155–159.

Selley, R.C. (1969). Torridonian alluvium and quicksands. Scottish. Journal of Geology, 5, 328–346.

Sims, J.D. (2013). Earthquake-induced load casts, pseudonodules, ball-and-pillow structures, and convolute lamination: Additional deformation structures for paleoseismic studies. In: Recent advances in North American paleoseismology and neotectonics East of the Rockies (Eds. R.T. Cox, M.P. Tuttle, O.S. Boyd and J. Locat). Geological Society of America Special Papers, 493, 191–201. https://doi.org/10.1130/2012.2493(09).

Stewart, H.B. (1958). Sedimentary reflections of depositional environments in San Miguel Lagoon, Baja California, Mexico. AAPG Bulletin, 42(11), 2567–2618.

Świątek, S. & Pisarska-Jamroży, M. (2025). Seismogenic liquefaction with M~3.5 in fine-grained sediments: An experimental approach. Sedimentary Geology, 478, 106833. https://doi.org/10.1016/j.sedgeo.2025.106833.

Świątek, S., Belzyt S., Pisarska-Jamroży, M. & Woronko, B. (2023). Sedimentary records of liquefaction: implications from field studies. Journal of Geophysical Research: Earth Surface, 128, e2023JF007152. https://doi.org/10.1029/2023JF007152.

Świątek, S., Lewińska, K., Pisarska-Jamroży, M. & Günter, C. (2025). An application of quartz grain analyses in earthquake-induced (palaeo)liquefaction studies. Journal of Structural Geology, 193, 105357. https://doi.org/10.1016/j.jsg.2025.105357.

Świątek, S., Lewińska, K., Pisarska-Jamroży, M. & Günter, C. *w recenzji*. Springer Nature.

Tang, X.W., Hu, J.L. & Qiu, J.N. (2016). Identifying significant influence factors of seismic soil liquefaction and analyzing their structural relationship. Journal of Civil Engineering, 20, 2655–2663. http://dx.doi.org/10.1007/s12205-016-0339-2.

Tuttle, M., Law, K.T., Seeber, L. & Jacob, K. (1990). Liquefaction and ground failure induced by the 1988 Saguenay, Quebec, earthquake. Canadian Geotechnical Journal, 27(5), 580–589. https://doi.org/10.1139/t90-073.

Umehara, Y. (1985). Evaluation of soil liquefaction potentials in partially drained conditions. Soils and Foundations, 25(2), 57-72.

Van Loon, A.J., Pisarska-Jamrożу, M. (2014). Sedimentological evidence of Pleistocene earthquakes in NW Poland induced by glacioisostatic rebound. Sedimentary Geology, 300(1), 1–10. https://doi.org/10.1016/j.sedgeo.2013.11.006.

Van Loon, A.J., Pisarska-Jamrożу, M. & Woronko, B. (2020). Sedimentological distinction in glacigenic sediments between load casts induced by periglacial processes from those induced by seismic shocks. Geological Quarterly, 64(3), 626–640. http://dx.doi.org/10.7306/gq.1546.

Van Loon, A.J., Pisarska-Jamrożу, M., Nartišs, M., Krievāns, M. & Soms, J. (2016). Seismites resulting from high-frequency, high-magnitude earthquakes in Latvia caused by Late Glacial glacio-isostatic uplift. Journal of Palaeogeography, 5(4), 363–380. https://doi.org/10.1016/j.jop.2016.05.002.

Van Loon, A.J. (2009). Soft-sediment deformation structures in siliciclastic sediments: and overview. Geologos, 15, 3–55.

Wahyudi, S., Koseki, J., Sato, T. & Miyashita, Y. (2013). Effects of pre-shearing history on repeated liquefaction behaviour of sand using stacked-ring shear apparatus. Bulletin of ERS, 46, 3–11.

Wang, W.S. (1979). Some findings in soil liquefaction. Earthquake Engineering Department, Water Conservancy and Hydroelectric Power Scientific Research Institute, Beijing, China.

Woronko, B., Pisarska-Jamrożу, M., Belzyt, S., Karmazienė, D., Bitinas, A. & Damušytė, A. (2018). Multi-type soft-sediment deformation structures in glaciolacustrine kame sediments (Licišķėnai outcrop, S Lithuania). Paper presented at International Palaeoseismological Field Workshop, Lithuanian Geological Survey, Lithuanian Geological Society, Vilnius, Lithuania.

Woźniak, P.P., Belzyt, S., Pisarska-Jamrożу, M., Woronko, B., Lamsters, K., Nartišs, M. & Bitinas, A. (2021). Liquefaction and re-liquefaction of sediments induced by uneven loading and glacigenic earthquakes: implications of results from the Latvian Baltic Sea coast. Sedimentary Geology, 421, 105944. https://doi.org/10.1016/j.sedgeo.2021.105944.

Youd, T.L. (1978). Packing changes and liquefaction susceptibility. Journal of the Geotechnical Engineering Division, 103(8), 918–922. https://doi.org/10.1061/AJGEB6.0000478.

Youd, T.L. & Perkins, D.M. (1973). Mapping liquefaction-induced ground failure potential. Journal of the Geotechnical Engineering Division, 104(4), 433–446. http://dx.doi.org/10.1061/AJGEB6.0000612.

Youd, T.L. & Idriss, I.M. (2011). Liquefaction resistance of soils: summary report from the 1996 NCEER and 1998 NCEER/NSF workshops on evaluation of liquefaction resistance of soils. Journal of Geotechnical and Geoenvironmental Engineering, 127(4), 297–313.

Zhang, J.M. & Wang, W.X. (1990). Effect of vibration frequency on dynamic behavior of saturated sand (in Chinese). Chinese Journal of Geotechnical Engineering, 12, 89–97.

Zhong, N., Jiang, H., Li, H., Su, D., Xu, H., Liang, L. & Fan, J. (2022). The potential of using soft-sediment deformation structures for quantitatively reconstructing paleo-seismic shaking intensity: progress and prospect. Environmental Earth Sciences, 81(408). https://doi.org/10.1007/s12665-022-10504-8.

Zhou, S.G. (1981). Influence of fines on evaluating liquefaction of sand by CPT. Paper presented at 1st International Conference on Recent Advances in Geotechnical Earthquake Engineering and Soil Dynamics. St. Louis, Missouri.

Finansowanie badań

Badania wchodzące w zakres rozprawy doktorskiej sfinansowano przez:

1. Narodowe Centrum Nauki w Polsce,
    - grant GREBAL nr 2015/19/B/ST10/0061 (kierownik: prof. dr hab. Małgorzata Pisarska-Jamroży) [A1]
    - grant nr 2019/35/N/ST10/03401 (kierownik: dr Szymon Belzyt) [A1]
    - grant nr 2023/49/N/ST10/00282 (kierownik: mgr Szymon Świątek) [A3]
2. Inicjatywa Doskonałości – Uczelnia Badawcza Uniwersytet im. Adama Mickiewicza w Poznaniu,
    - wniosek nr 021/13/UAM/0040 (kierownik: mgr Szymon Świątek) [A2]
    - wniosek nr 054/13/SNP/0001 (kierownik: mgr Szymon Świątek) [A2 oraz A3]
    - wniosek nr 133/13/UAM/0044 (kierownik: mgr Szymon Świątek) [A3]
3. International Association of Sedimentologists, [A2 oraz A3]
4. Środki statutowe Wydziału Nauk Geograficznych i Geologicznych,
5. Środki prywatne.

Prezentacja wyników badań

Wyniki badań w ramach rozprawy doktorskiej były prezentowane podczas:

1. Świątek, S., Belzyt, S., Pisarska-Jamroży, M., 2022 – Sediments prone to liquefaction – implications from field studies: review. 5th WGSG Meeting, 28-30.06.2022, Mediolan. [A1]
2. Świątek, S., Pisarska-Jamroży, M., 2023 – Soft-sediment deformation structures – development in laboratory conditions. 36th IAS Meeting of Sedimentologists, 12-16.06.2023, Dubrovnik. [A2]
3. Belzyt, S., Świątek, S., Pisarska-Jamroży, M., Woronko, B., 2023 – Jakie osady ulegają upłynnieniu? Cechy teksturalne osadów upłynnionych na podstawie przykładów terenowych. POKOS 8, 05-07.09.2023, Chęciny. [A1]
4. Świątek, S., Lewińska, K., Pisarska-Jamroży, M., 2024 – Wpływ warunków redukcyjno-oksydacyjnych na powstanie i rozwój struktur deformacyjnych powstałych w wyniku upłynnienia osadu – wstępne wyniki badań eksperymentalnych. IV Polski Kongres Geologiczny, 10-14.06.2024, Poznań. [A3]
5. Świątek, S., Belzyt, S., Pisarska-Jamroży, M., Woronko, B., 2024 – Which sediments are most prone for liquefaction? Textural characteristics of liquefied sediments based on field studies. 37th IAS Meeting of Sedimentologists, 25-27.06.2024, Aberdeen. [A1]
6. Świątek, S., Pisarska-Jamroży, M., 2024 – Earthquake's sedimentological evidence – experimental approach as key to better understanding seismically-induced liquefaction phenomenon. 6th WGSG Meeting, 02-04.07.2024, Londyn. [A2]
7. Świątek, S., Lewińska, K., Pisarska-Jamroży, M., Günter, C., 2025 – Seismically-induced quartz grain alterations as indicators of past earthquake events. European Geoscience Union General Assembly, 27.04-02.05.2025, Wiedeń. [A3]

Oświadczenia Autorów oraz kopie artykułów naukowych wchodzących w skład rozprawy doktorskiej

Oświadczenie Autorów

Świątek, S., Belzyt S., Pisarska-Jamroży, M., Woronko, B. 2023. Sedimentary records of liquefaction: implications from field studies. *Journal of Geophysical Research: Earth Surface* 128, e2023JF007152. https://doi.org/10.1029/2023JF007152

Niniejszym oświadczam, że wkład Pana Szymona Świątka w wyżej wymieniony artykuł naukowy wynosi 50%.

Pan Szymon Świątek był odpowiedzialny za przygotowanie wstępnej wersji artykułu, opracowanie wyników badań oraz wykonanie większości rycin i tabel zamieszczonych w publikacji. Autor brał również aktywny udział w pozostałych etapach przygotowania artykułu, w tym w edycji i recenzji manuskryptu, interpretacji wyników oraz formułowaniu wniosków.

Pełnił również rolę autora korespondencyjnego.

Materiał wykorzystany w publikacji pochodził zarówno z wcześniejszych badań terenowych, jak i z już wcześniej opublikowanych źródeł.

Szymon Świątek	09.04.2025	Świątek
Szymon Belzyt	15.04.2025	Szymon Belzyt
Małgorzata Pisarska-Jamroży	07.05.2025	
Barbara Woronko	10.04.2025	B Woronko

Oświadczenie Autorów

Świątek, S., Pisarska-Jamroży, M. 2025. Seismogenic liquefaction with M~3.5 in fine-grained sediments: An experimental approach. *Sedimentary Geology* 478, 106833. https://doi.org/10.1016/j.sedgeo.2025.106833

Niniejszym oświadczam, że wkład Pana Szymona Świątka w wyżej wymieniony artykuł naukowy wynosi 80%.

Pan Szymon Świątek był odpowiedzialny za przygotowanie wstępnej wersji artykułu, przeprowadzenie badań laboratoryjnych, opracowanie wyników badań oraz wykonanie większości rycin i tabel zamieszczonych w publikacji. Autor brał również aktywny udział w pozostałych etapach przygotowania artykułu, w tym w edycji i recenzji manuskryptu, interpretacji wyników oraz formułowaniu wniosków.

Pełnił również rolę autora korespondencyjnego.

Szymon Świątek	09.04.2025	Szymon Świątek
Małgorzata Pisarska-Jamroży	07.05.2025	

Declaration of Authors

Świątek, S., Lewińska, K., Pisarska-Jamroży, M., Günter, C. 2025. An application of quartz grain analyses in earthquake-induced (palaeo)liquefaction studies. *Journal of Structural Geology* 193, 105357. https://doi.org/10.1016/j.jsg.2025.105357

I hereby declare that the contribution of Mr. Szymon Świątek in the preparation of the publication can be estimated at 65%.

Mr. Szymon Świątek was responsible for preparing the initial draft of the article, conducting laboratory analyses, processing the research results, and creating the majority of the figures and tables included in the publication. The author also actively participated in other stages of the manuscript preparation, including editing and internal review, interpretation of the results, and formulation of the conclusions.

He also served as the corresponding author.

Szymon Świątek	09.04.2025	Świątek
Karolina Lewińska	07.05.2025	Lewińska
Małgorzata Pisarska-Jamroży	07.05.2025	
Christina Günter	z powodu ciężkiej choroby autorki brak możliwości uzyskania podpisu	

JGR Earth Surface

RESEARCH ARTICLE
10.1029/2023JF007152

Special Section:
Controls and Biasing Factors in Sediment Generation, Routing, and Provenance: Models, Methods, and Case Studies

Sedimentary Records of Liquefaction: Implications From Field Studies

Szymon Świątek[1], Szymon Belzyt[2], Małgorzata Pisarska-Jamroży[1], and Barbara Woronko[3]

[1]Faculty of Geographical and Geological Sciences, Institute of Geology, Adam Mickiewicz University in Poznań, Poznań, Poland, [2]Faculty of Earth Sciences and Spatial Management, Nicolaus Copernicus University in Toruń, Toruń, Poland, [3]Faculty of Geology, University of Warsaw, Warsaw, Poland

Key Points:

- Liquefaction-induced soft-sediment deformation structures were divided into active and passive concave up structures and active and passive concave down structures
- Content of silt is the main factor for deformation processes initiating the further development of all deformation structures
- Concave up structures zone, concave down structures zone and transitional zone were distinguished on the basis of grain-size composition of liquefied sediments

Correspondence to:
S. Świątek,
szymon.swiatek@amu.edu.pl

Citation:
Świątek, S., Belzyt, S., Pisarska-Jamroży, M., & Woronko, B. (2023). Sedimentary records of liquefaction: Implications from field studies. *Journal of Geophysical Research: Earth Surface*, *128*, e2023JF007152. https://doi.org/10.1029/2023JF007152

Received 6 MAR 2023
Accepted 16 JUL 2023

Abstract The susceptibility of grains in sediment to the liquefaction process causes the development of deformation structures. Some sediments undergo liquefaction, others do not. There is a group of sediments especially prone to liquefaction, which was proven during laboratory experiments. However, the field results are often slightly different from those obtained experimentally because of many unpredictable factors influencing the course of the liquefaction process. For this reason, we tested 144 samples of unconsolidated Quaternary-age sediments, collected from eight study sites in Germany, Lithuania and Latvia, which have been liquefied. We also present some new dating results. These samples were divided into two groups of soft-sediment deformation structures: concave up (e.g., injection structures) and concave down (e.g., load casts, pseudonodules). The granulometry of all deformation types was statistically evaluated, which allowed identifying textural differences between sediment contained in concave up and concave down structures. We suggest that the mobilization of silt fraction is responsible for the further deforming process. We also confirm that the maximum content of clay in sediment prone to liquefaction cannot exceed 14%, but only with a significant content of coarser fractions (silt and sand). Moreover, we identified two separate zones of the specific grain size in which only concave down structures or only concave up structures develop as an effect of liquefaction, and the third "transitional zone" where all forms occur. The "transitional zone" is separated from the concave up structures and concave down structures zones by two "gap zones" in which no liquefied sediments were observed.

Plain Language Summary Liquefaction is a process of temporary loss of shear strength of water-saturated sediments, during which the solid-state sediment behaves like a plastic mass or a viscous solid. It can be triggered in natural conditions by numerous factors, including waving, rapid sedimentation, earthquakes and the fall of meteorites. Sandy silt and silty sand are commonly known as the most liquefaction-prone sediments, but the specific granulometric features are still insufficiently characterized. We analyzed 144 samples of unconsolidated Quaternary-age sediments deposited in lacustrine, shallow marine and fluvial environments, which were liquefied. We divided all liquefaction-induced soft-sediment deformation structures into active and passive concave up (e.g., injection structures) and active and passive concave down (e.g., load structures). As a result of statistical tests, provided for each group separately, we observed that the silt content is the main factor for sediment deformation processes initiating the further development of all deformation structures. On the basis of grain-size composition of liquefied sediments, we also identified two separate zones for which only concave down structures or only concave up structures develop as an effect of liquefaction, and the third "transitional zone" where all forms occur. These zones are separated by two "gap zones," where no liquefied sediments were observed.

1. Introduction

Some geological processes can lead to temporary or permanent changes in sediment fabrics. Unconsolidated sediments are particularly susceptible to mobilization because pore pressure can increase relatively easily in them, which results in the loss of inter-grain contacts and mobilization of the grains (Maltman & Bolton, 2003; Seed, 1979; Van Rensbergen et al., 2003). Grain mobilization arises when the driving forces have got sufficient energy to set grains in motion. The potential energy can be released by several trigger mechanisms. Their existence causes the increase of stresses and lithostatic loading and, consequently, liquefaction and fluidization of sediments (He et al., 2018; Maltman & Bolton, 2003; Owen & Moretti, 2011; Youd, 1973; Zhong et al., 2022). The possible trigger mechanisms are among others wave action, storms, turbulent movements in water, tsunamis,

tidal shear, rapid sedimentation, periglacial processes related to the thawing of permafrost, earthquakes and the fall of meteorites (e.g., Allen, 1982; Vandenberghe, 2013; Van Loon et al., 2019).

In natural conditions, liquefaction and fluidization occur together and are known as liquidization. The fluidization occurs when a sufficiently vigorous upward flow of pore fluid flows through the porous medium, thereby counteracting their weight and reducing enough their strength to deform sediment (cf. Allen, 1977, 1982; Campbell, 2003; Davies et al., 2004; Nichols et al., 1994; Owen, 2003). Water-saturation, overpressure or insufficient compaction are required for a liquidization of sediments (Allen, 1982; Owen, 2003). The most important factors controlling both the liquefaction and fluidization are the hydraulic gradient, permeability, and resistance to deformation (Brandes & Winsemann, 2013; Lowe, 1976).

The liquefaction is known as a temporary loss of shear strength (Brandes & Winsemann, 2013; Müller et al., 2020; Owen & Moretti, 2011; Wahyudi et al., 2013). This phenomenon occurs when the sediment weight is transferred into the pore fluid because of the loss of cohesion, repacking of loose sediment, loading of overlying layers, or a rapid and sudden increase of fluid pressure in the pores (Galli, 2000; Maltman & Bolton, 2003; Seed, 1979). The sediment with the pore water behaves rheologically like a plastic mass (Van Loon et al., 2020) or a viscous solid (e.g., Allen, 1982; Owen & Moretti, 2011). The shear strength depends on the resistance of strength, which is a linear function of cohesion, inter-grain friction force, and effective stress (Allen, 1982). The liquefaction can be (a) complete, that is, all inter-grain contacts are lost and the primary sediment structure is interrupted or (b) partial, that is, some inter-grain contacts are preserved causing a partially disturbed primary structure (Doe & Dott, 1980). After liquefaction, the driving force is terminated, and the inter-grain contacts are restored (Campbell, 2003). The duration of the liquefaction phenomenon is a function of the grain size, which determines the velocity of particle deposition and the thickness of the liquefied layer (Allen, 1982; Owen, 2003). However, it is estimated that it does not last longer than several to a dozen seconds (Owen, 2003).

Liquefaction traces in sediments were noted up to the maximum depth of 10 m, but most often not deeper than 2 m (Bronikowska et al., 2021; Davies et al., 2004; Obermeier, 1996). Sediments closer to the surface have a greater potential for mobilization and plastic deformation (Maltman & Bolton, 2003; Youd, 1978). The critical deformation state increases with depth, which reduces the susceptibility of liquefaction. According to Wang (1979) and Seed et al. (1983), the water limit in sediments that undergo liquefaction is higher than 90%. One of the main factors that control the style of deformation and the possibility of sediment liquefaction is grain size distribution of the potentially liquefied sediments and the surrounding sediments. Previous studies were focused on relatively "clean" sand, that is, without silt or clay (Andrews & Martin, 2000; Obermeier, 1996; Owen, 1996). Sediments with significant content of clay, causing cohesion, are claimed to be less prone to liquefaction. Commonly accepted maximum content of clay obtained on the basis of field examples and laboratory experiments in sediments, above which the liquefaction does not occur, reaches >10% (for clay particles <2 μm: Andrews & Martin, 2000; Figueroa et al., 1995; Kishida, 1970; Tuttle et al., 1990; Wang, 1979; Zhou, 1981) or >15% (for clay particles <5 μm: Wang, 1979). Coarser grains, for example, gravels, usually do not undergo liquefaction because they have a greater weight and they require a more powerful trigger mechanism; only in some special cases gravel can be liquefied, for example, as an effect of a strong earthquake or because of being entrained by the surrounding liquefied sand (e.g., Postma, 1983; Wang & Manga, 2021). Grain-size distribution of sediments affected by known, recent and ancient earthquakes suggests that the liquefaction occurs mainly in loosely packed, and suitably water-saturated coarse-grained silt, silty sand and fine-grained sand (Andrews & Martin, 2000; Obermeier, 1996; Owen, 2003). Maltman and Bolton (2003) and Collinson et al. (2019) conclude that the greater the porosity, permeability and sorting of the sediment, the greater the susceptibility of the sediment to liquefaction.

Here, we describe the statistically developed granulometric composition of Quaternary-age sediments, deposited in lacustrine, shallow marine and fluvial environments, which have been liquefied (Belzyt et al., 2021; Hoffmann & Reicherter, 2011; Nartišs et al., 2018; Pisarska-Jamroży et al., 2018, 2019a, 2022; Woronko et al., 2018; Woźniak et al., 2021). The primary porosity and structure of the sediments is unknown as well as primary water saturation. We particularly aim (a) to describe grain-size characteristics of liquefied sediments in loaded and injected sediments, (b) to show statistically significant differences and relationships in textural features of loaded and injected sediments, and (c) to determine any interdependencies of the share of each fraction of sediments which the specific types of liquefaction-induced forms are composed of. We do not analyze the trigger mechanisms and their impact on the behavior of sediments during liquefaction, but the textural features of liquefied sediments in the distinguished concave up structures and concave down structures.

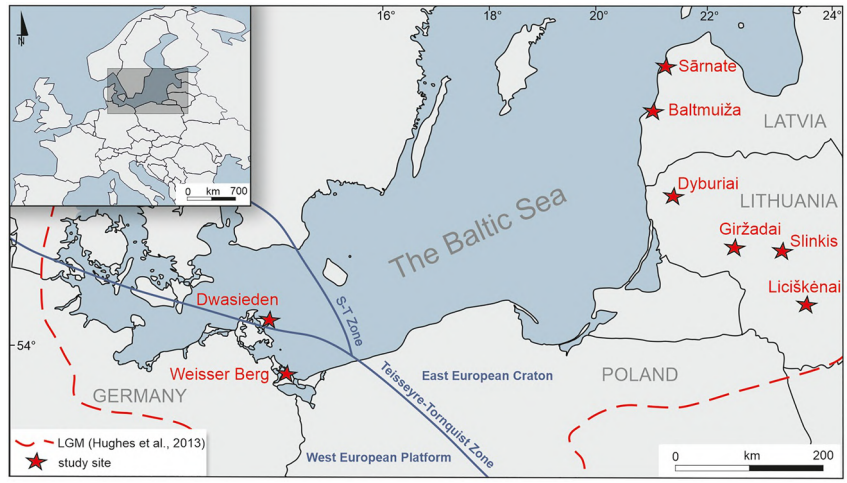

Figure 1. Location of the study sites (S-T Zone—Sorgenfrei-Tornquist Fault Zone, LGM—the maximal extent of Fennoscandian Ice Sheet during the Last Glacial Maximum—MIS2).

2. Geological Setting

The study presents results of the grain-size analysis of the samples collected from eight study sites from three Baltic countries (Figure 1): Latvia (Sārnate and Baltmuiža), Lithuania (Slinkis, Dyburiai, Liciškėnai, Giržadai) and Germany (Weisser Berg and Dwasieden). The study sites (Figure 1) are located in the area south and east of the Baltic Sea that forms a part of the European Plains, which was overrode by the Fennoscandian Ice Sheet several times during the Pleistocene. The German sites are located within the West European Platform, while all the remaining sites are located in the East European Craton. The samples were collected from natural exposures of Quaternary deposits in the area south and east of the Baltic Sea coastline (coastal bluffs, slopes of river valleys) and sand pits. The age of sediments taken into consideration varies between Marine Isotope Stage (MIS) 5d and MIS 2 (Table 1).

3. Material and Methods

3.1. Terminology

In the present paper, we particularly focus on the detailed recognition of concave down structures (e.g., load casts, pseudonodules, balls-and-pillows) and concave up structures (e.g., injections, clastic dykes, water/sediment escape structures, flame structures) from which the sediments were collected and analyzed. For the purpose of this paper, we use the classification of concave up structures and concave down structures involved in the liquefaction process and with the new genetic terms: active concave up structures, active concave down structures, passive concave up structures and passive concave down structures. Concave up structures and concave down structures analyzed in the study were developed mostly in two-layer systems (Figure 2a and 2b): a lower, finer-grained (mostly silty) layer and an upper, coarser-grained (mostly sandy) layer. Our division was based on the following features of the deformed structures: shape (geometry), co-relationships between the given deformation structures and the surrounding undeformed sediment and/or other deformation structures, internal structure of the single deformation structure, textural features and the order of recognized processes responsible for sediment deformation within a layer (sediment injection vs. sediment loading). Moreover, in most cases, we checked the spatial geometry of the deformation structures performing horizontal and vertical cross-sections.

The **active concave up structures (AU)** are represented by injection structures, such as clastic dykes and water-escape structures (Figure $2a_2$, 2c–2g and 2i). They are characterized by (a) irregular shape, (b) narrow and sharp ends, (c) different heights, (d) usually massive structure, and (e) occurrence mostly at irregular intervals. The AU are formed because of high pore pressure discharge associated with rapid fluidization and liquefaction of the sediment in the lower layer (source layer for AU). The AU presence initiates the further development of SSDS, also in the upper layer. The AU can develop when the lower layer (=deforming layer) is fluidized and liquefied (Figures 2d–2g, 2i and 2j), but the upper layer (=deformed layer) remains static (Figure 2c). The AU

Table 1
Age, Origin and Number of Samples From Each Study Site (SSDS—Soft-Sediment Deformation Structures)

Country	Study site and references	Estimated age of sediment deposition and deformation	Sedimentary environment	Architecture of layers with SSDS	Number of samples: Concave up structures	Number of samples: Concave down structures
Latvia	Sārnate (Nartišs et al., 2018)	Between 17.0 ± 1.2 ka and 16.7 ± 1.3 ka	Shallow marine	SSDS occur within 2 internally deformed layers (thickness from 1 to 2 m)	9	8
	Baltmuiža (Woźniak et al., 2021)	Between 30.5 ± 1.8 ka and 26.3 ± 1.5 ka	Shallow marine	SSDS occur within 7 internally deformed layers (thickness from 5 to 20 cm)	4	4
Lithuania	Slinkis (Pisarska-Jamroży et al., 2019a)	Between 22.6 ± 1.4 ka and 22.4 ± 1.2 ka	Glacifluvial, floodplain of meandering river	SSDS occur within 2 internally deformed layers (thickness from 10 to 35 cm)	9	6
	Dyburiai (Belzyt et al., 2021)	Between 111.9 ± 7.8 ka and 98.7 ± 7.6 ka	Lacustrine	SSDS occur within 10 internally deformed layers (thickness from 5 to 50 cm)	10	12
	Liciškėnai (Woronko et al., 2018)	Between 68.0 ± 6.2 ka and 56.8 ± 5.1 ka	Glacilacustrine	SSDS occur chaotically in 5 m thick exposure	5	20
	Giržadai	Between 19.3 ± 0.13 ka and 17.88 ± 0.95 ka	Glacilacustrine	SSDS occur within a few internally deformed layers (thickness from 4 to 15 cm)	10	8
Germany	Weisser Berg (Hoffmann & Reicherter, 2011; Pisarska-Jamroży et al., 2022)	Between 20.6 ± 2.6 ka and 16.7 ± 2.2 ka	Glacilacustrine	SSDS occur within 3 internally deformed layers (thickness from 4 to 35 cm)	19	11
	Dwasieden (Pisarska-Jamroży et al., 2018, 2019a)	Between 22.7 ± 1.9 ka and 19.0 ± 2.3 ka	Glacilacustrine	SSDS occur within 2 internally deformed layers (thickness from 20 to 40 cm)	6	3

co-occur mainly with the passive concave down structures, but can also be associated with the evolution of active concave down structures (Figure 2j).

The **active concave down structures (AD)** are represented by load structures as load casts or pseudonodules (Figure $2b_2$, 2h, and 2j). They are characterized by (a) regular, mostly rounded shape, (b) well-marked internal lamination usually co-shaped with the external shape of the form, (c) their occurrence mostly at irregular intervals, and (d) reaching the similar depths that depend on the thickness of the lower layer. The AD develop in the upper layer (=deforming layer), the sediments of which sink downwards (=loading) and cause deformation of the lower layer (=deformed layer). The AD occur in sediments where at least one (lower) layer undergo liquefaction and the second (upper) layer is prone for plastic deformation. The AD co-occur mostly with the passive concave up structures.

The **passive concave up structures (PU)** are represented by flame structures and diapir-like structures (Figure $2b_2$ and 2h) which are characterized by (a) massive or laminated, curved structure, (b) mostly similar heights, (c) relatively regular rounded shape, directed upward, and (d) occurrence mostly at regular intervals. The PU develop in the source lower layer (=deformed layer) and do not lead to breaking the continuity of the upper layer (=deforming layer). Their formation is related to the liquefaction of both layers or liquefaction of one (lower) layer and plasticity of the second (upper) layer. The pore pressure in the lower layer is insufficiently strong for upward injection and the loading of sediments initiates deformation process from the upper layer. The PU co-occur with the AD.

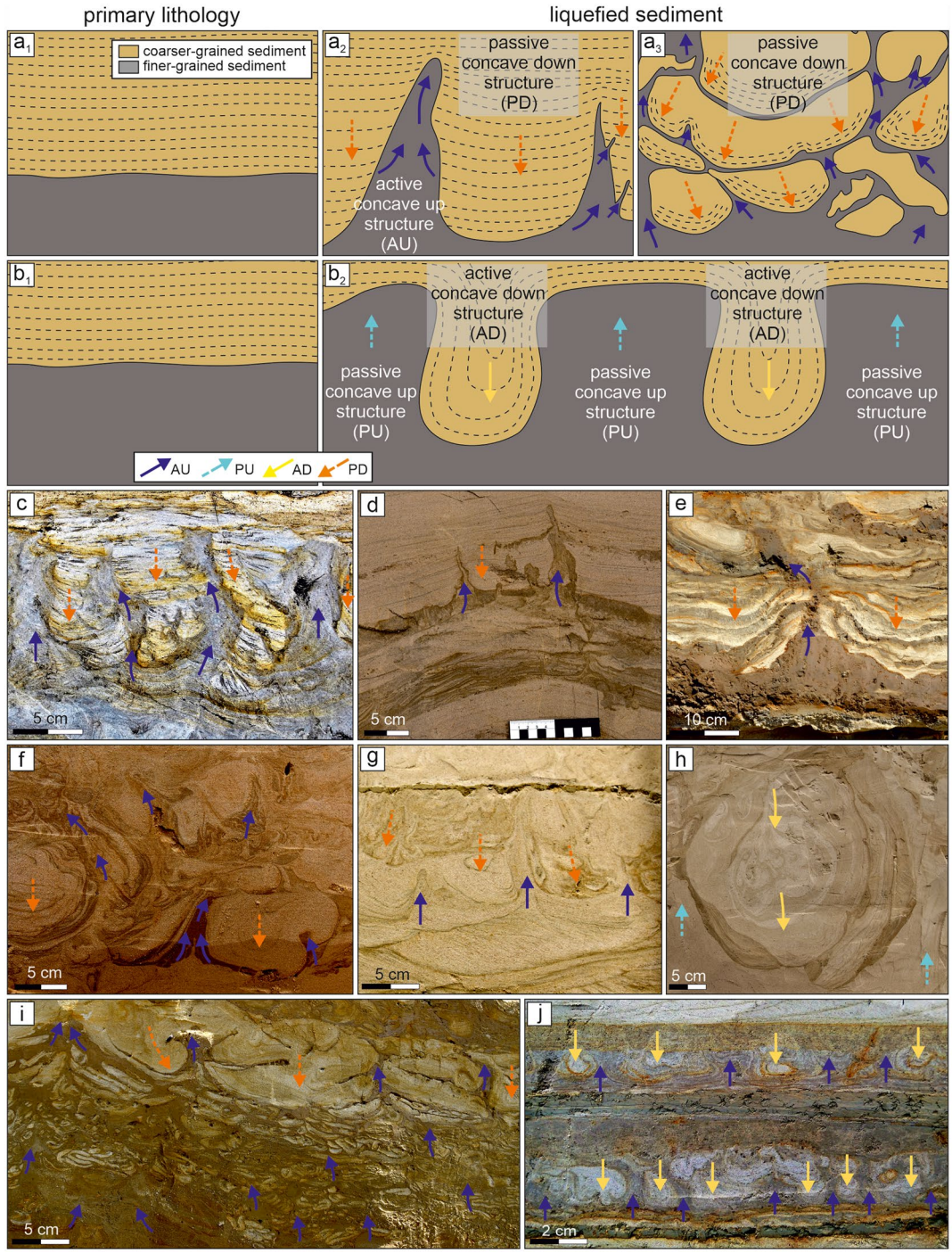

Figure 2. Characteristics of active concave down structures (AD), active concave up structures (AU), passive concave up structures (PU) and passive concave down structures (PD) and their field examples. (a, b) Schematic evolution of AD, AU, PU and PD and their relationships. (c) PD (load casts with preserved non-deformed internal structure) accompanied by AU (irregular upward injections with narrow and sharp ends creating branching structure), Slinkis site. (d) AU (irregular injections with sharp and narrow ends) reaching different heights accompanied by PD (load casts), Sārnate site. (e) AU (irregular injection) accompanied by PD (load casts and ball-and-pillow structures), Dwasieden site. (f) AU (irregular injections with sharp and narrow ends) reaching different heights accompanied by PD (load casts), Liciškėnai site. (g) AU (irregular injections) reaching different heights accompanied by PD (load casts), Dyburiai site. (h) AD (regular, rounded shape load cast) with well-marked internal lamination co-shaped their shape, Liciškėnai site. (i) PD (strongly irregular load casts and pseudonodules) accompanied by AU (clastic dykes, injections), Weisser Berg site. (j) Two levels with AD (load casts and pseudonodules of regular shapes reaching the similar depths) separated by AU, Dyburiai site.

The **passive concave down structures (PD)** are represented by load structures, such as load casts and pseudonodules, but their names do not correspond to the loading process itself, which is commonly known to be responsible for their development (Figure 2a$_3$, 2c–2g, and 2i). In 2019, the process of the development of such concave down structures was explained by Pisarska-Jamroży et al. (2019a) and named as pseudoloading by Belzyt et al. (2021). The PD are characterized by (a) strongly irregular shape, (b) similar heights, (c) well-marked primary internal structure, which is not plastically deformed or is only slightly curved but exclusively in the outermost parts, (d) being attached or detached to the upper source layer (Figure 2c). The sediments that the PD are composed of are usually not mobilized, and they develop as an effect of a rapid act of injections (often multi-directional) of the underlying liquefied sediments (=deforming layer), leaving no visible evidence of loading. Injection structures cause the disruption and separation of the overlying sediments (=deformed layer). The PD co-occur with the AU.

3.2. Materials

We present the results of grain-size analysis of 144 samples collected from eight study sites, where SSDS, induced by liquefaction, were recognized (Nartišs et al., 2018; Pisarska-Jamroży et al., 2018, 2019a, 2019b; Woronko et al., 2018; Woźniak et al., 2021), and the age of sediment deformation was estimated using the Optically Simulation Luminescence (OSL) method (Table 1). We analyzed the deformed sediments occurring within separate, laterally continuous layers interbedded by undeformed sediments, recorded over a large area of the outcrop. The exceptions are the Licišķėnai and Sārnate sites, where the deformed sediments are not limited to laterally continuous layers and cover almost the entire vertical sequence of the outcrop (Nartišs et al., 2018; Woronko et al., 2018).

3.3. Methods

We analyzed samples from 72 concave down structures (51 passive, 21 active) and 72 concave up structures (69 active and only 3 passive). From each concave up structures and concave down structures a 4 g sample was collected, and then the particle size was analyzed by the laser diffraction method using Malvern Mastersizer 2000 (with Hydro 2000G analyzer). The relatively small samples were collected to avoid sediment mixing and the possible contamination of the surrounding sediments. In cases of very small structures (e.g., pseudonodules or load casts with diameter below 2 cm, see Figures 2i and 2j), we carefully collected samples of the whole structure. In other cases of bigger structures, we collected multiple (two to four) samples from the central parts. The volumetric distribution, informing about the percentage share of individual sediment fractions for all 144 samples, was obtained. In each sample, grain-size distribution was analyzed using the GRADISTAT software (Blott & Pye, 2001). The grain size was classified according to Friedman and Sanders (1978) (Figure 3). The statistical analysis was based on determining the basic parameters such as mean diameter, skewness, sorting and kurtosis. The calculations were made using the logarithmic graphical measures of Folk and Ward (1957). We calculated (using STATISTICA software) the ratio of one fraction to the other, the Pearson correlation coefficient ($p < 0.05$) between all designated dependent and independent variables and we performed the Mann-Whitney tests (Cohen, 1988; Mann & Whitney, 1947; Wilcoxon, 1949). The median is a measure of the central tendency for the test used. The following alternative and zero hypotheses were used to compare the statistical significance between the values for concave up and concave down structures, for example,:

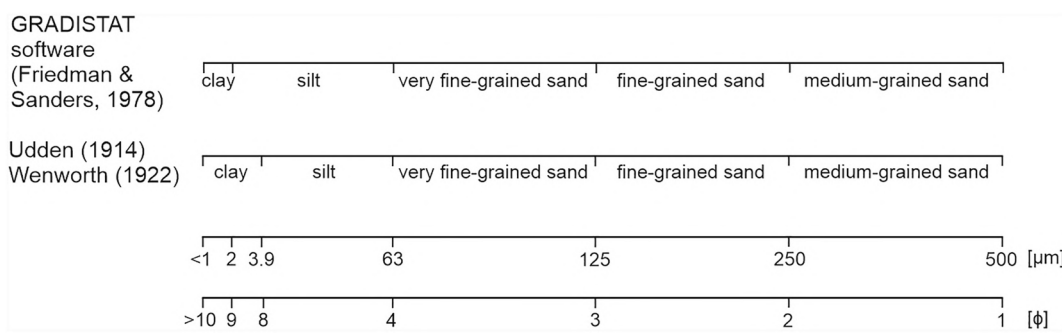

Figure 3. Grain-size distribution used in the present study (Friedman & Sanders, 1978) with relation to the Udden (1914) and Wentworth (1922) scale.

H_0: the median content of the clay fraction in the tested samples is the same in the population of concave up structures and concave down structures:

$$H_0 : \theta_1 = \theta_2$$

H_1: the median content of the clay fraction in the tested samples is different for the population of concave up structures and concave down structures:

$$H_1 : \theta_1 \neq \theta_2$$

where: θ_1, θ_2 are the medians of the clay fraction content in samples of concave up structures and concave down structures, respectively.

The p value was determined and then compared with the significance level α (0.05 and 0.001).

$$\text{If } p \leqslant \alpha \text{ then we reject } H_0, \text{assuming } H_1,$$

$$\text{if } p > \alpha \text{ then we assume the hypothesis } H_0.$$

In the analyses, the Mann-Whitney test continuity correction was applied (Marascuilo & McSweeney, 1977). In addition, a similar parametric Student's t-test was carried out, comparing the arithmetic means of the studied variables. Analogously to the Mann-Whitney test, the zero hypothesis (the means are the same) and the alternative hypothesis (the means differ significantly) were used. If $p \leqslant \alpha$, the Fisher-Snedocor F test was additionally performed, examining the statistical significance of the variance in both populations (Fisher, 1925). Due to the small number of PU samples, we did not take them into account in statistical analyses.

Most of the research is aimed to predict the occurrence of liquefaction in the specific sediments and to calculate the liquid limit (Andrews & Martin, 2000; Chang et al., 2015; Othman et al., 2018; Othman & Marto, 2018). The liquid limit criterion together with the clay content criterion are key sediment parameters that help in partitioning the silty sediments into liquefiable and non-liquefiable (Andrews & Martin, 2000). The liquid limit of a sediment is a measure of the grain spacing at which the net attractive force produces a shear strength of approximately 25 g/cm^2 (Seed et al., 1964). The sediments studied in this paper underwent liquefaction in the past. Thus, intentionally, we do not calculate the liquid limit, commonly used to determine the probability of liquefaction of a sediment. Thus far, the sedimentological analyses of sediments prone to liquefaction have been limited to the grain size fraction content and distribution analysis, and have not included the determination of interdependencies between each fraction content or the detailed statistical characteristics. Even the basic sorting value has most often been presented as a descriptive feature without providing the exact statistical data.

4. Results

4.1. Comparison of Basic Features of Sediments in Concave Down Structures and Concave Up Structures

The grain size analysis of the 144 samples of sediments allowed us to determine the fraction distribution, mean diameter, skewness, sorting and kurtosis (Table 2; Figures 4 and 5).

Concave up structure sediments are generally characterized (Table 2; Figure 4) by very high content of silt and relatively low content of very fine- and fine-grained sand (Figure 4a). Concave down structure sediments are characterized by a predominance of very fine- and fine-grained sand and a much lower content of silt than in concave up structures (Figure 4a). The content of the clay in concave up structure sediments varies between 2% and 14%, while in concave down structure sediments between 0% and 3% (Figure 4a).

The concave up structure sediments (Table 2; Figure 4b) are characterized by a finer mean grain diameter and wider range than concave down sediments. Significant differences in parameter values are noted between passive and active structures (Table 2; Figure 5b).

The sediment sorting value is over twice higher in concave up structures, which are mainly poorly/very poorly sorted, than in concave down structures, which are moderately/moderately well sorted (Table 2; Figure 4c). Kurtosis values for concave up structures and concave down structure sediments are comparable (Table 2). Most sediments in concave up structures and concave down structures (Table 2; Figure 4d) have leptokurtic/very and

Table 2
Comparison of Quantitative Features of Concave Up Structures and Concave Down Structures Divided Into Active and Passive ($\bar{x}$, Arithmetic Value; Me, Median)

	Concave up structures (n = 72)		Concave down structures (n = 72)	
	AU—active concave up structures (n = 69)	PU—passive concave up structures (n = 3)	AD—active concave down structures (n = 21)	PD—passive concave down structures (n = 51)
Fraction content	Clay 2%–14% ($\bar{x}$ = 5%; Me = 4%)		Clay 0%–3% ($\bar{x}$ = Me = 1%)	
	Silt 40%–89% ($\bar{x}$ = 69%; Me = 73%)		Silt 3%–45% ($\bar{x}$ = 22%, Me = 20%)	
	V. fine sand 0%–50% ($\bar{x}$ = 22%; Me = 20%)		V. fine sand 9%–74% ($\bar{x}$ = Me = 47%)	
	Fine sand 0%–18% ($\bar{x}$ = 3%; Me = 2%)		Fine sand 5%–51% ($\bar{x}$ = Me = 27%)	
	Medium sand 0%–3% ($\bar{x}$ = Me = 0%)		Medium sand 0%–35% ($\bar{x}$ = 3%, Me = 0%)	
	Clay 2%–14% ($\bar{x}$ = 5%; Me = 4%)	Clay 2%–3% ($\bar{x}$ = Me = 2%)	Clay 0%–3% ($\bar{x}$ = Me = 1%)	Clay 0%–3% ($\bar{x}$ = Me = 1%)
	Silt 40%–89% ($\bar{x}$ = 70%; Me = 75%)	Silt 45%–55% ($\bar{x}$ = 49%, Me = 47%)	Silt 10%–42% ($\bar{x}$ = Me = 25%)	Silt 3%–45% ($\bar{x}$ = 21%, Me = 19%)
	V. fine sand 0%–50% ($\bar{x}$ = 21%; Me = 20%)	V. fine sand 35%–40% ($\bar{x}$ = Me = 38%)	V. fine sand 21%–57% ($\bar{x}$ = 48%, Me = 50%)	V. fine sand 9%–74% ($\bar{x}$ = 46; Me = 45%)
	Fine sand 0%–18% ($\bar{x}$ = 3%; Me = 2%)	Fine sand 8%–14% ($\bar{x}$ = 12%, Me = 13%)	Fine sand 15%–43% ($\bar{x}$ = 25, Me = 23%)	Fine sand 5%–51% ($\bar{x}$ = Me = 28%)
	Medium sand 0%–3% ($\bar{x}$ = Me = 0%)	Medium sand 0% ($\bar{x}$ = Me = 0%)	Medium sand 0%–24% ($\bar{x}$ = 2%, Me = 0%)	Medium sand 0%–35% ($\bar{x}$ = 4%, Me = 1%)
Mean diameter	2.25–5.38ϕ ($\bar{x}$ = 3.59ϕ; Me = 3.46ϕ)		1.36–2.57ϕ ($\bar{x}$ = 2.23ϕ; Me = 2.26ϕ)	
	2.26–5.38ϕ ($\bar{x}$ = 3.64ϕ; Me = 3.55ϕ)	2.25–2.32ϕ ($\bar{x}$ = 2.29ϕ; Me = 2.30ϕ)	1.65–2.50ϕ ($\bar{x}$ = 2.29ϕ; Me = 2.34ϕ)	1.36–2.57ϕ ($\bar{x}$ = 2.20ϕ; Me = 2.22ϕ)
Skewness	−0.19–0.74 ($\bar{x}$ = 0.40; Me = 0.46)		−0.26–0.37 ($\bar{x}$ = 0; Me = −0.02)	
	−0.13–0.74 ($\bar{x}$ = 0.42; Me = 0.51)	−0.19–0.40 ($\bar{x}$ = 0.14; Me = 0.21)	−0.26–0.26 ($\bar{x}$ = −0.08; Me = −0.16)	−0.26–0.37 ($\bar{x}$ = 0.04; Me = 0.07)
Sorting	0.57–2.07ϕ ($\bar{x}$ = 1.46ϕ; Me = 1.57ϕ)		0.46–1.37ϕ ($\bar{x}$ = 0.79ϕ; Me = 0.70ϕ)	
	Poorly & very p. 80%		Poorly 21%	
	Moderately 20%		Moderately & m. well 75%	
			Well sorted 4%	
	0.65–2.07ϕ ($\bar{x}$ = 1.53ϕ; Me = 1.62ϕ)	0.57–0.92ϕ ($\bar{x}$ = 0.69ϕ; Me = 0.59ϕ)	0.46–1.28ϕ ($\bar{x}$ = 0.68ϕ; Me = 0.63ϕ)	0.46–1.37ϕ ($\bar{x}$ = 0.84ϕ; Me = 0.77ϕ)
	Poorly & very poorly 84%	Moderately 100%	Poorly 8%	Poorly 25%
			Moderately & m. well 82%	Moderately & m. well 73%
	Moderately 16%		Well sorted 10%	Well sorted 2%
Kurtosis	0.63–3.31 ($\bar{x}$ = 1.56; Me = 1.07)		0.75–3.10 ($\bar{x}$ = 1.52; Me = 1.22)	
	Leptokurtic, very l. & extremely l. 47%		Leptokurtic, very l. & extremely l. 58%	
	Platykurtic & very p. 44%		Platykurtic 25%	
	Mesokurtic 9%		Mesokurtic 17%	
	0.63–3.31 ($\bar{x}$ = 1.55; Me = 0.99)	1.23–2.65 ($\bar{x}$ = 1.78; Me = 1.42)	0.80–2.39 ($\bar{x}$ = 1.32; Me = 1.15)	0.75–3.10 ($\bar{x}$ = 1.60; Me = 1.62)
	Platykurtic & very p. 47%	Leptokurtic 100%	Platykurtic 33%	Leptokurtic, very l. & extremely. l. 63%
	Leptokurtic, very l. & extremely l. 44%			Platykurtic 21%
			Leptokurtic & very l. 48%	
	Mesokurtic 9%		Mesokurtic 19%	Mesokurtic 16%

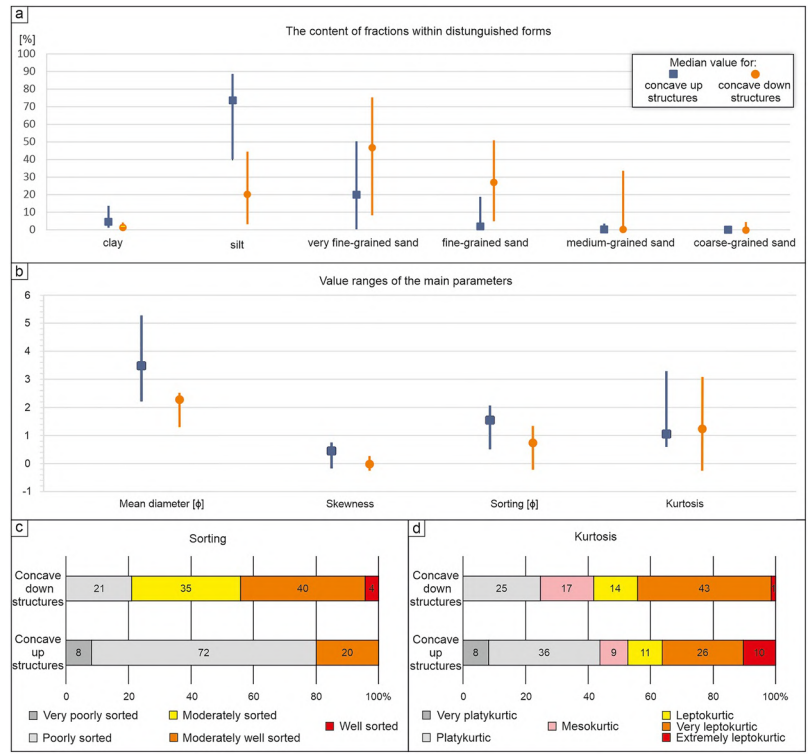

Figure 4. Individual values of fractions and parameters and their share for concave up structures and concave down structures for (a) fractions, (b) basic statistical parameters, (c) sorting and (d) kurtosis.

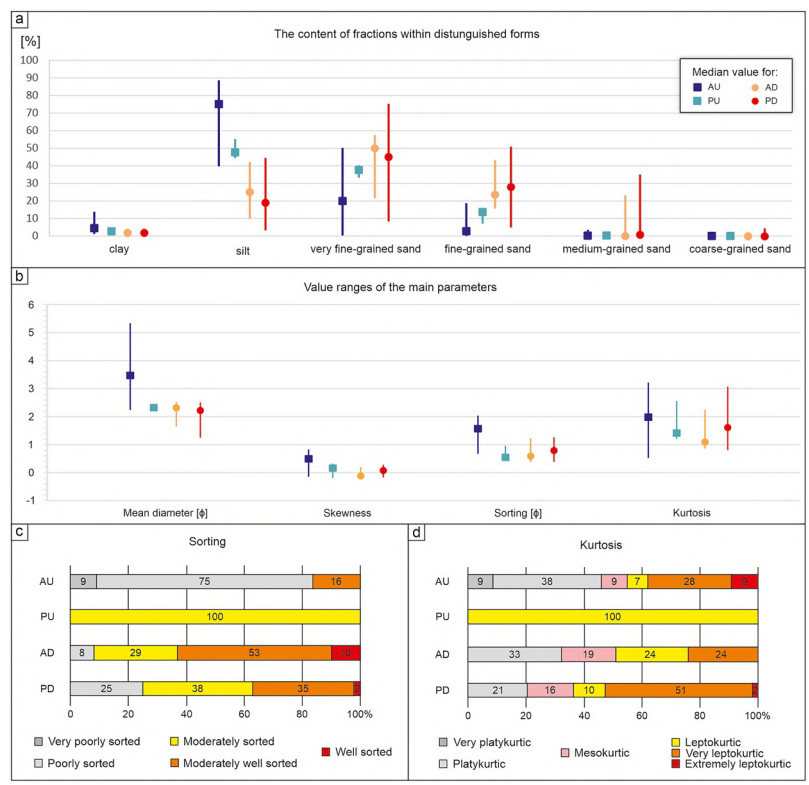

Figure 5. Individual values of fractions and grain-size parameters and their share for active and passive concave up structures and active and passive concave down structures for (a) fractions, (b) basic statistical parameters, (c) sorting and (d) kurtosis.

extremely leptokurtic distribution. More platykurtic distributions were noted in concave up structure sediments than in concave down structure sediments (Table 2; Figure 5d).

The common ranges of fractions content and granulometric parameters for both concave up structures and concave down structures were recognized (Figure 6). The common range is very narrow for clay (2%–3%), silt (40%–45%) and medium-grained sand (0%–3%), whereas for very fine-grained sand they are wide (9%–50%) (Figure 6a). The common ranges are also noticed in the mean diameter (2.26–2.57ϕ), the sorting (0.57–1.37ϕ), the skewness (−0.19–0.37), and in the case of the kurtosis (0.75–3.1) (Figure 6b).

4.2. Comparison of Cumulative Curves

The shape of cumulative curves, prepared separately for each study site (Figure 7), clearly differentiate sediments within concave up structures and concave down structures. Three curve types (A–C) were distinguished on the basis of their shapes resulting from the variable content of clay, silt and very fine-grained sand fraction (Figure 3).

The A type includes those where cumulative curves for concave up structures and concave down structures have a different shape and are clearly separated from each other. Concave down structure sediments are characterized by a low share of the clay fraction (up to 3%), a low share of the silt fraction (7%–27%) and a high share of the sand fraction (70%–90%), while in the concave up structure sediments the share of clay and silt fractions are similar.

The B type includes one curve with similar shape for concave up structures and concave down structures, but clearly shifted to each other. The samples from concave down structures are characterized by the absence of a clay fraction, a low share of the silt fraction (up to 10%) and a very high share of the sand fraction (especially very fine sand—90% to 97%), while in concave up structures, the content of clay is up to 3% and the silt fraction is in the range from 50% to 93%.

The C type includes curves whose shape is very similar for concave up structures and concave down structures (only slightly steeper for concave up structures than for concave down structures). The content of the clay fraction is low and does not exceed 4%. Concave up structures differ from concave down structures in terms of the content of the silt fraction. There is also a difference in the share of the sand fraction. For concave up structures it does not exceed 50%, while for concave down structures it reaches even 90% but never drops below 80%.

4.3. Relationships and Trend Analysis for Sediments in Concave Up Structures and Concave Down Structures

Five zones were distinguished on the basis of fractions content: a concave down structures zone, concave up structures zone, “transitional zone” and two gap zones I and II (Figure 8). The concave down structures zone contains sediments characterized by very small content of silt and clay fractions, with high content of fine- and very fine-grained sand. The concave up structures zone includes sediments with high content of silt (>55%),

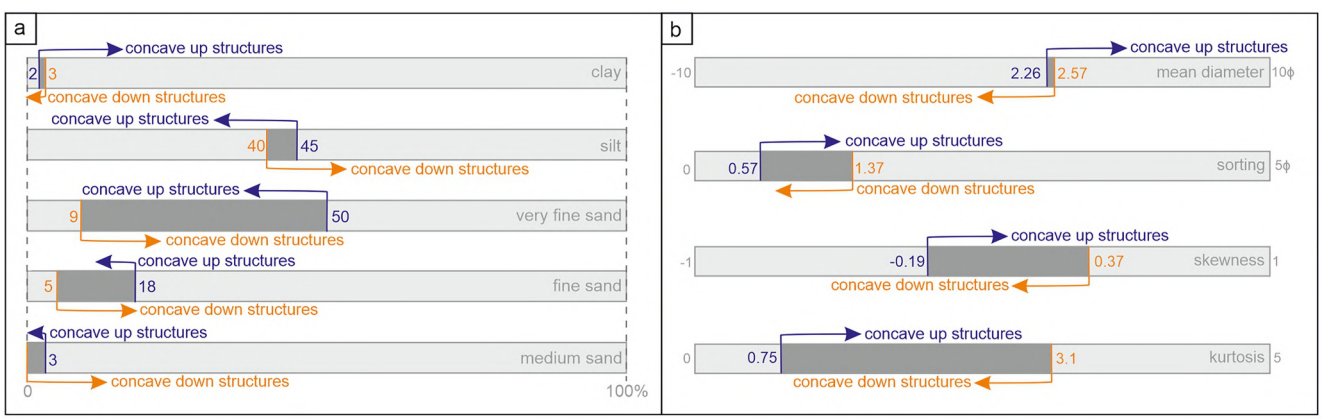

Figure 6. Range of common (dark gray color): (a) grain size content [%] in concave up structures and concave down structures, (b) grain size statistical parameters according to Folk and Ward (1957) in concave up structures and concave down structures.

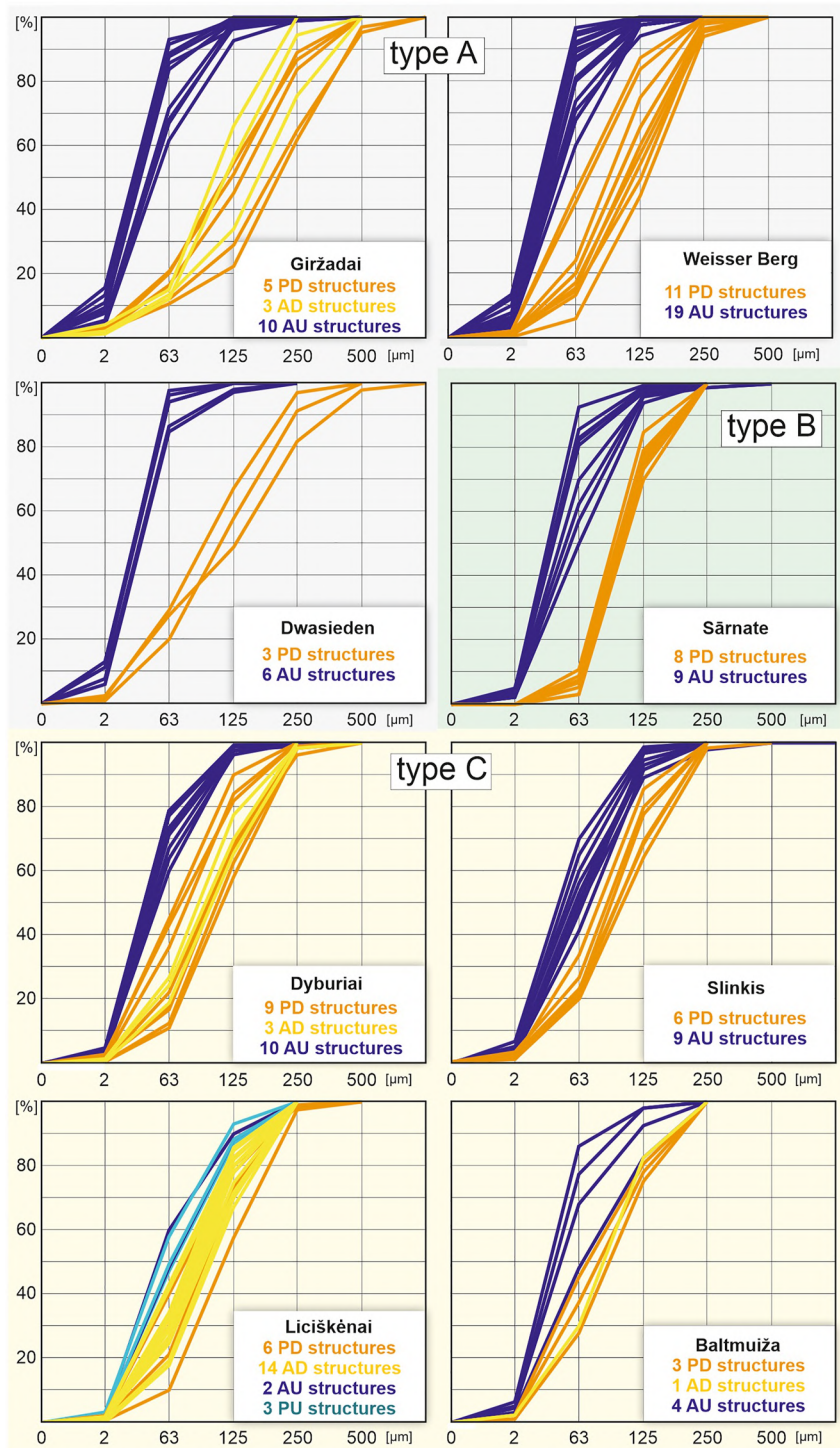

Figure 7. Three distinguished types of cumulative curves of all samples.

maximum 14% of clay and up to 45% of sand (fine and very fine-grained). We also distinguished a zone that we called a "transitional zone," wherein concave up structure and concave down structure sediments overlap (Figure 8). The "transitional zone" is characterized by sediments with similar content of sand and the sum of silt and clay fractions (ca. 50:50). Furthermore, the sediments creating a "transitional zone" are distinctly separated from the sediments in the concave up structures and concave down structures zones by two "gap zones" (Figure 8), where no samples were recorded. We called those two zones: "gap zone I" and "gap zone II." The

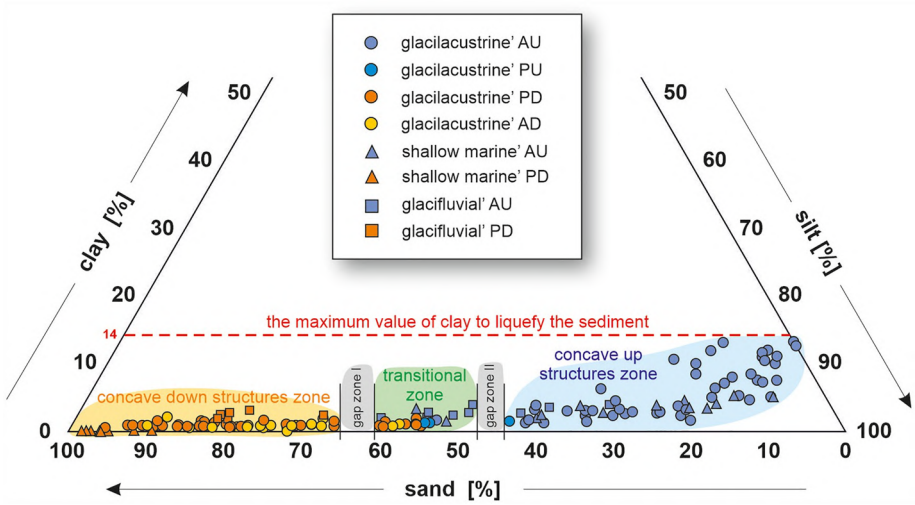

Figure 8. Triangle texture classification with division into sedimentary environments and distinguished active (AU) and passive concave up structures (PU), as well as active (AD) and passive concave down structures (PD). For details, see Figure 2.

"gap zone I" occurs for sand values of ca. 60%–65% and silt of ca. 35%–40%, while the "gap zone II" occurs for ca. 45%–50% of sand and ca. 50%–55% of silt (Figure 8).

Very strong statistically significant relationships were observed between some fractions (see red numbers in Table 3). An upward trend between the share of the very fine-grained sand fraction and the sum of the whole sand fraction (Figure 9a) is visible for concave up structures ($R = 0.92$). Concave down structures show no trend ($R = -0.24$). The general share of sand fraction increases only with the increasing share of very fine sand (Figure 9a). In the case of concave down structures, it was determined that the content of the sand fraction is between 53% and 97% (Figure 9a), and the share of very fine-grained sand varies (Figure 9b). For both concave up structures and concave down structures, the trend of the share of the sand fraction and the share of the silt fraction is downward, that is, the more silt, the lower the sand fraction share ($R = -0.99$; Figure 9b).

Relationships between the content of the clay fraction and other fractions were also observed. In the case of concave up structures, a downward trend was noticed, that is, the more clay, the less very fine-grained sand

Table 3
Correlation Coefficient Between the Examined Parameters

Fractions	Clay (<2.0 μm)	Silt (2.0-63 μm)	Clay + silt (<63 μm)	Very fine sand (63-125 μm)	Fine sand (125-250 μm)	Medium sand (250-500 μm)	Sand (>63 μm)
Clay (<2.0 μm)	X	0.53	0.74	-0.5	-0.22	0.21	-0.58
Silt (2.0-63 μm)	0.62	X	0.99	-0.64	-0.7	-0.26	-0.99
Clay + silt (<63 μm)	0.58	0.99	X	-0.24	-0.69	-0.24	-1
Very fine sand (63-125 μm)	-0.76	-0.96	-0.98	X	-0.2	-0.47	0.24
Fine sand (125-250 μm)	-0.48	-0.82	-0.8	0.71	X	0.5	0.69
Medium sand (250-500 μm)	-0.08	-0.09	-0.09	0.14	0.3	X	0.24
Sand (>63 μm)	-0.75	-0.99	-1	0.98	0.8	0.09	X

concave up structures concave down structures -0.98 very strong correlation ($p<0.05$)

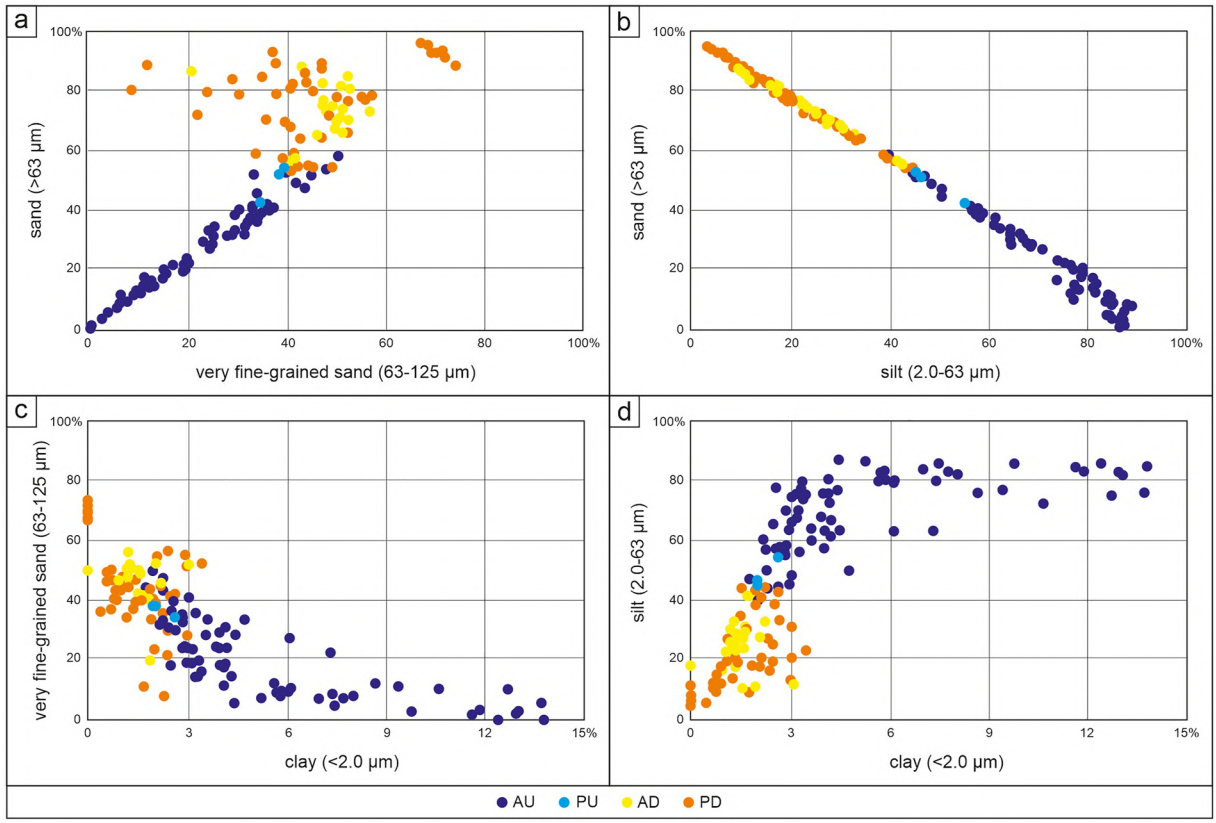

Figure 9. Relationship between the content of fractions.

(Figure 9c). For concave down structures, in turn, no regularity was noticed. However, it should be emphasized that most of the samples have a content of very fine-grained sand between 35% and 60%, with clay content of 0%–3% (Figure 9c). The clay fraction slightly increases (from 0% to 2%–3%) with the increase of the silt fraction (Figure 9d). However, concave down structures are also characterized by a low content of the silt fraction and an increased content of the clay fraction (Figure 9d). In concave up structure sediments, two tendencies were noticed: (a) an increase of the silt fraction in the range of 45%–75% co-occurs with a very slight increase of the clay fraction (Figure 9d), and (b) with the content of silt in the range of 75%–90%, the share of the clay fraction changes in a large range, that is, from 5% to 14% (Figure 9d).

In the case of concave up structure sediments, the higher grains mean diameter [ϕ], the poorer sorting ($R = 0.92$). Concave down structure sediments are characterized mainly by moderate sorting (Figure 10a) in the range of 0.5–1.0ϕ ($R = -0.53$) and more negative skewness values (Figure 10b) than concave up structures. In the case of concave down structures—the more positive the skewness, the poorer sorting of sediments ($R = 0.82$) (Figure 10b). The relationship between the mean diameter and skewness shows several regularities (Figure 10c). Most concave down structures samples are in the range of 2–3ϕ and skewness values between −0.2 and 0.4. For concave up structures, three zones are visible: (a) when the diameter grows [ϕ], the skewness increases (range 2–3ϕ), (b) in the range of 3.2–3.8ϕ, the skewness remains at the level of 0.6, and (c) above 3.8ϕ, the skewness decreases. A certain trend between sorting and kurtosis was observed for concave up structure and concave down structure sediments (Figure 10d)—the poorer the sorting, the lower the kurtosis value ($R = -0.81$ for concave up structures) or the higher the kurtosis value ($R = 0.55$ for concave down structures). The same and slightly more pronounced trends were observed between the mean diameter and kurtosis (Figure 10e; $R = 0.31$ for concave down structures; $R = -0.81$ for concave up structures). No relationship was observed for concave up structures between skewness and kurtosis (Figure 10f). It is worth noting that for the value of kurtosis 0.5–1.0, the value of skewness occurs in the entire range, that is, −0.3–0.7 ($R = 0.33$ for concave up structure; $R = 0.81$ for concave down structures).

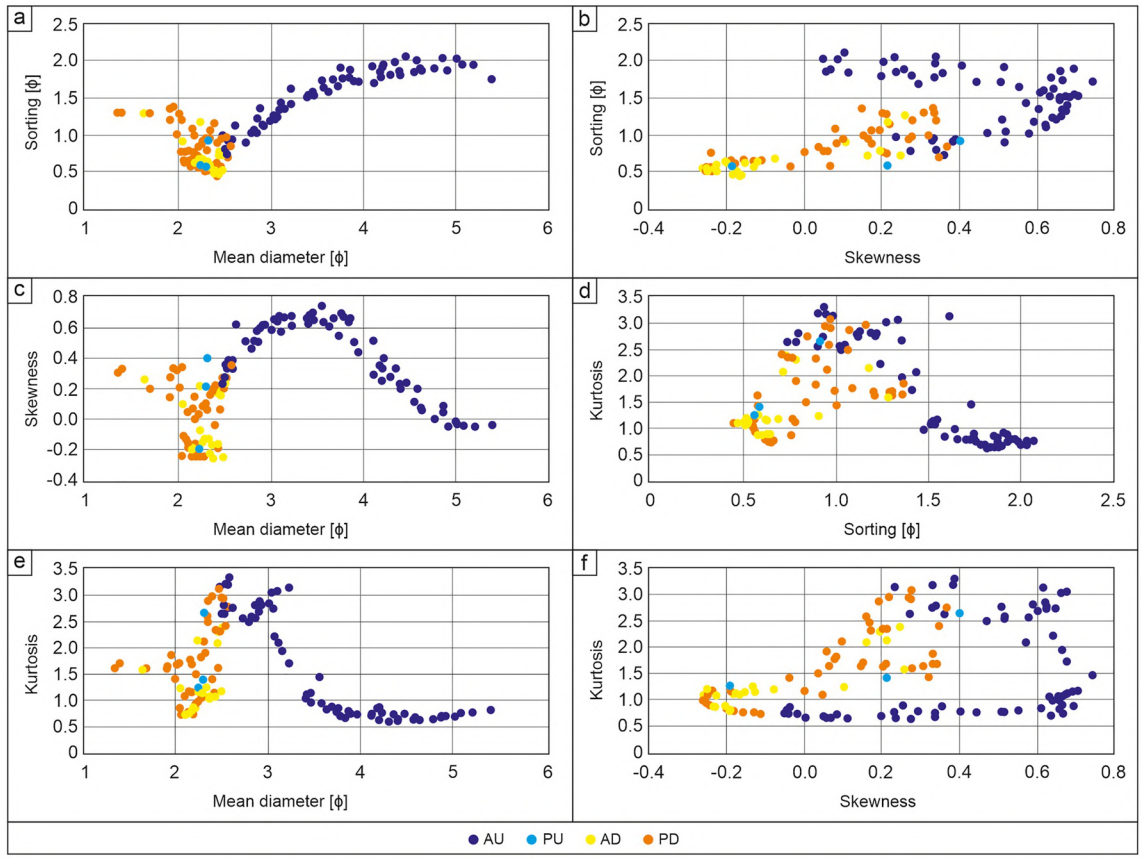

Figure 10. Relationships between basic statistical parameters.

Very strong linear correlations and regressions were also observed between the analyzed fractions, where the correlation coefficient $R \geq |0.99|$ (Table 4). Statistical significance tests allowed us to check the significance of the studied variables, that is, each detected sediment fraction (>0ϕ) and four basic statistical parameters: mean diameter, sorting, skewness and kurtosis. In the Mann-Whitney test ($p < 0.05$) there was a statistically significant difference between the studied variables (Table 5). Complementary analyses of the *t*-Student's test and the Fisher-Snedocor test showed that the most statistically significant differences (in all four analyses) were visible for the content of the clay fraction, fine-grained sand fraction, medium-grained sand fraction, medium diameter, sorting and skewness. None of the tests showed a statistically significant difference for the 0–1ϕ fraction and kurtosis parameter.

Table 4
Trend Function Equations for the Correlation $r \geq |0.99|$ ($p < 0.05$)

Y and X values	Concave up structures	Concave down structures
Y: silt, *X*: silt + clay,	$Y = 0.844x + 6.413$	$Y = 0.958x - 0.465$
Y: silt, *X*: sand,	$Y = -0.844x + 90.807$	$Y = -0.958x + 95.335$
Y: sand, *X*: silt + clay,	$Y = -1x + 100.003$	$Y = -1x + 100$

5. Discussion

The studied sediments (Table 1), deposited in lacustrine, shallow marine or fluvial environments (Belzyt et al., 2021; Bitinas et al., 2021; Pisarska-Jamroży et al., 2019a, 2022; Woźniak et al., 2021), had a high potential for their liquefaction. The sediments were water-saturated during deposition and may have remained saturated for a long time after deposition. In all study sediments, the water content and sediment permeability were crucial for sediment saturation and affected the course and depositional effect of the liquefaction process (cf. Cui et al., 2022; Owen & Moretti, 2011). The water-saturated condition of sediments above 90%, necessary for the liquefaction to occur, has certainly been met in the case of studied sediments (cf. Seed et al., 1983; Wang, 1979).

Table 5
Trend Function Equations for the Correlation $r \geq |0.99|$ ($p < 0.05$)

	Mann-Whitney test		*t*-Student's test	*F* Fisher-Snedocor test
Analyzed parameters	Statistical significance ($p < 0.05$)	Statistical significance ($p < 0.001$)	Statistical significance ($p < 0.05$)	
Fraction content of 2.0 μm	Yes	Yes	Yes	Yes
Fraction content of 2.0–63 μm	Yes	Yes	Yes	No
Fraction content of 63–125 μm	Yes	Yes	Yes	No
Fraction content of 125–250 μm	Yes	Yes	Yes	Yes
Fraction content of 250–500 μm	Yes	No	Yes	Yes
Fraction content of 500–1,000 μm	No	No	No	No
Value of mean diameter (ϕ)	Yes	Yes	Yes	Yes
Value of sorting (ϕ)	Yes	Yes	Yes	Yes
Value of skewness	Yes	Yes	Yes	Yes
Value of kurtosis	No	No	No	No

The grain size distribution of sediments within concave up structures and concave down structures is related to the pre-deposition history of the environment in which the sediments were deposited (including the energy of transport). According to Youd and Perkins (1978), the possibility for sediment liquefaction depends on their sedimentary environment, and sediment textural and structural features. The features of the primary sediments have the main impact on the course and effect of the liquefaction process.

5.1. Mobilization of Silts

Previous studies were mainly focused on the critical share of the clay fraction in the sediments that undergo deformation, while the content of the silt fraction was often overlooked (Andrews & Martin, 2000; Figueroa et al., 1995; Kishida, 1970; Tuttle et al., 1990; Wang, 1979; Zhou, 1981). However, the presented results show that the abundance of silt and its role in the deformation process are decisive. The mobility of the silt fraction in the sediment initiates the deformation structures development, especially in the case of AU and PU, that is, injection features. Concave up structure sediments contain higher percentage of silt (Me = 73%) than concave down structure sediments (Me = 20%), which was confirmed by many field studies (Belzyt et al., 2021; Pisarska-Jamroży et al., 2018, 2019a, 2019b, 2022; Van Loon et al., 2016; Van Loon & Pisarska-Jamroży, 2014; Woźniak et al., 2021) as well as during laboratory experiments (Othman et al., 2018; Othman & Marto, 2018), and by mathematical models (Bronikowska et al., 2021). Both active structures, that is, AU and AD contain higher percentage of silt (Me = 75% and 25%, respectively) than passive structures (PU and PD) (Table 2). However, the highest silt content in AD is recorded in the "transitional zone," as described in subsections 4.3 and 5.4 (Figure 8), and is always lower than all concave up structure sediments (Table 2). This suggests that the silty sediment is the most prone to mobilization during the liquefaction and fluidization phenomena and facilitates further sand grains mobilization. In addition, it seems that the presence of the silt fraction determines the style of deformation and the nature (i.e., shape) of the structures formed during this process (e.g., injection/load casts).

The mobilization of sediments, that form concave up structures, occurs when the content of the silt fraction is higher than 45% and it does not exceed 90%. Most of the samples have silt content between 60% and 90% (Table 2). It is most likely that the share of silt in sediments subjected to deformation must be a significant admixture in relation to the very fine- and fine-grained sand (Figure 9b). At the same time, these sediments contain a very low share of clay, not exceeding 3% (Figures 8 and 9d). On this basis, it can be concluded that the proportions of the silt fraction to very fine-grained sand fraction may be very diverse (Figures 8 and 9). The obtained results show that the admixture of clay or sand (up to 45%) to the silt fraction is of great importance in the case of silty sediments that undergo liquefaction. Sand grains can increase the porosity of silty sediments, which can affect their permeability and water capacity. On the other hand, the clay mineral characteristics, especially their layered structure, causing their volume increase in contact with water, makes them able to swell. Thus, the clay minerals are agents of sediments plasticizing (Izdebska-Mucha & Wójcik, 2016), which may increase the mobility of liquefied silty sediments under the influence of any driving force (e.g., loading).

When the grain diameter drops below the sand fraction, the skewness becomes very variable in the concave up structure sediments, ranging from ca. 0.5 to ca. 0 (Table 2). These sediments contain the highest amount of clay (Table 2) and represent type A of cumulative curves (Figure 7). It shows that the silty sediments associated with concave up structures (i.e., injected sediments) must be enriched with a slightly coarser sediment—most likely with fine-grained sand, which would balance the high content of the clay fraction and reduce the cohesion of the sediment. This conclusion is confirmed by the lowest sorting values and the lowest values of kurtosis, which is leptokurtic for these sediments (Table 2). Therefore, we can conclude that in the case of concave up structure sediments, two subgroups can be distinguished on the basis of their common textural features: (a) the first, where the silt fraction constitutes a significant admixture in very fine-grained sand, and (b) the second, where the silt fraction constitutes more than 75%, and the clay and fine-grained sand fractions are admixed. Both groups are clearly visible on the cumulative curves and the triangle graph (Figures 7 and 8) as well as on the individual plots of the relationship between basic statistical parameters (Figure 10).

Our observations are in contradiction with Obermeier (1996), who noted that the more silt and clay content is added to sandy sediments, the slimmer the chance of the liquefaction of the sediment. According to our research, water-saturated silt is easily prone to mobilization, while sediments with clay can be mobilized only when their percentage is not too high (it will be discussed in details in subsection 5.3). We strongly recommend considering the percentage of silt and clay not together but separately; additionally in relation with all other individual fractions.

AU are formed in response to high pressure, energy and driving force, giving them a characteristic convex upward shape (Alsop et al., 2022; Cui et al., 2022; Liang et al., 2018). In most cases, the upward injections of water-saturated sediment that create concave up structures should be regarded as the primary and main cause of the whole deformation process. We claim that the injection is often followed by sediment loading and the development of load structures.

5.2. Mobilization of Sands

Sandy sediments are easily mobilized under load due to gravity (Nichols, 1995). In the studied samples, the sand fractions are generally associated with concave down structures. It should be emphasized that this applies to a narrow range of the mean diameter, that is, 2–2.5ϕ, with a large range of skewness from −0.2 to 0.2. This means that the mobilization of these sediments can occur when they have an admixture of coarser and finer grains, in this case most likely silty (cf. Mycielska-Dowgiałło & Rutkowski, 2007). Two subgroups of sands can be distinguished: (a) the first characterized by negative skewness, good sorting, related mainly to AD, and (b) the second characterized by positive skewness, poor sorting and very diverse kurtosis value, typical mainly for PD (Figure 10).

AD are better sorted than AU, that is, most of the sediments in AD (82% of samples) are moderately and moderately well sorted. Porosity and permeability of these sandy sediments are greater, and their saturation could also be greater. Water fills the pores of the sediment and adds to the sediment's weight, which has resulted in greater density differences between the sediments in AD and the surrounding sediments.

The relationship between the porosity and the ability to mobilize sediment grains may also confirm the poorer sorting of sediments in PD than in AD. The mobilization of sandy grains in sandy sediments is hampered by effective internal friction, that is, sandy sediments when pressure is applied (e.g., during liquefaction) behave like sandpapers in contact with each other, which becomes much more resistant to the movement. Such an arrangement changes the increase of the finer fraction (e.g., silt) in sediments, which improves the plasticity of the sediments and their mobilization. The finer grains partially infill the pores between the coarser ones, as a result of which the saturated sediment behaves during liquefaction as a homogeneous plastic mass (cf. Van Loon et al., 2020).

Concave down structures (load casts, pseudonodules and also ball-and-pillow structures) arise as a result of the liquefaction and coexistence of unstable density layering. The key factors giving them a concave shape are mass and gravity (Moretti et al., 2001). The participation of external factors (force, pressure) is definitely smaller. Concave down structures are characterized by higher content of the sand fraction than the silt fraction. Saturated sand overlying saturated finer sediment is gravitationally unstable, allowing the sand to sink into a finer sediment when they are liquefied (Mills, 1983; Owen & Moretti, 2011). During the formation of concave down structures, the lower layers composed of finer sediments strive to achieve a density equilibrium by forming, for example, flame structures (Oliveira et al., 2011).

Although the concave down structures contain a very high content of sand, no significant relationships between the other fractions were noted. In the case of concave up structures, the content of sand depends on both the

content of the clay and silt fractions. Moreover, the fraction of very fine-grained sand plays the greatest role. The share of sand above 40% significantly reduces the susceptibility of sediments to liquefaction and the development of concave up structures. The content of all the sand fractions between 50% and 60% is a "transitional zone" in which all the tested types of forms are found.

5.3. Clay Fraction—For and Against Mobilization

The highest percentage content of clay occurs in AU (four times higher than in AD and PD and twice higher than in PU). The clay grains population influences the cohesive strength of sediments. Andrews and Martin (2000) noted that clay content can be regarded as a "key" soil parameter that partitions liquefiable and non-liquefiable silty soils. It seems to be confirmed, but only if the share of clay in the sediment is very high. Our results clearly show that the share of the clay fraction in sediments subject to plastic deformation cannot be higher than 14%, assuming additionally that the sediment is both very silty and has a small admixture of sand (Figures 7 and 8). This is consistent with the results obtained by Andrews and Martin (2000) and Seed et al. (1983), who suggest that the maximum content of the clay fraction in sediments, which allows sediment plastic deformation, is 15%. According to others, this value should not exceed 8%–10% (Figueroa et al., 1995; Kishida, 1970). As is known, the cohesion influences the plasticity of sediments (e.g., Tchakalova & Ivanov, 2022) and the degree of plasticity depends on the type and size of grains as well as the amount of water (e.g., Moreno-Maroto & Alonso-Azcárate, 2018; Muttashar et al., 2020; Yong, 1999; Yong & Warkentin, 1966). All the samples analyzed by us are characterized by a low content of the clay fraction (<14%), which allows the liquefaction and fluidization of the sediments.

5.4. Sediments in "Transitional Zone"

The results of the grain size analysis of sediments deformed in natural conditions point to the existence of a group/zone of sediments in which it is difficult to clearly determine which kind of deformation structures (concave up structures or concave down structures) will develop. This zone includes the overlapped sediments of different genesis and all forms (AU, PU, AD, PD), and is characterized by the content of sand of 48%–60%, silt of 39%–50% and very low content of clay (1%–3%). This so-called "transitional zone" (Figures 7–11) is most likely composed of sediments in which the proportion of the silt and sand fractions is at the level of concave up structures and concave down structures threshold values. Thus even slight changes in the silt content can determine whether the loading or injection process will take place, and—as a consequence—whether the concave up structures and concave down structures will develop. This emphasizes the importance of the silt fraction in the development of deformation structures during the liquefaction process.

Although no samples of liquefied sediments were observed in the gap zones, we can estimate the possible ranges of the individual fractions content using data interpolation (Figures 11 and 12, Table 4). The interpolated data (Figure 11) have a high Pearson correlation coefficient (R = 0.95 for concave down structures, R = 0.98 for

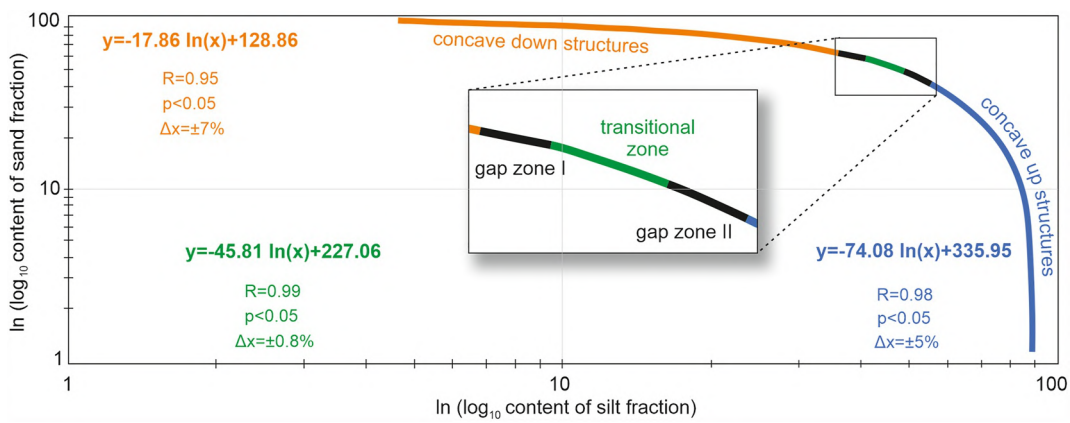

Figure 11. Relationship between the content of silt and sand fractions, their logarithmic trends and equations of functions for concave up structures and concave down structures.

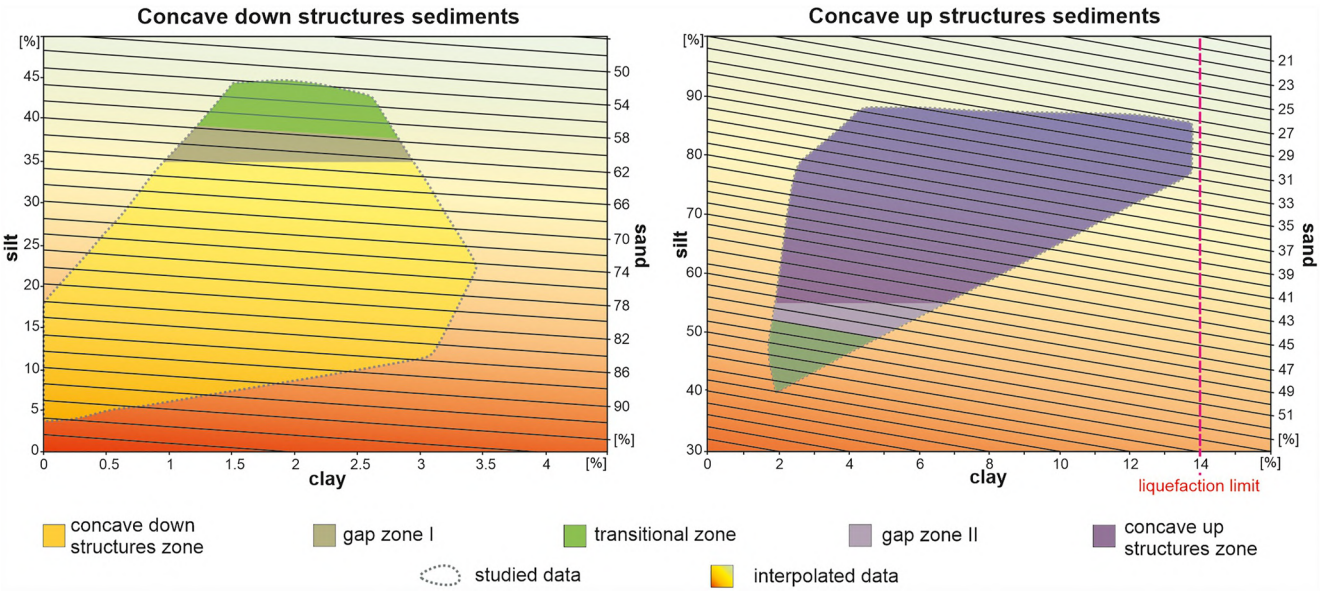

Figure 12. Studied and interpolated data susceptible to liquefaction.

concave up structures, $R = 0.99$ for sediments in the transitional zone) and allow estimating the grain size of sediments located in the transitional zone with high accuracy ($p < 0.05$) and very small absolute error (±0.8%). In addition, the ratio (share) of the fractions for the sediments outside our samples to which we applied our results was also calculated (Figure 12).

We can only speculate why there are no samples in the gap zones, despite the good representation and equal distribution of all the collected sediment samples in all other zones. This may be due to the character of the depositional environments and the following of the primary sediment texture. Alternatively, it may indicate the existence of a specific range of fractions' content that are not susceptible to liquefaction. This requires further research and sediment analysis to confirm the presence of these gaps and also explain their causes.

The presence of the "transitional zone" and the common ranges of fractions content and all statistical parameters for concave up structures and concave down structures indicate that, in addition to textural features, there must exist some other factors that influence the type of deformation that we are not able to qualitatively and quantitatively determine, for example, grain shape and primary grain arrangement, primary sedimentary structures, pore water content, bed thickness and primary surface geometry. At the same time, it indicates that nature is more complicated—in the natural environment, the occurrence of deformations, and above all how they will proceed, depends on the co-occurrence of several factors together.

6. Conclusions

The following conclusions can be drawn.

1. Soft-sediment deformation structures were recognized in the liquefied sediments of the Pleistocene age in eight study sites. 144 samples of liquefied sediments were described in detail using granulometric composition, statistical parameters and relationships between them. All deformation structures were then divided into four groups: active concave up (AU) and active concave down (AD), passive concave up (PU) and passive concave down (PD).
2. The concave up structure sediments contain a higher content of clay (2%–14%) and silt (4%–89%) than the concave down structure sediments (0%–3% and 3%–45%, respectively). In addition, some other trends are visible: (a) the larger the mean diameter of the concave up structure sediment, the greater the value of sorting and (b) the greater the skewness of the concave down structure sediments, the greater the value of sorting. The poor sorting of sediment (mainly within concave up structures) may result from (a) collecting finer,

lighter grains of the surrounding sediments directly present during the sediment escape, (b) leaching from the surrounding sediments, or (c) mixing of sediments as a result of a rapid and strong geological event. Concave down structure sediments are characterized by a dominant sand content.

3. In none of the analyzed concave down structure and concave up structure sediments, the content of the clay fraction (<2 μm) exceeded 14%. This value, in accordance with the results of the previous studies, seems to be the maximum content of clay in the liquefaction-prone sediments. The high content of clay (14%) is connected with a high content of silt (>75%).
4. The mobilization of the silt fraction during the liquefaction and fluidization initiates the further deforming process and facilitates the further sand grains mobilization, especially in the case of concave up structures (e.g., injection features). In concave up structure sediments the share of the silt fraction subjected to liquefaction must be significant in relation to the very fine- and fine-grained sand. Thus, we strongly recommend considering the percentage of silt and clay in liquefaction-prone sediments not together but separately; additionally in relation with all other individual fractions.
5. Moderately and moderately well-sorted sandy sediments undergo loading more easily due to the greater differences in density between the loaded sandy sediments and the surrounding silty sediments (due to the higher porosity and permeability of the loaded sediments, their greater water saturation and specific weight).
6. Two specific grain size zones were identified for which concave down structures (concave down structures zone) or concave up structures (concave up structures zone) develop during liquefaction. However, there is also the "transitional zone," in which all groups of forms can develop. The "transitional zone" is separated from the concave up structures zone and concave down structures zone by two "gap zones" in which no liquefied sediments were observed.

Conflict of Interest

The authors declare no conflicts of interest relevant to this study.

Data Availability Statement

All data to reproduce the work in the paper are available in the repository https://doi.org/10.5281/zenodo.8089572. Data are stored in this in-text data citation reference: Hoffmann & Reicherter, 2011; Nartišs et al., 2018; Woronko et al., 2018; Pisarska-Jamroży et al., 2018, 2019a, 2022; Belzyt et al., 2021; Woźniak et al., 2021.

Software for this research is available in these in-text data citation references: Blott & Pye, 2001, http://onlinelibrary.wiley.com/doi/10.1002/esp.261/suppinf (GRADISTAT), https://www.statsoft.pl/ (STATISTICA).

Acknowledgments

The authors are grateful to the Editorial Board and the two Reviewers for their detailed evaluation, helpful comments and suggestions that significantly improved our manuscript. This work was supported by the National Science Centre, Poland, Grants 2015/19/B/ST10/00661 and 2019/35/N/ST10/03401. The authors thank all the participants of the GREBAL project (https://grebal.amu.edu.pl).

References

Allen, J. R. L. (1977). The possible mechanics of convolute lamination in graded sand beds. *Journal Geology of Society*, *134*(1), 19–31. https://doi.org/10.1144/gsjgs.134.1.0019

Allen, J. R. L. (1982). *Developments in sedimentology. Sedimentary structures, their character and physical basis* (Vol. 30A). Elsevier Scientific Publishing Company.

Alsop, G. I., Weinberger, R., Marco, S., & Levi, T. (2022). Recognising surface versus sub-surface deformation of soft-sediments: Consequences and considerations for palaeoseismic studies. *Journal of Structural Geology*, *154*, 104493. https://doi.org/10.1016/j.jsg.2021.104493

Andrews, C. A. D., & Martin, G. R. (2000). Criteria for liquefaction of silty soils. Paper presented at 12th World Conference on Earthquake Engineering, Auckland, New Zealand.

Belzyt, S., Pisarska-Jamroży, M., Bitinas, A., Woronko, B., Phillips, E. R., Piotrowski, J. A., & Jusienė, A. (2021). Repetitive Late Pleistocene soft-sediment deformation by seismicity-induced liquefaction in north-western Lithuania. *Sedimentology*, *68*(7), 3033–3056. https://doi.org/10.1111/sed.12883

Bitinas, A., Lazauskienė, J., & Pisarska-Jamroży, M. (2021). Soft-sediment deformation structures in the Eastern Baltic Region: Implication in seismicity and glacially-induced faulting. In H. Steffen, O. Olesen, & R. Sutinen (Eds.), *Glacially triggered faulting* (pp. 320–338). Cambridge University Press. https://doi.org/10.1017/9781108779906.023

Blott, S. J., & Pye, K. (2001). GRADISTAT: A grain size distribution and statistics package for the analysis of unconsolidated sediments. *Earth Surface Processes and Landforms*, *26*(11), 1237–1248. https://doi.org/10.1002/esp.261

Brandes, C., & Winsemann, J. (2013). Soft-sediment deformation structures in NW Germany caused by Late Pleistocene seismicity. *International Journal of Earth Sciences*, *102*(8), 2255–2274. https://doi.org/10.1007/s00531-013-0914-4

Bronikowska, M., Pisarska-Jamroży, M., & Van Loon, A. J. (2021). First attempt to model numerically seismically-induced soft-sediment deformation structures – A comparison with field examples. *Geological Quarterly*, *65*(4), 60. https://doi.org/10.7306/gq.1629

Campbell, C. S. (2003). Rapid granular flows. *Annual Review of Fluid Mechanics*, *22*(1), 57–90. https://doi.org/10.1146/annurev.fl.22.010190.000421

Chang, C. S., Wang, J., & Ge, L. (2015). Modelling of minimum void ratio for sand-silt mixtures. *Engineering Geology*, *196*, 293–304. https://doi.org/10.1016/j.enggeo.2015.07.015

Cohen, J. (1988). *Statistical power analysis for the behavioral sciences* (2nd ed.). Lawrence Erlbaum Associates. https://doi.org/10.4324/9780203771587

Collinson, J. D., Mountney, N., & Thompson, D. B. (2019). *Sedimentary structures* (4th ed.). Dunedin Academic Press.

Cui, M., Peng, N., Liu, Y., Wang, Z., Li, C., Xu, K., & Kuang, H. (2022). Recognizing deformation origins: A review of deformation structures and hypothesis on the perspective of sediment consolidation. *International Geology Review*, *65*(9), 1500–1523. https://doi.org/10.1080/00206814.2022.2094840

Davies, N., Turner, P., & Sansom, I. J. (2004). Soft-sediment deformation structures in the Late Silurian Stubdal Formation: The result of seismic triggering. *Norwegian Journal of Geology*, *85*(3), 233–243.

Doe, T. W., & Dott, R. H., Jr. (1980). Genetic significance of deformed cross bedding; with examples from the Navajo and Weber sandstones of Utah. *Journal of Sedimentary Petrology*, *50*(3), 793–812. https://doi.org/10.1306/212F7AEF-2B24-11D7-8648000102C1865D

Figueroa, J. L., Saada, A. S., & Liang, L. (1995). Effect of the grain size on the energy per unit volume at the onset of liquefaction. Paper presented at 3rd International Conference on Recent Advances in Geotechnical Earthquake Engineering and Soil Dynamics. St. Louis, Missouri.

Fisher, R. A. (1925). *Statistical methods for research workers* (5th ed.). Oliver and Boyd.

Folk, R., & Ward, W. (1957). Brazos River bar: A study and mineral composition in sedimentary rock nomenclature. *The Journal of Geology*, *62*, 344–359.

Friedman, G., & Sanders, J. (1978). *Principles of sedimentology*. Wiley.

Galli, P. (2000). New empirical relationships between magnitude and distance for liquefaction. *Tectonophysics*, *324*(3), 169–187. https://doi.org/10.1016/S0040-1951(00)00118-9

He, B., Qiao, X., Li, H., & Su, D. (2018). Soft sediment deformation structures triggered by the earthquakes: Response to the high frequent tectonic events during the main tectonic movements. In E. Sharkov (Ed.), *Tectonics – Problems of regional settings*. ⁅IntechOpen. https://doi.org/10.5772/intechopen.72941

Hoffmann, G., & Reicherter, K. (2011). Soft-sediment deformation of Late Pleistocene sediments along the southwestern coast of the Baltic Sea (NE Germany). *International Journal of Earth Sciences*, *101*(1), 351–363. https://doi.org/10.1007/s00531-010-0633-z

Hughes, P. D., Gibbar, P. L., & Ehlers, J. (2013). Timing of glaciation during the last glacial cycle: Evaluating the concept of a global 'Last Glacial Maximum' (LGM). *Earth-Science Reviews*, *125*, 171–198. https://doi.org/10.1016/j.earscirev.2013.07.003

Izdebska-Mucha, D., & Wójcik, E. (2016). Identyfikacja składu mineralnego i pęcznienia gruntów spoistych na podstawie współczynnika swobodnego pęcznienia. *Biuletyn Panstwowego Instytutu Geologicznego*, *466*(0), 77–86. https://doi.org/10.5604/01.3001.0009.4756

Kishida, H. (1970). Characteristics of liquefaction of level sandy ground during the Tokachioki earthquake. *Soils and Foundations*, *10*(2), 103–111. https://doi.org/10.3208/sandf1960.10.2_103

Liang, L., Dai, F., Jiang, H., & Zhong, N. (2018). A preliminary study on the soft-sediment deformation structures in the Late Quaternary lacustrine sediments at Tashkorgan, northeastern Pamir. *Acta Geologica Sinica*, *92*(4), 1574–1591. https://doi.org/10.1111/1755-6724.13644

Lowe, D. R. (1976). Subaqueous liquefied and fluidised sediment flows and their deposits. *Sedimentology*, *23*(2), 285–308. https://doi.org/10.1111/j.1365-3091.1976.tb00051.x

Maltman, A. J., & Bolton, A. (2003). How sediments become mobilized. In P. van Rensbergen, R. R. Hillis, A. J. Maltman, & C. K. Morley (Eds.), *Subsurface sediment mobilization* (Vol. 216, pp. 9–20). Geological Society Special Publications. https://doi.org/10.1144/GSL.SP.2003.216.01.02

Mann, H., & Whitney, D. (1947). On a test of whether one of two random variables is stochastically larger than the other. *The Annals of Mathematical Statistics*, *18*(1), 50–60. https://doi.org/10.1214/aoms/1177730491

Marascuilo, L. A., & McSweeney, M. (1977). *Nonparametric and distribution-free method for the social sciences*. Brooks/Cole Publishing Company.

Mills, P. C. (1983). Genesis and diagnostic value of soft-sediment deformation structures—A review. *Sedimentary Geology*, *35*(2), 83–104. https://doi.org/10.1016/0037-0738(83)90046-5

Moreno-Maroto, J. M., & Alonso- Azcárate, J. (2018). What is clay? A new definition of "clay" based on plasticity and its impact on the most widespread soil classification system. *Applied Clay Science*, *161*, 57–63. https://doi.org/10.1016/j.clay.2018.04.011

Moretti, M., Miguel, J., Alfaro, P., & Walsh, N. (2001). Asymmetrical soft-sediment deformation structures triggered by rapid sedimentation in turbiditic deposits (Late Miocene, Guadix Basin, Southern Spain). *Facies*, *44*(1), 283–294. https://doi.org/10.1007/BF02668179

Muttashar, W. R., Bryson, L. S., McGlue, M., & Woolery, E. (2020). The integration of grain-size distribution and plasticity parameters for characterizing and classifying unconsolidated fine-grained sediments. *Bulletin of Engineering Geology and the Environment*, *79*(2), 925–939. https://doi.org/10.1007/s10064-019-01588-x

Müller, K., Winsemann, J., Pisarska-Jamroży, M., Lege, T., Spies, T., & Brandes, C. (2020). Limitations of soft-sediment deformation structures as indicators for paleo-earthquakes in formerly periglacial and glaciated areas. Paper presented at EGU General Assembly 2020.

Mycielska-Dowgiałło, E. & Rutkowski, J. (Eds.) (2007). *Badania cech teksturalnych osadów czwartorzędowych i wybrane metody oznaczania ich wieku*. Wydawnictwo Szkoły Wyższej Przymierza Rodzin.

Nartišs, M., Woronko, B., Pisarska-Jamroży, M., Belzyt, S., & Bitinas, A. (2018). Injection structures and load casts in lagoon sediments (Sārnate outcrop, W Latvia). Paper presented at International Palaeoseismological Field Workshop, Lithuanian Geological Survey, Lithuanian Geological Society, Vilnius, Lithuania.

Nichols, R. J. (1995). *The liquefaction and remobilization of sandy sediments* (Vol. 64, pp. 63–76). Geological Society Special Publications. https://doi.org/10.1144/GSL.SP.1995.094.01.06

Nichols, R. J., Sparks, R. S. J., & Wilson, C. J. N. (1994). Experimental studies of the fluidization of layered sediments and the formation of fluid escapes structures. *Sedimentology*, *41*(2), 233–253. https://doi.org/10.1111/j.1365-3091.1994.tb01403.x

Obermeier, S. (1996). Use of liquefaction-induced features for paleoseismic analysis – An overview of how seismic liquefaction features can be distinguished from other features and how their regional distribution and properties of source sediment can be used to infer the location and strength of Holocene paleo-earthquakes. *Engineering Geology*, *44*(1–4), 1–76. https://doi.org/10.1016/S0013-7952(96)00040-3

Oliveira, C. M. M., Hodgson, D. M., & Flint, S. S. (2011). Distribution of soft-sediment deformation structures in clinoform successions of the Permian Ecca Group, Karoo Basin, South Africa. *Sedimentary Geology*, *235*(3–4), 314–330. https://doi.org/10.1016/j.sedgeo.2010.09.011

Othman, B. A., & Marto, A. (2018). Laboratory test on maximum and minimum void ratio of tropical sand matrix soils. *IOP Conference Series: Earth and Environmental Science*, *140*(1), 012084. https://doi.org/10.1088/1755-1315/140/1/012084

Othman, B. A., Marto, A., Yunus, N. Z. M., Soon, C. T., & Pakir, F. (2018). The grading effect of coarse sand on consolidated undrained strength behaviour of sand matrix soils. *International Journal of Recent Technology and Engineering*, *7*(5), 88–92.

Owen, G. (1996). Experimental soft-sediment deformation: Structures formed by the liquefaction of unconsolidated sands and some ancient examples. *Sedimentology*, *43*(2), 279–293. https://doi.org/10.1046/j.1365-3091.1996.d01-5.x

Owen, G. (2003). Load structures: Gravity-driven sediment mobilization in the shallow subsurface. In P. van Rensbergen, R. R. Hillis, A. J. Maltman, & C. K. Morley (Eds.), *Subsurface sediment mobilization* (Vol. 216, pp. 21–34). Geological Society Special Publications. https://doi.org/10.1144/GSL.SP.2003.216.01.03

Owen, G., & Moretti, M. (2011). Identyfying triggers for liquefaction-induced soft-sediment deformation in sands. *Sedimentary Geology*, *235*(3–4), 141–147. https://doi.org/10.1016/j.sedgeo.2010.10.003

Pisarska-Jamroży, M., Belzyt, S., Bitinas, A., Jusienė, A., Damušytė, A., & Woronko, B. (2018). A glaciolacustrine succession (Dyburiai outcrop, NW Lithuania) with numerous deformed layers sandwiched between undeformed layers. Paper presented at International Palaeoseismological Field Workshop, Lithuanian Geological Survey, Lithuanian Geological Society, Vilnius, Lithuania.

Pisarska-Jamroży, M., Belzyt, S., Bitinas, A., Jusienė, A., & Woronko, B. (2019a). Seismic shocks, periglacial conditions and glaciotectonics as causes of the deformation of a Pleistocene meandering river succession in central Lithuania. *Baltica*, *32*(1), 63–77. https://doi.org/10.5200/baltica.2019.1.6

Pisarska-Jamroży, M., Belzyt, S., Börner, A., Hoffmann, G., Hüneke, H., Kenzler, M., et al. (2019b). The sea cliff at Dwasieden: Soft-sediment deformation structures triggered by glacial isostatic adjustment in front of the advancing Scandinavian Ice Sheet. *DEUQUA Special Publications*, *2*, 61–67. https://doi.org/10.5194/deuquasp-2-61-2019

Pisarska-Jamroży, M., Belzyt, S., Börner, A., Hoffmann, G., Kenzler, M., Rother, H., et al. (2022). Late Pleistocene earthquakes imprinted on glaciolacustrine sediments on Gnitz Peninsula (Usedom Island, NE Germany). *Quaternary Science Reviews*, *296*, 107807. https://doi.org/10.1016/j.quascirev.2022.107807

Postma, G. (1983). Water escape structures in the context of a depositional model of a mass flow dominated conglomeratic fandelta (Abrioja Formation, Pliocene, Almeria Basin, SE Spain). *Sedimentology*, *30*(1), 91–103. https://doi.org/10.1111/j.1365-3091.1983.tb00652.x

Seed, H. B. (1979). Soil liquefaction and cyclic mobility evaluation for level ground during earthquakes. *Journal of the Geotechnical Engineering Division*, *105*(2), 201–255. https://doi.org/10.1061/AJGEB6.0000768

Seed, H. B., Idriss, I. M., & Arango, I. (1983). Evaluation of liquefaction potential using field performance data. *Journal of Geotechnical Engineering*, *109*(3), 458–482. https://doi.org/10.1061/(ASCE)0733-9410(1983)109:3(458)

Seed, H. B., Woodward, R. J., & Lundgren, R. (1964). Fundamental aspects of the Atterberg limits. *Journal of the Soil Mechanics and Foundations Division*, *90*(6), 75–105. https://doi.org/10.1061/JSFEAQ.0000685

Tchakalova, B., & Ivanov, P. (2022). Correlation between effective cohesion and plasticity index of clay. *Geologia Balcanica*, *51*(3), 45–49. https://doi.org/10.52321/GeolBalc.51.3.45

Tuttle, M., Law, K. T., Seeber, L., & Jacob, K. (1990). Liquefaction and ground failure induced by the 1988 Saguenay, Quebec, earthquake. *Canadian Geotechnical Journal*, *27*(5), 580–589. https://doi.org/10.1139/t90-073

Udden, J. (1914). Mechanical composition of clastic sediments. *Bulletin of the Geological Society of America*, *25*(1), 655–744. https://doi.org/10.1130/GSAB-25-655

Vandenberghe, J. (2013). Permafrost and periglacial features. Cryoturbation structures. In S. A. Elias & C. J. Mock (Eds.), *Encyclopedia of quaternary science* (2nd ed., pp. 430–435).

Van Loon, A. J., & Pisarska-Jamroży, M. (2014). Sedimentological evidence of Pleistocene earthquakes in NW Poland induced by glacioisostatic rebound. *Sedimentary Geology*, *300*(1), 1–10. https://doi.org/10.1016/j.sedgeo.2013.11.006

Van Loon, A. J., Pisarska-Jamroży, M., Nartišs, M., Krievāns, M., & Soms, J. (2016). Seismites resulting from high-frequency, high-magnitude earthquakes in Latvia caused by Late Glacial glacio-isostatic uplift. *Journal of Palaeogeography*, *5*(4), 363–380. https://doi.org/10.1016/j.jop.2016.05.002

Van Loon, A. J., Pisarska-Jamroży, M., & Woronko, B. (2020). Sedimentological distinction in glacigenic sediments between load casts induced by periglacial processes from those induced by seismic shocks. *Geological Quarterly*, *64*(3), 626–640. https://doi.org/10.7306/gq.1546

Van Loon, A. J., Soms, J., Nartišs, M., Krievāns, M., & Pisarska-Jamroży, M. (2019). Sedimentological traces of ice-raft grounding in a Weichselian glacial lake near Dukuli (NE Latvia). *Baltica*, *32*(2), 170–181. https://doi.org/10.5200/baltica.2019.2.4

VanRensbergen, P., Hillis, R. R., Maltman, A. J., & Morley, C. K. (Eds.) (2003)., *Subsurface sediment mobilization* (Vol. 216). Geological Society Special Publications. https://doi.org/10.1144/GSL.SP.2003.216

Wahyudi, S., Koseki, J., Sato, T., & Miyashita, Y. (2013). Effects of pre-shearing history on repeated liquefaction behaviour of sand using stacked-ring shear apparatus. *Bulletin of ERS*, *46*, 3–11.

Wang, C. Y., & Manga, M. (2021). *Water and earthquakes. Lecture notes in Earth system sciences*. Springer. https://doi.org/10.1007/978-3-030-64308-9

Wang, W. S. (1979). *Some findings in soil liquefaction*. Earthquake Engineering Department, Water Conservancy and Hydroelectric Power Scientific Research Institute.

Wentworth, C. (1922). A scale of grade and class terms for clastic sediments. *The Journal of Geology*, *30*(5), 377–392. https://doi.org/10.1086/622910

Wilcoxon, F. (1949). Some rapid approximate statistical procedures. *Annals of the New York Academy of Sciences*, *52*(6), 808–814. https://doi.org/10.1111/j.1749-6632.1950.tb53974.x

Woronko, B., Pisarska-Jamroży, M., Belzyt, S., Karmazienė, D., Bitinas, A., & Damušytė, A. (2018). *Multi-type soft-sediment deformation structures in glaciolacustrine kame sediments (Ličiškėnai outcrop, S Lithuania)*. Lithuanian Geological Survey, Lithuanian Geological Society. Paper presented at International Palaeoseismological Field Workshop.

Woźniak, P. P., Belzyt, S., Pisarska-Jamroży, M., Woronko, B., Lamsters, K., Nartišs, M., & Bitinas, A. (2021). Liquefaction and re-liquefaction of sediments induced by uneven loading and glacigenic earthquakes: Implications of results from the Latvian Baltic Sea coast. *Sedimentary Geology*, *421*, 105944. https://doi.org/10.1016/j.sedgeo.2021.105944

Yong, R. N. (1999). Soil suction and soil-water potentials in swelling clays in engineered clay barriers. *Engineering Geology*, *54*(1–2), 3–13. https://doi.org/10.1016/S0013-7952(99)00056-3

Yong, R. N., & Warkentin, B. P. (1966). *Introduction to soil behavior*. Macmillan Series in Civil Engineering.

Youd, T. L. (1973). *Liquefaction, flow, and associated ground failure* (Vol. 688). USGS Circular. https://doi.org/10.3133/cir688

Youd, T. L. (1978). Packing changes and liquefaction susceptibility. *Journal of the Geotechnical Engineering Division*, *103*(8), 918–922. https://doi.org/10.1061/AJGEB6.0000478

Youd, T. L., & Perkins, D. M. (1978). Mapping liquefaction-induced ground failure potential. *Journal of the Geotechnical Engineering Division*, *104*(4), 433–446. https://doi.org/10.1061/AJGEB6.0000612

Zhong, N., Jiang, H., Li, H., Su, D., Xu, H., Liang, L., & Fan, J. (2022). The potential of using soft-sediment deformation structures for quantitatively reconstructing paleo-seismic shaking intensity: Progress and prospect. *Environmental Earth Sciences*, *81*(408), 408. https://doi.org/10.1007/s12665-022-10504-8

Zhou, S. G. (1981). Influence of fines on evaluating liquefaction of sand by CPT. Paper presented at 1st International Conference on Recent Advances in Geotechnical Earthquake Engineering and Soil Dynamics. St. Louis, Missouri.

Sedimentary Geology 478 (2025) 106833

Contents lists available at ScienceDirect

Sedimentary Geology

journal homepage: www.elsevier.com/locate/sedgeo

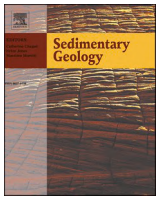

Seismogenic liquefaction with M ~ 3.5 in fine-grained sediments: An experimental approach

Szymon Świątek *, Małgorzata Pisarska-Jamroży

Institute of Geology, Adam Mickiewicz University in Poznań, B. Krygowskiego 12, 61-680 Poznań, Poland

ARTICLE INFO

Dr. Basilici Giorgio

Keywords:
Seismically-induced liquefaction
Soft-sediment deformation structures
Seismites
Low-magnitude experiment
Morphometric analysis
Water-saturated sediments
Fine-grained sandy and silty sediments

ABSTRACT

Seismically liquefaction-induced soft-sediment deformation structures are key to understanding the geological history of earthquakes and sedimentary environments. These evidences usually have been associated with high-magnitude seismic events, above 5. However, the precise thresholds and mechanisms, especially for lower-magnitude earthquakes, remained unclear. This study aims to address this gap by experimentally investigating the development of deformation structures under controlled laboratory conditions. Using three sediment types arranged in five sequences, the sediments were subjected to low-magnitude seismic vibrations. Developed liquefaction features such as clastic volcanoes, pseudonodules, flame structures, and load casts were measured by a novel morphometric analysis to quantify their size and shape. The findings revealed that even at a magnitude of ~3.5, liquefaction and deformation structures can occur, especially in high water-saturated fine-grained sediments. These results provide new insights into the thresholds of seismically-induced liquefaction and highlight the importance of considering lower-magnitude events in seismic risk assessments, offering significant implications for the study of sedimentary processes and earthquake-related deformation.

1. Introduction

Earthquakes create traces near the epicentre, like fissures and faults, and farther away as deformed layers called seismites (Seilacher, 1969). Seismites are typically found within 30–40 km of the epicentre (Galli, 2000; Bronikowska et al., 2021), though stronger earthquakes can cause liquefaction hundreds of kilometers away (Galli, 2000; He and Qiao, 2015). Seismites form when S-type seismic waves reduce the shear resistance in water-saturated clastic sediments (Tokimatsu and Uchida, 1990; Owen and Moretti, 2011).

Regardless of the trigger mechanism (e.g. seismic shock, volcanic activity, storm waves etc.), if the driving force is higher than the sediment's strength, the sediment deforms, altering its structure. The dissipation of pore overpressure and the drainage of pore fluid re-establish intergrain contact, leading to the formation of soft-sediment deformation structures (SSDS). When the plasticity limit is exceeded, brittle deformation processes are initiated (Youd, 1973; Seed, 1979; Moretti et al., 1999). SSDS in seismites are linked to sediment fluidisation and liquefaction (cf. Allen, 1982; Owen, 2003). Fluidisation causes water to escape, while liquefaction increases pore pressure, destroying intergranular contacts and mobilising grains (e.g. Galli, 2000; Maltman and Bolton, 2003; Owen, 2003). Common seismically liquefaction-induced SSDS include water-escape structures, dish-and-pillar structures, clastic dykes, load casts, pseudonodules, flame structures, convolute lamination, ball-and-pillow structures, intrusions, sand / clastic volcanoes, blows, craters, microfolds, and deformation bands (Lowe, 1976; Allen, 1982; Obermeier, 1996, 2009; Owen, 2003; Davies et al., 2004; Castilla and Audemard, 2007; Van Loon, 2009; Owen and Moretti, 2011; Brandes and Winsemann, 2013; Pisarska-Jamroży et al., 2019; Pisarska-Jamroży and Woźniak, 2019; Müller et al., 2020; Van Loon et al., 2020). Other seismically-induced features include pinch-and-swell structures (Cox et al., 2014; Lakshmi, 2021) and boudinage-like SSDS (Hou et al., 2019). Seismic shocks can also deform sediment laminae or layers, creating disaggregation bands, fragmented laminae, broken-up parts of laminae (Van Loon et al., 2016; Belzyt et al., 2021; Brandes et al., 2022; Jiménez-Millán et al., 2022; Pisarska-Jamroży et al., 2022, 2024), and liquefied breccia (He et al., 2014).

Liquefaction is more likely to occur in environments with the presence of water (e.g. river, sea, glacial, lacustrine) (Youd and Perkins, 1978). It occurs when the water content in the sediment reaches at least 90 % of the liquid limit (water content to change itself state to liquid form), indicating the sediment's capacity to maintain a liquid-like state

* Corresponding author.
E-mail address: szymon.swiatek@amu.edu.pl (S. Świątek).

https://doi.org/10.1016/j.sedgeo.2025.106833
Received 23 December 2024; Received in revised form 29 January 2025; Accepted 7 February 2025
Available online 10 February 2025

under stress (Seed et al., 1983; Cui et al., 2022). Sediments with water content between 18 and 26 % (Puri and Prakash, 2010) and a minimum 90 % of the liquid limit are prone to liquefaction during seismic activity (Andrews and Martin, 2000). That is why modern sediments are most prone to liquefaction, while more consolidated, older sediments are less so (Obermeier, 1996; Tang et al., 2016). Tang et al. (2016) suggested liquefaction occurs if the relative density between layers is below 50 %, though it has been observed at densities of 58–92 % (Nakai, 2005) or 80 % (Wahyudi et al., 2013). The minimum sediment layer thickness for liquefaction is generally a few centimeters (Zhong et al., 2022), but can be 10–30 cm (Nichols, 1995; Ecemis, 2021) or up to a metre (Obermeier, 1996).

Fluidisation and liquefaction phenomena are recorded in susceptible sediments, such as coarse-grained silt and/or fine-grained sand (Obermeier, 1996; Owen, 2003). Liquefaction usually concerns sand-sized sediment from 0.01 mm (cf. Obermeier, 1996; Terzaghi, 1996) to 2 mm (cf. Moretti et al., 1999). However, recent research by Minarelli et al. (2022) and Świątek et al. (2023) contrasts with this by indicating that silt and clay fractions are almost always needed together. The clay content in the sediment enhances resistance to liquefaction by increasing plasticity and cohesion, with optimal resistance observed at clay contents between 10 and 20 %: 10 % (Andrews and Martin, 2000), 14 % (Świątek et al., 2023) or 20 % (de Magistris et al., 2013). According to Ashmawy et al. (2003) particle shape can also have impact on liquefaction, increasing porosity and susceptibility to that. The most frequently mentioned criterion for sediment liquefaction is the magnitude of the seismic event. Green and Bommer (2019) argued that the absolute minimum magnitude is close to 4.5–5.0. Higher earthquake magnitudes, usually above 5 (Allen, 1986; Owen and Moretti, 2011), increase the liquefaction potential, with some cases reaching magnitudes as high as 7 or more (Papadopoulos and Lefkopoulos, 1993). In contrast to the above, results obtained by Phillips et al. (2018) and Zhong et al. (2022) suggest that magnitudes of 3.0 and 3.6, respectively, can also cause liquefaction.

The duration of shocks also affects the likelihood of liquefaction, as it determines the grain deposition rate and the thickness of the liquefied layer (Allen, 1982; Owen, 2003). Longer durations increase the chance of liquefaction (Tang et al., 2016). Zhang and Wang (1990)) assumed that the greater the frequency of seismic waves (even 100 Hz), the greater the potential to liquefy. However, according to Jain et al. (2022), liquefaction can occur at frequencies of 0.1–1.5 Hz. This is consistent with Fuławka et al. (2022), who demonstrated that lower frequencies (0.8–1 Hz) can cause a greater seismic load, and consequently, a higher risk of liquefaction.

Despite the increased number of studies on palaeoearthquake traces (cf. Belzyt et al., 2021; Woźniak et al., 2021; Pisarska-Jamroży et al., 2022; McCalpin et al., 2023), there is still a significant knowledge gap regarding quantitative results related to seismites and liquefaction-induced SSDS. Sediment type, water saturation, magnitude, and frequency of seismic events play major roles in the occurrence of liquefaction and the development of SSDS, but still we do not know how the above factors interact and how their threshold values can be determined. We fully acknowledge that laboratory studies have their limitations and cannot serve as direct evidence of phenomena occurring in nature. However, they can provide a valuable starting point for more precise monitoring of liquefaction processes in natural environments. The following questions remain open: How do seismic shocks affect unconsolidated sediments of various textural and structural features? What are the limit values of the shock parameters necessary to develop SSDS? What are the relationships between different SSDS morphologies?

The main aims of this study are: (1) to present a new approach to developing liquefaction-induced SSDS under laboratory conditions with lower magnitude than commonly applied, (2) to determine the relationships between the development of SSDS, their textural features, and seismological parameters, and (3) to attempt a qualitative description of the geometry of SSDS.

2. Material and Methods

2.1. Sediments

In the experiment, three types of unconsolidated sediments were used (Fig. 1A): silt, fine-grained sand, and coarse-grained sand. These sediments were collected from natural outcrops (silt in the Słonów site, sand in the Bielice Nowe site – both in NW Poland), then dried, sieved, and classified according to the Friedman and Sanders (1978).

2.2. Experiment design

Five variants of sediment sequences (A, B, C, D and E), with five duplicates each (subvariants), varying in the number and arrangement of layers relative to each other, were prepared. The sediments were placed in transparent plexiglass cylinders with a diameter of 10 cm and a height of 10 cm (Fig. 1B). The thickness of layers varied between 1.5 and 3 cm, and the thickness of the entire sequences ranged from 6.5 up to 7.5 cm. All layers were water-saturated separately. In other words, one layer was placed at the bottom of the plexiglass cylinder, sprayed with water, covered by next layer, sprayed, and so on. Samples were left for 30 min to allow gravitational infiltration to occur. The sediment sequence was designed to replicate lacustrine deposits, representing undisturbed, water-saturated sediment layers with an overlying water film (Appendix S1). Such settings were recognised and analysed in a few field sites (cf. Woźniak et al., 2021; Pisarska-Jamroży et al., 2024).

The liquefaction was conducted under strictly controlled laboratory conditions, using Analysette 3 Spartan (Fritsch) device, imitating the shaking table with specific parameters (Fig. 1C). This seismological instrument was characterised by the following features: magnitude (~3.5), frequency (50 Hz), amplitude (3 mm) and duration of the seismic shocks does not exceed 15 s. The technical data and parameters are provided by the device manufacturer. This instrument is made in such a way that it does not allow **us** to change, frequency and amplitude. To calculate value of magnitude, we used equations proposed by Boore (1983), Atkinson and Boore (1995), Boore et al. (1997), Arias (1970), and Katsumata (2001) with modification to the following:

$$M = log_{10}(PGA) + 1.1 \cdot log_{10}(R) + 3.2$$

where:

PGA – Peak Ground Acceleration = 2 g = 2 · 9.81 m/s^2 = 19.62 m/s^2;
R – distance to epicentre = 10 cm = 0.1 m.

Each specimen was subjected to seismic vibrations carefully and separately. After the simulation, morphometric analyses of SSDS were done.

2.3. Morphometric analyses of SSDS

Each sediment sequence and the SSDS that occurred in the sediments were described in detail and photographed before (Appendix S1) the experiment and after the seismic shock simulation. The morphometry of each deformation structure was described, including its shape, orientation, width, height, length, number of features, location within the sequence, and the layers from which originated, as part of the following experiment description. Based on these values, various shape coefficients were calculated (Fig. 2). These shape coeficient usually was described as height to width ratio. It is worth noting that the dimensions of SSDS and thickness of the layers after seismic wave propagation was measured along the walls of the cylinder.

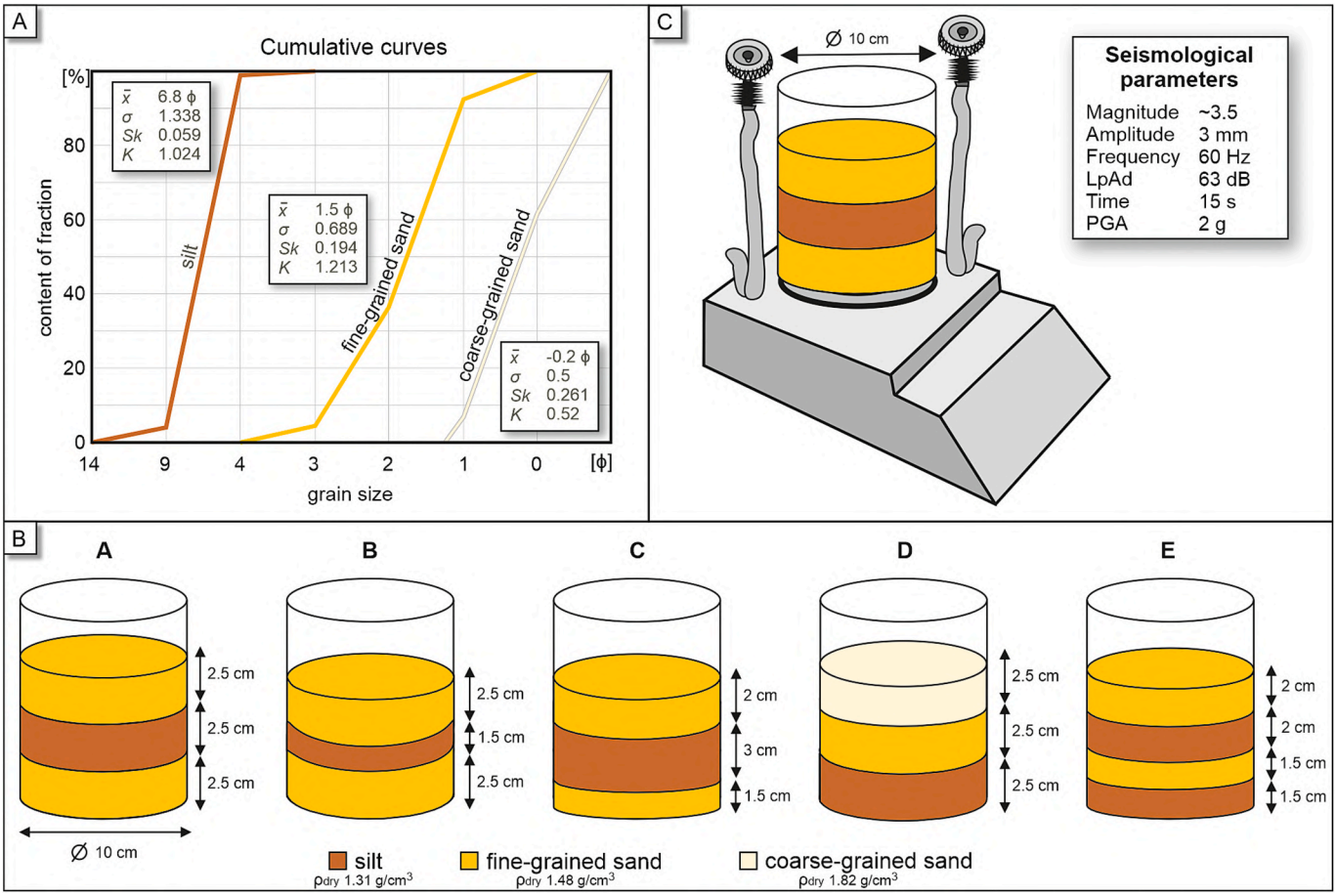

Fig. 1. Experiment design: A – cumulative curves and basic statistical parameters: mean diameter ($\bar{x}$), sorting (δ), skewness (Sk) and kurtosis (K) of sediments used in the experiment, B – variants of sediment sequences, and C – device (Analysette 3 Spartan Vibratory Sieve Shaker by Fritsch) imitating a shaking table with parameters modelled during the experiment (LpAd – 60 dB; PGA – 2 g).

3. Results

3.1. *Experimentally-induced features of seismic shock in five sedimentary sequences*

As a result of the seismic shock simulation, the water-saturated sediments in five variants of sedimentary sequences underwent fluidisation and liquefaction.

3.1.1. *Variant A*

3.1.1.1. Description. The thickness of a lower sandy layer (Fig. 3A_0) in all subvariants decreased by 20–30 %, the middle silty layer increased by up to 30 %, while the upper sandy layer decreased by 10 %. The boundary between the lower sandy layer and the middle silty layer is sharp (Figs. 3A_1 and A_2); however, in some places, contorted bedding occurs (Fig. 3A_3). A gradational boundary is present only there where sandy injections (0.33–0.6 cm wide, 0.28–1.13 cm high) are found (Fig. 3A_3). The boundary between the middle silty layer and the upper sandy layer is blurred and sometimes difficult to identify (Fig. 3A_1).

A wide range of SSDS occurs within layers in variant A (Figs. 3 and 4A). There is a visibly increased amount of SSDS in the upper part of the sequence compared to the lower. (1) Silty flame structures average 1.2 cm wide and 0.53 cm high (Figs. 3A_4 and A_5). Their shape coefficient, in subvariants A1-A4, reaches from 0.23 to 0.73, while for A5, from 0.45 to 1.28. (2) Load casts are characterised by an average width of 1.1 cm and a height of 0.63 cm (Figs. 3A_4 and A_5). The load coefficient has an average value of 0.54. (3) Silty injection structures with a shape coefficient of 0.9–2.5 are recorded in each subvariant except A3 (Figs. 3A_3 and 4A). (4) Pseudonodules (occurring in subvariants A3 and A5) are 1.5–1.8 cm wide and 0.7 cm high (Fig. 3A_3). The pseudonodule parameter is estimated at 0.44. (5) Clastic volcanoes, occurring in subvariants A2-A5 (Fig. 3A_1), are characterised by wide diversity; their vein width ranges from 0.32 to 2.48 cm, and length from 0.65 to 1.45 cm. The height of the silt blow ranges from 0.18 to 0.43 cm, while their width varies from 1.5 to 5.23 cm. The shape coefficient in all subvariants is similar, except for the V_5 coefficient. Together with clastic volcanoes, a new layer of sediments (extrudites) is formed, reaching approximately 0.6 cm in thickness (Fig. 3A_1). Furthermore, in each of the subvariants, the (6) polygonisation of silt grains is observed (Figs. 3A_1 and A_2). These features occur in the middle of the silt layer and are brighter than the rest.

3.1.1.2. Interpretation. The decreased thickness of the sandy layers is caused by the consolidation and reorganisation of grains. The lower sandy layer experienced greater compaction due to intense shaking and its position at the bottom of the sedimentary sequence. This process resulted in a tightly packed structure in the lower sandy layer, maintaining a clear and sharp boundary with the overlying silty layer. The relative increase in silty layer thickness can be attributed to the swelling of clay minerals commonly occurring in silty sediments (Aksu et al., 2015; Tan et al., 2017). The sharp boundary between the lower sandy layer and the middle silty layer is due to their different responses to seismic shocks. The fewer deformations at the boundary of the lower sandy and middle silty layers are probably due to greater pressure from the overlying sediments compared to the upper sandy layer.

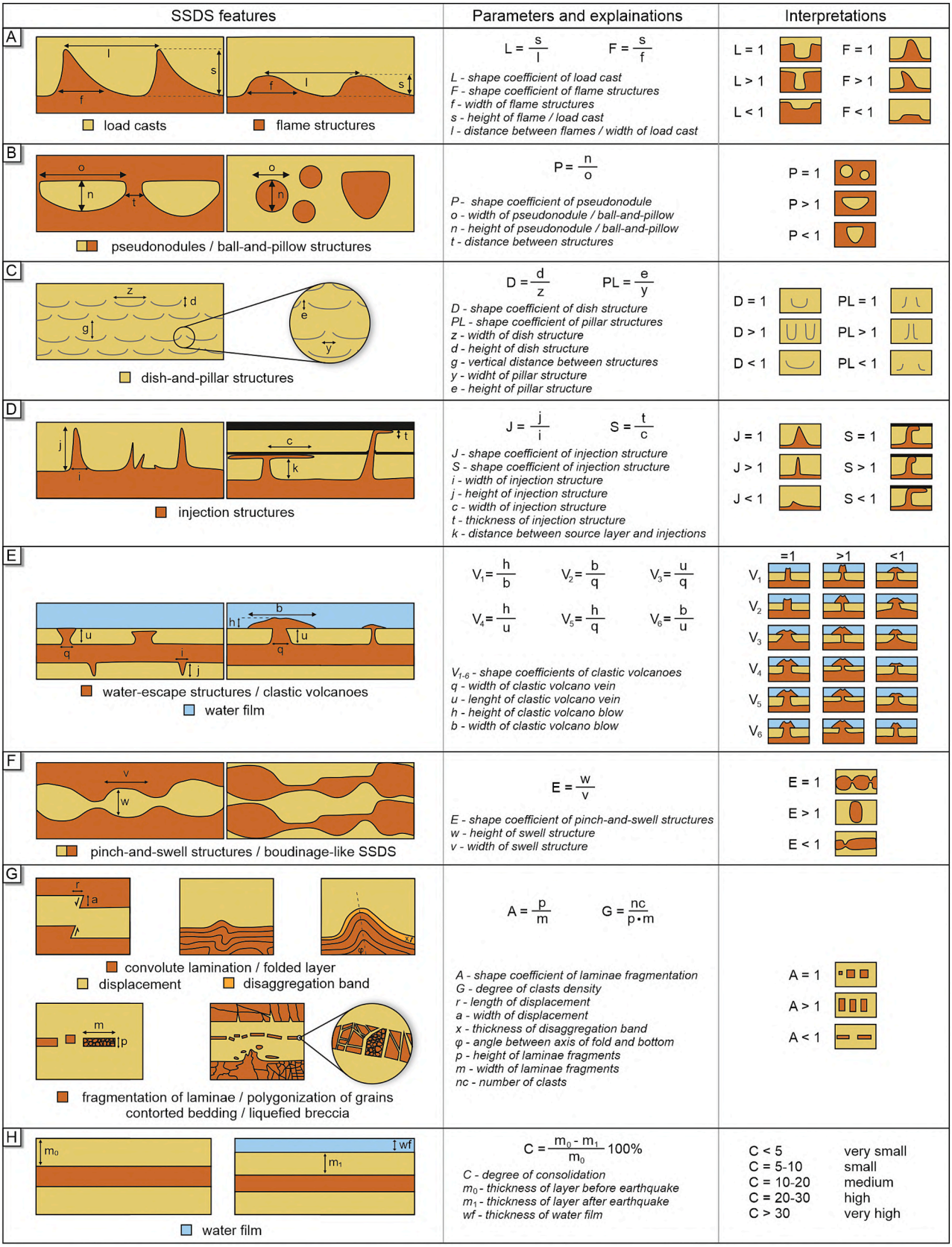

Fig. 2. Features and morphometric parameters of seismically-induced soft-sediment deformation structures (orange colour – finer-grained sediments e.g. silt or sandy silt, yellow colour – coarser-grained sediments, e.g. silty sand or sand, blue colour – water): A – load structures, B – pseudonodules and ball-and-pillow structures, C – dish-and-pillar structures, D – injection structures, E – water-escape and volcano structures, F – pinch-and-swell structures, G – other features, H – consolidation.

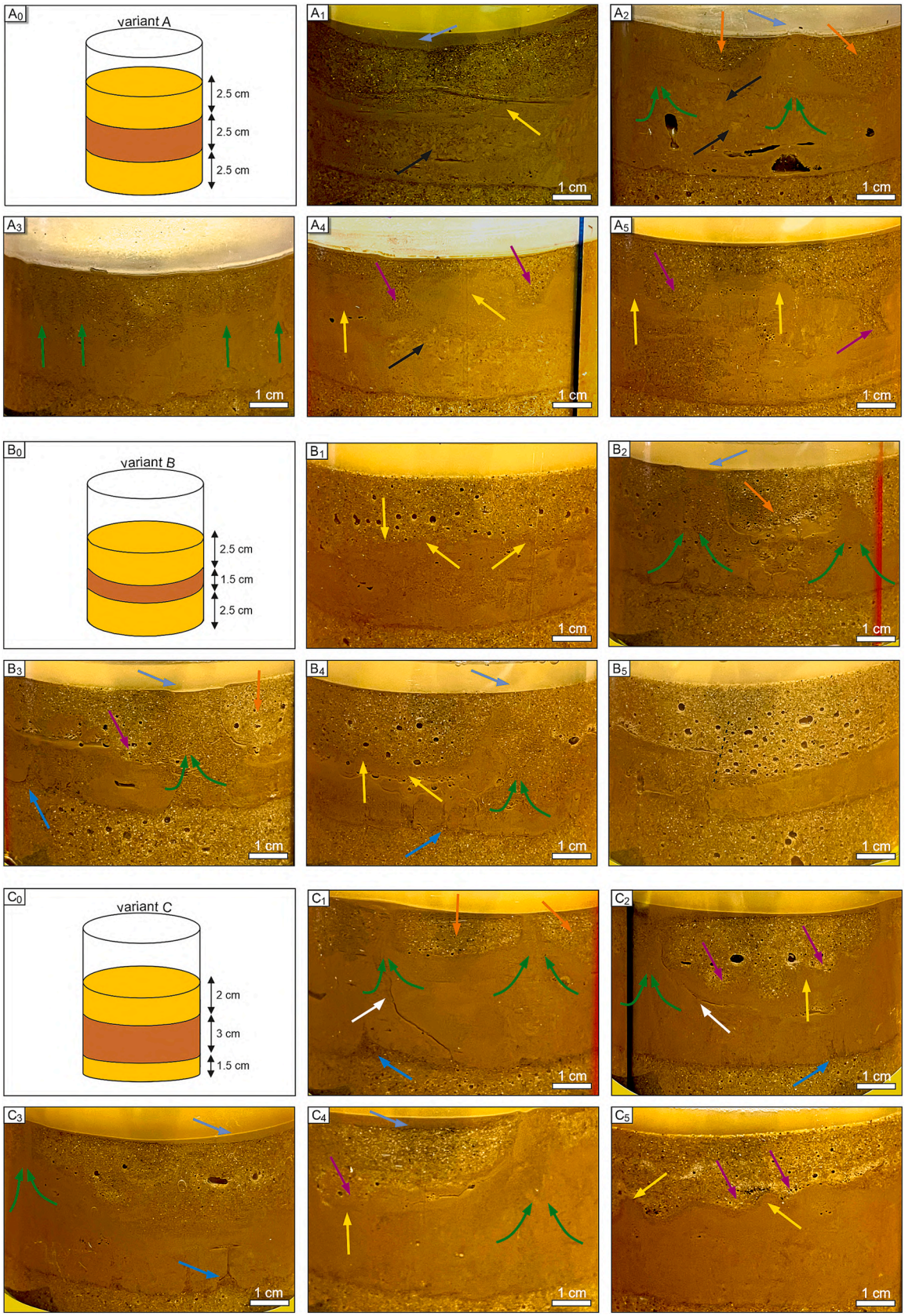

Fig. 3. Features of deformed sediments in variants A-E: A_0-E_0 – sketch presenting the original sediment sequence in the variants A-E; A_1 – poligonisation of grains in the lower part of photo, flame structures between the middle silty layer and the upper sandy layer (in the middle part of photo), clastic volcano deposits at the top of sequence, A_2 – poligonisation of grains and injection structures in the middle part of photo; load casts and clastic volcano deposits in the top part of sequence, A_3 – injection structures of the silty sediments, A_4 – poligonisation of grains and flame structures in the middle part of photo, load casts in the upper part of photo, A_5 – load casts and related flame structures, B_1 – silty flame structures, B_2 – sandy pseudonodule surrounded by an injection structure and clastic volcano, B_3 – sandy

injection structures in the lower layer and the middle silty injection structure with sandy load cast and pseudonodule, B_4 – injection structures with flame structures and clastic volcano deposits, B_5 – fault caused by the movement of the silty mass, C_1 – pseudonodules cut by two clastic volcanoes with sandy injection structure, C_2 – clastic volcano with load cast, C_3 – injection structures, C_4 – silty injection structure with flame structures and load cast, C_5 – co-occurence of load casts and flame structures, D_1 and D_2 – air bubbles occurring in a zone parallel to silty layer, D_3 and D_5 – filling of coarse-grained sand pores by fine-grained sand grains, D_4 – swelling and bulging of the silty layer, E_1-E_5 – co-occurence of sandy injection structures in the lower layer and silty injection structures / volcanoes in the middle layer with pseudonodules alternately, E_2 – flame structures related to load casts. White arrows indicate the feeding channel.

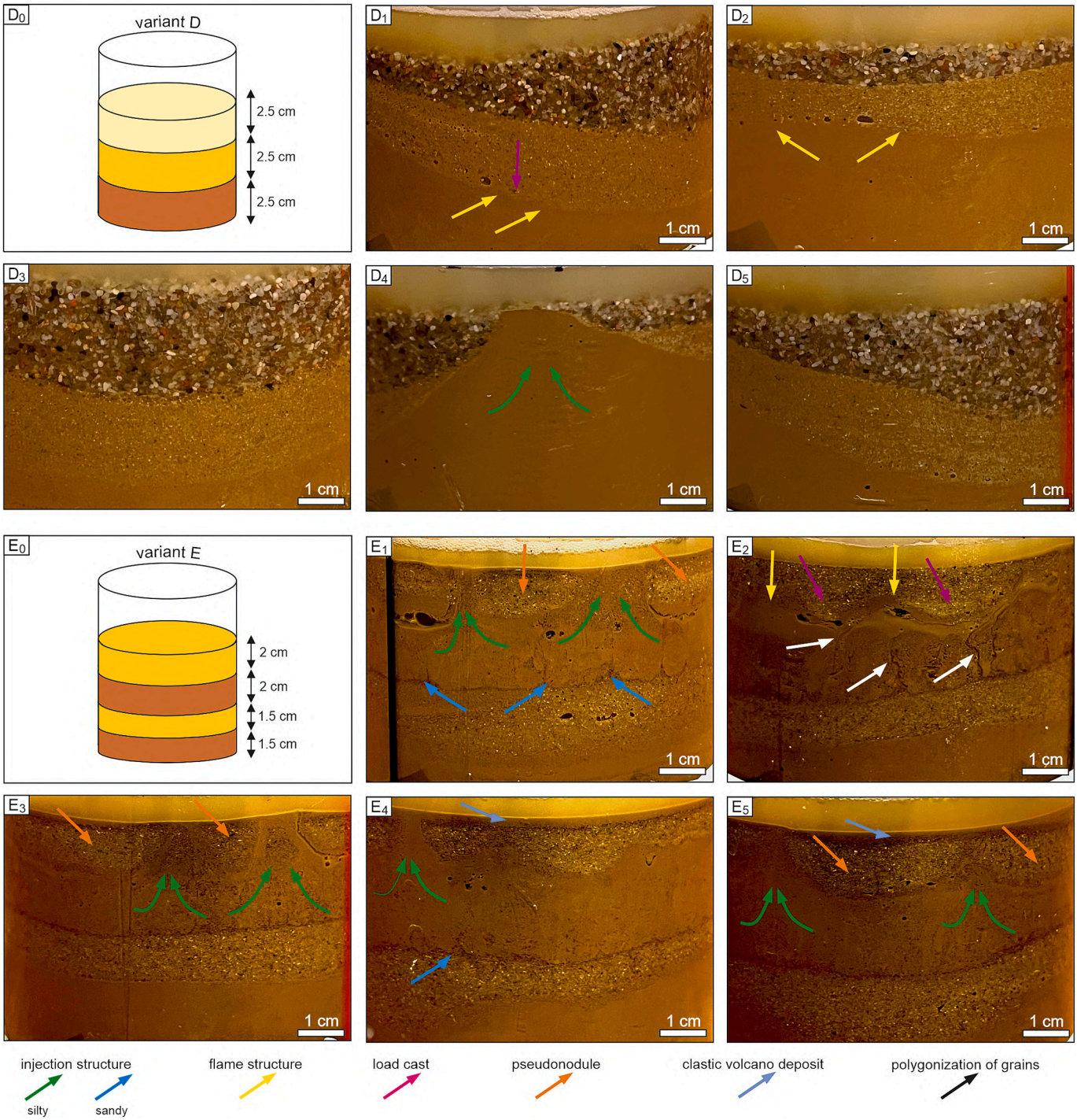

Fig. 3. (*continued*).

Consequently, the lower sandy layer was less prone to deformation, while the upper sandy layer was more affected by seismic activity (cf. Wiemer et al., 2015).

Seismic shocks can transfer energy nonlinearly through the sediment sequence, dissipating and attenuating in the lower sandy layer causing the upper sandy layer more prone to vibrations. Resonance with the frequency of seismic shocks (cf. Foda and Chang, 1996; Van der Baan, 2009) could have intensified deformation in the upper sandy layer. Additionally, an appropriate silt thickness responded more effectively to the shocks, promoting SSDS typical of seismic wave (cf. Świątek et al., 2023).

The alternating occurrence of sediments and the increase in pore

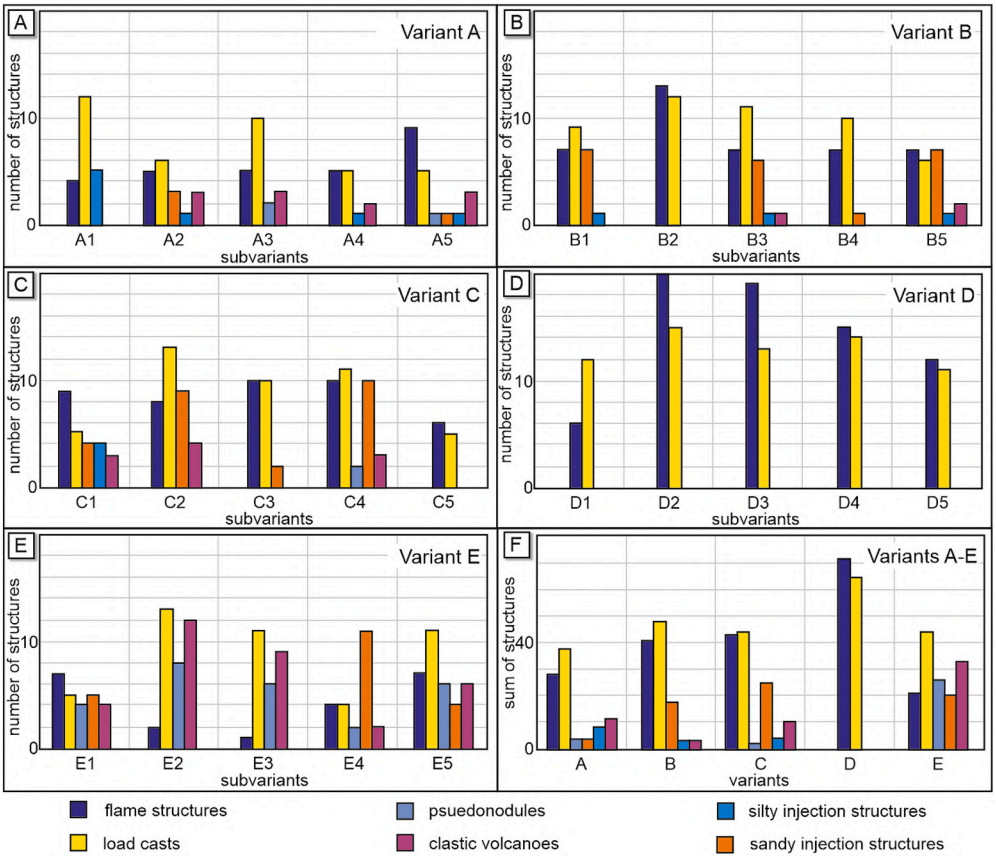

Fig. 4. Comparison of SSDS developed experimentally in the following subvariants (A-E) and variants (F).

pressure resulted in differences in the density and consistency of the layers, leading to the development of unstable layering structures such as flame structures, load casts and pseudonodules. A similar shape coefficient of flame structures ($F < 1$) suggests that the intensity and nature of seismic events equally influenced their formation, as well as the homogeneity of the sediment. Seismic events can reduce the shear strength of sediments, leading to these formations. In each subvariant (A1-A5), the shape coefficients, ranging from 0.29 to 0.87 (medians~0.5), indicating flattened and shallow structures, but values of 0.5–1.0 resemble more rounded and spherical objects. Injection structures formed in both the lower sandy layer and the middle silty layer. Despite the different granulometric compositions of these sediments, the average value of the shape coefficient and the dimensions of the structures are similar, suggesting a resemblance in deformation style. The shape coefficient indicates that sandy injections tend to form as narrow and tall structures, resulting from differences in pore pressure and local sediment properties influencing water and sediment flow during seismic events. The very low coefficient V_1 of clastic volcanoes suggests they have wide blows compared to their height. These structures may indicate mild, widespread eruptions, where silt spreads sideways rather than building tall cones. This may relate to a moderate pressure gradient and stable outflow of pore fluids. A medium V_2 value indicates varying cone formation conditions, with differential sediment eruptions – some concentrated and some extensive – suggesting variable pressure and fluid flow conditions in the sediments. Lower V_3 values indicate that veins are wider relative to their length, indicating shallow, wide channels. Low and medium V_4 values indicate the cone height is small compared to the vein length, implying more scattered eruptions with deep veins relative to the cone. Various V_5 values indicate that cone height is much smaller than vein width, suggesting low and wide cones consistent with mild, broad eruptions, potentially due to evenly distributed fluid pressure. Lower V_6 values suggest wider cones relative to vein length, indicating more widespread eruptions. Volcanoes did not develop in variant A1, which is characterised by a higher number of injection structures. This suggests that local and specific conditions (e.g. insufficient water-saturated sediments, pore pressure, or a too-thick upper layer) prevented the development of volcanoes. In other words, the conditions were not sufficient to break through the upper layer.

Reducing interparticle friction and effective stress allows grains to move and reconfigure during the polygonisation phenomenon. It occurs when silty grains arrange themselves into multi-sided shapes due to the system's tendency to minimize energy and maximize packaging efficiency under new stress conditions.

3.1.2. *Variant B*

3.1.2.1. Description. The thickness of the lower sandy layer (Fig. 3B_0) in all subvariants decreased by 9–17 %, the middle silty layer increased by up to 25 %, while the upper sandy layer decreased by 4–10 %. The boundary between the lower sandy layer and the middle silty layer is sharp, although contorted bedding is occasionally observed (Figs. 3B_3 and B_4). In contrast, the boundary between the middle silty layer and the upper sandy layer is less distinct, sometimes becoming difficult to identify (Fig. 3B_4).

The following SSDS are recognised in variant B (Figs. 3B and 4B). (1) Silty flame structures, with widths ranging from 0.3 to 2.1 cm and heights from 0.2 to 0.8 cm, are observed (Fig. 3B_1). Their shape coefficient ranges from 0.24 to 1.19. (2) Load casts are characterised by widths from 0.38 to 2.55 cm and heights from 0.3 to 0.9 cm. Their shape coefficient is similar for all subvariants, ranging from 0.26 to 0.95, with an average of 0.46. (3) Silty injection structures, ranging from 0.5 to 1.25 cm in height and 0.5 to 1.75 cm in width, have a shape coefficient from 1.0 to 1.4 (Figs. 3B_2—B_4). (4) Sandy injection structures vary in height from 0.3 to 1 cm and in width from 0.25 to 0.8 cm; their shape

coefficient ranges from 0.5 to 1.6 (Figs. 3B_3—B_4). (5) Clastic volcanoes are observed in subvariants B3 and B5 (Figs. 3B_2—B_4). The width of the clastic volcano veins is 1.5–2.5 cm and the length is 1.15–1.9 cm. Silt blows reach 0.15–0.3 cm in height and 3–4.2 cm in width. Their average shape coefficients are as follows: $V_1 = 0.5$, $V_2 = 1.93$, $V_3 = 0.82$, $V_4 = 0.11$, $V_5 = 0.09$, and $V_6 = 2.35$. Furthermore, a displacement similar to a (6) fault is observed in the B1 subvariant (Fig. 3B_5). This displacement has a 1 cm vertical range.

3.1.2.2. Interpretation. The decrease in the thickness of both sandy layers, together with an increase in the silty layer, suggests a redistribution of grains within the sedimentary profile. This rearrangement may be attributed to the consolidation and reorganisation of sandy grains and the swelling of silty grains, potentially in response to seismic shock (see section 3.1.1). The sharp boundary between the lower sandy layer and the middle silty layer, occasionally disrupted by contorted bedding, points to a strong contrast in grain size and sediment properties, leading to a differential response under stress. Conversely, the less distinct boundary between the upper sandy layer and the silty layer implies a more gradual transition between sediments, possibly due to co-seismic mixing or weaker initial contrasts (cf. Allen, 1982).

The occurrence of silty flame structures and load casts across all subvariants highlights inverse density differences, supporting the idea of seismic-induced liquefaction and subsequent reorganisation of sediments (cf. Owen, 2003). The flatness of flame structures and load casts suggests that the sediment layers experienced limited vertical movement and compaction. This is likely due to seismic disturbances, which prevented significant vertical deformation, causing the structures to spread laterally. The presence of silty and sandy injection structures indicates fluidisation processes, where sediments were injected into overlying layers due to liquefaction (Owen and Moretti, 2011). The relatively higher shape coefficient of the silty injection structures compared to the sandy injection structures suggests that silty sediment was more prone to forming elongated structures, likely due to its finer grain size and cohesive properties. The clastic volcanoes, with varying shape coefficients, indicate significant disruptions within the sedimentary layers, caused by the upward movement of fluidised sediment (Collignon et al., 2018). These variations suggest a wide range of sedimentary conditions during volcano formation. Broad cones indicate high-pressure expulsion, while shape coefficients reflect differences in sediment viscosity and the resistance of overlying layers. Simulated seismic activity likely caused liquefaction, leading to sediment injection through overlying layers, shaping the observed volcanic structures. The displacement similar to a fault in the B1 subvariant suggests intense and localised microstress that these sedimentary layers experienced (cf. Lewis et al., 2002).

3.1.3. Variant C

3.1.3.1. Description. The thickness of the lower sandy layer (Fig. 3B) decreased by 5–15 %, the middle silty layer increased by 6–11 %, while the upper sandy layer decreased by 8–30 %. The lithological boundary between the lower sandy layer and the middle silty layer is sharp (Figs. 3C_1C_4), whereas the boundary between the middle silty layer and the upper sandy layer is less distinct and sometimes difficult to identify (Figs. 3C_2 and C_3).

A wide range of SSDS is observed in variant C (Figs. 3 and 4C). (1) Silty flame structures, with widths ranging from 0.3 to 1 cm and heights from 0.5 to 2 cm, are observed in all subvariants (Figs. 3C_2—C_5). The shape coefficient ranges from 0.31 to 0.93. (2) Sandy load casts have widths ranging from 0.4 to 1 cm and heights from 0.4 to 4.3 cm (Figs. 3C_2 and C_5). The shape coefficient is consistently similar across all subvariants, ranging from 0.24 to 0.62. (3) Pseudonodules, with a shape coefficient of 0.29–0.31, are observed in subvariant C4 (Fig. 3C_1). (4) Sandy injection structures, with 25 instances showing heights ranging from 0.2 to 0.4 cm and widths from 0.3 to 0.4 cm (Figs. 3C_1—C_3). These structures have shape coefficients varying from 0.5 to 1.3 cm. (5) Silty injection structures are observed in subvariant C1. These structures range from 0.3 to 0.9 cm in height and 0.3 to 1.6 cm in width, with shape coefficients between 1.0 and 1.7. No injection structures, either sandy or silty, are found in subvariants C5. (6) Clastic volcanoes are identified in subvariants C1, C2, and C4 (Figs. 3C_3 and C_4). Their veins' widths range from 0.6 to 1.7 cm and lengths from 0.8 to 1.9 cm. The clastic volcano cones reach heights of 0.2 to 0.5 cm and widths of 3 to 5 cm. The shape coefficients are as follows: $V_1 = 0.08$, $V_2 = 3.95$, $V_3 = 1.37$, $V_4 = 0.23$, $V_5 = 0.31$, and $V_6 = 2.94$.

3.1.3.2. Interpretation. The reduction in the thickness of the lower and the upper sandy layers indicates consolidation under the seismic forces. The greater reduction in thickness in the upper sandy layer compared to the lower sandy layer might be due to the different initial conditions and/or the impact of the original thin sandy layer, which likely had less porosity than the upper one. The increase in the thickness of the middle silty layer indicates swelling and expansion of the silt due to the stress (cf. Barbosa et al., 2023) and water content. The sharply defined boundary between the lower sandy layer and the middle silty layer suggests no mixing and a clear separation between these layers. This distinct boundary indicates that the lower sandy layer and middle silty layer responded differently to the seismic activity, possibly due to differences in their grain size, composition, and consolidation properties (cf. Foda and Chang, 1996; Van der Baan, 2009). A less distinct boundary between the middle silty layer and the upper sandy layer suggests a greater degree of mixing or interaction between these layers during the seismic event (cf. Owen, 1985). The seismic activity caused partial fluidisation and mixing of the silts and upper sands, leading to less defined lithological contacts. This could be caused by the uppermost position of these layers in the sedimentary sequence and the lack of top loading.

The flat and wide flame structures and load casts indicate horizontal spreading and low vertical displacement. This morphology suggests that the sediments experienced lateral forces that caused them to spread out rather than penetrate vertically. The elongated downward pseudonodules in subvariant C4 indicate differential settling where the reversed density phenomenon occurs. This elongation signifies that the sediments underwent vertical displacement due to gravitational settling in a fluidised state (Sims, 2013). The sandy injection structures present a mix of small, wide forms and narrow, long forms. The small, wide injection structures likely formed under conditions of lower vertical stress but significant lateral pressure, causing the sediments to spread horizontally. In contrast, the narrow, long silty injections indicate higher vertical stress, forcing the sediments to intrude upwards through narrower channels.

The clastic volcanoes exhibit various morphologies based on their shape coefficients. Structures with wide sediment cones and extensive lateral spread indicate that the extruded sediment predominantly moved sideways across the surface, rather than ascending vertically. This suggests relatively low resistance to horizontal movement and ample space for lateral dispersion. When the cone is wider than the volcanic vein, it underscores the predominance of lateral extrusion over vertical movement, pointing to an ease of lateral flow. Structures, where the vertical veins are longer than their width, indicate a more significant vertical extrusion path, suggesting that the force driving the sediment upwards was strong enough to overcome vertical resistance. This results in a more focused and pronounced upward movement with less lateral spread.

3.1.4. Variant D

3.1.4.1. Description. The thickness of the lower silty layer (Fig. 3) increased by 7–44 %, the middle fine-grained sandy layer decreased by 30–50 %, and the upper coarse-grained sandy layer decreased by 19–29

%. The angle of layers, especially silt and fine-grained sand, changed by up to 45° (Fig. 3D_1). The boundary between the lower silty layer and the middle fine-grained sandy layer is indistinct (Fig. 3D_3), whereas the boundary between the fine-grained sandy layer and the coarse-grained sandy layer is well-marked (Figs. 3D_1D_5). The fine-grained sands infilled the pores in the upper coarse-grained sands (Fig. 3D_3). Air / water bubbles formed parallel to the boundary planes (Figs. 3D_1 and D_2).

The two following SSDS are developed (Figs. 3 and 4D). (1) Silty flame structures, with heights between 0.1 and 1 cm and widths from 0.1 to 0.3 cm, have a shape coefficient between 0.46 and 1.6, averaging 0.79 (Figs. 3D_1- and D_2). (2) Sandy load casts, with heights from 0.2 to 1.3 cm and widths from 0.1 to 0.4 cm, have a shape coefficient ranging from 0.24 to 0.78 (Figs. 3D_1 and —D_2).

3.1.4.2. Interpretation. The simulated seismic liquefaction affected all layers in variant D. However, more deformation structures developed in the lower and middle layers. Thickness decrease resulted in compaction of sediments within the profile, contributing to their ability to liquefy (cf. Świątek et al., 2023). The change in the thickness of the silt later indicates swelling and expansion of the silt (see section 3.1.1). The middle fine-grained sand infilled pores in the upper coarse-grained sand. The formation of air / water bubbles parallel to the boundary plane suggests the release of previously entrapped air / water during rapid expulsion by liquefaction. These bubbles are a direct consequence of the sudden reduction in pore pressure and the subsequent escape of water from the liquefied layers (cf. Pralle et al., 2003). The reorientation of the middle sandy layer (tilting up to 45°) developed during seismic shaking and is typical in environments where liquefaction-induced ground movements cause tilting and bending of the sediment strata (cf. Abd-Elhamed and Mahmoud, 2019).

The presence of flat and wide as well as tall and wide, silty flame structures reflects variations in sediment response to liquefaction. The flat and wide sandy load casts suggest that the coarser sands settled into the underlying, more fluidised fine-grained sands or silts, creating the characteristic load cast shapes. The absence of injection structures and clastic volcanoes can be explained by the insufficient pressure and energy required to force sediments upwards through overlying layers (cf. Postma, 1983).

3.1.5. Variant E

3.1.5.1. Description. The thickness of the lowermost silty layer (Fig. 3) increased by 10–40 %, the lower sandy layer decreased by 1–10 %, the upper silty layer increased by 1–12 %, and the uppermost sandy layer decreased by 30–40 %. The boundary between the lowermost silty layer and the lower sandy layer is indistinct and gradual (Fig. 3E_1); between the lower sandy layer and the upper silty layer is sharp (Fig. 3E_1-E_5), while between the upper silty layer and uppermost sandy layer is usually less distinct but well marked in some places (Fig. 3E_4).

Six SSDS are recognised in the layers of variant E (Figs. 3 and 4E). (1) Silty flame structures vary in height from 0.3 to 3.5 cm and in width from 0.3 to 0.9 cm (Fig. 3E_2). Their shape coefficients range from 0.22 to 2.0, showing slight differences between subvariants. (2) Sandy load casts, with heights from 0.6 to 1.3 cm and widths from 0.8 to 4.4 cm, have a shape coefficient ranging from 0.26 to 0.93 (Fig. 3E_2). (3) Pseudonodules are observed across all subvariants (Figs. 3E_1 and E_3), with widths from 0.8 to 2.7 cm and heights from 0.5 to 1.4 cm. The shape coefficient for pseudonodules is similar across all subvariants, ranging from 0.23 to 0.97, with an average of 0.55. (4) Sandy injection structures, present in subvariants E1, E4, and E5, are noted between the lowermost sandy layer and the upper silty layer (Figs. 3E_1 and E_4). Their height ranges from 0.1 to 0.6 cm while their width ranges from 0.2 to 0.9 cm; their shape coefficients range from 1.0 to 1.8. (5) Clastic volcanoes are abundant in all subvariants (Figs. 3E_4-E_5). The veins of clastic volcanoes range from 0.3 to 1.5 cm in width and 0.7 to 1.2 cm in length. The volcanic cones have heights from 0.1 to 0.3 cm and widths from 1.3 to 7.25 cm. The average value of shape coefficients reaches for V_1 = 0.09, V_2 = 3.03, V_3 = 1.2, V_4 = 0.22, V_5 = 0.26, and V_6 = 2.72. (6) Disaggregation bands were observed in subvariants E1 and E3. These structures co-occur with silty volcano veins.

3.1.5.2. Interpretation. The changes are observed in all layers and all subvariants. The increase in the thickness of both silty layers and the decrease in the thickness of both sandy layers suggest that the silt experienced expansion and redistribution, while the sand underwent compaction and thinning. The lithological boundaries reflect these changes, with indistinct and gradual transitions between the lowermost silty layer and lower sandy layer, and a sharper boundary between the upper silty layer and uppermost sandy layer.

The variation in morphology of flame structures reflects different conditions of sediment movement and fluidisation during seismic events. The flat and wide sandy load casts suggest that they were formed in broad depressions. Pseudonodule structures co-occur between volcano veins. The presence of sandy injection structures in subvariants E1, E4, and E5, between the lower sandy layer and upper silty layer, highlights the movement of liquefied sand into overlying silt. The narrow and elongated injection structures suggest flow through confined spaces. However, the absence of silty injection structures may indicate that the silty layers did not liquefy to the same degree or lacked the necessary pressure to form injections.

The abundant clastic volcanoes, with their wide sediment cones and varying vein dimensions, originating from the middle silty layer, indicate upward movement of liquefied silt through fractures or weak zones. The lack of structures originating from the lowermost silty layer suggests that this layer did not experience the same level of liquefaction, had more cohesive properties, or had a higher degree of consolidation preventing the formation of such features. Disaggregation bands observed in subvariants E1 and E3 support the idea of intense seismic activity causing the separation and movement of sediment grains.

3.2. Features of experimentally-induced SSDS

Six major SSDS were developed in 25 plexiglass cylinders as a result of seismic shock simulation in water-saturated sedimentary sequences (Fig. 4E; see Appendix S2 for a table comparing the shape coefficient between variants and subvariants).

3.2.1. Flame structures

Simulated seismic shocks led to the development of 205 flame structures (Fig. 5A). The largest number of structures was identified in variant D, and the fewest in variant E. They are 0.1–3.5 cm wide and 0.1–1 cm high. Values for variant E have a wider spread, while values for variant D are more clustered, indicating less variability in conditions during their development. The highest rate of changes in the morphology of flame structures occurs in variant E. Strong and very strong relationships were observed for all variants A-E (Fig. 5A). An upward trend between the width and the height of flame structures is visible (R = 0.83 for all subvariants). Individual coefficients of correlation, as well as trend equations, are similar to each other (R ranges from 0.7 to 0.78).

3.2.2. Load casts

The experiment resulted in the formation of 195 load casts (Fig. 5B). Variant D showed the highest number of load casts, while variant A had the fewest. Load casts range in size, with widths from 0.1 to 4.2 cm and heights from 0.1 to 4.5 cm. For variants A-D, the trend is positive with slope coefficients near 0.3, while variant E has a negative trend and a slope coefficient of 3.3 (Fig. 5B). There is a strong and very strong correlation between the height and width of load casts (R = 0.86 for all subvariants). Variant B demonstrated the highest correlation coefficient

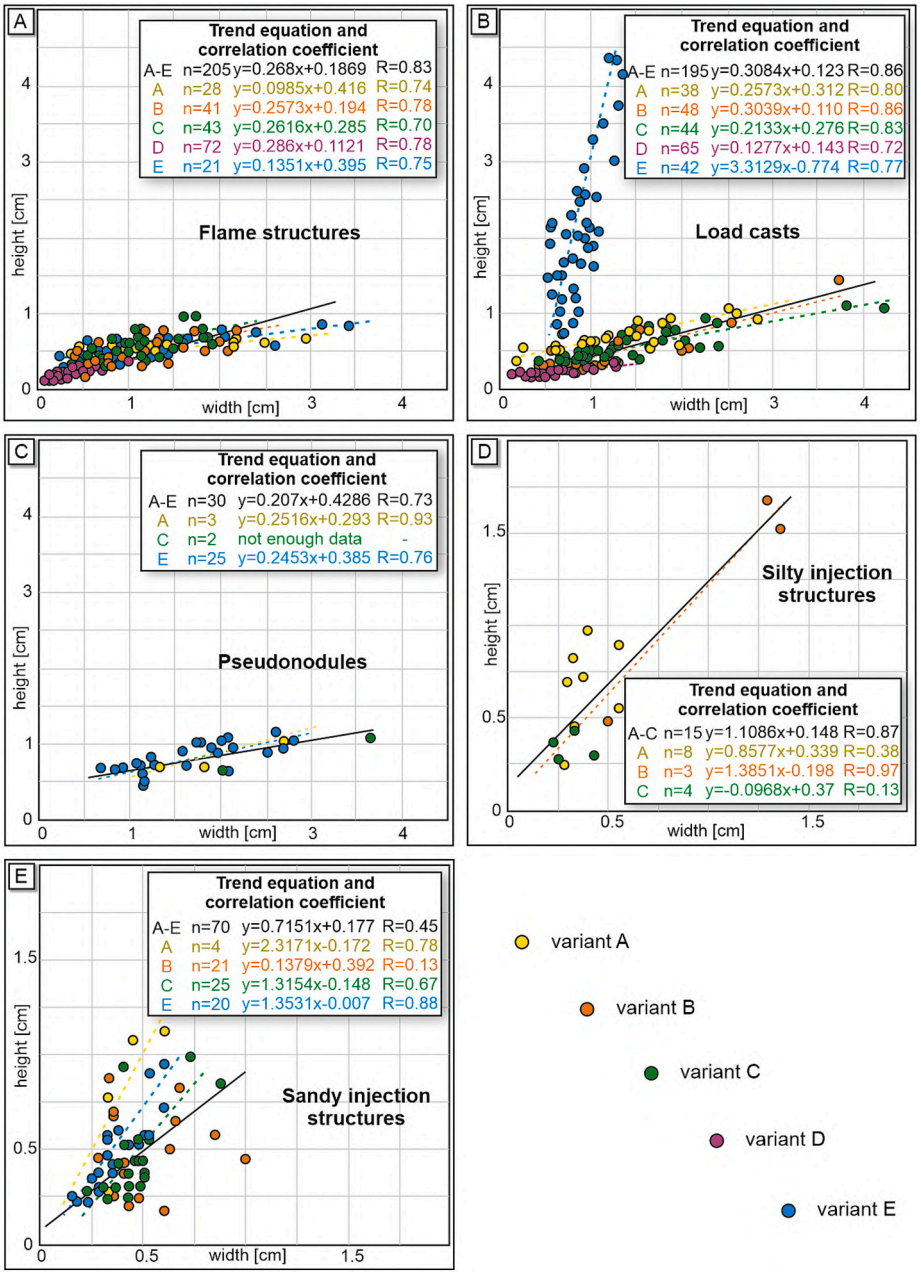

Fig. 5. Relationships between the dimensions of the major SSDS developed during seismic shock simulation: A – flame structures, B – load casts, C – pseudonodules, D – silty injection structures, E – sandy injection structures.

(0.86), while variant D had the lowest correlation coefficient (0.72). Despite these differences, an overall upward trend in the morphology of load casts is clear across all variants.

3.2.3. Pseudonodules

Simulated seismic shocks led to the formation of 30 pseudonodules, with the highest number in variant E (Fig. 5C). Pseudonodules had widths from 0.6 to 3.7 cm and heights from 0.4 to 1.3 cm. An upward trend (the greater the width, the greater the height) is apparent and supported by strong correlation coefficients (R = 0.73 for all subvariants, 0.76 for variant E).

3.2.4. Silty injection structures

Fifteen silty injection structures were identified (Fig. 5D) during the experiment. The highest number was found in variant A. Their dimensions vary, with widths from 0.2 to 1.3 cm and heights ranging from 0.25 to 1.7 cm. A notable strong positive correlation between the width and height of these structures was observed, with an overall correlation coefficient (R = 0.87).

3.2.5. Sandy injection structures

Experimental seismic activity resulted in the formation of 70 sandy injection structures (Fig. 5E). The highest number of these structures was recognised in variant C, while no structures were present in variant D. The sandy injection structures vary in widths from 0.2 to 1 cm and heights from 0.2 to 1.3 cm. Despite a visible upward trend between width and height, the overall correlation for all subvariants is weak (R = 0.45). However, strong correlations were observed within specific variants, particularly variant E (R = 0.88) and variant C (R = 0.67), indicating that as the width increases, the height of the sandy injection structures also increases significantly.

3.2.6. Clastic volcanoes

The simulated shock caused the development of 57 clastic volcanoes, with the highest number found in variant E and none observed in variant D (Fig. 6). The vein widths of the volcanoes ranged from 0.3 to 3.5 cm, and their lengths varied between 0.6 and 2 cm. The volcanic cones exhibited heights from 0.1 to 0.5 cm and widths from 1 to 5.5 cm.

The overall correlation between the width and length of the vein is weak ($R = 0.57$; Fig. 6A); however, individual variants show strong to very strong correlations, indicating an upward trend ($R = 0.72$–0.84). The relationship between vein width and blow height is very weak ($R = 0.21$; Fig. 6B). The correlation between the width of the vein and the width of the volcanic blow is very high (R = 0.7 for all subvariants; Fig. 6C), and remains consistently high across individual variants, also showing an upward trend (R = 0.72–0.88). There is no significant correlation between vein length and blow height (Fig. 6D), with the highest correlation coefficient observed in variant E ($R = 0.59$). A relatively strong and positive correlation exists between vein length and cone width ($R = 0.61$ for all subvariants; $R = 0.71$ for variant E; Fig. 6E). Although there is no strong correlation between cone height and width (Fig. 6F).

4. Discussion

4.1. "Strength"

We deliberately titled this section "Strength" rather than "Magnitude" because the magnitude of the seismic shocks simulated in our experiments was estimated based on calculations rather than direct measurements. The estimated value of M~3.5 is derived solely from empirical studies and is specific to the laboratory conditions, including the distance of the cylinders from the wave source, their weight, and their dimensions. Our experimental results do not fully align with earlier findings, which suggest that seismic shocks of low magnitude (~M3.5) are insufficient to induce liquefaction in sediments. In previous studies, it has often been assumed that the minimum earthquake magnitude required to trigger sediment liquefaction is at least M4.2 (Youd, 1977; Galli, 2000), and in many cases, a higher magnitude threshold was suggested (Ambraseys, 1988). The prevailing view has been that smaller seismic events, below this threshold, do not generate sufficient energy to destabilize sedimentary layers, limiting the potential of such events to induce liquefaction (Papadopoulos and Lefkopoulos, 1993). Higher magnitudes, generally above M5.0, were believed to be necessary for the formation and development of significant SSDS such as clastic dikes, flame structures, and sand blows (Allen, 1986; Owen and Moretti, 2011). According to Zhong et al. (2022), it is not possible to develop SSDS below M5, and the development of ball-and-pillow structures or pseudonodules is only likely by M6 and M6.5, respectively. However, these authors have marked that low-magnitude earthquakes (M3.6) occurred during the 1966 in Lompoc, with a focal depth of only 1.1 km, causing surface ruptures and probably liquefaction phenomenon.

Previous studies have demonstrated that SSDS can form at varying levels of Peak Ground Acceleration (PGA). For instance, Seed and Idriss (1971) reported PGA values as low as 0.09 g, while Kramer and Seed (1988) documented thresholds of 0.2–0.03 g. Higher PGA values

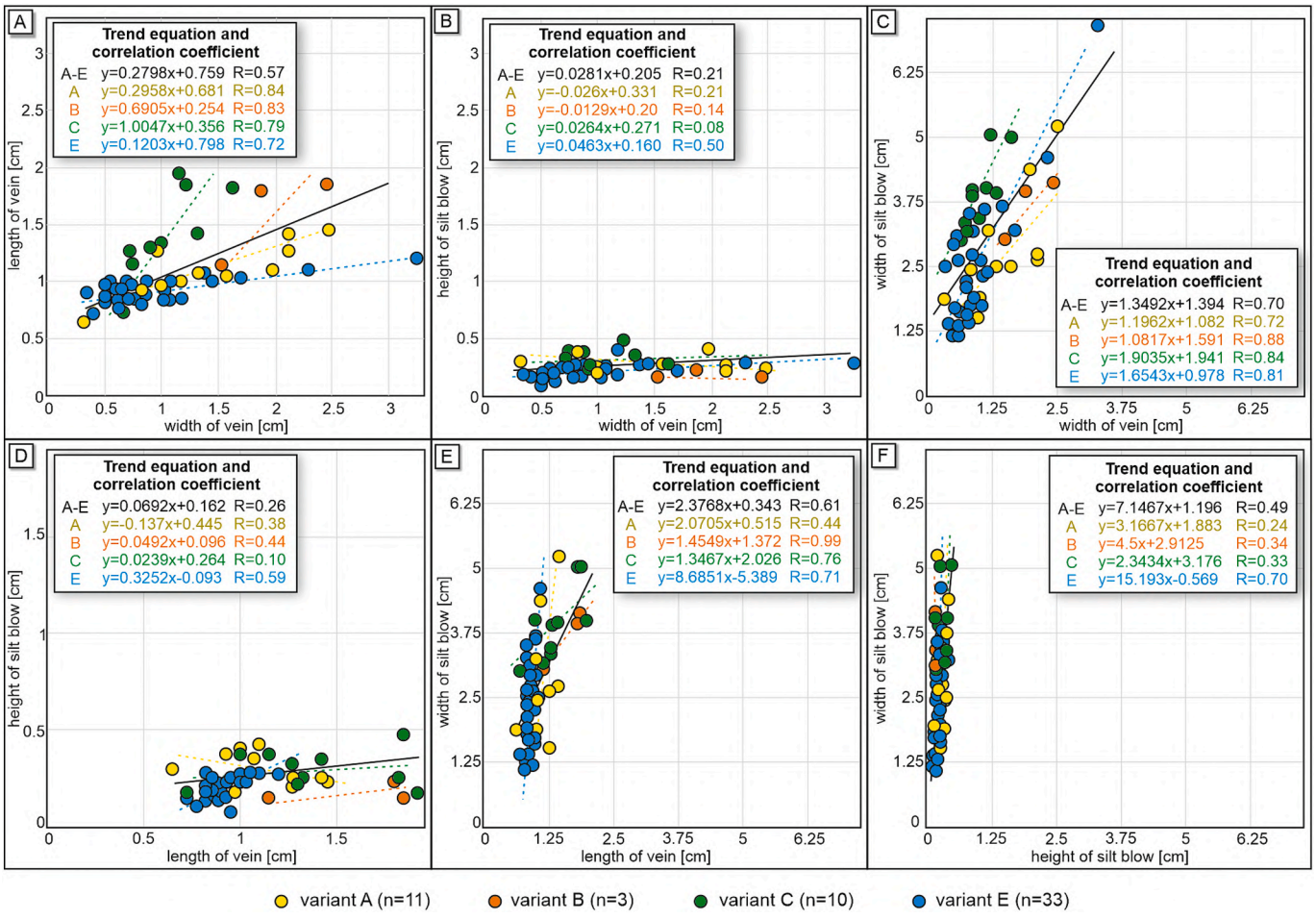

Fig. 6. Relationships between the dimensions of clastic volcanoes developed during seismic shock simulation: A – width of vein and length of vein, B – width of vein and height of blow, C – width of vein and width of blow, D – length of vein and height of blow, E – length of vein and width of blow, F – height of blow and width of blow.

between 0.1 and 0.2 g were noted by Quigley et al. (2013) and Varghese and Latha (2014), with González de Vallejo et al. (2005)) identifying a range of 0.22–0.35 g. Owen (1996) observed deformation at 0.29–1.15 g. In contrast, this study provided a PGA of approximately 2 g, significantly exceeding the thresholds documented in most previous research. This high acceleration led to extensive sediment mobilization and the formation of complex deformation features, such as clastic volcano, load structures, and flame structures, similar to those observed experimentally by Liang et al. (2024) at PGA levels of 0.5–0.8 g. The extreme PGA applied in this study provides valuable insights into sediment behaviour under seismic conditions, contributing to a better understanding of liquefaction and SSDS formation under dynamic loading, with implications for paleoseismic analysis and seismic hazard assessments.

Moreover, our experiments provided that such processes are more likely to occur in sediments which are highly water-saturated (>40 % of sediment volume) (cf. Świątek and Pisarska-Jamroży, 2023; Świątek et al., 2023). Detailed morphometric analysis of the deformation structures showed that, although the lower magnitude generated less seismic stress, it was still capable of producing complex SSDS in properly prepared sediment sequences.

4.2. Sediment arrangement

The arrangement of sedimentary layers played a critical role in determining the type, extent, number, and distribution of deformation structures observed in the experiment (Figs. 3–6). Each sediment sequence, consisting of varying combinations of silt, fine-grained sand, and coarse-grained sand, reacted differently to the simulated seismic shocks. The differences in grain size (cf. Obermeier, 1996; Moretti et al., 1999), sediment compaction (Tang et al., 2016), and water content between layers (cf. Cui et al., 2022), as well as the thickness of layer (Tuttle and Seeber, 1991; Alfaro et al., 2010; Zhong et al., 2022) directly influenced the deformation response, as previously documented in field studies of seismically-induced liquefaction structures. Field and experimental blast data clearly indicate that the lateral confinement of buried sandy bodies, their thickness, and the occurrence of anon-liquefiable crust influence the dissipation of the excess pore water pressure, and therefore the duration of liquefaction phenomena, according to the local stratigraphy (Minarelli et al., 2024). The experimental results demonstrated that the upper sandy layers consistently exhibited more pronounced deformation compared to the lower sandy and silty layers (Fig. 3). This can be attributed to their position within the sediment sequence, where the upper layers experience less vertical confinement and are, therefore, more susceptible to liquefaction-induced fluidisation and reorganisation under seismic loading (cf. Morsilli et al., 2020). The increased deformability of these upper layers is consistent with earlier findings suggesting that the energy dissipation during seismic shaking is often more pronounced in deeper layers, leading to more significant deformation in the uppermost, less constrained sediment (Owen and Moretti, 2011; Wiemer et al., 2015).

The textural contrast between silt and coarse-grained sand further promoted the development of SSDS. At the interface between these sediment types, liquefaction was more likely to occur due to the differences in permeability and shear resistance, as noted in previous research (cf. Owen, 2003; Kokusho, 1999; Wahyudi et al., 2013; Chiaradonna and Reder, 2019; Müller et al., 2023). The sharp boundaries between sandy and silty layers in some of the experimental variants (Fig. 3) led to the formation of load casts, pseudonodules, and injection structures, confirming the role of grain size and layer arrangement in shaping these SSDS (Allen, 1982; Owen and Moretti, 2011).

4.3. SSDS – Field analogy and recognition criteria

In field studies, SSDS have been extensively used as indicators of past seismic activity, particularly in the identification of palaeoseismic events (Zhong et al., 2022; McCalpin et al., 2023). These deformation features, formed as a result of liquefaction and fluidisation, provide a crucial tool for understanding the intensity and dynamics of seismic events in regions where historical seismic records may be incomplete or unavailable (McCalpin and Nelson, 1996; Tuttle et al., 2019).

The morphometric analysis conducted in the experiment provides additional criteria for recognizing and interpreting SSDS in the field (cf. Obermeier et al., 1990; Hilbert-Wolf et al., 2009; Owen and Moretti, 2011; Owen et al., 2011; Moretti et al., 2014; He and Qiao, 2015; Świątek et al., 2025). For instance, the shape coefficients of flame structures, pseudonodules, and clastic volcanoes exhibit consistent trends in relation to their width, height, and overall dimensions (Figs. 7 and 8), which can be used to infer the intensity of past seismic events (Owen and Moretti, 2011; Belzyt and Pisarska-Jamroży, 2017). The correlation between these morphological parameters and factors controlling liquefaction in this study (sediment arrangement, magnitude, water content) suggests that similar approaches could be applied in field studies to estimate the processes responsible for deformation – whether it was a single process or multiple processes involving similar or differing forces. (Figs. 7 and 8).

The deformation structures observed in the laboratory simulations have been similar to those documented in natural settings (Fig. 9), providing a strong analogy between experimental and field-based seismically-induced SSDS. Many of the structures formed in our experiments, including clastic volcanoes, load casts, flame structures, and pseudonodules, are commonly identified in sedimentary sequences affected by past seismic events (Nichols et al., 1994; Moretti and Sabato, 2007; Moretti et al., 2016; Cox et al., 2014; McCalpin et al., 2023).

In our experiment, mud volcanoes were formed (Fig. 3), which is consistent with field observations (cf. Hommels et al., 2003; Pryce et al., 2023). Some studies present sand volcano reproduction and observations (cf. Bardet and Kapuskar, 1993; Obermeier, 1996; Moretti et al., 1999) However, it is important to note that in natural conditions, mud volcanoes are more frequently observed than sand volcanoes (Mazzini and Etiope, 2017). When the overlying sediment layers are sufficiently thin, injection structures have enough force to penetrate through and evolve into clastic volcanoes (cf. Figs. 3A_3 and A_2), with the displaced material forming a new layer on top, commonly referred to as extrudites (Fig. 3A_1, e.g., Hurst et al., 2021). The sizes of the deformation structures vary significantly, primarily depending on the lithological properties and the relationship between the two interfacing layers (Müller et al., 2023), where contrasts in grain size, permeability, and compaction play crucial roles in determining the extent and morphology of the structures formed.

4.4. Limitations of this study

Like all experimental research, it has also its limitations and reduced assumptions:

1. Water-saturated sediments had a limited volume, as well as limited directions of deformation due to the plexiglass cylinder's walls. We do not know accurately the role they played (negative or positive) in relation to the liquefaction phenomenon and the development of deformation structures. Firstly, the walls of the cylinder could act as a barrier and, under the pore-pressure effect, liquefied sediment may have fluidised along the weak zone, seeking the fastest escape route (see Fig. 1B). On the other hand, we observed clastic dykes and clastic volcanoes forming in the middle of cylinders. However, in nature, specific conditions can confine unconsolidated sediments, such as ice sheet (periglacial processes, cf. Van Loon et al., 2020), glacier (icequakes, cf. Phillips et al., 2018), and blocks of dead ice (kame, cf. Bitinas et al., 2004; Ozols, 2009; Gorbatov, 2020).
2. Experimental research cannot fully replicate conditions in which the analysed phenomenon occurs. We also used limited values and reduced numbers of factors influencing seismically-induced liquefaction, especially seismological parameters and some sediment

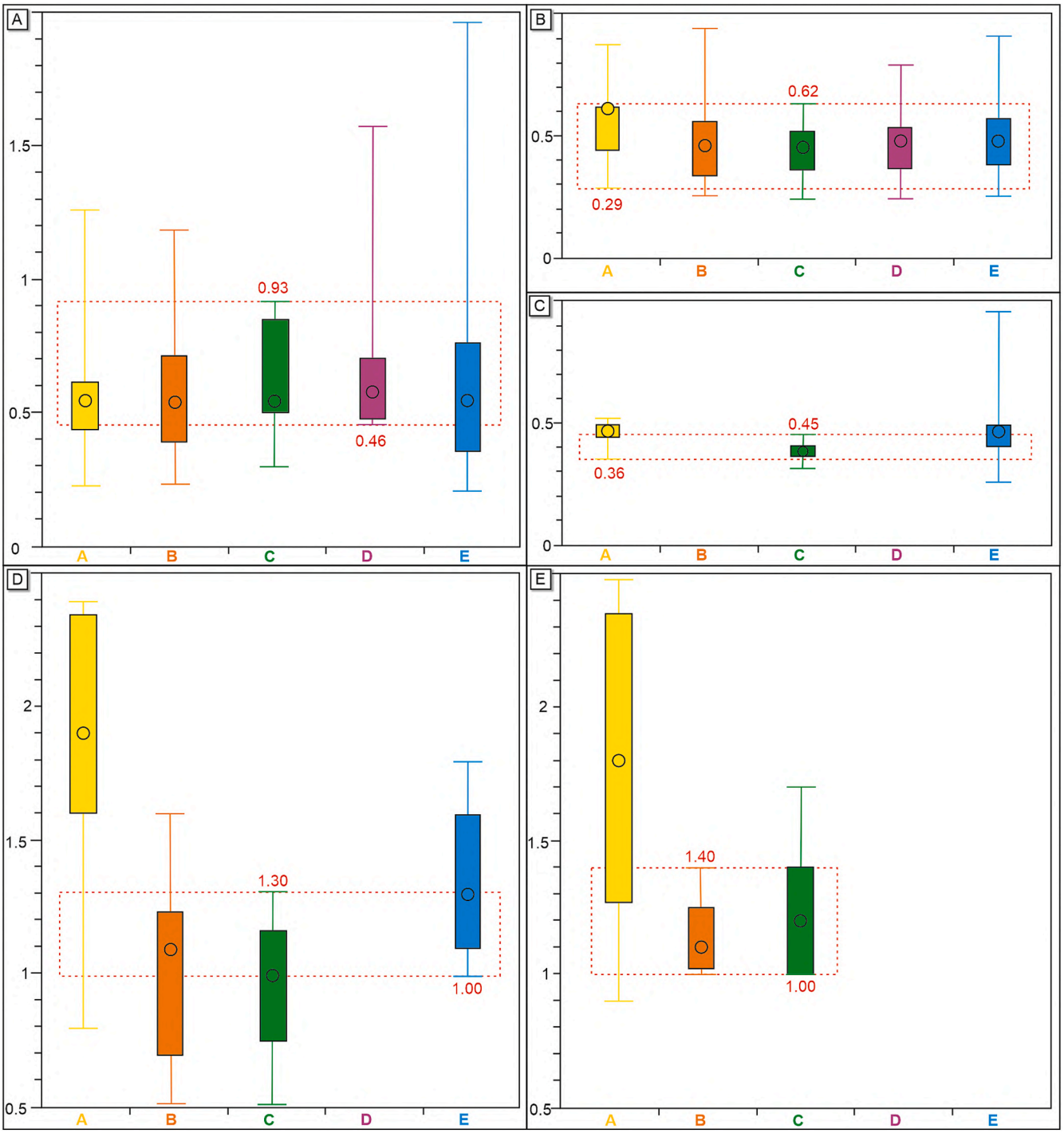

Fig. 7. Comparison of box plots for the shape coefficient of: A – flame structures, B – load casts, C – pseudonodules, D – sandy injection structures, and E – silty injection structures. The area marked with a red dashed lines indicates common values for all variants. See Appendix S1 for a table comparing the shape coefficient between variants and subvariants.

textural features (Fig. 1). Moreover, it is truly a challenge to use all feasible factors to accurately mimic natural conditions. It is possible that there are components controlling liquefaction that are not yet understood – e.g. geochemistry, soil-forming processes, and biological processes. Nevertheless, liquefaction is a very complex process, and each experimental setup contributes to a better understanding of its mechanisms.

3. The complex nature of liquefaction and its induced SSDS prevents accounting for all components influencing it. Therefore, it is infeasible to conduct experiments using all possible combinations. In this study, we focused on low magnitude and its consequences, such as the sizes and shapes of deformation structures.
4. Seismically-induced liquefaction is often linked to strong earthquakes, landslides, or volcano eruptions. These geological processes occur not only on a global scale but also on smaller local scales. The aim of our research was to show that some earthquake-induced features can be recorded in unconsolidated sediments on a small scale. These features are associated with small magnitudes and proximity to the hypocenter, as well as the epicentre. Although, in this study, the hypocenter was a few centimeters away instead of tens

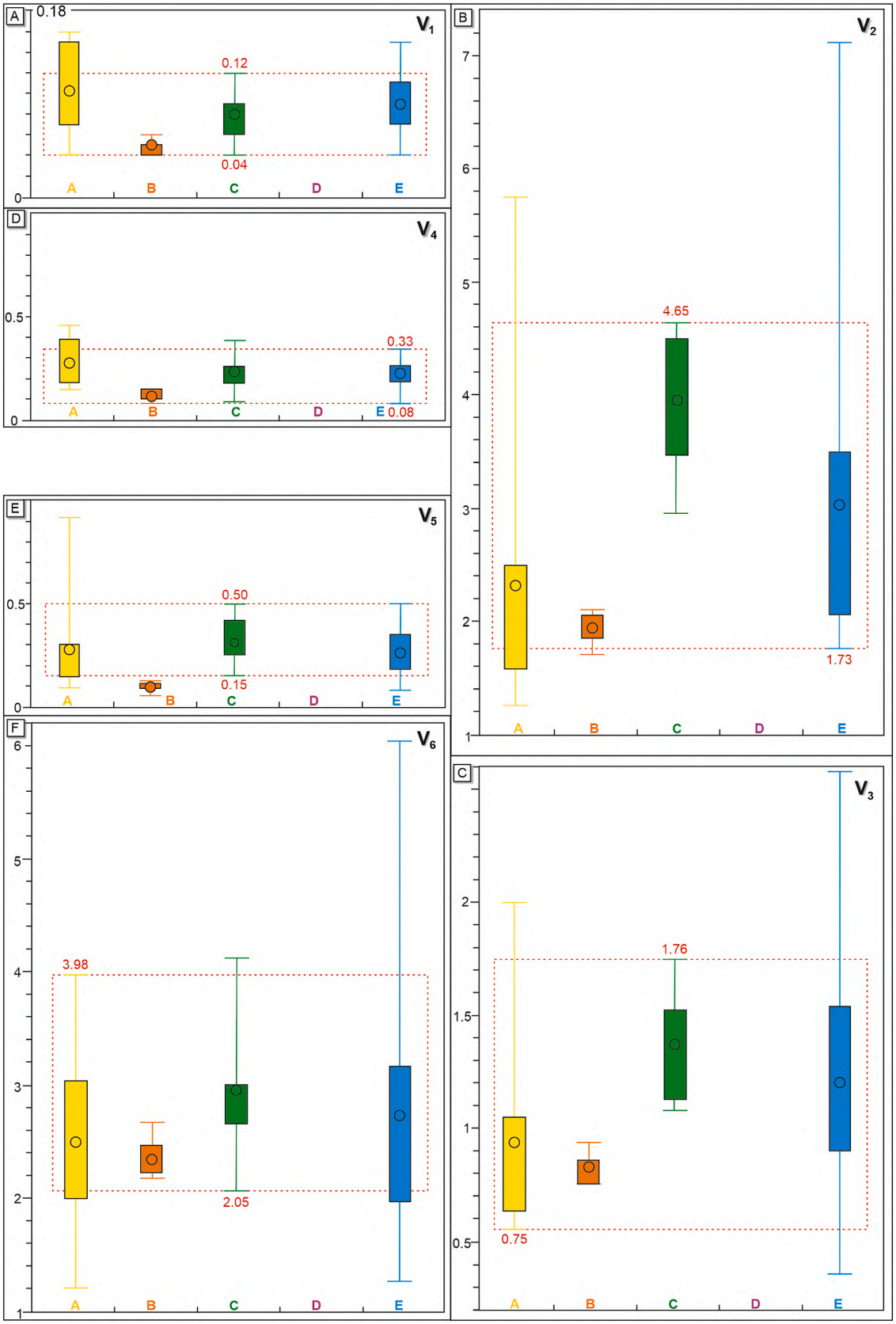

Fig. 8. Comparison of box plots for the volcano's shape coefficients of: V_1, V_2, V_3, V_4, V_5 and V_6 (for explanation see Fig. 2). The area marked with a red dashed line indicates common values for variants A, C-E. See Appendix S1 for a table comparing the shape coefficient between variants and subvariants.

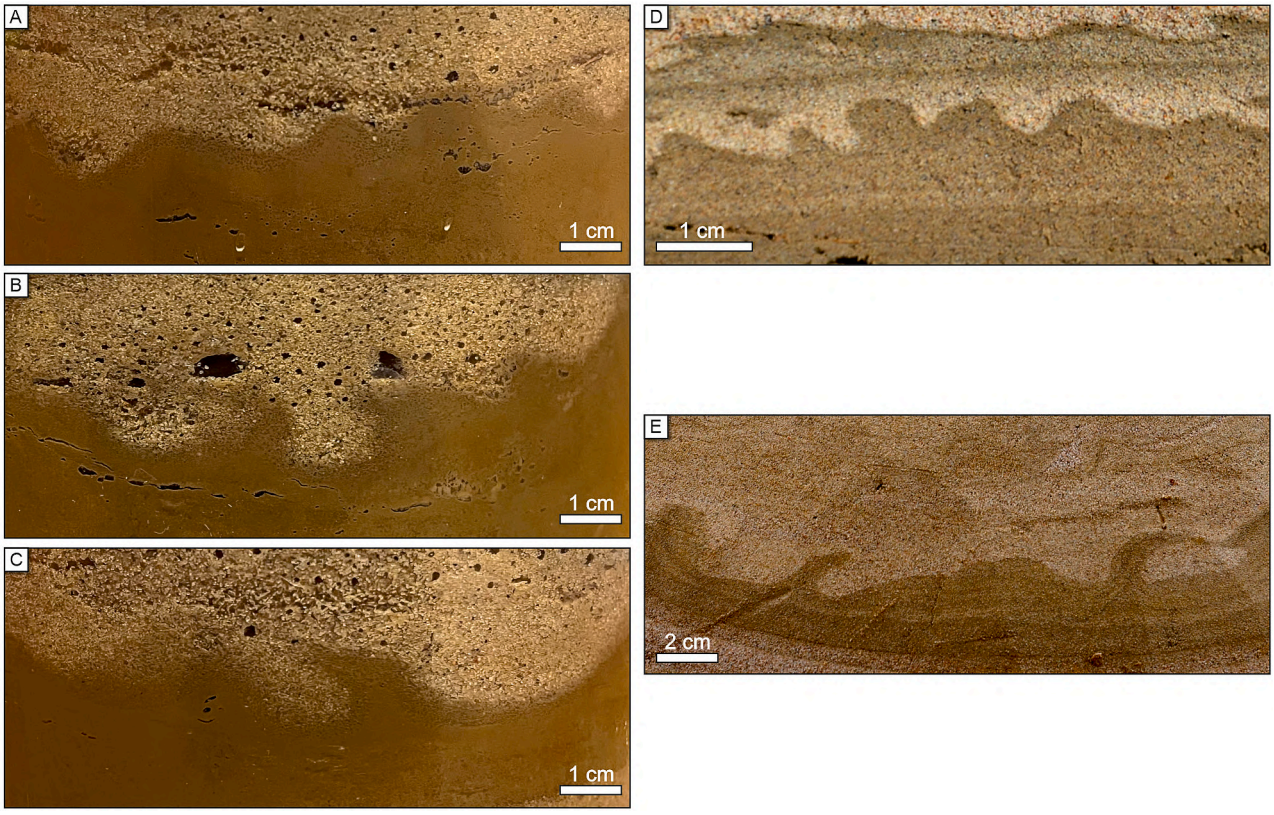

Fig. 9. Examples of developed flame structures and load casts in this study (A-C) and recognised in the field (D-E). A – subvariant C3, B and C – subvariant C2, D – silty and sandy SSDS from the Rakvere site (after Woźniak et al., 2021), E – silty and sandy SSDS from the Pikametsa site (Pisarska-Jamroży et al., 2024).

of kilometers (as in natural conditions), we should not exclude this scenario. Moreover, seismic shocks have been recognised in sandstone and mudstone cores at great deep (Nakashima and Komatsubara, 2016; Yang et al., 2016), which may confirm that such seismic events could occur near their recorded evidence.

5. To conduct our experiment we used only three types of sediment, as well as a limited number of stratigraphic combinations. However, our research did not focus on determining which sediment types liquefied, because this is already known from previous results (Świątek et al., 2023). We also used random but susceptible sediments to induce liquefaction. Moreover, some analyses have shown SSDS composed of silt similar to our analysed samples. In addition, sediment sequences were linked to naturally occurring layers (cf. Woźniak et al., 2021; Pisarska-Jamroży et al., 2024).

5. Conclusions

The following conclusions can be drawn:

1. The experiment demonstrated that seismic liquefaction and the development of soft-sediment deformation structures (SSDS) can occur at magnitudes as low as ~3.5, challenging the widely held belief that higher magnitudes (typically above 4.5) are necessary for significant liquefaction. These findings suggest that lower-magnitude seismic events, under certain sedimentary and water-saturated conditions, can still pose liquefaction risks.
2. The arrangement and composition of sediment layers play a crucial role in the development and morphology of SSDS. The experimental results demonstrated that the upper sandy layer, due to less packing, was more prone to liquefaction compared to the lower sandy layer, consistent with findings from previous studies. The contrast in grain size and permeability between silty and sandy layers promoted the development of flame structures, pseudonodules, and load casts, emphasizing the importance of sedimentological properties in liquefaction processes.
3. The innovative use of morphometric analysis provided detailed insights into the size, shape, and distribution of SSDS. This method showed a clear relationship between the height and width of the structures. Clastic volcanoes and flame structures displayed a strong correlation, with taller structures generally having greater widths. Pseudonodules exhibited more variability in their dimensions, ranging from elongated to compact forms. The analysis suggests that the size of SSDS is closely related to the seismic forces and the sediment's physical properties. The morphometric analysis offer a new approach to identifying and interpreting past seismic events in sedimentary records.
4. The SSDS observed in the experiment, such as clastic volcanoes, flame structures, load casts, and pseudonodules, closely resemble those found in natural environments. This suggests that the experimental setup successfully replicated forces responsible for liquefaction processes occurring in the field, providing valuable insights into the mechanisms driving seismic deformation in natural settings.
5. Ultimately, the experimental approach presented in this study offers a reliable analogue for understanding the formation and distribution of SSDS in the field (Fig. 9). The recognition criteria derived from this work – such as the shape, size, and spatial arrangement of SSDS – provide a valuable toolset for others seeking to identify seismic signatures in the geological record. These criteria not only aid in recognizing liquefaction-induced structures but also provide clues about the seismological parameters of past events, such as magnitude, duration, and frequency, contributing to a deeper understanding of the seismic history preserved in sedimentary environments.
6. The findings highlight the need to reconsider the liquefaction risk posed by lower-magnitude seismic events, particularly in regions with highly water-saturated sediments. This could have significant

implications for seismic hazard assessments in areas previously considered at low risk for liquefaction.

CRediT authorship contribution statement

Szymon Świątek: Writing – review & editing, Writing – original draft, Visualization, Validation, Project administration, Methodology, Investigation, Formal analysis, Data curation, Conceptualization. **Małgorzata Pisarska-Jamroży:** Writing – review & editing, Visualization, Supervision, Methodology, Conceptualization.

Declaration of competing interest

The authors declare that they have no known competing financial interests or personal relationships that could have appeared to influence the work reported in this paper.

Acknowledgments

This work was supported by the UAM Research University – Excellence Initiative (grant numbers 021/13/UAM/0040 and 054/13/SNP/0001). Szymon Świątek is also a scholar of Adam Mickiewicz University's Foundation for the academic year 2023/2024, as well as a scholar of the International Association of Sedimentologists. The authors thank Karolina Lewińska and Dariusz Kasztelan for field assistance. We greatly appreciate the in-depth review and major constructive comments of the Editor Giorgio Basilici, Prof. Daniela Fontana and the anonymous reviewer who led to significant improvement of the manuscript.

Appendix A. Supplementary data

Supplementary data to this article can be found online at https://doi.org/10.1016/j.sedgeo.2025.106833.

Data availability

All data created the work in the paper are available in the repository doi:https://doi.org/10.5281/zenodo.14525719

References

Abd-Elhamed, A., Mahmoud, S., 2019. Seismic response evaluation of structures on improved liquefiable soil. Eur. J. Environ. Civ. Eng. 25, 1–23. https://doi.org/10.1080/19648189.2019.1595738.

Aksu, I., Bazilevskaya, E., Karpyn, Z.T., 2015. Swelling of clay minerals in unconsolidated porous media and its impact on permeability. Georesources Journal 7, 1–13. https://doi.org/10.1016/j.grj.2015.02.003.

Alfaro, P., Gibert, L., Moretti, M., García-Tortosa, F.J., de Galdeano, C.S., Galindo-Zaldívar, J., López-Garrido, A.C., 2010. The significance of giant seismites in the Plio-Pleistocene Baza palaeo-lake (S Spain). Terra Nova 22, 172–179. https://doi.org/10.1111/j.1365-3121.2010.00930.x.

Allen, J.R.L., 1982. Developments in Sedimentology. Sedimentary Structures, their Character and Physical Basis, vol. 30A. Elsevier Scientific Publishing Company.

Allen, J.R.L., 1986. Earthquake magnitude-frequency, epicentral distance, and soft-sediment deformation in sedimentary basin. Sediment. Geol. 46, 67–75. https://doi.org/10.1016/0037-0738(86)90006-0.

Ambraseys, N.N., 1988. Engineering seismology: part I. Earthq. Eng. Struct. Dyn. 17, 1–105. https://doi.org/10.1002/eqe.4290170101.

Andrews, C.A.D., Martin, G.R., 2000. Criteria for liquefaction of silty soils. In: Paper Presented at 12th World Conference on Earthquake Engineering. New Zealand, Auckland.

Arias, A., 1970. A measure of earthquake intensity. In: Hansen, Robert J. (Ed.), Seismic Design for Nuclear Power Plants. Mass. Massachusetts Inst. of Tech. Press, Cambridge.

Ashmawy, A.K., Sukumaran, B., Hoang, V.V., 2003. Evaluating the influence of particle shape on liquefaction behavior using discrete element modeling. Proc. 13th International Offshore and Polar Engineering Conference. ISOPE 2, 542–549.

Atkinson, G.M., Boore, D.M., 1995. Ground-motion relations for eastern North America. Bull. Seismol. Soc. Am. 85, 17–30. https://doi.org/10.1785/BSSA0850010017.

Barbosa, V.H.R., Marques, M.E.S., Guimarães, A.C.R., 2023. Predicting Soil Swelling potential using Soil Classification Properties. Geotech. Geological Engineering 41, 4445–4457. https://doi.org/10.1007/s10706-023-02525-2.

Bardet, J.P., Kapuskar, M., 1993. Liquefaction sand boils in San Francisco during 1989 Loma Prieta earthquake. J. Geotech. Eng. 119 (3), 543–562.

Belzyt, S., Pisarska-Jamroży, M., 2017. W jaki sposób badać sejsmity? Przegląd metod badawczych. Acta Geographica Lodziensia 106, 171–180.

Belzyt, S., Pisarska-Jamroży, M., Bitinas, A., Woronko, B., Phillips, E.R., Piotrowski, J.A., Jusienė, A., 2021. Repetitive late Pleistocene soft-sediment deformation by seismicity-induced liquefaction in North-Western Lithuania. Sedimentology 68, 3033–3056. https://doi.org/10.1111/sed.12883.

Bitinas, A., Karmazienė, D., Jusienė, A., 2004. Glaciolacustrine kame terraces as an indicator of conditions of deglaciation in Lithuania during the last Glaciation. Sediment. Geol. 165, 285–294. https://doi.org/10.1016/j.sedgeo.2003.11.012.

Boore, D.M., 1983. Stochastic simulation of high-frequency ground motions based on seismological models of the radiated spectra. Bull. Seismol. Soc. Am. 73, 1865–1894.

Boore, D.M., Joyner, W.B., Fumal, T.E., 1997. Equations for estimating Horizontal Response Spectra and Peak Acceleration from Western north American Earthquakes: a Summary of recent work. Seism. Res. Letters 68, 128–153.

Brandes, C., Winsemann, J., 2013. Soft-sediment deformation structures in NW Germany caused by late Pleistocene seismicity. Seismol. Res. Lett. 102, 2255–2274. https://doi.org/10.1007/s00531-013-0914-4.

Brandes, C., Polom, U., Winsemann, J., Sandersen, P.B.E., 2022. The near-surface structure in the area of the Børglum fault, Sorgenfrei-Tornquist Zone, northern Denmark: Implications for fault kinematics, timing of fault activity and fault control on tunnel valley formation. Quat. Sci. Rev. 289, 107619. https://doi.org/10.1016/j.quascirev.2022.107619.

Bronikowska, M., Pisarska-Jamroży, M., Van Loon, A.J., 2021. First attempt to model numerically seismically-induced soft-sediment deformation structures – a comparison with field examples. Geological Quarterly 65, 60. https://doi.org/10.7306/gq.1629.

Castilla, R.A., Audemard, F.A., 2007. Sand blows as a potential tool for magnitude estimation of pre-instrumental earthquakes. J. Seismol. 11, 473–487. https://doi.org/10.1007/s10950-007-9065-z.

Chiaradonna, A., Reder, A., 2019. Influence of initial conditions on the liquefaction strength of an earth structure. Bull. Eng. Geol. Environ. 79, 687–698. https://doi.org/10.1007/s10064-019-01594-z.

Collignon, M., Schmid, D.W., Galerne, C., Lupi, M., Mazzini, A., 2018. Modelling fluid flow in clastic eruptions: Application to the Lusi mud eruption. Mar. Pet. Geol. 90, 173–190. https://doi.org/10.1016/j.marpetgeo.2017.08.011.

Cox, R.T., Lowe, C.C., Hao, Y., Mahan, S.A., 2014. Use of small-scale liquefaction features to assess paleoseismicity: an example from the Saline River fault zone, Southeast Arkansas, USA. Front. Earth Sci. 2, 31. https://doi.org/10.3389/feart.2014.00031.

Cui, M., Peng, N., Liu, Y., Wang, Z., Li, C., Xu, K., Kuang, H., 2022. Recognizing deformation origins: a review of deformation structures and hypothesis on the perspective of sediment consolidation. Int. Geol. Rev. 65, 1500–1523. https://doi.org/10.1080/00206814.2022.2094840.

Davies, N., Turner, P., Sansom, I.J., 2004. Soft-sediment deformation structures in the late Silurian Stubdal Formation: the result of seismic triggering. Nor. J. Geol. 85, 233–243.

De Magistris, F.S., Lanzano, G., Forte, G., Fabbrocino, G., 2013. A database for PGA threshold in liquefaction occurrence. Soil Dyn. Earthq. Eng. 54, 17–19. https://doi.org/10.1016/j.soildyn.2013.07.011.

Ecemis, N., 2021. Experimental and numerical modeling on the liquefaction potential and ground settlement of silt-interlayered stratified sands. Soil Dyn. Earthq. Eng. 144, 106691. https://doi.org/10.1016/j.soildyn.2021.106691.

Foda, M.A., Chang, Y.H., 1996. Faraday resonance in thin sedimentary layers. Paper presented at 11th World Conference on Earthquake Engineering.

Friedman, G., Sanders, J., 1978. Principles of Sedimentology. Wiley, New York.

Fuławka, K., Kwietniak, A., Lay, V., Jaśkiewicz-Proć, I., 2022. Importance of seismic wave frequency in FEM-based dynamic stress and displacement calculations of the earth slope. Studia Geotechnica et Mechanica. 44, 82–96. https://doi.org/10.2478/sgem-2022-0002.

Galli, P., 2000. New empirical relationships between magnitude and distance for liquefaction. Tectonophysics 324, 169–187. https://doi.org/10.1016/S0040-1951(00)00118-9.

González de Vallejo, L.I., Tsigé, M., Cabrera, L., 2005. Paleoliquefaction features on Tenerife (Canary Islands) in Holocene sand deposits. Eng. Geol. 76, 179–190. https://doi.org/10.1016/j.enggeo.2004.07.006.

Gorbatov, E.S., 2020. Particularity of formation of the kame Sharvaozero (North Karelia) and syngenetic deformations in its section. Geophysical Processes and the Biosphere 19, 33–50. https://doi.org/10.21455/GPB2020.3-3.

Green, R.A., Bommer, J.J., 2019. What is the smallest earthquake magnitude that needs to be considered in assessing liquefaction hazard? Earthquake Spectra 35, 1441–1464.

He, B., Qiao, X., 2015. Advances and overview of the study on paleo-earthquake events: a review of seismite. Acta Geol. Sin. 89, 1702–1746.

He, B., Qiao, X., Jaio, C., Xu, Z., Cai, Z., Guo, T., Zhang, Y., 2014. Palaeo-earthquake events during the late early Palaeozoic in the Central Tarim Basin (NW China): evidence from deep drilling cores. Geologos 20, 105–123.

Hilbert-Wolf, H.L., Simpson, E.L., Simpson, W.S., Tindall, S.E., Wizevich, M.C., 2009. Insights into syndepositional fault movement in a foreland basin; trends in seismites of Upper cretaceous Wahweap Formation, Kaiparowits Basin, Utah, USA. Basin Res. 21, 856–871.

Hommels, A., Scholte, K.H., Sabater, J.M., Hanssen, R.F., van der Meer, F.D., Kroonenberg, S.B., Aliyeva, E., Huseynov, D., Guliev, I., 2003. Preliminary ASTER and INSAR imagery combination for mud volcano dynamics, Azerbaijan. International Geoscience and Remote Sensing Symposium 1573–1575. https://doi.org/10.1109/IGARSS.2003.1294179.

Hou, Z., Chen, S., Zhang, S., Yang, H., 2019. Sedimentary deformation features as evidence for paleoseismic events in the middle Eocene in the Dongying Depression of the southern Bohai Bay Basin, eastern China. Can. J. Earth Sci. 57, 954–970. https://doi.org/10.3133/cir688.

Hurst, A., Grippa, A., Silcock, S.Y., Huuse, M., Bowman, M., Cobain, S.L., 2021. Introduction: subsurface sand remobilization and injection. Geological Society of London Special Publications 493, 1–10. https://doi.org/10.1144/SP493-2020-268.

Jain, A., Mittal, S., Shukla, S.K., 2022. Cyclic behaviour of stratified soils under liquefied states. Mar. Georesour. Geotechnol. 41, 721–742. https://doi.org/10.1080/1064119X.2022.2095946.

Jiménez-Millán, J., Abad, I., García-Tortosa, F.J., Jiménez-Espinosa, R., 2022. Structural Diagenesis in Clay Smearing Bands developed on Plio-Pleistocene Sediments Affected by the Baza Fault (S Spain). Minerals 12, 1255. https://doi.org/10.3390/min12101255.

Katsumata, A., 2001. Magnitude determination of deep-focus earthquakes in and around Japan with regional velocity-amplitude data. Earth, Planets and Space 53, 333–346. https://doi.org/10.1186/BF03352390.

Kokusho, T., 1999. Formation of water film in liquefied sand and its effect on lateral spread. J. Geotech. Geoenviron. 125, 817–826.

Kramer, S.L., Seed, H.B., 1988. Initiation of Soil Liquefaction under Static Loading Conditions. J. Geotech. Eng. 114, 412–430. https://doi.org/10.1061/(ASCE)0733-9410(1988)114:4(412).

Lakshmi, B.V., 2021. Seismically-Induced Soft Sediment Deformation Structures in and around Chamoli, Garhwal Himalaya, India. Journal of Earth and Environmental Science Research 156.

Lewis, H., Olden, P., Couples, G.D., 2002. Geomechanical simulations of top seal integrity. Norwegian Petroleum Society Special Publications 11, 75–87. https://doi.org/10.1016/S0928-8937(02)80008-X.

Liang, L., Lu, Z., Zhang, Q., Tian, H., Dai, F., Jiang, H., 2024. Shaking table simulation of soft sediment deformation structures in lacustrine sediments. Sediment. Geol. 472, 106756. https://doi.org/10.1016/j.sedgeo.2024.106756.

Lowe, D.R., 1976. Subaqueous liquefied and fluidised sediment flows and their deposits. Sedimentology 23, 285–308. https://doi.org/10.1111/j.1365-3091.1976.tb00051.x.

Maltman, A.J., Bolton, A., 2003. How sediments become mobilized. In: Subsurface Sediment Mobilization (Eds R.R. Van Rensbergen, a.J. Hillis and C.K. Maltman). Geological Society of London Special Publications 216, 9–20. https://doi.org/10.1144/GSL.SP.2003.216.01.02.

Mazzini, A., Etiope, G., 2017. Mud volcanism: an updated review. Earth Sci. Rev. 168, 81–112. https://doi.org/10.1016/j.earscirev.2017.03.001.

McCalpin, J.P., Nelson, A.R., 1996. Introduction to Paleoseismology. In: Paleoseismology (Ed.), J.P McCalpin. Academic Press.

McCalpin, J.P., Ferrario, F., Figueiredo, P., Livio, F., Grützner, C., Pisarska-Jamroży, M., Quigley, M., Reicherter, K., Rockwell, T., Štěpančíková, P., Táboříki, P., 2023. New developments in onshore paleoseismic methods, and their impact on Quaternary tectonic studies. Quat. Int. 664, 59–76. https://doi.org/10.1016/j.quaint.2023.03.008.

Minarelli, L., Amoroso, S., Civico, R., De Martini, P.M., Lugli, S., Martelli, L., Molisso, F., Rollins, K.M., Salocchi, A., Stefani, M., Cultrera, G., Milana, G., Fontana, D., 2022. Liquefied sites of the 2012 Emilia earthquake: a comprehensive database of the geological and geotechnical features (Quaternary alluvial Po plain, Italy). Bull. Earthq. Eng. 20, 3659–3697. https://doi.org/10.1007/s10518-022-01338-7.

Minarelli, L., Fontana, D., Lugli, S., Rollins, K.M., Stefani, M., Tonni, L., Amoroso, S., 2024. Sediment stacking pattern effect on sand liquefaction inferred from full-scale experiments in the Emilia alluvial plain (Italy). Eng. Geol. 231, 107735. https://doi.org/10.1016/j.enggeo.2024.107735.

Moretti, M., Sabato, L., 2007. Recognition of Trigger Mechanisms for Soft-Sediment Deformation in the Pleistocene Lacustrine Deposits of the Sant' Arcangelo Basin (Southern Italy): Seismic shock vs. Overloading. Sedimentary Geology 196, 31–45. https://doi.org/10.1016/j.sedgeo.2006.05.012.

Moretti, M., Alfaro, P., Caselles, O., Canas, J.A., 1999. Modelling seismites with a digital shaking table. Tectonophysics 304, 369–383.

Moretti, M., Van Loon, A.J., Liu, M., Wang, Y., 2014. Restrictions to the application of 'diagnostic' criteria for recognizing ancient seismite. J. Palaeogeogr. 3, 162–173. https://doi.org/10.3724/SP.J.1261.2014.00050.

Moretti, M., Alfaro, P., Owen, G., 2016. The environmental significance of soft-sediment deformation structures: key signatures for sedimentary and tectonic processes. Sediment. Geol. 344, 1–4. https://doi.org/10.1016/j.sedgeo.2016.10.002.

Morsilli, M., Giona Bucci, M., Gliozzi, E., Lisco, S., Moretti, M., 2020. Sedimentary features influencing the occurrence and spatial variability of seismites (late Messinian, Gargano Promontory, southern Italy). Sediment. Geol. 401, 105628. https://doi.org/10.1016/j.sedgeo.2020.105628.

Müller, K., Winsemann, J., Pisarska-Jamroży, M., Lege, T., Spies, T., Brandes, C., 2020. Limitations of soft-sediment deformation structures as indicators for paleo-earthquakes in formerly periglacial and glaciated areas. Paper presented at EGU General Assembly 2020.

Müller, P., Tamburelli, S., Menegoni, N., Perozzo, M., Amadori, C., Crispini, L., Federico, L., Seno, S., Maino, M., 2023. Concurrence of load-and-flame structures, balls-and-pillows, clastic injectites and shear deformation bands as indicator of seismicity in mixed siliciclastic-carbonate successions (Finale Ligure Basin, Italy). Mar. Pet. Geol. 155, 106345. https://doi.org/10.1016/j.marpetgeo.2023.106345.

Nakai, K., 2005. An Elasto-Plastic Constitutive Modeling of Soils Based on the Evolution Laws Describing Collapse of Soil Skeleton Structure, Loss of Overconsolidation and Development of Anisotropy. Nagoya University, Doctoral Thesis (in Japanese).

Nakashima, Y., Komatsubara, J., 2016. Seismically induced soft-sediment deformation structures revealed by X-ray computed tomography of boring cores. Tectonophysics 683, 138–147. https://doi.org/10.1016/j.tecto.2016.05.044.

Nichols, R.J., 1995. The liquefaction and remobilization of sandy sediments. Geological Society of London Special Publications 64, 63–76. https://doi.org/10.1144/GSL.SP.1995.094.01.06.

Nichols, R.J., Sparks, R.S.J., Wilson, C.J.N., 1994. Experimental studies of the fluidization of layered sediments and the formation of fluid escapes structures. Sedimentology 41, 233–253. https://doi.org/10.1111/j.1365-3091.1994.tb01403.x.

Obermeier, S., 1996. Use of liquefaction-induced features for paleoseismic analysis – an overview of how seismic liquefaction features can be distinguished from other features and how their regional distribution and properties of source sediment can be used to infer the location and strength of Holocene paleo-earthquakes. Eng. Geol. 44, 1–76. https://doi.org/10.1016/S0013-7952(96)00040-3.

Obermeier, S., 2009. Using Liquefaction-Induced and Other Soft-Sediment Features for Paleoseismic Analysis. In: Paleoseismology (Ed J.P. McCalpin). International Geophysics 95, 497–564.

Obermeier, S., Jacobson, R.B., Smoot, J.P., Weems, R.E., Gohn, G.S., Monroe, J.E., Powars, D.S., 1990. Earthquake-induced liquefaction features in the coastal setting of South Carolina and in the fluvial setting of the New Madrid seismic zone. US Geological Survey Professional Papers 1504, 44.

Owen, G., 1985. Mechanisms and Controls of Deformation in Unconsolidated Sands: An Experimental Approach. Unpublished PhD thesis,. University of Reading.

Owen, G., 1996. Experimental soft-sediment deformation: structures formed by the liquefaction of unconsolidated sands and some ancient examples. Sedimentology 43, 279–293.

Owen, G., 2003. Load structures: gravity-driven sediment mobilization in the shallow subsurface. In: Subsurface Sediment Mobilization (Eds R.R. Van Rensbergen, a.J. Hillis and C.K. Maltman). Geological Society of London Special Publications 216, 21–34. https://doi.org/10.1144/GSL.SP.2003.216.01.03.

Owen, G., Moretti, M., 2011. Identifying triggers for liquefaction-induced soft-sediment deformation in sands. Sediment. Geol. 235, 141–147. https://doi.org/10.1016/j.sedgeo.2010.10.003.

Owen, G., Moretti, M., Alfaro, P., 2011. Recognising triggers for soft-sediment deformation: current understanding and future directions. Sediment. Geol. 235, 133–140.

Ozols, D., 2009. Subglacial meltwater discharge within and around North Latvia Uplands during the last Glaciation. Polish Geological Institute Special Papers 25, 49–58.

Papadopoulos, G.A., Lefkopoulos, G., 1993. Magnitude–distance relations for liquefaction in soil from earthquakes. Bull. Seismol. Soc. Am. 83, 925–938. https://doi.org/10.1785/BSSA0830030925.

Phillips, E.R., Evans, D.J.A., van der Meer, J.J.M., Lee, J.R., 2018. Microscale evidence of liquefaction and its potential triggers during soft-bed deformation within subglacial traction tills. Quat. Sci. Rev. 181, 123–143. https://doi.org/10.1016/j.quascirev.2017.12.003.

Pisarska-Jamroży, M., Woźniak, P.P., 2019. Debris flow and glacioisostatic-induced soft-sediment deformation structures in a Pleistocene glaciolacustrine fan: the southern Baltic Sea coast, Poland. Geomorphology 326, 225–238.

Pisarska-Jamroży, M., Belzyt, S., Bitinas, A., Jusienė, A., Woronko, B., 2019. Seismic shocks, periglacial conditions and glaciotectonics as causes of the deformation of a Pleistocene meandering river succession in Central Lithuania. Baltica 32, 63–77. https://doi.org/10.5200/baltica.2019.1.6.

Pisarska-Jamroży, M., Belzyt, S., Börner, A., Hoffmann, G., Kenzler, M., Rother, H., Steffen, R., Steffen, H., 2022. Late Pleistocene earthquakes imprinted on glaciolacustrine sediments on Gnitz Peninsula (Usedom Island, NE Germany). Quat. Sci. Rev. 296, 107807. https://doi.org/10.1016/j.quascirev.2022.107807.

Pisarska-Jamroży, M., Woronko, B., Woźniak, P.P., Rosentau, A., Hang, T., Steffen, H., Steffen, R., 2024. Deformation structures as key hints for interpretation of ice sheet dynamics - a case study from northeastern Estonia. Quat. Sci. Rev. 306, 108788. https://doi.org/10.1016/j.quascirev.2024.108788.

Postma, G., 1983. Water escape structures in the context of a depositional model of a mass flow dominated conglomeratic fandelta (Abrioja Formation, Pliocene, Almeria Basin, SE Spain). Sedimentology 30, 91–103. https://doi.org/10.1111/j.1365-3091.1983.tb00652.x.

Pralle, N., Kulzer, M., Gudehus, G., 2003. Experimental evidence on the role of gas in sediment liquefaction and mud volcanism. Geological Society of London Special Publications 216, 159–171. https://doi.org/10.1144/GSL.SP.2003.216.01.11.

Pryce, E., Kirkham, C., Cartwright, J., 2023. Crater formation during the onset of mud volcanism. Geology 51, 252–256. https://doi.org/10.1130/G50713.1.

Puri, V.K., Prakash, S., 2010. Foundations for dynamic loads. In: Art of Foundation Engineering Practice (Eds M.H. Hussein, J.B. Anderson and W.M. Camp). Geotechnical Special Publications. doi:https://doi.org/10.1061/41093(372)26.

Quigley, M.C., Bastin, S., Bradley, B.A., 2013. Recurrent liquefaction in Christchurch, New Zealand, during the Canterbury earthquake sequence. Geology 41, 419–422. https://doi.org/10.1130/G33944.1.

Seed, H.B., 1979. Soil liquefaction and cyclic mobility evaluation for level ground during earthquakes. Journal of Geotechnical Engineering Division 105, 201–255. https://doi.org/10.1061/AJGEB6.0000768.

Seed, H.B., Idriss, I.M., 1971. Simplified Procedure for evaluating Soil Liquefaction potential. Journal of Soil Mechanics and Foundations Division 97, 1249–1273.

Seed, H.B., Idriss, I.M., Arango, I., 1983. Evaluation of liquefaction potential using field performance data. J. Geotech. Eng. 109, 458–482. https://doi.org/10.1061/(ASCE)0733-9410(1983)109:3(458).

Seilacher, A., 1969. Fault-graded beds interpreted as seismites. Sedimentology 13, 155–159.

Sims, J.D., 2013. Earthquake-induced load casts, pseudonodules, ball-and-pillow structures, and convolute lamination: additional deformation structures for paleoseismic studies. In: recent advances in north American paleoseismology and

neotectonics East of the Rockies (Eds. R.T. Cox, M.P. Tuttle, O.S. Boyd and J. Locat). Geol. Soc. Am. Spec. Pap. 493, 191–201. https://doi.org/10.1130/2012.2493(09).
Świątek, S., Lewińska, K., Pisarska-Jamroży, M., Günter, C., 2025. An application of quartz grain analyses in earthquake-induced (palaeo)liquefaction studies. J. Struct. Geol., 105357 https://doi.org/10.1016/j.jsg.2025.105357.
Świątek, S., Pisarska-Jamroży, M., 2023. Soft-sediment deformation structures – Development in laboratory conditions. In: Paper Presented at 36th International Meeting of Sedimentology. https://doi.org/10.13140/RG.2.2.25225.83045. Dubrovnik, Croatia.
Świątek, S., Belzyt, S., Pisarska-Jamroży, M., Woronko, B., 2023. Sedimentary records of liquefaction: Implications from field studies. Journal of Geophysical Research: Earth Surface 128, e2023JF007152. https://doi.org/10.1029/2023JF007152.
Tan, X., Liu, F., Hu, L., Reed, A.H., Furukawa, Y., Zhang, G., 2017. Evaluation of the particle sizes of four clay minerals. Appl. Clay Sci. 135, 313–324. https://doi.org/10.1016/j.clay.2016.10.012.
Tang, X.W., Hu, J.L., Qiu, J.N., 2016. Identifying significant influence factors of seismic soil liquefaction and analyzing their structural relationship. J. Civ. Eng. 20, 2655–2663. https://doi.org/10.1007/s12205-016-0339-2.
Terzaghi, K., 1996. Soil Mechanics in Engineering Practice, 3rd edition. New York.
Tokimatsu, K., Uchida, A., 1990. Correlation between Liquefaction Resistance and Shear Wave Velocity. Soils Found. 30, 33–42. https://doi.org/10.3208/sandf1972.30.2_33.
Tuttle, M.P., Seeber, L., 1991. Historic and prehistoric earthquake-induced liquefaction in Newbury. Massachusetts. Geology 19, 594–597. https://doi.org/10.1130/0091-7613(1991)019%3C0594:HAPEIL%3E2.3.CO;2.
Tuttle, M.P., Hartleb, R., Wolf, L., Mayne, P.W., 2019. Paleoliquefaction Studies and the Evaluation of Seismic Hazard. Geosciences 9, 311. https://doi.org/10.3390/geosciences9070311.
Van der Baan, M., 2009. The origin of SH-wave resonance frequencies in sedimentary layers. Geophys. J. Int. 178, 1587–1596. https://doi.org/10.1111/j.1365-246X.2009.04245.x.
Van Loon, A.J., 2009. Soft-sediment deformation structures in siliciclastic sediments: and overview. Geologos 15, 3–55.
Van Loon, A.J., Pisarska-Jamroży, M., Nartišs, M., Krievāns, M., Soms, J., 2016. Seismites resulting from high-frequency, high-magnitude earthquakes in Latvia caused by late Glacial glacio-isostatic uplift. J. Palaeogeogr. 5, 363–380. https://doi.org/10.1016/j.jop.2016.05.002.
Van Loon, A.J., Pisarska-Jamroży, M., Woronko, B., 2020. Sedimentological distinction in glacigenic sediments between load casts induced by periglacial processes from those induced by seismic shocks. Geological Quarterly 64, 626–640. https://doi.org/10.7306/gq.1546.
Varghese, R.M., Latha, G.M., 2014. Shaking Table Studies on the Conditions of Sand Liquefaction. Geo-characterization and Modeling for Sustainability. https://doi.org/10.1061/9780784413272.121.
Wahyudi, S., Koseki, J., Sato, T., Miyashita, Y., 2013. Effects of pre-shearing history on repeated liquefaction behaviour of sand using stacked-ring shear apparatus. Bulletin of the Earthquake Research Society 46, 3–11.
Wiemer, G., Moernaut, J., Stark, N., Kempf, P., De Batist, M., Pino, M., Urrutia, R., De Guevara, B.L., Strasser, M., Kopf, A., 2015. The role of sediment composition and behavior under dynamic loading conditions on slope failure initiation: a study of a subaqueous landslide in earthquake-prone South-Central Chile. Int. J. Earth Sci. 104, 1439–1457. https://doi.org/10.1007/s00531-015-1144-8.
Woźniak, P.P., Belzyt, S., Pisarska-Jamroży, M., Woronko, B., Lamsters, K., Nartišs, M., Bitinas, A., 2021. Liquefaction and re-liquefaction of sediments induced by uneven loading and glacigenic earthquakes: implications of results from the Latvian Baltic Sea coast. Sediment. Geol. 421, 105944. https://doi.org/10.1016/j.sedgeo.2021.105944.
Yang, R., Van Loon, A.J., Yin, W., Fan, A., Han, Z., 2016. Soft-sediment deformation structures in cores from lacustrine slurry deposits of the late Triassic Yanchang Fm. (Central China). Geologos 22, 201–211. https://doi.org/10.1515/logos-2016-0021.
Youd, T.L., 1973. Liquefaction, flow, and associated ground failure. USGS Circular 688, Washington.
Youd, T.L., 1977. Packing changes and liquefaction susceptibility. Journal of Geotechnical Engineering Division 103, 918–922. https://doi.org/10.1061/AJGEB6.0000478.
Youd, T.L., Perkins, D.M., 1978. Mapping liquefaction-induced ground failure potential. J. Geotech. Eng. Division 104 (4), 433–446. https://doi.org/10.1061/AJGEB6.0000612.
Zhang, J.M., Wang, W.X., 1990. Effect of vibration frequency on dynamic behavior of saturated sand (in Chinese). Chinese Journal of Geotechnical Engineering 12, 89–97.
Zhong, N., Jiang, H., Li, H., Su, D., Xu, H., Liang, L., Fan, J., 2022. The potential of using soft-sediment deformation structures for quantitatively reconstructing paleo-seismic shaking intensity: progress and prospect. Environ. Earth Sci. 81, 408. https://doi.org/10.1007/s12665-022-10504-8.

Journal of Structural Geology 193 (2025) 105357

Contents lists available at ScienceDirect

Journal of Structural Geology

journal homepage: www.elsevier.com/locate/jsg

An application of quartz grain analyses in earthquake-induced (palaeo) liquefaction studies

Szymon Świątek [a,*], Karolina Lewińska [a], Małgorzata Pisarska-Jamroży [a], Christina Günter [b]

[a] Faculty of Geographical and Geological Sciences, Adam Mickiewicz University, Krygowskiego 12, 61-680, Poznań, Poland
[b] Institute of Geosciences, University of Potsdam, Karl-Liebknecht-Str. 24-25, 14476, Potsdam, Germany

ARTICLE INFO

Keywords:
(palaeo)seismic event
Liquefaction
Soft-sediment deformation structures
Seismites
Quartz grains
Gold

ABSTRACT

This study investigates the micromorphological changes in quartz grains as a result of seismically-induced liquefaction and their potential for distinguishing seismogenic soft-sediment deformation structures from other trigger mechanisms. The experimental analysis revealed distinct subtle and pronounced quartz cracks, edge corrosion, and advanced grain defragmentation. The findings suggest that these quartz alterations are strongly influenced by the degree of water mineralisation and the duration of exposure on it. Moreover, the study identified gold forms within quartz cracks, which developed after seismic activity and serve as a direct evidence of such activity. These microstructures provide new insights into the role of seismicity in the redistribution and deposition of minerals. Geochemical conditions, including pH and Eh, also played a critical role in the sediment's liquefaction behaviour. Our results highlight how chemical interactions, combined with seismic forces, contribute to quartz grains damage. These findings provide a novel approach for identifying seismically-induced deformation structures and assessing past seismic events in sedimentary records. The results also emphasize the significance of integrating quartz grain analysis in seismic risk assessments, improving the understanding of liquefaction mechanisms and potential hazards.

1. Introduction

Liquefaction usually occurs when fine-grained sediments, such as silt and fine-grained sand, lose their strength due to an increase in pore water pressure (Seed, 1979; Owen, 2003). Consequently, the grains lose contact with each other, allowing the sediment to become mobilised (Maltman and Bolton, 2003; Van Rensbergen et al., 2003). Seismic waves reduce the shear strength of water-saturated sediments, triggering liquefaction and fluidisation, which in turn leads to the development of soft-sediment deformation structures (SSDS; Galli, 2000; Montenat et al., 2007; Owen and Moretti, 2011; Belzyt et al., 2021; Woźniak et al., 2021). This phenomenon is especially common in environments with high water-saturated sediments, like fluvial, glacial, lacustrine, coastal plains and lagoonal (Youd and Perkins, 1978). SSDS can form directly at the sediment-water interface and are entirely surficial, or alternatively may form in the shallow subsurface where they are interstitial (Alsop et al., 2022). Depending on the depth of SSDS, this may have consequences for structures produced (and their interpretation).

The SSDS are often a result of liquefaction (Allen, 1982; Van Loon, 2009; Owen and Moretti, 2011), including structures like load casts, dish and pillar structures, pseudonodules, flame structures, and clastic dykes or sills (Obermeier, 1996, 2009; Owen, 2003; Brandes and Winsemann, 2013; Pisarska-Jamroży et al., 2019; Pisarska-Jamroży and Woźniak, 2019; Müller et al., 2020). These features, while common in liquefied sediments resulting from seismic events, can also be an effect of non-seismic processes (e.g., storm, tsunami, volcanic activity), making the identification of seismogenic SSDS a critical challenge (Van Loon, 2014; Müller et al., 2023; McCalpin et al., 2023). The distinction between seismogenic and non-seismic liquefaction is essential for reconstructing past earthquake events, and understanding the kinematic and dynamic behaviour of seismic shocks (McCalpin and Nelson, 1996; Tuttle et al., 2019). A range of criteria has been proposed to help differentiate seismically-induced SSDS from those caused by other deformation trigger mechanisms (cf. Obermeier et al., 1990; Hilbert-Wolf et al., 2009; Owen and Moretti, 2011; Owen et al., 2011; Moretti et al., 2014; He and Qiao, 2015). These include, among others, the lateral extent and vertical repetition of SSDS within sedimentary

* Corresponding author.
E-mail addresses: szymon.swiatek@amu.edu.pl (S. Świątek), karolina.lewinska@amu.edu.pl (K. Lewińska), pisanka@amu.edu.pl (M. Pisarska-Jamroży), christina.guenter@geo.uni-potsdam.de (C. Günter).

https://doi.org/10.1016/j.jsg.2025.105357
Received 15 January 2025; Received in revised form 31 January 2025; Accepted 3 February 2025
Available online 4 February 2025

sequences, their proximity to seismic faults, and the co-occurrence of brittle and plastic deformations. A seismically-deformed layer, known as seismite, is a key piece of evidence for past seismic events preserved in the sedimentary record (He and Qiao, 2015; Zhong et al., 2022; McCalpin et al., 2023). Seismites usually form within 30–40 km of an epicentre or known plate boundary as with Dead Sea transform or southern California San Andreas Fault, though larger earthquakes can trigger liquefaction and deformation at distances stretching hundreds of kilometres (Galli, 2000). Additionally, modern seismites provide analogues for identifying ancient seismic events through comparative studies of sediment deformation (cf. Alsop et al., 2019).

Most traditional studies on SSDS have focused on macro- and mesoscale features visible in field or labs (cf. Montenat et al., 2007; Owen and Moretti, 2011; Owen et al., 2011; McCalpin et al., 2023). Less attention has been given to the microscale deformation of individual sediment grains, especially quartz. Quartz grains are widely used in geological and geomorphological research, particularly in areas such as sediment provenance analyses (cf. Ackerson et al., 2015; Moliner-o-García et al., 2022), paleoenvironmental reconstructions (cf. Sleep and Hessler, 2006; Woronko, 2016), as well as soil and sediment transport analysis (cf. Drees et al., 1989). Its physical and chemical properties allow changes in micromorphology to be investigated, such as edge and boundary abrasion, fracturing, and grain boundary alteration, which can provide critical insights into the forces that have acted upon the sediments (cf. Moss, 1966; Helland and Holmes, 1997). This gap in paleoseismological research can be significant, as quartz morphology has the potential to reveal subtle differences between seismically-induced liquefaction and other deformation processes. Moreover, recent findings have shown that seismic shocks can lead to the deposition of gold in quartz grains association (Voisey et al., 2024).

The objectives of this experimental study are: (1) to analyse the morphological characteristics of quartz grains in order to differentiate between seismogenic and non-seismic liquefaction in sedimentary deposits, (2) to investigate the occurrence and relationships between micro-fragments of gold on quartz grains as a result of seismic activity, (3) to determine the influence of chemical compounds and geochemical conditions on the liquefaction record in quartz grains, and (4) to establish a methodology for utilising quartz grain morphology as a tool for assessing geochemical conditions of sedimentation and predicting potential future liquefaction risks.

2. Material and methods

2.1. Sediments, water and reagent

Two types of unconsolidated siliclastic sediments were used in the experiment: silt (93% for 2–63 μm) and fine-grained sand (56% for 125–250 μm), which were collected from natural outcrops (Fig. 1A; Słonów and Bielice Nowe sites), then dried at room temperature (20–22°C), cleaned, sieved, and classified according to the Friedman and Sanders's classification (Friedman and Sanders, 1978).

Three types of water with varying degrees of mineralisation and chemical properties were used to saturate the sediments: distilled water, medium-mineralised water, and highly-mineralised water (Fig. 1B). The mineralised waters were commercially available bottled waters, each with different concentrations of mineral components (Fig. 1B). To ensure a natural iron content typically found in fine-grained sands, iron (II) sulphate (~2.72%) was purchased from WarChem (Poland).

2.2. Experimental setup

The experiment was conducted under controlled laboratory conditions. Sediments were placed in 36 transparent plexiglass cylinders with a height of 10 cm and a diameter of 15 cm (Fig. 1C). A single layer of sand was placed at the bottom of the cylinders, which was then saturated with a solution of water and iron (II) sulphate. The solution used to saturate the sediments was prepared at a ratio of 7 g *per* 250 ml of water, to imitate natural content of iron, i.e., 0.5–1% (cf. Zhou et al., 2004).

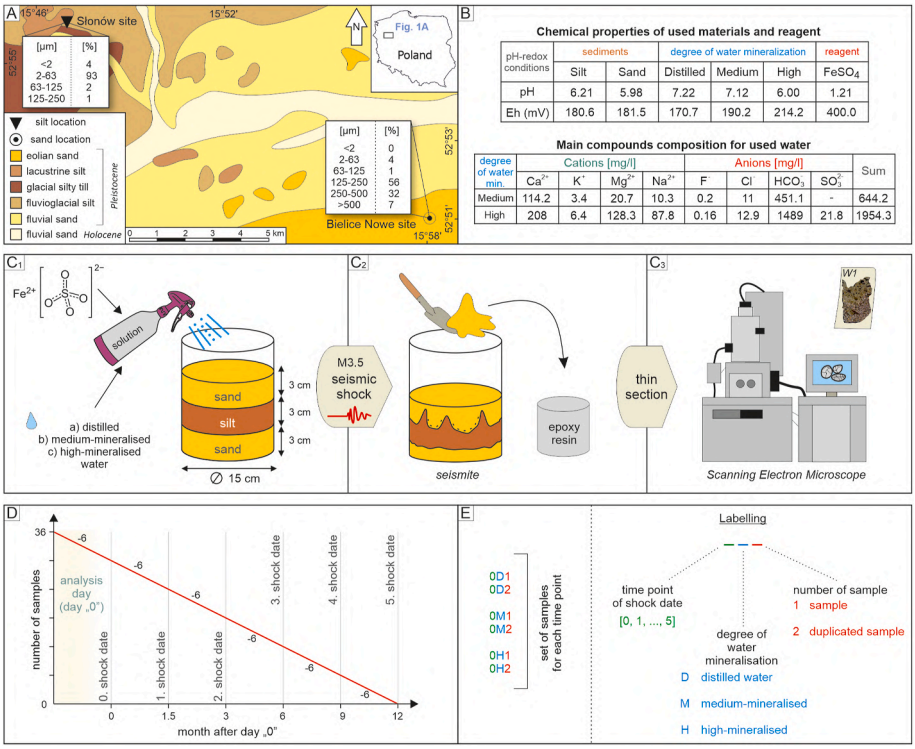

Fig. 1. Experiment design. A – location and simplified lithogenetic map of the Słonów and Bielice Nowe sites in the northwest Poland. B – chemical properties of used materials and chemical composition of water. C_1-C_3 – workflow of preparation and technical conditions of samples. D – time chart of experiment duration. E – set of samples for each analysis day, with the labelling.

After waiting a few minutes, another layer of sediment was added. The cylinders were incubated in low-light conditions and securely closed to minimize evaporation, aiming to induce reductive conditions.

All 36 cylinders were prepared on the same day, referred to "day 0," and divided into six analysis time points, with the first time point occurring on the preparation day. The subsequent analyses were conducted sequentially after 1.5, 3, 6, 9, and 12 months from day 0 (Fig. 1D). Each time point included a fixed set of 6 samples: two samples with distilled water, two samples with medium- and two with highly-mineralised water, respectively (Fig. 1E).

At scheduled time points (see Fig. 1D), the cylinders were carefully opened, and measurements of the pH and redox potential were taken at a depth of 2–3 cm from the top layer of the sediments. A seismic shock simulations also performed. The liquefaction phenomenon was conducted under controlled laboratory conditions, using Analysette 3 Spartan (Fritsch) device, imitating the shaking table with specific parameters. This instrument was characterised by the following features: magnitude (3.5), frequency (50 Hz), amplitude (3 mm) and duration of the seismic shocks does not exceed 15 s (for detailed description of simulation, see Świątek and Pisarska-Jamroży, 2023). Each specimen was subjected to seismic vibrations gingerly and separately.

After each seismic simulation, the pH and redox potentials were measured again. The samples were air-dried at room temperature, and approximately 100 g of undisturbed sediment were carefully collected and placed into a PVC tube, which was properly closed. The prepared samples were then immersed in Araldite 2020 epoxy resin for several days to solidify the sediment (Fig. 1C_2). Then, thin sections were prepared and analysed using a Scanning Electron Microscope (*SEM*; Fig. 1C_3).

2.3. Morphological analysis

The carbon-coated thin sections were used to micromorphological analyses at the Faculty of Geographical and Geological Sciences (Adam Mickiewicz University in Poznań, Poland), the Faculty of Geology (University of Warsaw, Poland) and at the University of Potsdam (Germany). The study focused on a detailed examination of the prepared thin sections, with 5–7 random SEM images taken at various magnifications (ranging from 20 to 500 μm). These images were used to analyse the micromorphology of quartz grain, especially edges, boundaries and their sphericity, degree of roundness, and additional features such as bays, or holes. The "edge" was defined as the outer line of the grain, while the "boundary" was considered a slightly deeper zone within the grain. The main focus of the study was on the analysis of cracks within the quartz grains, their interrelations, and the degree of mechanical destruction and corrosion. The simplified nomenclature of features and characteristics was applied based on Helland and Holmes (1997), Newsome and Ladd (1998), Mahaney (2002), Piazolo et al. (2002), Andò et al. (2012) and Voisey et al. (2024) with some modification presented in Appendix S1.

Furthermore, quartz grains were analysed for additional features, such as the coexistence of other chemical compounds. To achieve this, the elemental composition of specific areas on the grain was determined through energy-dispersive X-ray spectroscopy (EDX) analysis, and their distribution was rendered visible using EDX mapping (SEM, ZEISS Sigma VP apparatus for University of Warsaw; JEOL JSM-6510 coupled with an XPlore EDX-detector from Oxford Instruments for University of Potsdam). The final analyses also took into account the geochemical conditions of the sediments in which the grains were found.

3. Referenced material

Morphological analyses were also conducted on the same sand that was not subjected to seismic shocks (Fig. 3A_1-A_6; Supplementary Material No. 1A), as well as on sediment collected directly from an outcrop at the Dwasieden site in Germany (Figs. 2 and 3B-M; Supplementary Material No. 1B), aiming to comparison grain features. This site is characterised by two seismites of Late Pleistocene age containing SSDS such as pseudonodules, load casts, flame structures, fluid-escape structures, and ball-and-pillow structures (cf. Pisarska-Jamroży et al., 2018; Pisarska-Jamroży et al., 2019). The sediments of Dwasieden site are quartz-rich sands and clayey silts with glacifluvial origin. The analysed seismite could be developed as a result of glacio-isostatic rebound at the front of advancing ice sheet. The characteristics of these grains were the basis for evaluating the occurrence and development of the quartz grains studied in the conducted experiment.

The quartz grains are aeolian in origin and came from inland dunes. They have not been subjected to seismic shocks and display a variety of forms and degrees of weathering. Some grains maintain their initial, unweathered, and spherical shapes (Fig. 3A_1), while others are unweathered but exhibit subrounded and slightly elongated in shape (Fig. 3A_2). In several cases, grains are spherical or subrounded (Fig. 3A_3). There are also slightly elongated grains that have undergone rounding and show evidence of corrosion (Fig. 3A_4). Some grains are elongated and subangular, with a notable corroded edge (Fig. 3A_5), while others display a more angular shape with minimal weathering (Fig. 3A_6). The quartz grains from the dune sand do not exhibit any visible or significant cracks.

The quartz grains from the Dwasieden site display a variety of damage features, reflecting different degrees of fracturing, and corrosion. Among the observed features are grains displaying both single and multiple cracks, with some grains experiencing partial detachment (Fig. 3B). Isolated, singular cracks are visible in certain grains (Fig. 3C), while others exhibit networks of intersecting cracks (Fig. 3D) or multiple cracks that do not cross each other (Fig. 3E). In many cases, mixed fracturing patterns are observed, with cracks occurring in various directions and orientations (Fig. 3F), as well as cracks of different sizes (Fig. 3G). Some grains exhibit both fracturing and corrosion, with cracks varying in size and degree of degradation (Fig. 3H), while others reveal symmetrical cracks running along grain boundaries (Fig. 3I). Additionally, advanced corrosion is visible on grains that have fragmented extensively (Fig. 3J). Certain grains take on more distinct shapes, such as rounded or angular forms, often connected by gold crystals forming pseudo-hexagonal structures (Fig. 3K). In other cases, elongated grains show signs of corrosion, often accompanied by clusters of gold (Fig. 3L). Recrystallisation processes have also affected some grains, altering their original structure (Fig. 3M).

4. Experiment results

4.1. Seismically-induced alterations in quartz morphology

4.1.1. Edge morphology

As a result of the seismic shock, significant changes were observed in the edge morphology of the quartz grains. The following features were distinguished: subtle cracks, pronounced cracks, edge corrosion, edge defragmentation, knocked out grain fragments, and corroded and reactive boundaries (Fig. 4; Appendix S1).

Throughout the study, subtle cracks were consistently observed in all samples (Fig. 4A and B), regardless of the degree of water mineralisation or the time point. In contrast, pronounced cracks were found in nearly all samples (Fig. 4C and D), except those containing distilled water, where they were not be observed within first to seismic simulations (at 0 and after 1.5 months). As for edge corrosion (Fig. 4F and G) and edge fragmentation (Fig. 4H), they appeared regularly in samples with highly-mineralised water, while they occurred less frequently in those with medium mineralisation and only occasionally in samples with distilled water. The same situation is related to angular fragmentations, as well as grain and edge fragmentation (Fig. 4I and J). Furthermore, knocked out grain fragments (Fig. 4K) were a common feature in samples exposed to highly-mineralised water, less frequent in medium-mineralised water, and rarely seen in samples with distilled water.

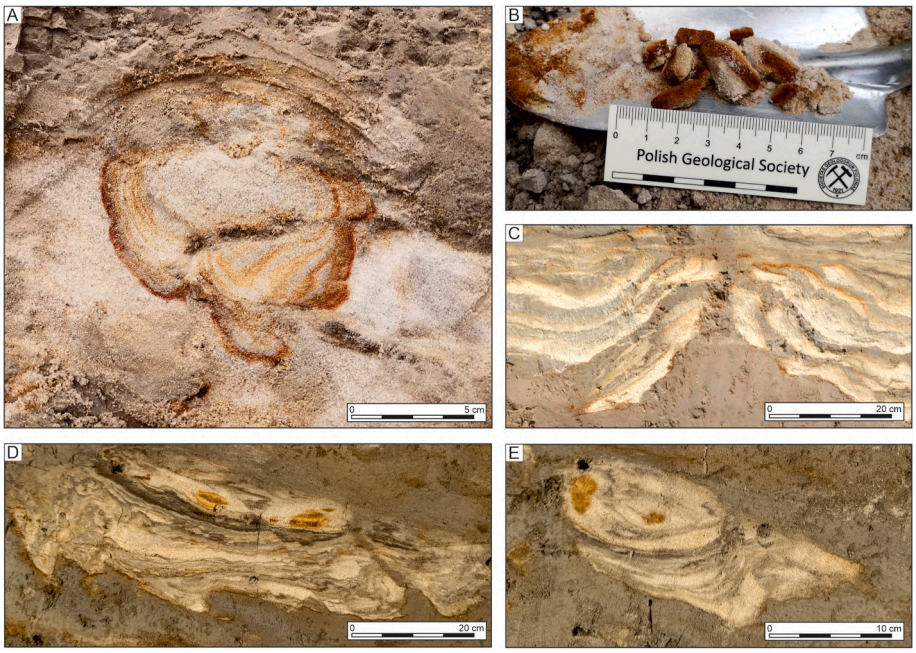

Fig. 2. Seismites from Dwasieden site with recognised (A) iron-rich load structure, (B) iron-rich sediments, (C) iron-rich water-escape structure, (D) iron-rich boundary between silty flames structures and load structures, and (E) iron-rich accumulation within load structure.

Corroded and reactive boundaries (Fig. 4L), on the other hand, appeared only after 1.5 months, initially in samples with highly-mineralised water. From that point forward, this feature became consistently present in both medium- and highly-mineralised water, yet it was never observed in samples saturated distilled water.

During the experiment, grains with spherical shapes were consistently observed across various samples and time points (Appendix S1). Spherical grains were identified at day 0 and in subsequent intervals, especially in samples exposed to medium- and highly-mineralised water. This morphology remained prevalent under most conditions (~75%). In contrast, slightly elongated grains were also recorded, appearing in several samples across multiple time points. These grains were particularly noticeable from day 0 onwards and continued to be observed during the later stages, with a stronger presence in both medium and highly-mineralised water. Although slightly elongated grains occurred less consistently than spherical ones, they were still identifiable at various stages of the experiment.

Grains with varying degrees of roundness were observed across different samples and time points. Rounded grains were identified primarily at later stages, with their presence being noted after significant intervals, particularly in samples with higher mineralisation degree. Subrounded grains, in turn, were consistently observed across a wide range of samples and time points. From day 0 onwards, subrounded grains were present in most conditions, appearing frequently in both medium- and highly-mineralised water. Subangular grains were also present in various samples, though their occurrence was somewhat less frequent compared to subrounded grains. These grains were observed at multiple time points and appeared regularly in medium- and highly-mineralised water samples, with only occasional occurrences in distilled water samples. In contrast, angular grains were rare, appearing only sporadically at specific time points and in fewer samples. They were primarily observed during the early stages of the experiment and were more common in environments with lower levels of mineralisation. Quartz grains were characterised by special features resulting from corrosion, i.e. bays and holes (Fig. 4F, G, K). Bays were a common feature, present across nearly all samples and time points. They appeared consistently in samples regardless of the water mineralisation degree, indicating their widespread occurrence throughout the study. Holes, on the other hand, were slightly less frequent but still appeared regularly in various samples. These were present at multiple time points, particularly in samples exposed to medium- and highly-mineralised water. Holes were less common in distilled water samples.

4.1.2. *Quartz grain state*

The microtexture of the quartz grains underwent significant alterations as a result of seismically-induced liquefaction. Various types of microcracks and fracturing developed across the samples, with distinct patterns emerging over time and under different conditions (Appendix S1).

Single fracturing affecting small fragments of the grain, was present in nearly all samples, except in distilled water at day 0 and after 1.5 months, but still evident in the mineralised water samples at day 0.

Tearing off involved the detachment or imminent decompression of previously fractured parts of the grains. It was observed mostly in the early stages of the experiment, then only in distilled water samples, but consistently reappeared across all samples after the 9 months.

Not only were single cracks observed, but much more frequently, the quartz grains were intersected by multiple cracks, indicating more complex patterns of damage. Single unconnected cracks, which could extend through an entire grain without connection to other cracks, were absent at day 0 and 1.5 months in distilled water samples, but were consistently observed in all other cases. Multiple intersecting cracks, which often formed at different times and crossed each other, were present in every sample across all time points, regardless of the water type or timing, making them one of the most frequently occurring features. Multiple non-intersecting cracks were characterised by numerous cracks within the grain texture, none of which were connected to each other, and they appeared in almost every sample. Multiple mixed cracks, which encompassed all types of cracks varying in size and intensity, were present irregularly throughout the experiment. Multi-sized fracturing, defined by cracks of various sizes that often intersected, were initially observed only in medium- and highly-mineralised water at the early stages, but appeared occasionally in all samples after 3 months, with their presence diminishing by the end of the experiment. Intergranular symmetric cracks, which were symmetrical across adjacent grains, appeared with varying frequency, showing no consistent pattern.

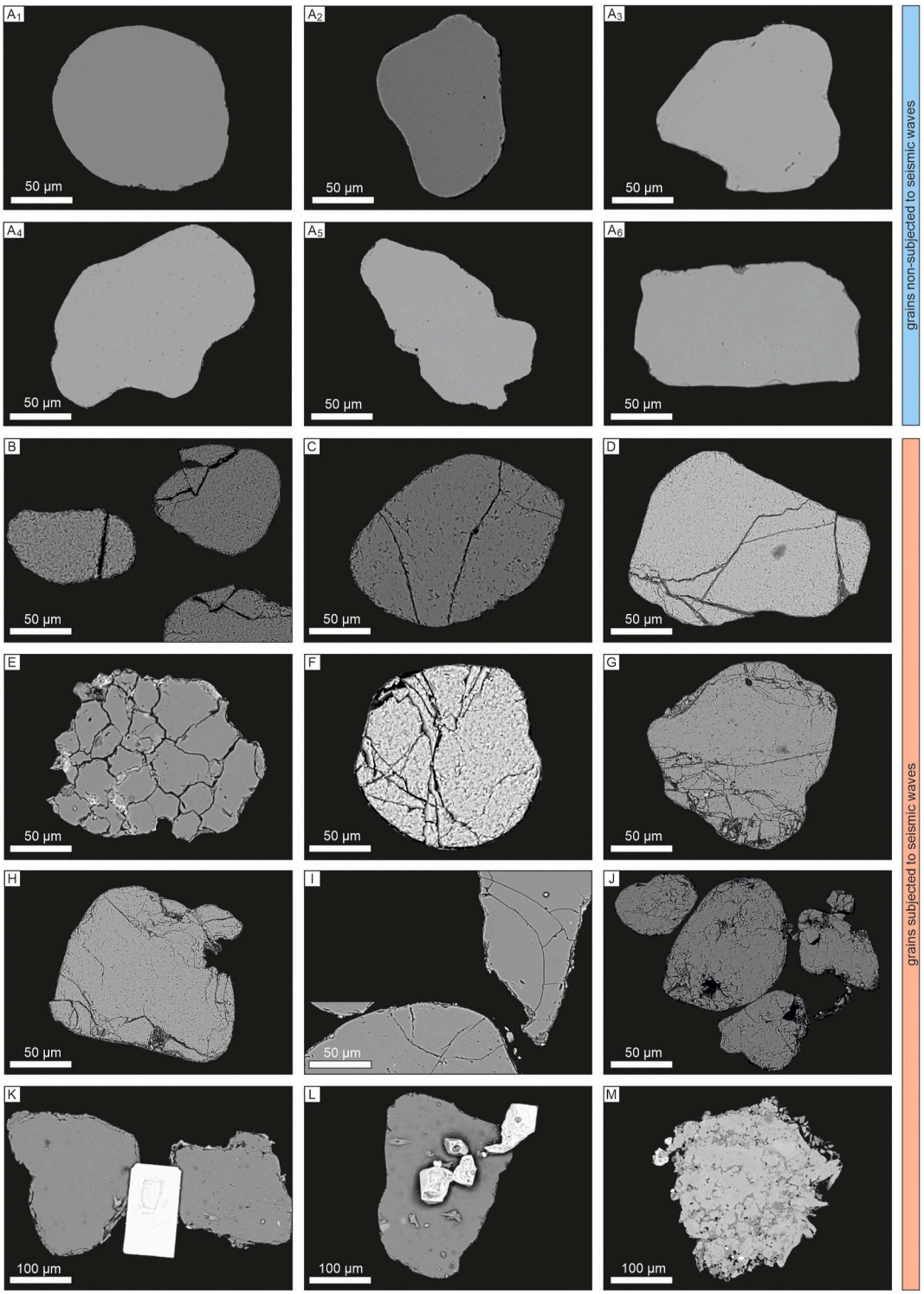

Fig. 3. Featured morphology of quartz grains based on intact grains not subjected to seismic waves from the Bielice Nowe site (A_1-A_6), and seismites from the Dwasieden study site (B–M). A_1 – initial, unweathered and spherical grain, A_2 – unweathered, subrounded and slightly elongated grain, A_3 – spherical, subrounded and corroded grain, A_4 – elongated, rounded and corroded grain, A_5 – elongated, subangular and corroded grain, A_6 – elongated and subangular grain, B – single and multiple grain fracturing, and tearing off, C – single unconnected cracks, D – multiple intersecting cracks, E – multiple non-intersecting cracks, F – multiple mixed cracks, G – multi-sized fracturing and cracks, H – multi-sized corroded fracturing, I – intergranular symmetric cracks, J – multi-advanced corrosion and defragmentation of grains, K – spherical, angular and corroded grains connected by pseudo-hexagonal gold crystal, L – elongated and corroded grain with gold clusters, and M – recrystallised quartz grain. (For interpretation of the references to colour in this figure legend, the reader is referred to the Web version of this article.)

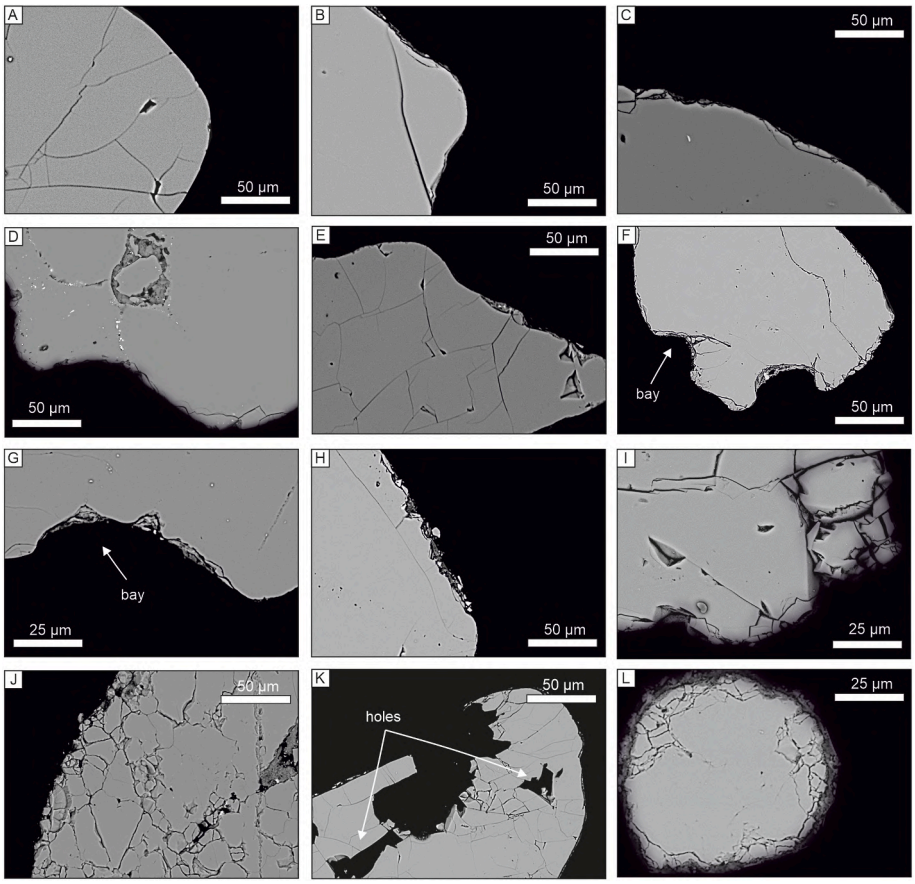

Fig. 4. Grains subjected to seismic waves during this experiment from the Bielice Nowe site. Featured of SEM images of representative edge morphology. A-B – subtle cracks, C – pronounced cracks, D – solution pit, E – mixed (subtle and pronounced) cracks, F-G – edge corrosion with visible bays, H – edge defragmentation, I – angular defragmentation and cracks, J – grain and edge defragmentation, K – knocked out grain fragments, and L – corroded and reactive boundary.

Lastly, multi-advanced corrosion and fragmentation, characterised by advanced corrosion and destruction of the grains, occurred exclusively in samples exposed to highly-mineralised water, with no instances found in other water types.

Progressive changes in quartz grain morphology and fracturing are shown over time, under varying degrees of water mineralisation. In the initial stages (Fig. 5A–D), the grains exhibit relative smoothness with minor fracturing. As the experiment progresses, the cracks become more pronounced (Fig. 5E–H), with some grains showing extensive internal fracturing and separation of fragments. By the later stages (Fig. 5G–L), the grains are characterised by significant fracturing and fragmentation, with multiple intersecting and non-intersecting cracks visible. The final phases are characterised by grains in an advanced state of damage (Fig. 5M–S), including complete separation of fragments and the development of complex crack networks.

4.2. Gold formation

Throughout the experiment, various forms of gold were observed across the samples at different time points (Fig. 6). Pseudo-hexagonal gold crystals occurred intermittently (Fig. Pseudo-hexagonal gold crystals occurred intermittently (Fig. 6A and B), but they were absent on day 0 in both medium- and highly-mineralised water samples. Furthermore, they were not observed after the 9 months in any of the samples. They reached sizes of up to 40 µm. In contrast, micrometre-sized gold particles were consistently present throughout the study (Fig. 6C), depositing in nearly all samples and time points, regardless of the water's mineralisation degree. Gold clusters followed a similar trend (Fig. 6D–F), being observed regularly from day 0 onwards and across most samples, particularly in those with medium and high mineralisation. Gold nanoparticles were also a persistent feature (Fig. 6A–G), consistently occurring in almost all samples and at every time point. On the other hand, gold droplets were much less frequent (Fig. 6H), observed exclusively in samples with highly-mineralised water and occurring occasionally at specific time points, but never in medium or distilled mineralisation conditions. They always occur in cracks of quartz grains.

4.3. Chemical elements distribution

Elemental mapping was conducted to visualize the distribution and intensity of the detected chemical elements on and around quartz grains (Figs. 6 and 7). EDX-mapping identified the following elements: aluminium (Al), calcium (Ca), sodium (Na), iron (Fe), phosphorus (P), magnesium (Mg), and potassium (K).

The presence of aluminium was primarily associated with clustering on each quartz grain (Fig. 7A). Notably, more intense concentrations of this element were observed in bays and holes, as well as in significant patches on the grain. Aluminium appeared on grains of various sizes, and a substantial amount was concentrated in smaller particles surrounding the quartz. Calcium was detected in smaller amounts and occasionally, usually appearing as patches covering significant areas of the grain (Fig. 7B). It was predominantly found on smaller grains compared to aluminium. Sodium co-occurred with quartz grains of different sizes but was present in small quantities similarly to Ca (Fig. 7C), manifesting as small clusters on the grain. Iron was detected, both on the grain and in the surrounding areas of the quartz (Fig. 7D). The intensity of iron was slightly lower than Al. The presence of Fe was particularly noticeable in bays and holes, as well as among smaller particles surrounding the

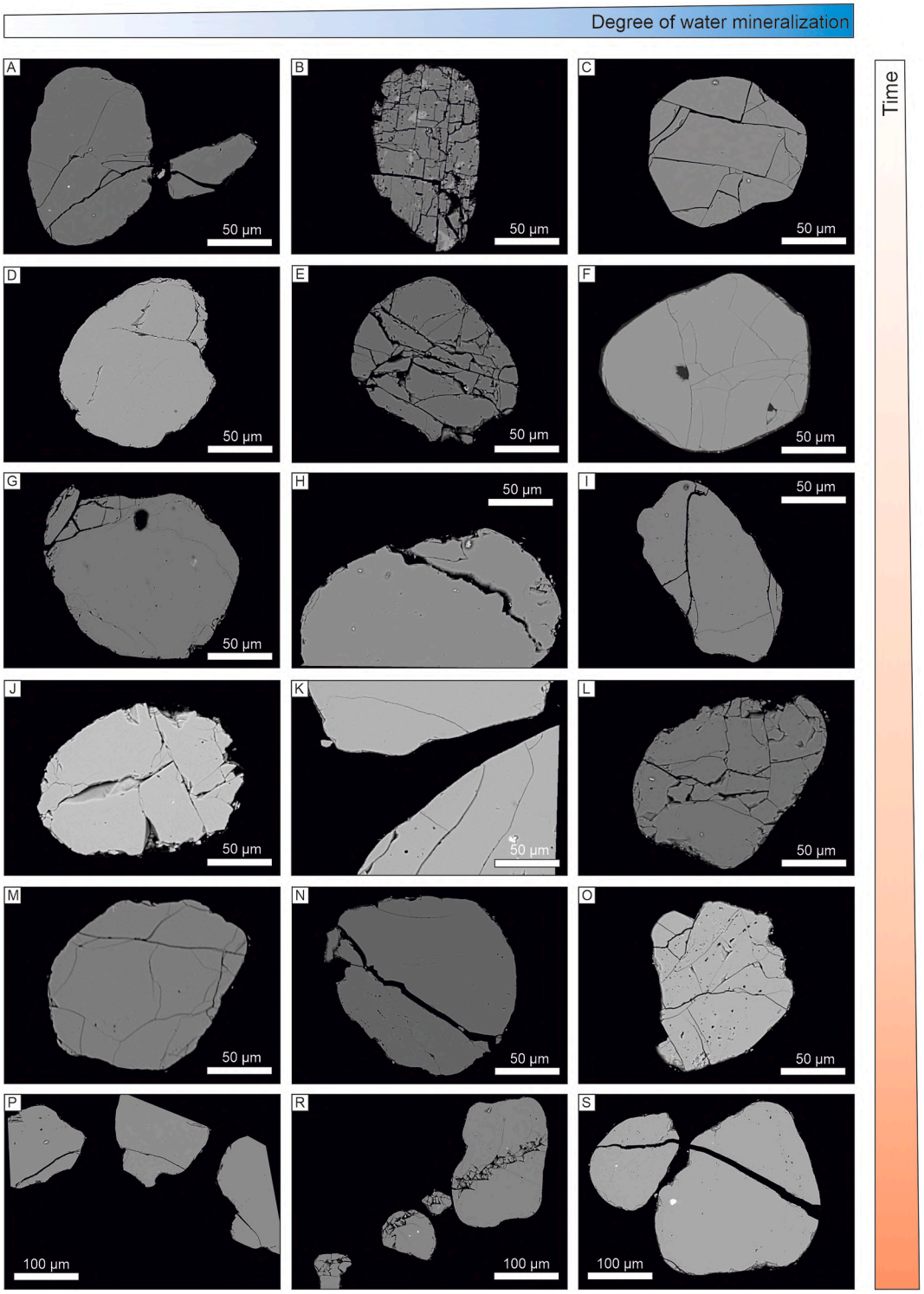

Fig. 5. Grains subjected to seismic waves during this experiment from the Bielice Nowe site. Examples of quartz grain cracks and defragmentation over time under varying degrees of water mineralisation. A – intergranular cracks with tearing off, B – multiple intersecting and corrosion, C – multiple intersecting cracks, D – multi-sized corroded fracturing and cracks, E – multi-advanced corrosion and fracturing, F – multiple intersecting cracks with holes, G – multiple mixed cracks with defragmentation and holes, H – single fracturing with tearing off, I – multiple mixed cracks, J – multi-advanced corrosion and cracks, K – intergranular symmetric cracks, L – multi-advanced corrosion and fracturing, M – multiple intersecting cracks, N – single fracturing with tearing off, O – multiple mixed cracks, P – intergranular symmetric cracks, R – intergranular cracks, S – intergranular symmetric cracks and tearing off. For higher resolution of P-S images, refer to Supplementary Material No. 2.

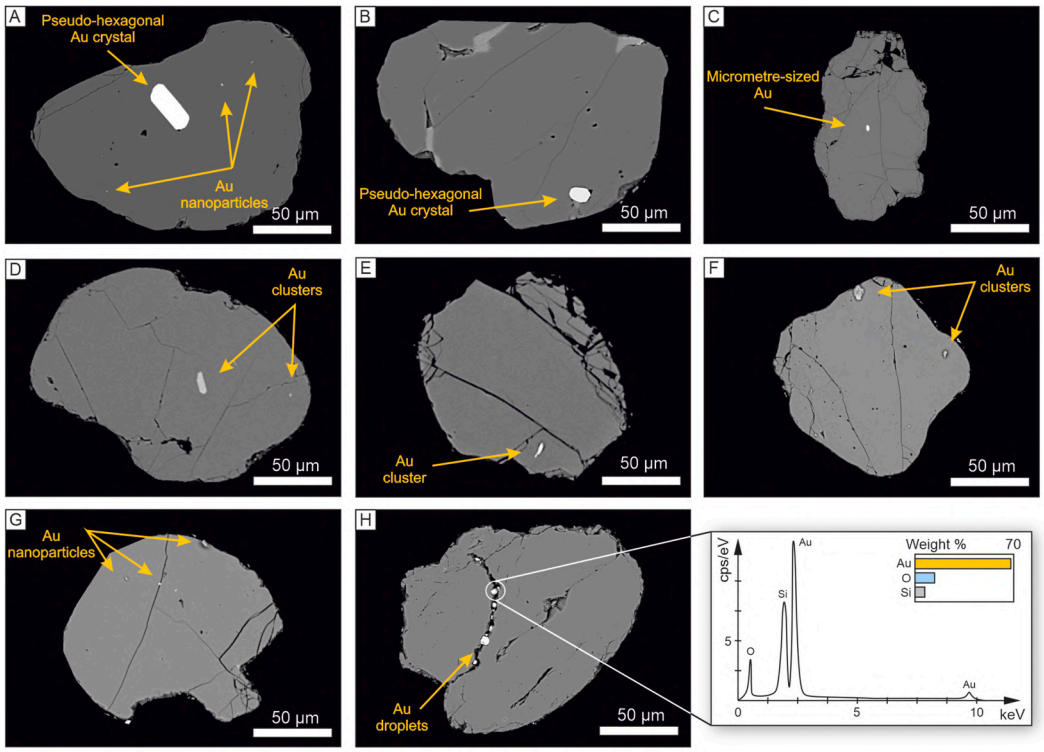

Fig. 6. The differential morphological form of gold deposit recognised with EDX spectrum: A-B – pseudo-hexagonal crystals, C – micrometre-sized gold, D-F – gold clusters, G – nanoparticles of gold, H – gold droplets. (*Au – gold, O – oxygen, Si – silicium, keV – kiloelectronvolt, cps – counts per second*). (For interpretation of the references to colour in this figure legend, the reader is referred to the Web version of this article.)

quartz grains. Unlike Al and Ca, Fe did not appear in the form of patches on the grain. Phosphorus and magnesium exhibited similar behaviour in relation to the quartz grains (Fig. 7E and F). They were generally found on larger grains rather than smaller ones. Both elements were present in clusters on the grains, as well as in the surrounding particles. Notably, there was no detection of these elements along the edges of the grains or in bays and holes, unlike the distribution pattern observed with Al. Potassium displayed behaviour similar to P and Mg (Fig. 7G). In addition to being found on the grains, K was highly visible along the edges of the quartz grains, particularly in bays, where its concentration was pronounced.

5. Discussion

5.1. Quartz transformations resulting from water mineralisation and duration of exposure

Fracturing in quartz grains can occur across various environments, including glacial, aeolian, littoral, and subglacial settings (Woronko, 2016). For example, edge-to-edge grain crushing is often observed in subglacial environments, where high pressure and grain-to-grain interactions dominate (Mahaney, 1995; Tulaczyk et al., 1998). Additionally, conchoidal cracks, a result of powerful impact or pressure, are commonly found in grains from glacial, periglacial, and aeolian environments (Mahaney, 2002; Vos et al., 2014). Despite extensive research on quartz grain fracturing in diverse environments, no previous studies have specifically investigated quartz grains and their characteristics in the context of seismically-induced liquefaction. The observed morphological changes in quartz grains due to seismic activity provide valuable insights into how water mineralisation influences edge, boundary and microtexture alterations, as well as the extent of physical damage to the grains. Systematic identification of features like cracks, corrosion, and grain defragmentation enhances our understanding of the post-seismic environment and highlights the role that water chemistry plays in quartz grain degradation.

5.1.1. Boundaries and morphology of quartz grains

The development of cracks in quartz grains, ranging from subtle to pronounced, was consistently influenced by the degree of water mineralisation (Appendix S1). Subtle cracks appeared in all samples, regardless of mineralisation, indicating that even low seismic stresses can initiate microfracturing in quartz grains. In contrast, pronounced cracks were absent in distilled water samples during early stages (day 0 and after 1.5 months), suggesting that water devoid of dissolved minerals provides a protective effect, reducing mechanical disruption during seismic events. The presence of pronounced cracks in medium- and highly-mineralised water highlights the role of chemical composition in promoting fracturing, potentially through enhanced ion exchange at grain boundaries, weakening the quartz structure (cf. Asumadu et al., 1998; Schulz and White, 1999; Wright, 2007). The similar situation is about edge corrosion and fragmentation of grain (Appendix S1).

Corroded and reactive boundaries emerged after 1.5 months in highly mineralised samples and remained present, highlighting a delayed yet significant effect of the chemical composition. This delay may result from progressive chemical reactions between water minerals and quartz grains, reinforcing the role of mineral content in morphology (cf. Asumadu et al., 1998; Schulz and White, 1999; Wright, 2007). The absence of these features in distilled water underscores the importance of ionic interactions in driving such processes.

Rounding of grains was more pronounced at later stages, especially in highly-mineralised water, while subrounded and subangular grains were consistently observed. The rarity of angular grains suggests their formation is tied to less intense seismic events or resistance to rounding effects in mineralised environments (cf. Crook, 1968).

Corrosion features, such as bays and holes, were more frequent in medium- and highly-mineralised water samples, highlighting the role of chemical dissolution in shaping quartz grains. Their reduced presence in

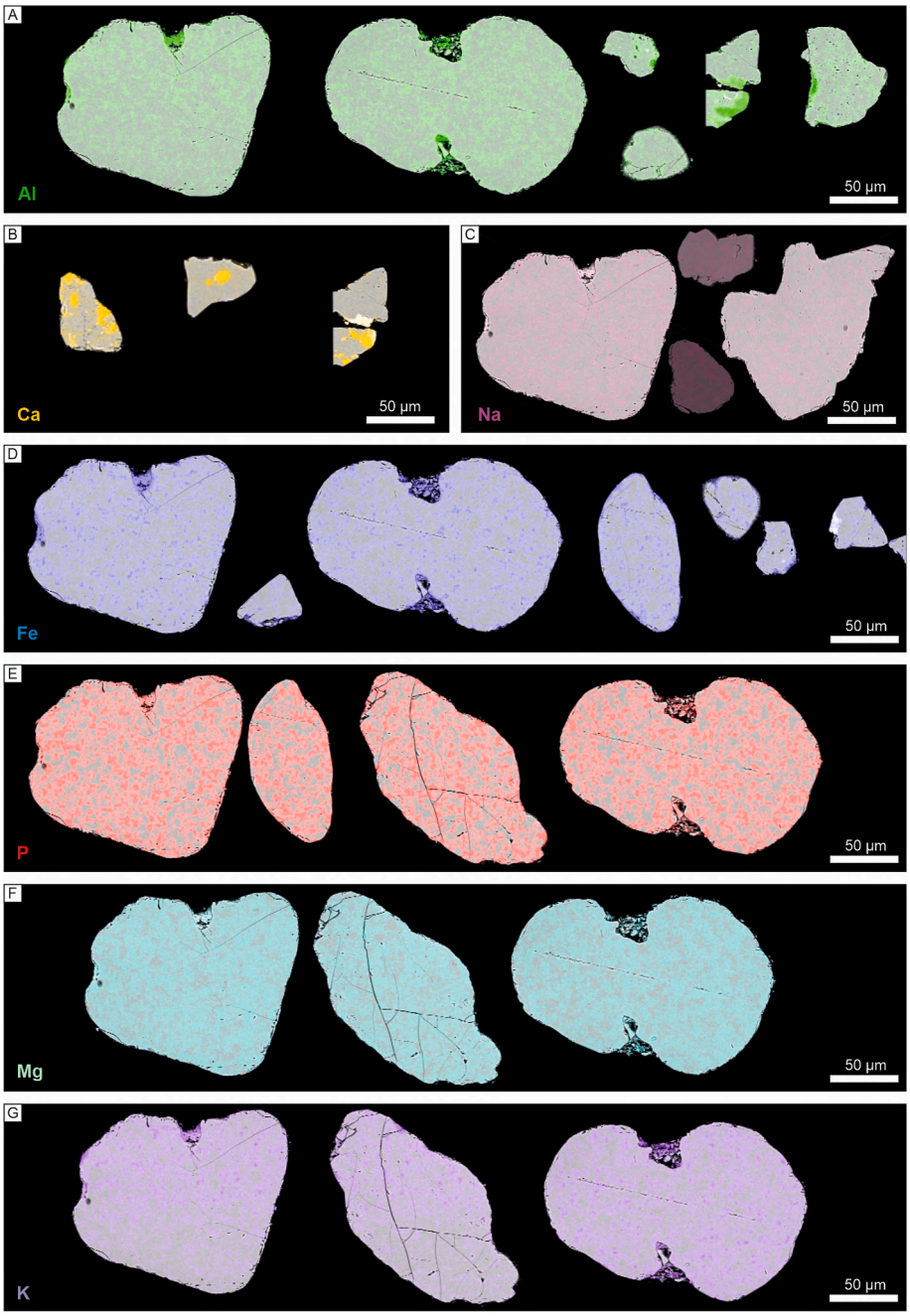

Fig. 7. Distribution of the following chemical elements basing on EDX-mapping: A – aluminium, B – calcium, C – sodium, D – iron, E – phosphorus, F – magnesium, and G – potassium.

distilled water further emphasizes the critical influence of mineral content in driving quartz corrosion.

5.1.2. *Microtextures of quartz*

A variety of fracture types were identified, each reflecting distinct temporal and environmental trends (Fig. 8). Single fracturing, which typically affected smaller grain fragments, was observed in most samples, except in those exposed to distilled water at the beginning of the experiment (day 0) and after 1.5 months. This suggests that mineral-rich environments facilitate earlier grain fracturing, whereas low-mineral environments delay its onset. The influence of water composition on quartz grain integrity aligns with findings from previous studies on chemical weathering in mineral-rich systems (e.g., Fu et al., 2023).

The predominance of multiple cracks, particularly intersecting cracks, across all samples and time points underscores the cumulative impact of seismic stress on quartz grains (Fig. 8). The consistent formation of intersecting cracks, regardless of water type, indicates that seismic forces are the primary driver of this feature, as previously suggested in studies on grain fracturing under dynamic stress conditions (e.g., Hurst et al., 2021). In contrast, multiple non-intersecting cracks occurred more frequently in mineralised water, suggesting that ionic interactions at the grain-water interface facilitate less structured crack propagation.

The presence of multi-advanced corrosion and fragmentation, exclusively in highly-mineralised water, highlights the significant role of mineral content in amplifying grain destruction under seismic stress. Advanced corrosion, characterised by progressive grain breakdown, was absent in distilled and medium-mineralised water, reinforcing the idea

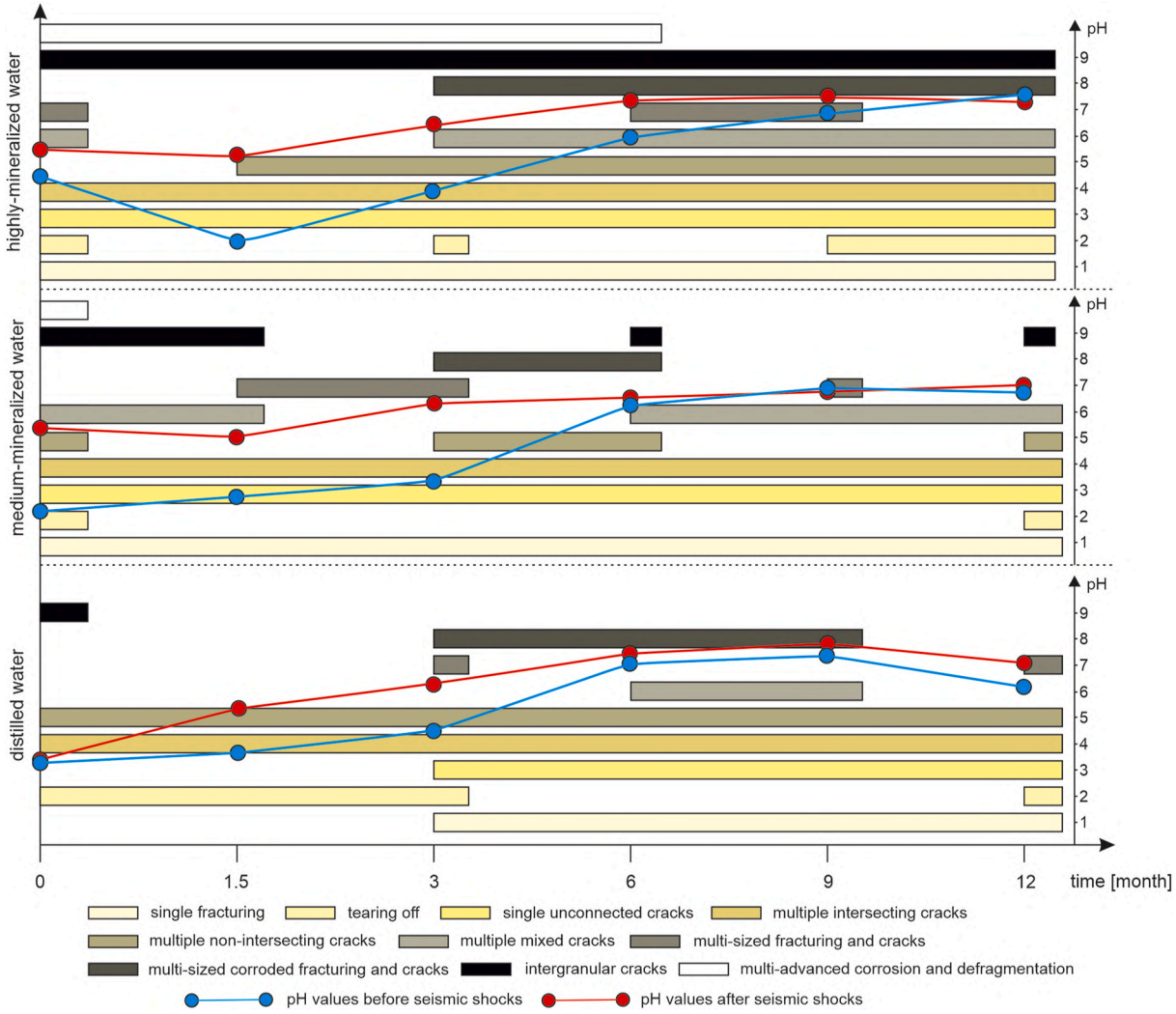

Fig. 8. Types of iron-rich quartz grain cracks over time in relation to the degree of water mineralisation and pH values.

that high ionic concentrations exacerbate chemical weakening processes (cf. Feucht and Logan, 1990; Dunning et al., 1994; Feng et al., 2001).

The irregular occurrence of intergranular symmetric cracks, with no consistent pattern, suggests that these features are influenced more by the direction and intensity of seismic forces than by water composition.

The progression of quartz grain damage over time provides key insights into how seismic activity and water chemistry jointly influence grain morphology (Fig. 8). In the early stages, the grains exhibited relatively smooth surfaces with minimal edge damage, suggesting that the initial seismic impacts may primarily targeted the grain boundaries. Over time, the increase in pronounced cracks and internal fracturing suggests deeper structural damage, consistent with accumulative effects of seismic stress. By the later stages, the dominance of intersecting and non-intersecting cracks, combined with significant fragmentation, particularly in mineralised water, underscores the compound effects of seismic and chemical stresses on quartz grain integrity.

5.2. *The seismic cycle of quartz grain – mechanical and chemical forces*

Based on the obtained results, the seismic cycle of quartz grain can be proposed, consisting of seven fundamental stages (Fig. 9A). Initially, the primary quartz grain undergoes damage and fracturing as a result of seismic shocks (Fig. 9A_1). These cracks vary in form and intensity depending on multiple factors, such as the degree of water mineralisation, the duration of exposure, and the parameters of the seismic events (magnitude, frequency). As physical forces continue to act on the grain, further destruction of the grain's morphological boundaries occurs (Fig. 9A_2), leading to the gradual spalling and fragmentation of the grain (Fig. 9A_3). The smaller detached fragments exhibit the capacity to form larger clusters through the combined effects of physical forces and chemical interactions in the environment (Fig. 9A_4). The thermodynamic energy and the increase in pressure during seismic activity can further accelerate and deepen this aggregation process (Fig. 9A_5). Smaller fragments move and align to form new grain boundaries. This process can ultimately lead to the complete recrystallisation of a new quartz grain (Fig. 9A_6). If subjected to additional seismic stress, the newly formed quartz grain re-enters the cycle, undergoing further damage and repeating the process of fracturing, disaggregation, and recrystallisation (Fig. 9A_7). This cyclical nature of quartz grain transformation highlights the dynamic interplay between mechanical and chemical factors, which together contribute to the continual evolution and modification of quartz grains in seismically active environments.

Certain processes and phenomena occurring during seismically-induced sediment liquefaction can be explained (Fig. 9B). The primary structure of water-saturated sediments defines the sediment's porosity, permeability, and compaction (Fig. 9B_1). At this stage, these parameters are at their most favourable for liquefaction (cf. Lowe, 1976; Maltman and Bolton, 2003; Brandes and Winsemann, 2013; Collinson et al., 2019). As the initial mobilisation of the sediment occurs, it enters a pre-liquefaction state, during which the water table rises, causing the

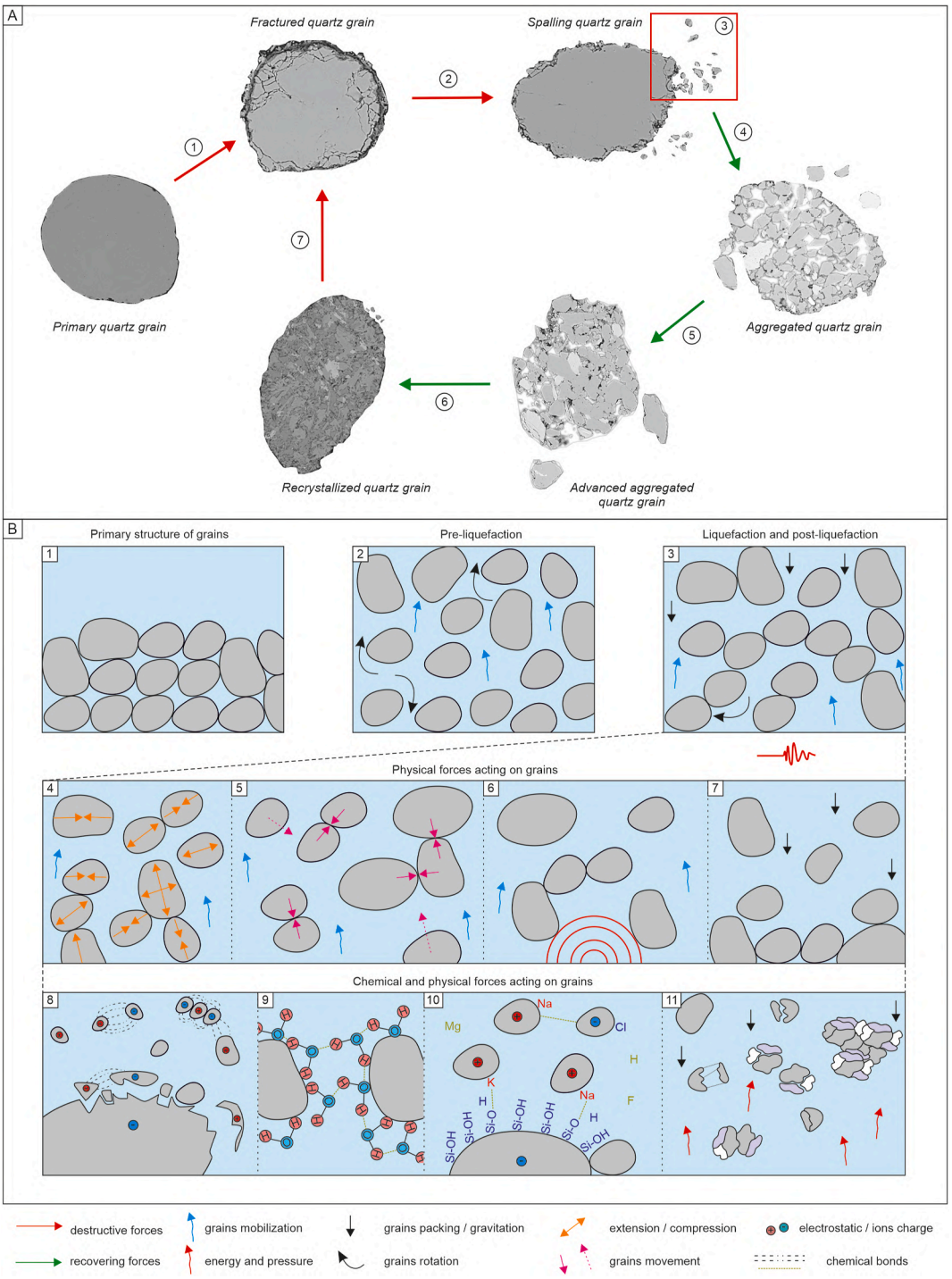

Fig. 9. Quartz grain changes caused by seismically-induced liquefaction. Main ways in: (A) the seismic cycle of quartz grain: 1 – fracturing, 2 – destruction, 3 – grain spalling and defragmentation, 4 – aggregation of smaller grains and particles, 5 – advanced aggregation, 6 – recrystallisation, 7 – re-entry to the seismic cycle, and (B) mechanisms of grains relationships during seismically-induced liquefaction: 1 – primary structure of grains, 2 – pre-liquefaction state, 3 – liquefaction and post-liquefaction state, 4 – compression and extension of grains, 5 – collision and grain movements, 6 – direct contact with seismic wave propagation, 7 – re-deposition of grains, 8 – electrostatic bonds, 9 – hydrogen bonds, 10 – ion bonds, 11 – pseudo-migration grain boundary.

grains to begin moving (Fig. 9B$_2$; cf. Maltman and Bolton, 2003). The next step is the actual seismogenic liquefaction of the sediment, during which intergranular contacts are lost (Fig. 9B$_3$; Seed, 1979; Van Rensbergen et al., 2003). The water-saturated sediment temporarily loses its strength and behaves like a viscous solid (e.g., Allen, 1982; Owen and Moretti, 2011) or plastic mass (Van Loon et al., 2020). After several seconds (depending on the duration of the seismic shocks, cf. Allen, 1982; Owen, 2003), the intergranular contacts are restored (Fig. 9B$_3$), and the liquefied sediment forms characteristic soft-sediment deformation structures (cf. Świątek et al., 2023). It is important to note that intergranular interactions persist and can continue even after the liquefaction process has concluded, contributing to the ongoing reorganisation of the sediment structure (cf. Campbell, 2003).

The greatest contribution to the formation of cracks and fracturing in quartz grains arises from physical phenomena, primarily compression and tension (Fig. 9B$_4$; cf. Yang and Zhang, 2019), as well as the collision

of grains during seismic events (Fig. 9B$_5$; cf. Barbot, 2019). These forces generate significant internal stress within the grains, leading to microfracturing and disaggregation. Grains can also be subjected to direct propagation of seismic waves, resulting in intra-grain fracturing, where cracks develop within a single grain, or symmetrical inter-grain cracks, which occur when adjacent grains are in direct contact and experience simultaneous stress (Fig. 9B$_6$). While these mechanical forces are dominant, gravitational forces, though less significant, still play a role in the overall fracturing process (Fig. 9B$_7$). During the post-liquefaction phase, "re-sedimentation" occurs as the liquefied sediment settles, and the falling grains may exert frictional forces upon each other. Although these gravitational effects are minor compared to the seismic forces, they can still contribute to grain abrasion and further microfracturing as the grains reposition and compact within the sedimentary layers.

Chemical forces operate somewhat differently compared to physical ones (Fig. 9B$_{8\text{-}10}$). Quartz in water almost always carries a negative electrostatic charge (Pan et al., 2022). During the propagation of seismic waves through water-saturated sediment and fractured quartz grains, this electrostatic charge can temporarily change (Fig. 9B$_8$; cf. Takeuchi and Nagahama, 2002). The detached quartz fragments carry both positive and negative static charges, which lead to the aggregation of smaller fragments (Dal Martello et al., 2012). These smaller fractions tend to combine with one another rather than attaching to larger quartz grains due to their increased boundary charge density (cf. Ledin et al., 1993). Additionally, larger grains have a more stable charge distribution, and their boundary are often already saturated with attached ions, making it less favourable for smaller fragments to aggregate with them (cf. Takeuchi and Nagahama, 2002; Zhang et al., 2023). The smaller particles, being more mobile and reactive due to their defragmented boundary, are more likely to interact and bind together through electrostatic forces (Fig. 8B$_8$; cf. Taboada-Serrano et al., 2006). Furthermore, the presence of water within the sediment exposes quartz grains to capillary forces, which arise from the interaction of water molecules with the quartz boundary (Fig. 9B$_9$). These forces promote the formation of hydrogen bonds between water molecules, which can contribute to the strengthen of clustering of smaller sediment particles (O'Melia, 1989; Xantheas, 2000). Though this effect is on a smaller scale, it may still play a role in the aggregation of finer sediment fractions, aiding in the formation of clusters of smaller particles.

A more significant influence, however, comes from the electric double layer that forms around water-saturated quartz (Fig. 9B$_{10}$; cf. Wander and Clark, 2008; Chen and Cheng, 2010). The boundary of quartz tends to develop hydroxyl hydration layer and silanol groups (-Si-O-H) due to the interaction between quartz and water (Zhang et al., 2023). These silanol groups further dissociate, leaving behind negatively charged boundaries (-SiO-). This negatively charged boundaries attracts cations from the surrounding solution (typically Na^+, K^+, Ca^{2+}), forming a double layer: one layer of negative charges on the quartz boundary and a corresponding layer of adsorbed cations from the solution (Fig. 9B$_{10}$; Leonardelli et al., 1992; Zhuravlev, 2000; Rimola et al., 2013; Dalstein et al., 2017). The presence of this double layer influences the behaviour of quartz grains in suspension, as it modulates the interaction between particles and ions in the solution (Zhang et al., 2023). As a result, selected cations from the solution adsorb onto the quartz boundary, leaving other cations and anions in the solution to interact with one another (Pan et al., 2022; Zhang et al., 2023). These interactions can lead to electrostatic repulsion or attraction between grains, affecting sediment cohesion and the aggregation of grains. The dynamic nature of this electric double layer, especially during seismic activity, may plays a crucial role in the mobility and reorganisation of quartz grains in water-saturated environments.

Pseudo-migration of grain boundary occurs when smaller quartz grain fragments, under favourable conditions, merge to form an aggregated or recrystallised, larger grain (Fig. 9B$_{11}$). This process is driven by several factors, including high thermodynamic energy, increased pressure, and the influence of physical and chemical forces (cf. Means and Jessel, 1986). As seismic activity generates significant mechanical stress, combined with the presence of water and mineralisation, these forces facilitate the gradual dissolution of the boundaries between the smaller grain fragments. Due to the high thermodynamic energy present during and after seismic events, the system tends to move towards a lower energy state, promoting the fusion of grain fragments. Pressure exerted during seismic activity also plays a crucial role by bringing the fragments into closer contact, allowing their boundaries to dissolve and merge more easily. In addition to these physical forces, chemical interactions further contribute to the dissolution of grain boundaries. The presence of water and dissolved ions in the surrounding environment promotes chemical reactions at the grain boundaries. This leads to a weakening and eventual loss of these boundaries, especially as the grains undergo reorganisation under stress. The result is a new, recrystallised quartz grain with no discernible internal boundaries between the original fragments. This process is not entirely the same as classical grain boundary migration, which is typically driven by grain growth through hydrothermal conditions, especially in metamorphic rocks (cf. Gower and Simpson, 1992; Masuda et al., 1997; Liebl et al., 2006; Tajčmanová et al., 2015). Instead, in pseudo-migration, the boundaries between fragments disappear due to the combined influence of seismic forces, high pressure, and chemical reactions. Over time, this creates a single, unified grain structure.

We have also identified additional indirect mechanisms responsible for the post-liquefaction state of quartz grains (Fig. 10). Often, though not always, grains were observed to crack into two or more parts (Fig. 10A). This phenomenon could be attributed to prolonged stresses over time, the separation of grain parts by mineral-rich fluids, or more commonly, the collision with other grains, or less during grains fall during re-sedimentation. Intergranular fracturing, in turn, may have occurred due to the direct propagation of seismic waves, with connected quartz grains serving as efficient conductors due to their piezoelectric properties (Fig. 10B; Baoyuan et al., 2007; Zhang et al., 2014; Barthelmy, 2021). In some cases, we found grains that had undergone near-total destruction or were heavily damaged (Fig. 10C). We suspect that these grains were already significantly fractured, and upon contact with another grain, they released stored stress through a sudden discharge, leading to further disintegration.

Additionally, many quartz grains appeared corroded, as evidenced by features such as bays and holes, as well as damaged and reactive grain boundaries (Figs. 5, 7 and 10D). Advanced corrosion of the grain, coupled with fragmentation caused by seismic shocks, may have contributed to the production of smaller grains, such as very fine-grained sand or even silt-sized grains. This process of breaking down larger quartz grains into finer would not only alter the grain size distribution in the sediment but also affect the overall sediment structure and behaviour during subsequent seismic events. Although the degree of mineralisation and the duration of water-saturation varied, we identified two key chemical compounds responsible for the degradation of quartz: hydrofluoric acid and orthosilicic acid. These compounds likely played a significant role in the corrosion of quartz grains (Larsen and Kleiv, 2016; Database, 2021), contributing to their deterioration, as further discussed in section 5.4 on corrosion.

5.3. Seismically-driven gold mobilisation and deposition

The presence of various morphological forms of gold in quartz grains association observed in this study provides compelling evidence of their deposition during or immediately after seismic events (Fig. 6). These findings significantly advance the understanding of the geological record of earthquakes, shedding light on the processes linking the association of gold and quartz. The presence of gold fragments filling cracks in quartz grains during a seismic event indicates a direct link between seismic activity and gold mobilisation. This is consistent with previous observations that quartz, as a piezoelectric material, can influence the precipitation of gold during episodes of stress (Voisey et al., 2024).

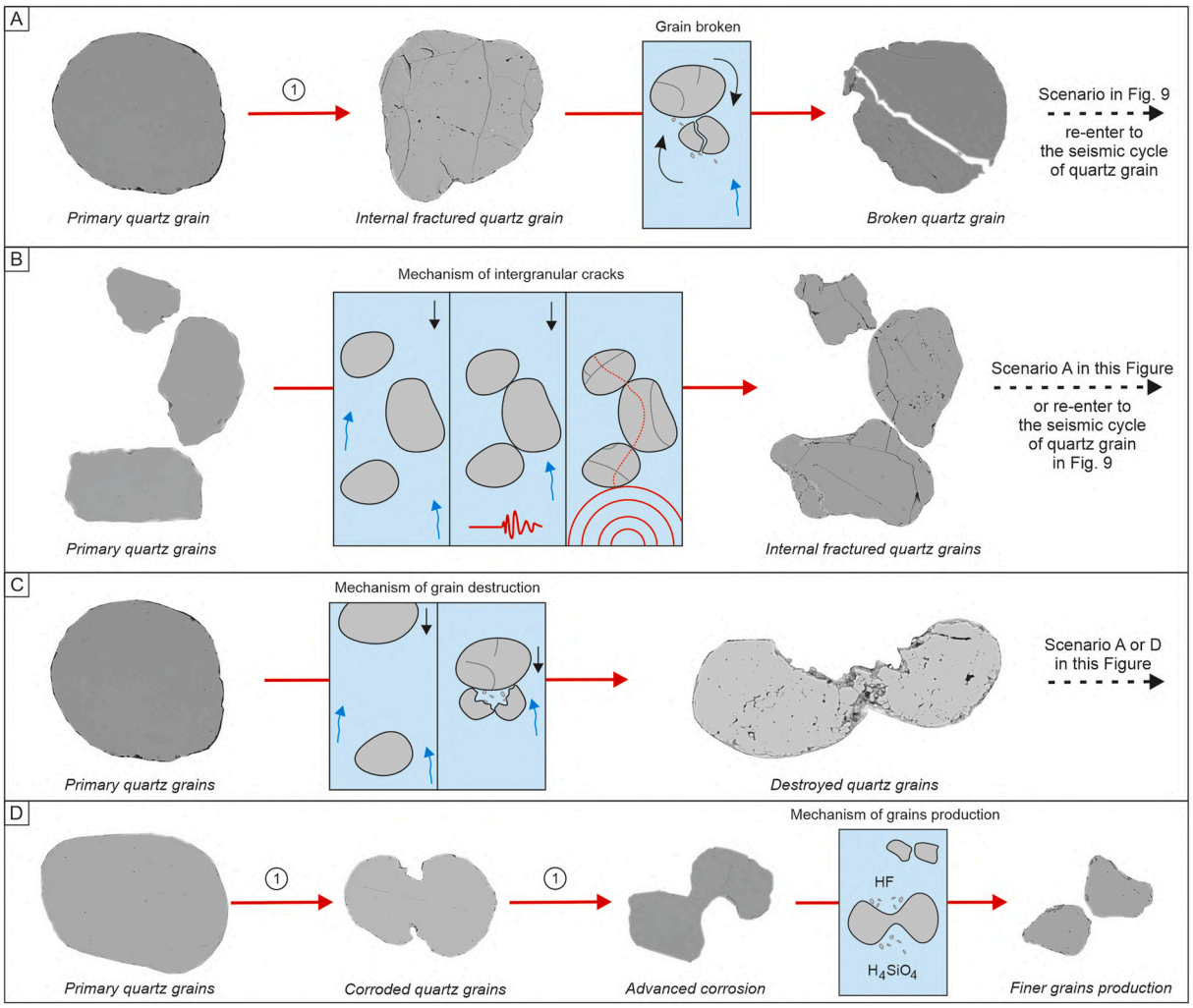

Fig. 10. Main stages with mechanisms of quartz grain defragmentation and destruction in this study. A – internal fracturing and tearing off, B – intergranular fracturing of grains, C – grain destruction, and D – corrosion and defragmentation. For explanations see Fig. 9.

In terms of the underlying mechanism, the main process of gold deposition on quartz grains during seismic events is thought to be driven by the piezoelectric effect of quartz (cf. Baoyuan et al., 2007; Zhang et al., 2014; Barthelmy, 2021). As seismic waves pass through quartz-rich environments, the mechanical stress applied to the quartz generates an electric charge, which in turn can facilitate the electrochemical reduction of gold from fluids present in the environment (Cox and Ruming, 2004; Voisey et al., 2024). This process, known as piezocatalysis, is enhanced under conditions where the quartz grains exhibit a strong preferred crystallographic orientation, as it amplifies the piezoelectric charge, creating localised environments favourable for gold nucleation and growth (Hong et al., 2010, 2012; Starr and Wang, 2013). The conditions accompanying seismicity, such as the rapid pressure changes and sediment-fluid system mobilisation associated with earthquake activity, further promote the deposition of gold within cracks of quartz grains (Fig. 6H). In particular, gold nanoparticles are often adsorbed onto quartz, which act as electrodes during the deformation, growing into larger gold clusters as deformation continues. This mechanism of piezoelectric gold deposition has been experimentally demonstrated, and our observations align with these findings, showing the accumulation of gold along quartz grain (cf. Tosi et al., 2012; Voisey et al., 2024)

One of the most intriguing implications of our results is the potential to use the morphology of gold deposits on quartz grains as a more precise indicator of seismic events, even at low-magnitude such this study.

5.4. Chemically-driven weathering

Geochemical conditions, particularly pH (acidity/alkalinity) and Eh (redox potential), may play a secondary role in influencing the ability, behaviour, and long-term record of sediment liquefaction, especially in tectonically active region. We specifically aimed to create incubation conditions that would actively promote the development of reductive environments. These parameters affect the chemical interactions within the sediment, altering processes such as mineral dissolution, precipitation, and grain cohesion during and after liquefaction events. Variations in pH can influence the solubility of minerals and the electrostatic charges on sediment grains, while Eh controls the oxidation-reduction reactions that can further modify the sediment structure (cf. Rao et al., 2009; Kicińska, 2018; Gorski, 2022; Zhang et al., 2023). However, no detailed studies have yet examined the specific impact of geochemical conditions on sediment liquefaction, which has been an unexpected and potentially significant factor in understanding this process. The literature only suggests that chemical agents may significantly influence on this phenomenon (Owen, 1987; Obermeier, 1996).

Low pH in the samples prior to the seismic shock may have allowed for the development of hydrofluoric acid (HF), particularly in samples with medium and high degree of water mineralisation that contained fluoride anions (Fig. 11). Another potential source of fluoride could have been mineral compounds or particles, such as apatite or topaz, which release fluoride into the solution (Bruun et al., 1983; Haroiuya and

Oelkers, 2004). The presence of HF was detected in samples analysed on day 0, as well as in samples analysed after 1.5 months (in the medium- and highly-mineralised water) and after 3 months of incubation (in the medium-mineralised water). Between 3 and 6 months, as well as after seismic shocks, the pH of the samples increased, causing HF to dissociate into free fluoride ions (Fig. 11A and B). During periods of low pH, hydrofluoric acid exerts a significant effect on the quartz grains, specifically by promoting corrosion and altering the structure of the grains (O'Meara et al., 1939; Ubara et al., 1984; Database, 2021). Highest pH has significant impact on dissociation (cf. Kuo and Klein, 2004). HF is known for its ability to attack silicon-oxygen bonds in quartz, leading to the etching of the quartz boundary and the formation of pits and micro-cracks (Larsen and Kleiv, 2015). This acid can penetrate the grain edge and boundary and weaken the overall structure, making the quartz grains more susceptible to mechanical fracturing. Despite quartz's typically stable physicochemical properties, even temporary exposure to HF created a chemically aggressive environment that further amplified intergranular interactions and, consequently, contributed to the

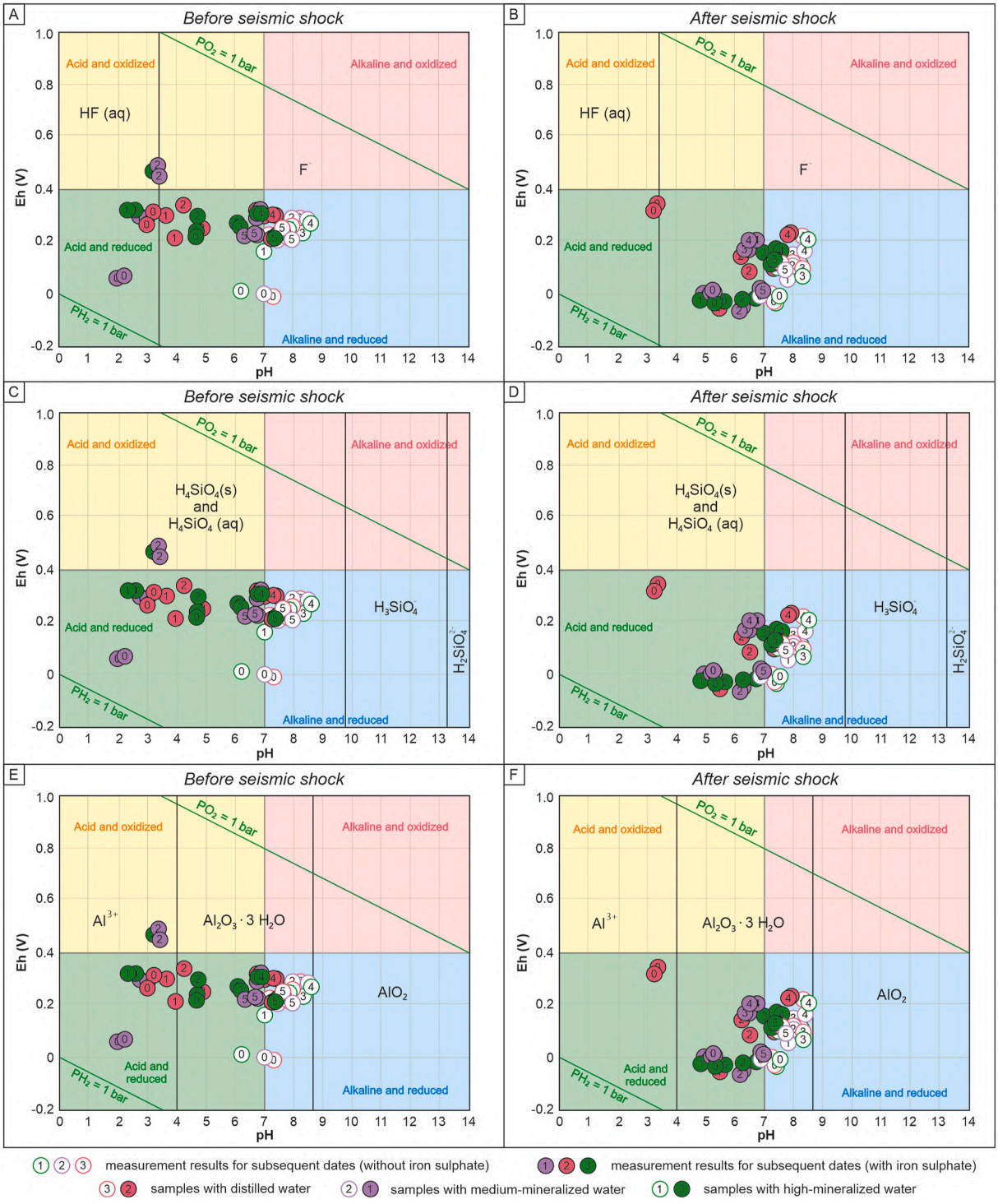

Fig. 11. Eh-pH diagrams of system F-H (A–B), Si-O-H (C–D) and Al-O-H (E–F) according to Pourbaix (1978) and Takeno (2005) for analysed samples before and after seismic shock.

fracturing of quartz grains (Larsen and Kleiv, 2015). Samples analysed at later time points were exposed to the effects of hydrofluoric acid for a longer duration, increasing the potential for more pronounced corrosion and structural damage to the quartz grains.

In addition to the presence of HF, orthosilicic acid may have been present (Fig. 11C and D), particularly due to its association with the electric double layer and the formation of silanol groups (-SiOH) on the quartz (Zhang et al., 2023). This acid could have reacted with the quartz grains, further weakening their structure by interacting with the silanol groups, leading to dissolution and weakening of the silicon-oxygen bonds:

$$SiO_2 + 2OH^- \rightarrow SiO_3^{2-} + H_2O \quad (1)$$

The hydroxide ions facilitate the dissociation of the silicon-oxygen bonds, leading to the release of silica into the solution. At pH levels above 4, the form of aluminium in the system changed from Al^{3+} to Al_2O_3, allowing it to react with orthosilicic acid and the formation of aluminosilicates (Fig. 11E, F), e.g., kaolinite (Li et al., 2020; Liu et al., 2020), as well as bicarbonates ions or mobility Si, Al and Fe (cf. Kicińska and Pomykała, 2023):

$$2SiO_2 + Al_2O_3 + 2H_2O \rightarrow Al_2Si_2O_5(OH)_4 \quad (2)$$

Kicińska and Pomykała (2023) suggest significantly the role of finer fractions (<63 μm) in adsorbing metals. The precipitation of aluminosilicates can lead to additional stress on the grain boundary, causing further fracturing and defragmentation. This transformation from quartz to aluminosilicates not only reduces the integrity of the quartz but also may promotes intergranular and intragranular fracturing, ultimately contributing to the grain's disintegration and altering its role in the sediment texture.

Determining the precise geochemical conditions and transitional changes between ions proves to be a complex task, given the multitude of forces and mechanisms interacting between the grains for liquefaction phenomenon. As we have demonstrated, the influence of time and the degree of water mineralisation play a secondary role in the formation of different types of cracks. Changes in pH and Eh, both before and after the seismic shock, further confirm this relationship. Identifying the mechanisms, particularly the mineralogical and crystallographic processes occurring during seismic events, requires further research, including experimental studies to provide a more comprehensive understanding.

6. Conclusions

The results of this study provide significant insights into the formation of seismically-induced soft-sediment deformation structures (SSDS) and the corresponding alterations in quartz grains. The following conclusions can be drawn.

1. Seismically-induced liquefaction causes a wide range of microstructural and microtextural changes in quartz grains, from subtle cracks to severe fracturing and corrosion features, which have not been studied until now. These alterations are strongly influenced by the degree of water mineralisation and the duration of exposure to seismic activity. Regardless of the depositional environment of the sediment (glaciofluvial, glaciolacustrine or aeolian), the features of quartz grains following seismic shocks exhibit remarkable similarity.
2. These studies offer a novel approach to differentiating seismically-induced liquefaction and deformation structures from those caused by other trigger mechanisms. Analysing microstructural changes and geochemical signatures in the quartz grains may enables the identification of deformation features unique to seismic events, enhancing the understanding of the geological record of earthquakes.
3. The observed deposition of gold on quartz grains during seismic events opens new possibilities for using these microstructures as indicators of past seismic activity. The gold formations, particularly in cracks, provide direct evidence of the role of seismicity in the redistribution and deposition of minerals, confirming results obtained by Voisey et al. (2024). The mineral composition in water may plays a crucial role in amplifying the effects of seismic stress on quartz grains. Highly-mineralised water accelerates corrosion and promote more pronounced grain damage, while distilled water provides a less destructive effect.
4. Changes in pH and Eh before and after seismic events highlight the importance of geochemical conditions in preserving liquefaction-induced deformation structures. These parameters not only affect the physical stability of the sediments but also influence chemical weathering processes that contribute to grain defragmentation.
5. The findings of this study suggest that further experimental and field investigations are necessary to fully understand the complex interactions between seismic forces, water chemistry, and sediment deformation. The proposed quartz seismic cycle, combining mechanical and chemical processes, offers a valuable framework for future studies aimed at reconstructing paleoseismic events.
6. The outcomes of this research hold valuable potential for enhancing seismic risk evaluations and understanding the hazards posed by seismic events by examining the chemical characteristics of sediments and the microstructural transformations of quartz grains.

CRediT authorship contribution statement

Szymon Świątek: Writing – review & editing, Writing – original draft, Validation, Project administration, Methodology, Investigation, Conceptualization. **Karolina Lewińska:** Writing – review & editing, Supervision, Methodology, Conceptualization. **Małgorzata Pisarska-Jamroży:** Writing – review & editing, Methodology, Conceptualization. **Christina Günter:** Writing – review & editing, Methodology.

Declaration of competing interest

The authors declare that they have no known competing financial interests or personal relationships that could have appeared to influence the work reported in this paper.

Acknowledgments

This work was supported by the UAM Research University – Excellence Initiative (grant numbers 054/13/SNP/0001 and 133/13/UAM/0044). The study has been supported in part by a grant PRELUDIUM-22 (No. 2023/49/N/ST10/00282) from the National Science Centre, Poland. The authors thank Konrad Proczek (Medical University of Warsaw) for lab assistance, as well as Nicolai Klitscher (GFZ-Potsdam) and Michał Jankowiak (UAM) for preparing thin sections. We greatly appreciate the in-depth review and major constructive comments of the Editor G. Ian Alsop, and the anonymous reviewers who led to significant improvement of the manuscript.

Appendix A. Supplementary data

Supplementary data to this article can be found online at https://doi.org/10.1016/j.jsg.2025.105357.

Appendix B

Appendix S1

Table comparing the occurrence of the microtextural and microstructural features between analysed samples (*D – distilled water, M – medium-mineralised water, H – high-mineralised water*)

Time					Day 0			1.5 month			3 months			6 months			9 months			12 months		
Date					0			1			2			3			4			5		
Features		Sample	Clean sand	Dwasieden	D	M	H	D	M	H	D	M	H	D	M	H	D	M	H	D	M	H
		pH	5.98	6.5	3.3	5.4	5.6	5.5	5.1	5.2	6.4	6.3	6.5	7.6	6.5	7.1	7.9	6.7	7.4	7.3	7	7.2
		Eh (mV)	181.5	330	340	20	−30	−58	0.4	−40	111	−44	180	95	186	175	223	204	187	134	40	121
		Reference																				
Edge and boundary morphology	Subtle cracks	Fig. 4A–B	x	x	x	x	x	x			x	x	x	x	x		x	x	x	x	x	x
	Pronounced cracks	Fig. 4C–D		x		x	x		x	x	x	x	x	x	x	x	x	x	x	x	x	x
	Edge corrosion	Fig. 4F–G		x	x		x	x		x			x		x	x		x	x	x		x
	Edge defragmentation	Fig. 4H		x		x		x	x	x		x	x	x	x	x	x		x	x	x	x
	Knocked out grain fragments	Fig. 4K		x		x	x		x	x			x	x		x			x		x	x
	Corroded and reactive boundary	Fig. 4L		x						x		x	x		x	x		x	x		x	x
Sphericity	Spherical	Fig. 3A$_1$	x	x				x	x	x	x	x	x	x	x		x	x	x	x	x	x
	Elongated	Fig. 3$_2$,	x	x	x	x	x								x	x			x	x		x
Roundness	Rounded	Fig. 3A$_4$	x																	x		
	Subrounded	Fig. 3A$_2$	x	x	x	x	x	x	x	x	x	x	x	x	x		x	x	x	x	x	x
	Subangular	Fig. 3A$_5$	x	x	x	x	x		x	x	x	x		x	x	x	x	x	x		x	x
	Angular	Fig. 3A$_6$		x	x											x						
Special features	Bay	Fig. 4F–G	x	x	x	x	x	x	x	x	x	x	x	x	x	x	x	x	x	x	x	x
	Hole	Fig. 4K	x	x		x	x	x		x	x	x	x	x	x	x	x	x	x	x	x	x
Microcracks and fracturing	Single fracturing	Fig. 3B		x		x	x		x	x	x	x	x	x	x	x	x	x	x	x	x	x
	Tearing off	Fig. 3B		x	x	x	x	x			x		x					x	x	x	x	x
	Single unconnected cracks	Fig. 3C		x		x	x		x	x	x	x	x	x	x	x	x	x	x	x	x	x
	Multiple intersecting cracks	Fig. 3D		x	x	x	x	x	x	x	x	x	x	x	x	x	x	x	x	x	x	x
	Multiple non-intersecting cracks	Fig. 3E		x	x	x		x		x	x	x	x	x	x	x	x		x	x	x	x
	Multiple mixed cracks	Fig. 3F		x		x	x		x				x	x	x		x	x			x	x
	Multi-sized fracturing and cracks	Fig. 3G		x			x		x		x	x				x		x	x	x		
	Multi-sized corroded fracturing and cracks	Fig. 3H		x							x	x	x		x	x	x		x			x
	Intergranular symmetric cracks	Fig. 3I		x	x	x	x		x	x			x	x	x	x	x		x	x	x	x
	Multi-advanced corrosion and defragmentation	Fig. 3J		x		x	x			x			x			x		x				
Gold formation	Pseudo-hexagonal Au crystal	Fig. 6A–B		x	x			x	x	x	x	x				x					x	x
	Micrometre-sized	Fig. 6C		x	x	x	x		x	x	x	x	x	x	x	x	x	x	x	x	x	x
	Au cluster	Fig. 6D–F		x	x	x	x	x		x	x	x	x	x	x	x	x	x	x	x		x
	Au nanoparticles	Fig. 6A–G		x	x	x	x	x	x		x	x	x	x	x	x	x	x	x	x	x	x
	Au droplets	Fig. 6H		x					x			x							x			x
The seismic cycle of quartz	Aggregated grain	Fig. 7A		x		x	x						x	x	x	x		x	x			x
	Advanced aggregated grain	Fig. 7A		x											x		x				x	
	Recrystallised	Fig. 3M, 7A		x				x	x	x			x	x			x			x		x
	Broken	Fig. 7A		x	x	x	x	x		x	x		x		x	x		x	x	x	x	x
	Internal fractured	Fig. 7A		x	x	x	x		x	x		x	x	x	x	x	x		x	x	x	x
	Destroyed grain	Fig. 7A													x						x	

Data availability

Data will be made available on request.

References

Ackerson, M.R., Tailby, N.D., Watson, E.B., 2015. Trace elements in quartz shed light on sediment provenance. Geochem. Geophys. Geosyst. 16, 1894–1904. https://doi.org/10.1002/2015GC005896.

Allen, J.R.L., 1982. Developments in Sedimentology. Sedimentary Structures: Their Character and Physical Basis, 30A. Elsevier Scientific Publishing Company.

Alsop, G.I., Marco, S., Levi, T., 2022. Recognising surface versus sub-surface deformation of soft-sediments: consequences and considerations for palaeoseismic studies. J. Struct. Geol. 154, 104493. https://doi.org/10.1016/j.jsg.2021.104493.

Alsop, G.I., Weinberger, R., Marco, S., Levi, T., 2019. Identifying soft-sediment deformation in rocks. J. Struct. Geol. 125, 248–255. https://doi.org/10.1016/j.jsg.2017.09.001.

Andò, S., Garzanti, E., Padoan, E., Limonta, M., 2012. Corrosion of heavy minerals during weathering and diagenesis: a catalog for optical analysis. Sed. Geol. 280, 165–178. https://doi.org/10.1016/j.sedgeo.2012.03.023.

Asumadu, K., Armitage, G.T.M., Churchward, H.M., 1998. The effects of chemical weathering on the morphology and strength of quartz grains–an example from S.W. Australia. Eur. J. Soil Sci. 39, 375–383. https://doi.org/10.1111/j.1365-2389.1988.tb01223.x.

Baoyuan, S., Jiantong, W., Changyin, G., Min, Q., 2007. Research on the torsional effect of piezoelectric quartz. Sens. Actuators A: Phys. 136, 329–334. https://doi.org/10.1016/j.sna.2006.08.028.

Barbot, S., 2019. Modulation of fault strength during the seismic cycle by grain-size evolution around contact junctions. Tectonophysics 765, 129–145. https://doi.org/10.1016/j.tecto.2019.05.004.

Barthelmy, D., 2021. Quartz mineral data. http://www.webmineral.com/data/Quartz.shtml. (Accessed 13 March 2023).

Belzyt, S., Pisarska-Jamroży, M., Bitinas, A., Woronko, B., Phillips, E.R., Piotrowski, J.A., Jusienė, A., 2021. Repetitive Late Pleistocene soft-sediment deformation by seismicity-induced liquefaction in north-western Lithuania. Sedimentology 68, 3033–3056. https://doi.org/10.1111/sed.12883.

Brandes, C., Winsemann, J., 2013. Soft-sediment deformation structures in NW Germany caused by Late Pleistocene seismicity. Int. J. Earth Sci. 102, 2255–2274. https://doi.org/10.1007/s00531-013-0914-4.

Bruun, C., Moe, D., Madsen, H.E.L., 1983. Study on the dissolution behaviour of calcium fluoride. Eur. J. Oral Sci. 91, 247–250. https://doi.org/10.1111/j.1600-0722.1983.tb00811.x.

Campbell, C.S., 2003. Rapid granular flows. Annu. Rev. Fluid Mech. 22, 57–90. https://doi.org/10.1146/annurev.fl.22.010190.000421.

Chen, Y.W., Cheng, H.P., 2010. Structure and stability of thin water films on quartz surfaces. Appl. Phys. Lett. 97, 161909. https://doi.org/10.1063/1.3504710.

Collinson, J.D., Mountney, N., Thompson, D.B., 2019. Sedimentary Structures, fourth ed. Dunedin Academic Press, London.

Cox, S.F., Ruming, K., 2004. The st ives mesothermal gold system, western Australia – a case of golden aftershocks? J. Struct. Geol. 26, 1109–1125. https://doi.org/10.1016/j.jsg.2004.04.006.

Crook, W.K.A., 1968. Weathering and roundness of quartz sand grains. Sedimentology 11, 171–182. https://doi.org/10.1111/j.1365-3091.1968.tb00851.x.

Dal Martello, E., Bernardis, S., Larsen, R.B., Tranell, G., Di Sabatino, M., Arnberg, L., 2012. Electrical fragmentation as a novel route for the refinement of quartz raw materials for trace mineral impurities. Powder Technol. 224, 209–216. https://doi.org/10.1016/j.powtec.2012.02.055.

Dalstein, L., Potapova, E., Tyrode, E., 2017. The elusive silica/water interface: isolated silanols under water as revealed by vibrational sum frequency spectroscopy. Phys. Chem. Chem. Phys. 19, 10343–10349. https://doi.org/10.1039/c7cp01507k.

Database Chemical Information, 2021. Silicon dioxide. https://www.drugfuture.com/chemdata/Silicon-Dioxide.html. (Accessed 13 March 2023).

Drees, L.R., Wilding, L.P., Smeck, N.E., Senkayi, A.L., 1989. Silica in soils: quartz and disordered silica polymorphs. In: Dixon, B., Weed, S.B. (Eds.), Minerals in Soil Environments, 1, second ed. Soil Science Society of America, pp. 913–974. https://doi.org/10.2136/sssabookser1.2ed.c19.

Dunning, J., Douglas, B., Miller, M., McDonald, S., 1994. The role of the chemical environment in frictional deformation: stress corrosion cracking and comminution. Pure and App. Geo 143, 151–178. https://doi.org/10.1007/BF00874327.

Feng, X.T., Chen, S., Li, S., 2001. Effects of water chemistry on microcracking and compressive strength of granite. Int. Rock Mech. Min. Sci. 38, 557–568. https://doi.org/10.1016/S1365-1609(01)00016-8.

Feucht, L.J., Logan, J.M., 1990. Effects of chemically active solutions on shearing behavior of a sandstone. Tectonophysics 175, 159–176. https://doi.org/10.1016/0040-1951(90)90136-V.

Friedman, G., Sanders, J.E., 1978. Principles of Sedimentology. Wiley, New York.

Fu, H., Jian, X., Pan, H., 2023. Bias in sediment chemical weathering intensity evaluation: a numerical simulation study. Earth Sci. Rev. 246, 104574. https://doi.org/10.1016/j.earscirev.2023.104574.

Galli, P., 2000. New empirical relationships between magnitude and distance for liquefaction. Tectonophysics 324, 169–187. https://doi.org/10.1016/S0040-1951(00)00118-9.

Gorski, C.A., 2022. Electrochemical analyses of redox-active minerals: insights and persisting challenges. In: Presented at the Electrochemical Society Meeting. The Electrochemical Society, vol. 2198.

Gower, R.J.W., Simpson, C., 1992. Phase boundary mobility in naturally deformed, high-grade quartzofeldspathic rocks: evidence for diffusional creep. J. Struct. Geol. 14, 301–313. https://doi.org/10.1016/0191-8141(92)90088-E.

Harouiya, N., Oelkers, E.H., 2004. An experimental study of the effect of aqueous fluoride on quartz and alkali-feldspar dissolution rates. Chem. Geol. 205, 155–167. https://doi.org/10.1016/j.chemgeo.2004.01.005.

He, B., Qiao, X., 2015. Advances and overview of the study on paleo-earthquake events: a review of seismite. Acta Geol. Sinica 89, 1702–1746.

Helland, P.E., Holmes, M.A., 1997. Surface textural analysis of quartz sand grains from ODP site 918 off the southeast coast of Greenland suggests glaciation of southern Greenland at 11 Ma. Palaeogeogr. Palaeoecol. 135, 109–121. https://doi.org/10.1016/S0031-0182(97)00025-4.

Hilbert-Wolf, H.L., Simpson, E.L., Simpson, W.S., Tindall, S.E., Wizevich, M.C., 2009. Insights into syndepositional fault movement in a foreland basin; trends in seismites of Upper Cretaceous Wahweap Formation, Kaiparowits Basin, Utah, USA. Basin Res. 21, 856–871.

Hong, K.-S., Xu, H., Konishi, H., Li, X., 2010. Direct water splitting through vibrating piezoelectric microfibers in water. J. Phys. Chem. Lett. 1, 997–1002.

Hong, K.-S., Xu, H., Konishi, H., Li, X., 2012. Piezoelectrochemical effect: a new mechanism for azo dye decolorization in aqueous solution through vibrating piezoelectric microfibers. J. Phys. Chem. C 116, 13045–13051.

Hurst, A., Luzinski, W., Zvirtes, G., Scott, A., Vigorito, M., Morton, A., Wu, F., 2021. Some petrographic and mineralogical diagnostics of sandstone intrusions. In: Silcock, S., Huuse, M., Bowman, M., Hurst, A., Cobain, S. (Eds.), Subsurface Sand Remobilization and Injection, vol. 493. Geological Society, London, Special Publications, pp. 287–302.

Kicińska, A., 2018. Health risk assessment related to an effect of sample size fractions: methodological remarks. Stoch. Environ. Res. Risk Assess. 32, 1867–1887. https://doi.org/10.1007/s00477-017-1496-7.

Kicińska, A., Pomykała, R., 2023. Incongruent dissolution of silicates and its impact on the environment: an example of a talc mine. Sci. Rep. 13, 22519. https://doi.org/10.1038/s41598-023-50143-y.

Kuo, J.R., Klein, M.L., 2004. Dissociation of hydrogen fluoride in $HF(H_2O)_7$. J. Chem. Phys. 120, 4690–4695. https://doi.org/10.1063/1.1644793.

Larsen, E., Kleiv, R.A., 2015. Towards a new process for the flotation of quartz. Miner. Eng. 83, 13–18.

Larsen, E., Kleiv, R.A., 2016. Flotation of quartz from quartz-feldspar mixtures by the HF method. Miner. Eng. 98, 49–51. https://doi.org/10.1016/j.mineng.2016.07.021.

Ledin, A., Karlsson, S., Allard, B., 1993. Effects of pH, ionic strength and a fulvic acid on size distribution and surface charge of colloidal quartz and hematite. Appl. Geochem. 8, 409–414. https://doi.org/10.1016/0883-2927(93)90009-6.

Leonardelli, S., Facchini, L., Fretigny, C., Tougne, P., Legrand, A.P., 1992. Silicon-29 NMR study of silica. J. Am. Chem. Soc. 114, 6412–6418. https://doi.org/10.1021/ja00042a018.

Li, S., He, H., Tao, Q., Zhu, J., Tan, W., Ji, S., Yang, Y., Zhang, C., 2020. Kaolinization of 2:1 type clay minerals with different swelling properties. Am. Mineral. 105, 687–696. https://doi.org/10.2138/am-2020-7339.

Liebl, C., Kuntcheva, B., Kruhl, J.H., Kunze, K., 2006. Effect of crystallography and temperature on the development of quartz high-angle grain boundaries in metamorphic rocks. In: Philipp, S., Leiss, B., Vollbrecht, A., Tanner, D., Gudmundsson, A. (Eds.), 11th Symposium "Tektonik, Struktur- und Kristallingeologie. Univ.-Verl. Göttingen, pp. 132–134. https://doi.org/10.23689/fidgeo-1878.

Liu, L., Zhang, T., Liu, J., Liu, Q., Li, K., Liu, D., Liu, W., 2020. Genesis of kaolinite deposits in the jungar coalfield, north China: petrological, mineralogical and geochemical evidence. Acta Geol. Sinica 95, 517–530. https://doi.org/10.1111/1755-6724.14527.

Lowe, D.R., 1976. Subaqueous liquefied and fluidised sediment flows and their deposits. Sedimentology 23, 285–308. https://doi.org/10.1111/j.1365-3091.1976.tb00051.x.

Mahaney, W.C., 1995. Pleistocene and Holocene glacier thicknesses, transport histories and dynamics inferred from SEM microtextures on quartz particles. Boreas 24, 293–304. https://doi.org/10.1111/j.1502-3885.1995.tb00781.x.

Mahaney, W.C., 2002. Atlas of Sand Grain Surface Textures and Applications. Oxford University Press, p. 237.

Maltman, A.J., Bolton, A., 2003. How sediments become mobilized. In: Van Rensbergen, P., Hillis, R.R., Maltman, A.J., Morley, C.K. (Eds.), Subsurface Sediment Mobilization, vol. 216. Geological Society Special Publications, pp. 9–20. https://doi.org/10.1144/GSL.SP.2003.216.01.02.

Masuda, T., Morikawa, T., Nakayama, Y., Suzuki, S., 1997. Grain-boundary migration of quartz during annealing experiments at high temperatures and pressures, with implications for metamorphic geology. J. Metamorph. Geol. 15, 311–322. https://doi.org/10.1111/j.1525-1314.1997.00023.x.

McCalpin, J.P., Ferrario, F., Figueiredo, P., Livio, F., Grützner, C., Pisarska-Jamroży, M., Quigley, M., Reicherter, K., Rockwell, T., Štěpančíková, P., Táboříki, P., 2023. New developments in onshore paleoseismic methods, and their impact on Quaternary tectonic studies. Quatern. Int. 664, 59–76. https://doi.org/10.1016/j.quaint.2023.03.008.

McCalpin, J.P., Nelson, A.R., 1996. Introduction to paleoseismology. In: McCalpin, J.P. (Ed.), Paleoseismology. Academic Press.

Means, W.D., Jessel, M.W., 1986. Accommodation migration of grain boundaries. Tectonophysics 127, 67–86.

Molinero-García, A., Müller, A., Martín-García, J.M., Simonsen, S.L., Delgado, R., 2022. Provenance of quartz grains from soils over Quaternary terraces along the

Guadalquivir River, Spain. Geoderma 414, 115769. https://doi.org/10.1016/j.geoderma.2022.115769.
Montenat, C., Barrier, P., d'Estevou, P.O., Hibsch, C., 2007. Sedimentary processes in seismically active regions. Sediment. Geol. 196, 5–30. https://doi.org/10.1016/j.sedgeo.2006.08.004.
Moretti, M., Van Loon, A.J., Liu, M., Wang, Y., 2014. Restrictions to the application of 'diagnostic' criteria for recognizing ancient seismite. J. Palaeogeogr. 3, 162–173. https://doi.org/10.3724/SP.J.1261.2014.00050.
Moss, A.J., 1966. Origin, shaping and significance of quartz sand grains. J. Geol. Soc. Aust. 13, 97–136. https://doi.org/10.1080/00167616608728607.
Müller, K., Winsemann, J., Pisarska-Jamroży, M., Lege, T., Spies, T., Brandes, C., 2020. Limitations of soft-sediment deformation structures as indicators for paleo-earthquakes in formerly periglacial and glaciated areas. Presented at EGU General Assembly 2020.
Müller, P., Tamburelli, S., Menegoni, N., Perozzo, M., Amadori, C., Crispini, L., Federico, L., Seno, S., Maino, M., 2023. Concurrence of load-and-flame structures, balls-and-pillows, clastic injectites, and shear deformation bands as indicators of seismicity in mixed siliciclastic-carbonate successions (Finale Ligure Basin, Italy). Mar. Petrol. Geol. 155, 106345. https://doi.org/10.1016/j.marpetgeo.2023.106345.
Newsome, D., Ladd, P., 1998. The use of quartz grain microtextures in the study of the origin of sand terrains in Western Australia. Catena 35, 1–17.
O'Meara, R.G., Norman, J.E., Hamond, W.E., 1939. Froth flotation and agglomerate tabling of feldspars. Bull. Am. Ceram. Soc. 18, 286–292.
O'Melia, C.R., 1989. Particle–particle interactions in aquatic systems. Colloids Surf. 39, 255–271. https://doi.org/10.1016/0166-6622(89)80191-X.
Obermeier, S., 1996. Use of liquefaction-induced features for paleoseismic analysis – an overview of how seismic liquefaction features can be distinguished from other features and how their regional distribution and properties of source sediment can be used to infer the location and strength of Holocene paleo-earthquakes. Eng. Geol. 44, 1–76. https://doi.org/10.1016/S0013-7952(96)00040-3.
Obermeier, S., 2009. Using liquefaction-induced and other soft-sediment features for paleoseismic analysis. In: McCalpin, J.P. (Ed.), Paleoseismology. Int. Geophys., vol. 95, pp. 497–564.
Obermeier, S., Jacobson, R.B., Smoot, J.P., Weems, R.E., Gohn, G.S., Monroe, J.E., Powars, D.S., 1990. Earthquake-induced liquefaction features in the coastal setting of South Carolina and in the fluvial setting of the New Madrid seismic zone. U. S. Geol. Surv. Prof. Pap. 1504, 44.
Owen, G., 1987. Deformation processes in unconsolidated sands. Geol. Soc. Lond. Spec. Publ 29, 11–24. https://doi.org/10.1144/GSL.SP.1987.029.01.0.
Owen, G., 2003. Load structures: gravity-driven sediment mobilization in the shallow subsurface. In: Van Rensbergen, P., Hillis, R.R., Maltman, A.J., Morley, C.K. (Eds.), Geol. Soc. Lond. Spec. Publ., Subsurface Sediment Mobilization, vol. 216, pp. 21–34. https://doi.org/10.1144/GSL.SP.2003.216.01.03.
Owen, G., Moretti, M., 2011. Identifying triggers for liquefaction-induced soft-sediment deformation in sands. Sediment. Geol. 235, 141–147. https://doi.org/10.1016/j.sedgeo.2010.10.003.
Owen, G., Moretti, M., Alfaro, P., 2011. Recognising triggers for soft-sediment deformation: current understanding and future directions. Sediment. Geol. 235, 133–140.
Pan, X., Li, S., Li, Y., Guo, P., Zhao, X., Cai, Y., 2022. Resource, characteristic, purification and application of quartz: a review. Miner. Eng. 183, 107600. https://doi.org/10.1016/j.mineng.2022.107600.
Piazolo, S., Bons, P.D., Jessell, M.W., Evans, L., Passchier, C.W., 2002. Dominance of microstructural processes and their effect on microstructural development: insights from numerical modelling of dynamic recrystallization. In: de Meer, S., Drury, M.R., de Bresser, J.H.P., Peynock, G.M. (Eds.), Geol. Soc. Lond. Spec. Publ., Deformation Mechanisms, Rheology and Tectonics: Current Status and Future Perspectives, vol. 200, pp. 149–170.
Pisarska-Jamroży, M., Belzyt, S., Börner, A., et al., 2018. Evidence from seismites for glacio-isostatically induced crustal faulting in front of an advancing land-ice mass (Rügen Island, SW Baltic Sea). Tectonophysics 745, 338–348.
Pisarska-Jamroży, M., Belzyt, S., Börner, A., Hoffmann, G., Hüneke, H., Kenzler, M., Obst, K., Rother, H., Steffen, H., Steffen, R., Van Loon, A.J., 2019. The Sea Cliff at Dwasieden: Soft-Sediment Deformation Structures Triggered by Glacial Isostatic Adjustment in Front of the Advancing Scandinavian Ice Sheet, vol. 2. DEUQUA Spec. Publ., pp. 61–67. https://doi.org/10.5194/deuquasp-2-61-2019
Pisarska-Jamroży, M., Woźniak, P.P., 2019. Debris flow and glacioisostatic-induced soft-sediment deformation structures in a Pleistocene glaciolacustrine fan: the southern Baltic Sea coast, Poland. Geomorphology 326, 225–238.
Pourbaix, M., 1978. Wykłady Z Korozji Elektrochemicznej. Państwowe Wydawnictwo Naukowe, Warszawa.
Rao, F., Song, S., Lopez-Valdivieso, A., 2009. Electrokinetic studies of minerals in aqueous solutions through electroacoustic measurement. Surf. Rev. Lett. 16, 65–71. https://doi.org/10.1142/S0218625X09012305.
Rimola, A., Costa, D., Sodupe, M., Lambert, J.F., Ugliengo, P., 2013. Silica surface features and their role in the adsorption of biomolecules: computational modeling and experiments. Chem. Rev. 113, 4216–4313. https://doi.org/10.1021/cr3003054.
Schulz, M.S., White, A.F., 1999. Chemical weathering in a tropical watershed, Luquillo Mountains, Puerto Rico III: quartz dissolution rates. Geo. Cosmo. Acta 63, 337–350. https://doi.org/10.1016/S0016-7037(99)00056-3.
Seed, H.B., 1979. Soil liquefaction and cyclic mobility evaluation for level ground during earthquakes. J. Geotech. Eng. Div. 105, 201–255. https://doi.org/10.1061/AJGEB6.0000768.
Sleep, N.H., Hessler, A.M., 2006. Weathering of quartz as an Archean climatic indicator. Earth Planet Sci. Lett. 241, 594–602.
Starr, M.B., Wang, X., 2013. Fundamental analysis of piezocatalysis process on the surfaces of strained piezoelectric materials. Sci. Rep. 3, 2160. https://doi.org/10.1038/srep02160.
Świątek, S., Belzyt, S., Pisarska-Jamroży, M., Woronko, B., 2023. Sedimentary records of liquefaction: implications from field studies. J. Geophys. Res.: Earth Surf. 128, e2023JF007152. https://doi.org/10.1029/2023JF007152.
Świątek, S., Pisarska-Jamroży, M., 2023. Soft-sediment deformation structures – development in laboratory conditions. Presented at the 36th International Meeting of Sedimentology, Dubrovnik, Croatia. https://doi.org/10.13140/RG.2.2.25225.83045.
Taboada-Serrano, P., Yiacoumi, S., Tsouris, C., 2006. Electrostatic surface interactions in mixtures of symmetric and asymmetric electrolytes: A Monte Carlo study. J. Chem. Phys. 125 (5), 054716. https://doi.org/10.1063/1.2238869.
Tajčmanová, L., Vrijmoed, J., Moulas, E., 2015. Grain-scale pressure variations in metamorphic rocks: implications for the interpretation of petrographic observations. Lithos 216–217, 338–351. https://doi.org/10.1016/j.lithos.2015.01.006.
Takeno, N., 2005. Atlas of eh-pH diagrams. Intercomparison of Thermodynamic Databases. National Institute of Advanced Industrial Science and Technology, Tsukuba, pp. 153–155.
Takeuchi, A., Nagahama, H., 2002. Surface charging mechanism and scaling law related to earthquakes. J. Atmos. Electr. 22, 183–190.
Tosi, P., Sbarra, P., De Rubeis, V., 2012. Earthquake sound perception. Geophys. Res. Lett. 39, 24. https://doi.org/10.1029/2012GL053180.
Tulaczyk, S., Kamb, B., Schierer, R.P., Engelhardt, H.F., 1998. Sedimentary processes at the base of a West Antarctic ice stream: constraints from textural and compositional properties of subglacial debris. J. Sediment. Res. 68, 487–496.
Tuttle, M.P., Hartleb, R., Wolf, L., Mayne, P.W., 2019. Paleoliquefaction studies and the evaluation of seismic hazard. Geosciences 9, 311. https://doi.org/10.3390/geosciences9070311.
Ubara, H., Imura, T., Hiraki, A., 1984. Formation of Si-H bonds on the surface of microcrystalline silicon covered with SiOx by HF treatment. Solid State Commun. 50, 673–675.
Van Loon, A.J., 2009. Soft-sediment deformation structures in siliciclastic sediments: an overview. Geologos 15, 3–55.
Van Loon, A.J., 2014. The life cycle of seismite research. Geologos 20, 61–66.
Van Loon, A.J., Pisarska-Jamroży, M., Woronko, B., 2020. Sedimentological distinction in glacigenic sediments between load casts induced by periglacial processes from those induced by seismic shocks. Geol. Q. 64, 626–640. https://doi.org/10.7306/gq.1546.
Van Rensbergen, P., Hillis, R.R., Maltman, A.J., Morley, C.K. (Eds.), 2003. Subsurface sediment mobilization. Geol. Soc. Lond. Spec. Publ. 216. https://doi.org/10.1144/GSL.SP.2003.216.
Voisey, C.R., Hunter, N.J.R., Tomkins, A.G., Brugger, J., Liu, W., Liu, Y., Luzin, V., 2024. Gold nugget formation from earthquake-induced piezoelectricity in quartz. Nat. Geosci. 17, 920–925. https://doi.org/10.1038/s41561-024-01514-1.
Vos, K., Vandenberghe, N., Elsen, J., 2014. Surface textural analysis of quartz grains by scanning electron microscopy (SEM): from sample preparation to environmental interpretation. Earth Sci. Rev. 128, 93–104. https://doi.org/10.1016/j.earscirev.2013.10.013.
Wander, M.C.F., Clark, A.E., 2008. Structural and dielectric properties of quartz−water interfaces. J. Phys. Chem. C 112, 19986–19994. https://doi.org/10.1021/jp803642c.
Woronko, B., 2016. Frost weathering versus glacial grinding in the micromorphology of quartz sand grains: processes and geological implications. Sediment. Geol. 335, 103–119. https://doi.org/10.1016/j.sedgeo.2016.01.021.
Woźniak, P.P., Belzyt, S., Pisarska-Jamroży, M., Woronko, B., Lamsters, K., Nartišs, M., Bitinas, A., 2021. Liquefaction and re-liquefaction of sediments induced by uneven loading and glacigenic earthquakes: implications of results from the Latvian Baltic Sea coast. Sediment. Geology 421, 105944. https://doi.org/10.1016/j.sedgeo.2021.105944.
Wright, J.S., 2007. An overview of the role of weathering in the production of quartz silt. Sed. Geo 202, 337–351. https://doi.org/10.1016/j.sedgeo.2007.03.024.
Xantheas, S.S., 2000. Cooperativity and hydrogen bonding network in water clusters. Chem. Phys. 258, 225–231. https://doi.org/10.1016/S0301-0104(00)00189-0.
Yang, X.L., Zhang, S., 2019. Seismic active earth pressure for soils with tension cracks. Int. J. GeoMech. 19, 06019009. https://doi.org/10.1061/(ASCE)GM.1943-5622.0001414.
Youd, T.L., Perkins, D.M., 1978. Mapping liquefaction-induced ground failure potential. J. Geotech. Eng. Div. 104, 433–446. https://doi.org/10.1061/AJGEB6.0000612.
Zhang, H., Xu, Z., Sun, W., Zhu, Y., Chen, D., Zhang, C., 2023. Hydroxylation structure of quartz surface and its molecular hydrophobicity. Appl. Surf. Sci. 612, 155884. https://doi.org/10.1016/j.apsusc.2022.155884.
Zhang, H.B., Zhang, Z.H., Jin, Y.D., Jiang, H.L., Fan, L.J., Yu, X.C., 2014. Experimental study on tertiary piezoelectric effect of X-cut quartz crystal. Key Eng. Mater. 620, 134–139. https://doi.org/10.4028/www.scientific.net/kem.620.134.
Zhong, N., Jiang, H., Li, H., Su, D., Xu, H., Liang, L., Fan, J., 2022. The potential of using soft-sediment deformation structures for quantitatively reconstructing paleo-seismic shaking intensity: progress and prospect. Environ. Earth Sci. 81, 408. https://doi.org/10.1007/s12665-022-10504-8.
Zhou, X., Guo, J., Zhao, J., 2004. Dynamics of nutrient element iron in soil-plant ecosystem of the Songnen Plain Leymus chinensis grassland. Yingyong Shengtai Xuebao 15 (12), 2250–2254.
Zhuravlev, L.T., 2000. The surface chemistry of amorphous silica. Zhuravlev model. Colloid Surf. A 173, 1–38. https://doi.org/10.1016/s0927-7757(00)00556-2.